



ELSEVIER GEO-ENGINEERING BOOK SERIES
SERIES EDITOR: JOHN A. HUDSON
Volume 4

ENGINEERING PROPERTIES OF ROCKS



LIANYANG ZHANG

Series Preface

The objective of the Elsevier Geo-Engineering Book Series is to provide high quality books on subjects within the broad geo-engineering subject area – e.g. on engineering geology, soil mechanics, rock mechanics, civil/mining/environmental/petroleum engineering, etc. The first three books in the Series have already been published:

- “Stability analysis and modelling of underground excavations in fractured rocks” by Weishen Zhu and Jian Zhao;
- “Coupled thermo-hydro-mechanical-chemical processes in geo-systems” edited by Ove Stephansson, John A Hudson and Lanru Jing; and
- “Ground Improvement — Case Histories” edited by Buddhima Indraratna and Jian Chu.

These three books already represent an admirable, high quality start to the Series. Now, I am delighted to introduce the fourth book in the Series,

- “Engineering Properties of Rocks” by Lianyang Zhang.

This book provides expert, up-to-date information on rock mechanics and rock engineering for both the engineering and academic communities. It is a particularly logical and helpful book because it sequentially outlines the key aspects of the rock mechanics problem: the rock stress, and then the intact rock, the discontinuities and rock masses, followed by the deformability, strength and permeability of these components.

The Author, in his own Preface, states that, “The typical values of and correlations between rock properties come in many forms and are scattered in different textbooks, reference manuals, reports and articles published in technical journals and conference proceedings. It is often difficult, time consuming, or even impossible for a practitioner to find appropriate information to determine the rock properties required for a particular project.” Not only is this true, but the rock property values are the key to rock engineering design, whether it be by an empirical approach or by numerical modelling – as is evident from the content of the first two books in the Geo-Engineering Series.

The rock engineer must be able to predict the consequences of a particular excavation design. This can only be done via an adequate model, and the model can only be adequate if it is supported by the appropriate rock property values. Thus, the content of this book has a value which transcends the direct explanations of the rock mechanics and the rock properties: it represents one of the fundamental and essential keys to good rock engineering design. I am more than pleased to recommend that you read the book from cover to cover.

We hope that you enjoy the book and we welcome proposals for new books. Please send these to me at the email address below.

Professor John A Hudson *FREng*
Geo-Engineering Series Editor
jah@rockeng.co.uk

Preface

For different reasons, it is often difficult for rock engineers to directly obtain the specific design parameter(s) of interest. As an alternative, they use the typical values or empirical correlations of similar rocks to estimate the specific parameter(s) of interest indirectly. For example, the unconfined compressive strength (UCS) of intact rock is widely used in designing surface and underground structures. The procedure for measuring UCS has been standardized by both the American Society for Testing and Materials (ASTM) and the International Society for Rock Mechanics (ISRM). Although the method is relatively simple, it is time consuming and expensive; also, it requires well-prepared rock cores, which is often difficult or even impossible for weak rocks.

Therefore, indirect tests are often conducted to estimate the UCS by using empirical correlations, such as point load, Schmidt hammer, sound velocity and impact strength tests. Another example is the determination of the deformation modulus of rock masses. Rock masses usually contain discontinuities. To obtain realistic values of rock mass deformation modulus, in situ tests, such as plate bearing, flat jack, pressure chamber, borehole jacking and dilatometer tests, need be conducted. The in situ tests, however, are time-consuming, expensive and, in some cases, even impossible to carry out. Therefore, the deformation modulus of rock masses is often estimated indirectly from correlations with classification indices such as RQD (Rock Quality Designation), RMR (Rock Mass Rating), Q (Q-System) and GSI (Geological Strength Index).

The typical values of and correlations between rock properties come in many forms and are scattered in different textbooks, reference manuals, reports and articles published in technical journals and conference proceedings. It is often difficult, time-consuming, or even impossible for a practitioner to find appropriate information to determine the rock properties required for a particular project. The main purpose of this book is to summarize and presents, in one volume, the correlations between different rock properties, together with the typical values of rock properties.

This book contains eight chapters which are presented in a logical order. Chapter 1 provides a general introduction to rock engineering problems and methods for determining rock properties, and presents examples on using empirical correlations to estimate rock properties. Chapter 2 describes in situ rock stresses and presents different empirical correlations for estimating them. Chapters 3–5 describe the classification of intact rock and rock masses and the characterization of rock

discontinuities. Chapters 6–8 present the typical values and correlations of deformability, strength and permeability of intact rock, rock discontinuities and rock masses. It need be noted that the typical values and correlations should never be used as a substitute for a proper testing program, but rather to complement and verify specific project-related information.

This book is intended for people involved in rock mechanics and rock engineering. It can be used by practicing engineers to determine the engineering properties of rocks required for particular projects. It will be useful for teaching to look into the typical values of different rock properties and the factors affecting them. It will also be useful for people engaged in numerical modeling to choose appropriate values for the properties included in the model.

Prof. Harun Sönmez of Hacettepe University, Turkey provided the deformation modulus data which was included in Fig. 6.14. The author sincerely thanks him.

Dr. Evert Hoek, Evert Hoek Consulting Engineer Inc., Canada sent the author his discussion papers and provided valuable information on the rock mass strength data included in Fig. 7.11. The author is grateful to him.

Portions of Chapters 4, 6 and 7 are based on the author's doctoral research conducted at the Massachusetts Institute of Technology. The author acknowledges the support and advice given by Prof. Herbert Einstein.

Finally, the author wants to thank Dr. Francisco Silva and Mr. Ralph Grismala of ICF Consulting for their support during the preparation of this book.

Lianyang Zhang
ICF Consulting
Lexington, MA
USA

1

Introduction

1.1 ROCK ENGINEERING PROBLEMS

Rock has been used as a construction material since the dawn of civilization. Different structures have been built on, in or of rock, including houses, bridges, dams, tunnels and caverns (Bieniawski, 1984; Goodman, 1989; Brown, 1993; Fairhurst, 1993; Hudson, 1993; Hudson & Harrison, 1997; Hoek, 2000). Table 1.1 lists some of the types of structures built on, in or of rock and their field of application. Brown (1993) produced this table by adding surface civil engineering structures to that given by Bieniawski (1984) in his book on rock mechanics design in mining and tunneling.

Rock differs from most other engineering materials in that it contains discontinuities such as joints, bedding planes, folds, sheared zones and faults which render its structure discontinuous. A clear distinction must be made between the intact rock or rock material and the rock mass. The intact rock may be considered as a continuum or polycrystalline solid between discontinuities consisting of an aggregate of minerals or grains. The rock mass is the in situ medium comprised of intact rock blocks separated by discontinuities such as joints, bedding planes, folds, sheared zones and faults. The properties of the intact rock are governed by the physical properties of the materials of which it is composed and the manner in which they are bonded to each other. Rock masses are discontinuous and often have heterogeneous and anisotropic properties.

Because rock masses are discontinuous and variable in space, it is important to choose the right domain that is representative of the rock mass affected by the structure analyzed. Fig. 1.1 shows a simplified representation of the influence exerted on the selection of a rock mass behavior model by the relation of the discontinuity spacing and the size of the problem domain. When the problem domain is much smaller than the blocks of rock formed by the discontinuities, such as the excavation of rock by drilling, the behavior of the intact rock material will be of concern. When the block size is of the same order of the structure being analyzed or when one of the discontinuity sets is significantly weaker than the others, the stability of the structure should be analyzed by considering failure mechanisms involving sliding or rotation of blocks and wedges defined by intersecting structural features. When the structure being analyzed is much larger than the blocks of rock formed by the discontinuities, the rock mass may be simply treated as an equivalent continuum (Brady & Brown, 1985; Brown, 1993; Hoek, 2000).

Table 1.1 Some of the types of structures on, in or of rock (after Brown, 1993).

Field of application	Types of structures on, in or of rock
Mining	Surface mining – slope stability; rock mass diggability; drilling and blasting; fragmentation. Underground mining – shaft, pillar, draft and stope design; drilling and blasting; fragmentation; cavability of rock and ore; amelioration of rockbursts; mechanized excavation; in situ recovery.
Energy development	Underground power stations (hydroelectric and nuclear); underground storage of oil and gas; energy storage (pumped storage or compressed air storage); dam foundations; pressure tunnels; underground repositories for nuclear waste disposal; geothermal energy exploitation; petroleum development including drilling, hydraulic fracturing, wellbore stability.
Transportation	Highway and railway slopes, tunnels and bridge foundations; canals and waterways; urban rapid transport tunnels and stations; pipelines.
Utilities	Dam foundations; stability of reservoir slopes; water supply tunnels; sanitation tunnels; industrial and municipal waste treatment plants; underground storages and sporting and cultural facilities; foundations of surface power stations.
Building construction	Foundations; stability of deep open excavations; underground or earth-sheltered homes and offices.
Military	Large underground chambers for civil defense and military installations; uses of nuclear explosives; deep basing of strategic missiles.

Hudson (1993) developed a general three-tier approach to all rock engineering problems as represented by the three borders shown in Fig. 1.2. The main project subjects concerned, such as foundations, rock slopes, shafts, tunnels and caverns, are illustrated within the three borders of the diagram. The words in the borders at the top of the diagram represent the entry into the design problem: the whole project complete with its specific objective in the outer border, the inter-relation between various components of the total problem in the middle border, and the individual aspects of each project in the central border. The words in the borders at the lower part of the diagram illustrate how the different components of the design might be executed. Different methods, such as the knowledge-based expert system, the rock mechanics interaction matrix analysis and the numerical analysis, can be used to consider the problem. It is noted that, for any project problem considered and any design method used, the material properties (highlighted as intact rock, discontinuities and permeability in Fig. 1.2) and the boundary conditions (highlighted as in situ stress and the hydrogeological regime in Fig. 1.2) should be known. Therefore, determination of engineering properties of rocks (including the boundary conditions) is an essential part of all rock engineering problems.

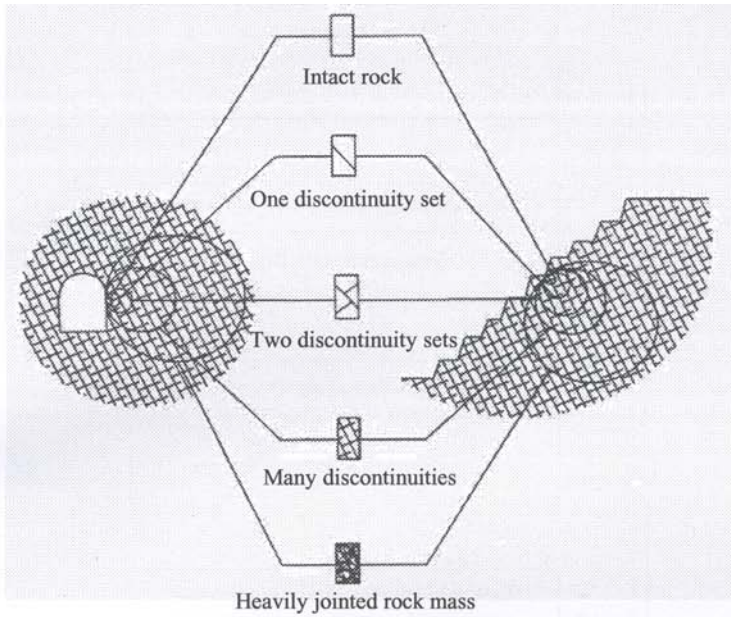


Fig. 1.1 Simplified representation of the influence of scale on the type of rock mass behavior (after Hoek et al., 1995).

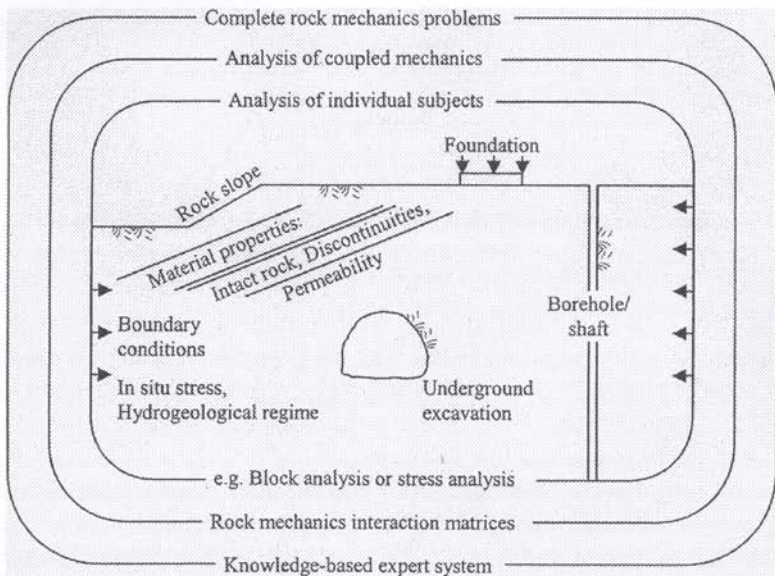


Fig. 1.2 Three-tier approach to all rock engineering problems (after Hudson, 1993).

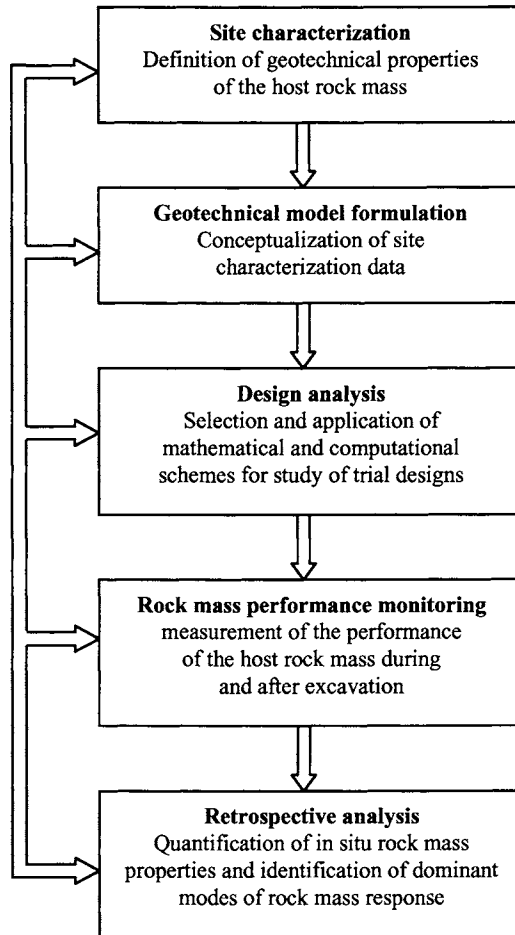


Fig. 1.3 Components of a general rock mechanics program (after Brady & Brown, 1985).

Fig. 1.3 shows the components of a general rock mechanics program for predicting the responses of rock masses associated with rock engineering projects (Brady & Brown, 1985). Determination of engineering (or geotechnical) properties of rock masses is an important part of the general rock mechanics program. Brown (1986) clearly stated the importance of site characterization for determining the engineering properties of rock masses: 'Inadequacies in site characterization of geological data probably present the major impediment to the design, construction and operation of excavations in rock. Improvements in site characterization methodology and techniques, and in the interpretation of the data are of primary research requirements, not only for large rock caverns, but for all forms of rock engineering.'

1.2 DETERMINATION OF ENGINEERING PROPERTIES OF ROCKS

As stated earlier, determination of the engineering properties of rocks is an important part of all rock engineering problems. Because of the discontinuous and variable nature of rock masses, however, it is complex and difficult to determine rock properties. As Hudson (1992) notes: 'The subject of rock characterization is far more complex and intractable than might appear at first sight. The subject does not merely concern the optimal length-to-diameter ratio for a compression test specimen and other similar tactical aspects of testing procedures; it concerns the whole strategic concept of how to characterize naturally occurring rock masses, which have been in existence for millions of years, have been operating as natural process – response systems for all that time and are about to be perturbed by engineers in order to achieve particular objectives.'

Despite the complexity and difficulty for determining the engineering properties of rocks, we still have to do the best we can to decide the specific rock properties required for a particular rock engineering problem and assign reliable values to them. Table 1.2 lists some typical rock engineering applications and the required accuracy for corresponding rock properties suggested by Pine and Harrison (2003).

There are different methods for determining rock mass properties, which can be divided into two general categories: direct and indirect methods (see Table 1.3). The direct methods include laboratory and in situ tests. Many rock mechanics and rock engineering textbooks provide information on conducting laboratory and in situ tests to determine rock properties. In addition, the American Society for Testing and Materials

Table 1.2 Suggested levels of accuracy required for rock mass properties in different applications (after Pine & Harrison, 2003).

Application	Strength	Deformability	Permeability/Hydraulic conductivity
Mining	Pillars Walls (10%) Roofs	Shafts (25%)	Total inflow rates (50%)
Civil excavations	Tunnels (25%) Caverns (10%)	Tunnels (25%) Caverns (25%) Pressure tunnels and shafts (10%)	Total inflow rates (50%) Total leakage rates (25%)
Nuclear/radioactive waste			Mass transport (factor of 10^{-2} to 10^2)
Oil and gas	Borehole stability (10%)	Reservoir subsidence (25%)	Connectivity/transmissivity (50%)
Civil foundations/ pile sockets		Settlement (25%)	

Table 1.3 Methods for determining rock mass properties (after Brown, 1993; Pine & Harrison, 2003; Zhang, 2004).

Direct methods	Indirect methods
Laboratory tests	Empirical or theoretical correlations
In situ tests	Combination of intact rock and discontinuity properties using analytical or numerical methods
	Back-analysis using field observations of prototype observations

Table 1.4 Categories of test methods suggested by ISRM (after Brown, 1981).

1. LABORATORY TESTS

(a) Characterization

- (i) Porosity, density, water content
- (ii) Absorption
- (iii) Hardness – Schmidt rebound, Shore scleroscope
- (iv) Resistance to abrasion
- (v) Point load strength index
- (vi) Uniaxial compressive strength and deformability
- (vii) Swelling and slake-durability
- (viii) Sound velocity
- (ix) Petrographic description

(b) Engineering design

- (i) Triaxial strength and deformability test
- (ii) Direct shear test
- (iii) Tensile strength test
- (iv) Permeability
- (v) Time dependent and plastic properties

2. IN SITU TESTS

(a) Characterization

- (i) Discontinuity orientation, spacing, persistence, roughness, wall strength, aperture, filling, seepage, number of sets, and block size
- (ii) Drill core recovery/RQD
- (iii) Geophysical borehole logging
- (iv) In situ sound velocity

(b) Engineering design

- (i) Plate and borehole deformability tests
 - (ii) In situ uniaxial and triaxial strength and deformability test
 - (iii) Shear strength – direct shear, torsional shear
 - (iv) Field permeability measurement
 - (v) In situ stress determination
-

(ASTM) and International Society for Rock Mechanics (ISRM) standards provide guidance related to the specific procedures for performing the actual laboratory and in situ tests. Table 1.4 lists the categories of the suggested test methods of ISRM (Brown, 1981).

The direct methods have different limitations. To obtain realistic results of rock mass properties, rock of different volumes having a number of different known discontinuity configurations should be tested at relevant stress levels under different stress paths. Such an experimental program is almost impossible to carry out in the laboratory. With in situ tests, such an experimental program would be very difficult, time-consuming and expensive.

The indirect methods include empirical or theoretical correlations, combination of intact rock and discontinuity properties using analytical or numerical methods, and back-analysis using field observations of prototype observations. Because of the limitations of the direct methods, current practice relies heavily on the indirect methods. The indirect methods can be used not only for determining rock properties but also for checking the test results. Data resulting from laboratory and in situ tests are often not completely consistent with other data obtained for a particular project. The indirect methods such as the empirical or theoretical correlations can be used to check the data from tests and investigate the reasons for the inconsistency. The two examples presented in next section clearly show the application of empirical correlations in the determination of the engineering properties of rocks.

1.3 EXAMPLES ON DETERMINING ENGINEERING PROPERTIES OF ROCKS

This section presents two examples on determining the engineering properties of rocks. They clearly show how the existing data and empirical correlations are used in the determination of the engineering properties of rocks.

a. Estimation of rock discontinuity shear strength (Wines & Lilly, 2003)

This example shows the estimation of rock discontinuity shear strength in part of the Fimiston open pit operation in Western Australia (Wines & Lilly, 2003). There are four major discontinuity sets at the pit site:

- Discontinuities in Set 1 are generally rough, planar and clean, with occasional quartz infill and have an average dip/dip direction of $65^{\circ}/271^{\circ}$.
- Discontinuities in Set 2 are generally rough and planar to undulating, with regular quartz infill and have an average dip/dip direction of $2^{\circ}/306^{\circ}$.
- Discontinuities in Set 3 are generally rough and planar, with regular quartz infill and have an average dip/dip direction of $82^{\circ}/323^{\circ}$.
- Discontinuities in Set 4 include tightly healed, rough and undulating quartz veins and have an average dip/dip direction of $86^{\circ}/001^{\circ}$.

Shear strength data of the discontinuities were required in order to design a major part of the eastern wall in the Fimiston open pit.

The empirical shear strength criterion proposed by Barton (1976) [equation (7.32) in Chapter 7] was used to describe the shear strength of discontinuities at the site. To use this criterion, the following three input parameters need be determined:

- JRC – Discontinuity roughness coefficient
- JCS – Discontinuity wall compressive strength
- ϕ_r – Residual friction angle of the discontinuity

JRC values for the four discontinuity sets were recorded during scanline mapping and diamond core logging using the profiles presented in Fig. 6.6. Since the discontinuities in the study area generally exhibited no wall softening due to weathering, JCS was assumed to be equal to the unconfined compressive strength of the intact rock. The estimated values of JRC and JCS are summarized in Table 1.5.

Since the discontinuities in the study area generally exhibited no wall softening due to weathering, the residual friction angle ϕ_r could be simply taken equal to the basic friction angle ϕ_b [see equation (6.20)]. The basic friction angle was determined using the following three different methods:

- (1) Direct shear testing along smooth and clean saw cut samples.
- (2) Tilt test on split core samples and using equation (6.21) to calculate the basic friction angle.
- (3) Using typical values available in the literature (Table 6.7).

The estimated values of the basic friction angle using the above three methods are shown in Table 1.6. It is noticed that the estimated values using the three methods are in good agreement except that the values of Paringa Basalt from the tilt testing a bit higher.

Table 1.5 Estimated values of JRC and JCS for the four main discontinuity sets (from Wines & Lilly, 2003).

Parameter	Statistic	Paringa Basalt			Golden Mine Dolerite			
		Set 1	Set 2	Set 4	Set 1	Set 2	Set 3	Set 4
JRC	Mean	6.4	7.1	4.7	7.8	7.3	5.9	7.0
	SD	3.0	2.9	2.9	2.7	2.3	2.2	3.1
	Min	2.0	2.0	2.0	2.0	2.0	2.0	2.0
	Max	14.0	12.0	10.0	16.0	14.0	10.0	14.0
JCS (MPa)	Mean	86.9	86.9	86.9	95.9	95.9	95.9	95.9
	SD	28.9	28.9	28.9	34.4	34.4	34.4	34.4
	Min	43.7	43.7	43.7	34.3	34.3	34.3	34.3
	Max	156.5	156.5	156.5	156.3	156.3	156.3	156.3

Table 1.6 Estimated values of the basic friction angle ϕ_b (from Wines & Lilly, 2003).

Rock	Direct shear testing				Tilt testing				Values from Table 6.7
	Mean	SD	Min	Max	Mean	SD	Min	Max	
Paringa Basalt	36.9	2.0	32.9	39.4	39.6	1.1	37.4	42.1	35-38
Golden Mine Dolerite	34.2	1.5	32.0	36.0	36.3	1.4	32.6	40	36

b. Estimation of strength and deformability of rock masses (Ozsan & Akin, 2002)

This example describes the estimation of strength and deformability of rock masses at the proposed Urus Dam site in Turkey (Ozsan & Akin, 2002). The site is located on volcanic rocks of the Neogene Age and on Quaternary deposits. Volcanic rocks consist of andesite, basalt and tuff (see Figs. 1.4 and 1.5).

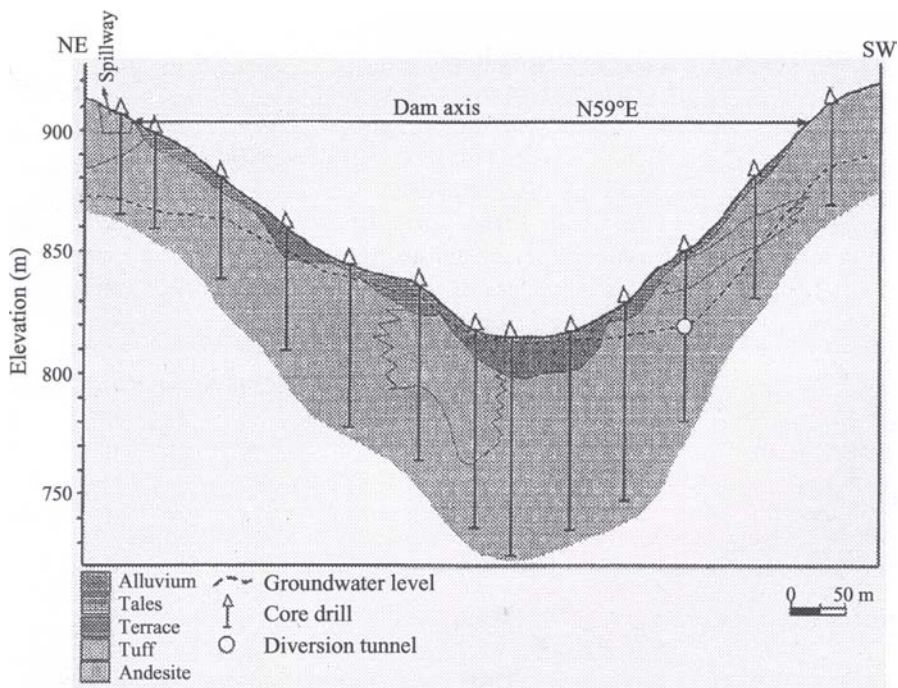


Fig. 1.4 Geological cross-section along dam axis at the Urus Dam site (from Ozsan & Akin, 2002).

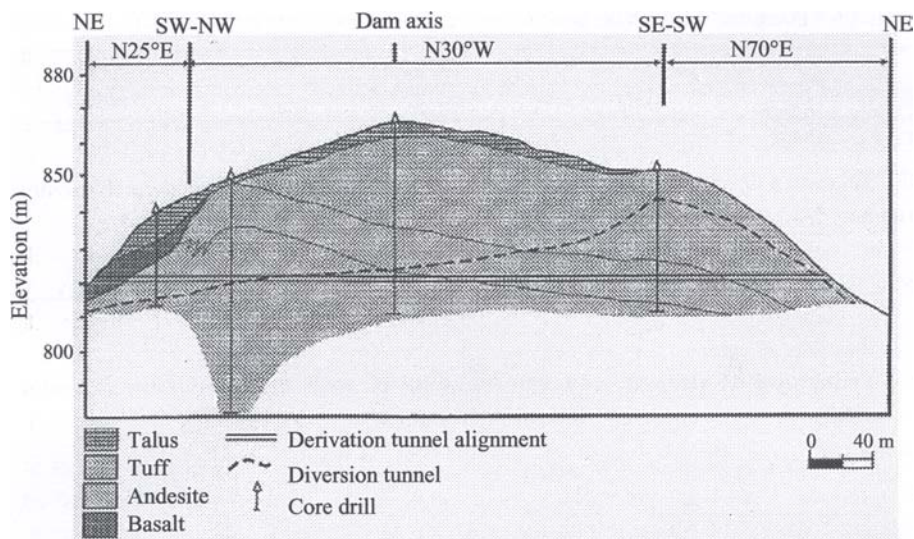


Fig. 1.5 Geological cross-section of the diversion tunnel alignment at the Urus Dam site (from Ozsan & Akin, 2002).

Table 1.7 Quantitative descriptions and statistical distributions of discontinuities of basalt and andesite at the Urus Dam site (from Ozsan & Akin, 2002).

	Range	Description	Distribution (%)	
			Basalt	Andesite
Spacing (mm)	< 20	Extremely close	4	-
	20-60	Very close	47	26
	60-200	Close	32	51
	200-600	Moderate	17	23
Persistence (m)	1-3	Low	17	13
	3-10	Medium	59	47
	10-20	High	24	40
Aperture ^a (mm)	0.25-0.5	Partly open	26	31
	0.5-2.5	Open	55	54
	2.5-10	Moderately wide	19	15
Roughness	1 ^b	0-2 ^c	25	23
	2	2-4	33	36
	3	4-6	19	25
	4	6-8	13	8
	5	8-10	10	8

^a Aperture of discontinuities contains mostly limonite, hematite and clay infilling materials.

^b Roughness profile numbers.

^c JRC values.

Characterization of discontinuities was carried out by exposure logging following ISRM (1978c). A total of 399 discontinuities, 372 on the left bank and 27 on the right bank, were measured. Three major discontinuity sets on the left bank ($29^\circ/3352^\circ$, $87^\circ/333^\circ$, $30^\circ/079^\circ$) and two ($85^\circ/146^\circ$, $60^\circ/2973^\circ$) on the right bank were determined. Table 1.7 shows the quantitative descriptions and statistical distributions of discontinuities of basalt and andesite at the site. Since tuff is moderately-highly weathered, no discontinuity was observed during exposure logging.

Borings were made at the site to verify foundation conditions and to obtain rock samples for laboratory testing. Rock quality designation (RQD) and total core recovery (TCR) values were determined for different structural areas of the dam site. Table 1.8 lists the average values.

Laboratory tests were carried out to determine physical and mechanical properties including unit weight, porosity, unconfined compressive and tensile strength, cohesion, internal friction angle and deformation parameters. The results are summarized in Table 1.9.

Table 1.8 Average RQD and TCR values obtained from core drilling at the Urus Dam site (from Ozsan & Akin, 2002).

Location	Andesite		Basalt		Tuff	
	RQD (%)	TCR (%)	RQD (%)	TCR (%)	RQD (%)	TCR (%)
Left bank	59	93	-	-	34	79
Dam axis	46	85	-	-	10	94
Right bank	35	100	-	-	34	87
Diversion tunnel	52	100	15	58	8	75
Spillwa	38	83	-	-	0	75

Table 1.9 Laboratory test results of rocks at the Urus Dam site (from Ozsan & Akin, 2002).

Parameter	Andesite		Basalt		Tuff	
	Range	Average	Range	Average	Range	Average
Unit weight (kN/m^3)	21.6-25.5	23.7	22.1-2.57	24.0	18.8-21.5	19.9
Porosity (%)	3.26-4.13	3.73	3.03-3.54	3.29	12.5-18.6	16.1
Unconfined compressive strength (MPa)	40-148	93	64-249	142	17-33	24
Tensile strength (MPa)	7.55-9.60	8.58	6.20-8.30	7.25	0.75-2.94	1.97
Cohesion (MPa)		9.72		10.81		9.29
Internal friction angle ($^\circ$)		53.21		43.18		36.77
Elastic modulus (GPa)		41.9		40.0		11.6
Poisson's ratio		0.22		0.30		0.21

To estimate the strength and deformability properties of the rock masses, the Geological Strength Index (GSI) was estimated using the quantified GSI chart proposed by Sonmez and Ulusay (1999, 2002) (see Fig. 5.2 in Chapter 5). Table 1.10 lists the estimated GSI values. The strength of rock masses at this site was expressed by using the Hoek-Brown criterion [equation (7.39) in Chapter 7]. Rock mass constants m_b , s and a for the Hoek-Brown criterion were estimated by using equation (7.44). Intact rock constants were selected from Hoek and Brown (1997). The unconfined compressive strength σ_{cm} of rock masses was determined by inserting the minor principal stress σ'_3 of zero into equation (7.39). The results are shown in Table 1.10.

The deformation modulus of rock masses at this site was estimated by using equation (6.45) in Chapter 6. The results are also shown in Table 1.10.

Table 1.10 GSI values, rock mass constants and deformations modulus of rock masses at the Urus Dam site (from Ozsan & Akin, 2002).

Parameter	Andesite	Basalt	Tuff
Unconfined compressive strength of intact rock σ_c (MPa)	93	142	24
Geological strength index (GSI)	41	42.5	31
Hoek-Brown intact rock constant m_i	19*	17*	15*
Hoek-Brown rock mass constant m_b	2.31	2.18	1.28
Hoek-Brown rock mass constant s	0.00142	0.00168	0.00047
Hoek-Brown rock mass constant a	0.5	0.5	0.5
Unconfined compressive strength of rock masses σ_{cm} (MPa)	3.51	5.82	0.52
Deformation modulus of rock masses E_m (GPa)	5.74	7.74	1.64

* Marinou and Hoek (2001) updated the table for m_i (see Table 7.9 in Chapter 7). If the updated table were used, the corresponding values of m_i would be, respectively, 25, 25 and 13.

1.4 CONTENT OF THE BOOK

This book focuses on the determination of the engineering properties of rocks. The emphasis is mostly on the indirect methods for determining the rock properties, including empirical or theoretical correlations and combination of intact rock and discontinuity properties using analytical or numerical methods. The direct methods – laboratory and in situ tests – have been well described in many rock mechanics and rock engineering textbooks. The American Society for Testing and Materials (ASTM) and International Society for Rock Mechanics (ISRM) standards provide guidance related to the specific procedures for performing the actual laboratory and in situ tests.

The last three decades have seen sustained research and development efforts to improve the methods for determining the engineering properties of rocks. Although

much has been learned on determining rock properties, all the major findings are scattered in different textbooks, reference manuals, reports and articles published in technical journals and conference proceedings. It is often difficult, time-consuming, or even impossible for a practitioner to find appropriate information to determine the rock properties required for a particular project. The main purpose of this book is to provide the reader a single source of information required for determining rock properties by summarizing and presenting the latest information in one volume.

The eight chapters in this book are presented in a logical order starting with this initial Chapter 1 that provides a general introduction to rock engineering problems and methods for determining rock properties, presents examples on determining rock properties, and describes the various topics covered by the main chapters of this book.

Chapter 2 describes in situ rock stresses and presents the empirical correlations and analytical solutions for estimating the in situ rock stresses.

Chapter 3 discusses the classification and index properties of intact rocks. The typical values of and empirical or theoretical correlations between different index properties are also presented.

The characterization of rock discontinuities is presented in Chapter 4. This chapter focuses on the geometric properties of discontinuities. The mechanical and hydraulic properties of discontinuities are discussed in later chapters.

Chapter 5 describes the classification of rock masses using different rock mass classification systems. The correlations between different classification indices are also presented.

The deformability of intact rocks, rock discontinuities and rock masses is discussed in Chapter 6. The typical values of the deformation parameters of different rocks are summarized in tables and figures. Different methods for determining the deformability of intact rocks, rock discontinuities and rock masses are presented and the factors affecting the deformability of rocks are discussed.

Chapter 7 deals with the strength of intact rocks, rock discontinuities and rock masses. The typical values of the strength parameters of different rocks are summarized in tables and figures. Different methods for determining the strength of intact rocks, rock discontinuities and rock masses are presented and the factors affecting the strength of rocks are discussed.

Finally, Chapter 8 discusses the permeability of rocks. The typical values of the permeability of intact rocks and rock masses are presented. The methods for considering the permeability of rock discontinuities are described and the factors affecting the permeability of rocks are discussed.

This book is intended for people involved in rock mechanics and rock engineering. It can be used by practicing engineers to determine the engineering properties of rocks required for particular projects. It will be useful for teaching to look into the typical values of different rock properties and the factors affecting them. It will also be useful for people engaged in numerical modeling to choose appropriate values for the properties included in the model.

This book focuses on the indirect methods with emphasis on empirical or theoretical correlations and combination of intact rock and discontinuity properties using analytical or numerical methods. It does not mean that the direct methods are not important. In practice, a project should always include some types of laboratory or in situ tests. The

indirect methods can only be used to supplement the direct methods. When describing the use of correlations, Sabatini et al. (2002) states:

‘Correlations in general should never be used as a substitute for an adequate subsurface investigation program, but rather to complement and verify specific project-related information.’

The above statement about correlations also applies to indirect methods covered in this book.

Preface

For different reasons, it is often difficult for rock engineers to directly obtain the specific design parameter(s) of interest. As an alternative, they use the typical values or empirical correlations of similar rocks to estimate the specific parameter(s) of interest indirectly. For example, the unconfined compressive strength (UCS) of intact rock is widely used in designing surface and underground structures. The procedure for measuring UCS has been standardized by both the American Society for Testing and Materials (ASTM) and the International Society for Rock Mechanics (ISRM). Although the method is relatively simple, it is time consuming and expensive; also, it requires well-prepared rock cores, which is often difficult or even impossible for weak rocks.

Therefore, indirect tests are often conducted to estimate the UCS by using empirical correlations, such as point load, Schmidt hammer, sound velocity and impact strength tests. Another example is the determination of the deformation modulus of rock masses. Rock masses usually contain discontinuities. To obtain realistic values of rock mass deformation modulus, in situ tests, such as plate bearing, flat jack, pressure chamber, borehole jacking and dilatometer tests, need be conducted. The in situ tests, however, are time-consuming, expensive and, in some cases, even impossible to carry out. Therefore, the deformation modulus of rock masses is often estimated indirectly from correlations with classification indices such as RQD (Rock Quality Designation), RMR (Rock Mass Rating), Q (Q-System) and GSI (Geological Strength Index).

The typical values of and correlations between rock properties come in many forms and are scattered in different textbooks, reference manuals, reports and articles published in technical journals and conference proceedings. It is often difficult, time-consuming, or even impossible for a practitioner to find appropriate information to determine the rock properties required for a particular project. The main purpose of this book is to summarize and presents, in one volume, the correlations between different rock properties, together with the typical values of rock properties.

This book contains eight chapters which are presented in a logical order. Chapter 1 provides a general introduction to rock engineering problems and methods for determining rock properties, and presents examples on using empirical correlations to estimate rock properties. Chapter 2 describes in situ rock stresses and presents different empirical correlations for estimating them. Chapters 3–5 describe the classification of intact rock and rock masses and the characterization of rock

2

In situ Stresses

2.1 INTRODUCTION

The distribution of in situ rock stresses is a major concern of rock mechanics and rock engineering, both with respect to understanding basic geological process such as plate tectonics and earthquakes, and the design of structures in and on rock masses (Amadei & Stephansson, 1997; Hudson & Harrison, 1997; Fairhurst, 2003). A list of activities requiring knowledge of in situ rock stresses is given in Table 2.1 which was produced by Amadei and Stephansson (1997). As stated by Hudson and Harrison (1997), ‘The basic motivations for in situ stress determination are two-fold.

1. To have a basic knowledge of the stress state for engineering, e.g. in what direction and with what magnitude is the major principal stress acting? What stress effects are we defending ourselves and our structures against? In what direction is the rock most likely to break? All other things being equal, in what direction will the groundwater flow? Even for such basic and direct engineering questions, a knowledge of the stress state is essential.
2. To have a specific and “formal” knowledge of the boundary conditions for stress analyses conducted in the design phase of rock engineering projects.’

Stress is a tensor quantity containing nine components: three normal stress components and six shear stress components [see Fig 2.1(a)]. With the complementary pairs of shear stresses being equal, the stress tensor has six independent components. Hence, to specify the in situ rock stress at a point, six independent pieces of information must be known. When the cube shown in Fig. 2.1(a) is rotated, the stress components on the faces change in value. At one, and only one, cube orientation, all the shear stress components on the faces will be zero [see Fig. 2.1(b)]. When this occurs, the cube faces represents the principal stress planes and the corresponding normal stresses are the principal stresses (Hudson et al., 2003). So the in situ rock stress at a point can also be specified if we know the orientations and magnitudes of the principal stresses.

There are many different methods for measuring in situ rock stresses. These methods can be classified into two main categories (Ljunggren et al., 2003). The first consists of methods that disturb the in situ rock conditions, i.e. by inducing strains, deformations or crack opening pressures, including hydraulic fracturing and/or hydraulic testing of

pre-existing fractures (HTPE) methods, borehole relief methods and surface relief methods. The second consists of methods based on observation of rock behavior without any major influence from the measuring method, including core discing, borehole breakouts, relief of large rock volumes (back analysis), acoustic methods (Kaiser effect), strain recovery methods, geological observational methods and earthquake focal mechanisms. Description of the various methods for measuring in situ rock stresses is out of the scope of this book. The reader can refer to Amadei and Stephansson (1997), Hudson and Harrison (1997) and the Rock Stress Estimation Special Issue of the International Journal of Rock Mechanics and Mining Sciences, 2003, Volume 40, Issue 7-8 for detailed description of the various methods. Instead, this book will concentrate on the various methods for estimating the in situ rock stresses, including empirical correlations or observations obtained from stress measurements made in the past and different analytical models. 'Estimating in situ stresses can be useful in the early stage of engineering design, for the planning process and when selecting stress measuring methods and the location of those measurements.' (Amadei & Stephansson, 1997).

Table 2.1 Activities requiring knowledge of in situ stresses (after Amadei & Stephansson, 1997).

Civil and mining engineering

- Stability of underground excavations (tunnels, mines, caverns, shafts, stopes, haulages)
- Drilling and blasting
- Pillar design
- Design of support systems
- Prediction of rock bursts
- Fluid flow and contaminant transport
- Dams
- Slope stability

Energy development

- Borehole stability and deviation
- Borehole deformation and failure
- Fracturing and fracture propagation
- Fluid flow and geothermal problems
- Reservoir production management
- Energy extraction and storage

Geology/geophysics

- Orogeny
- Earthquake prediction
- Plate tectonics
- Neotectonics
- Structural geology
- Volcanology
- Glaciation

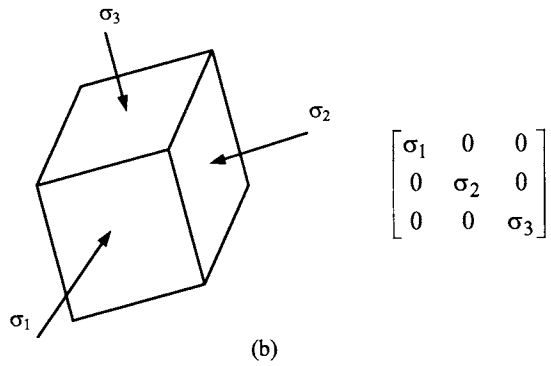
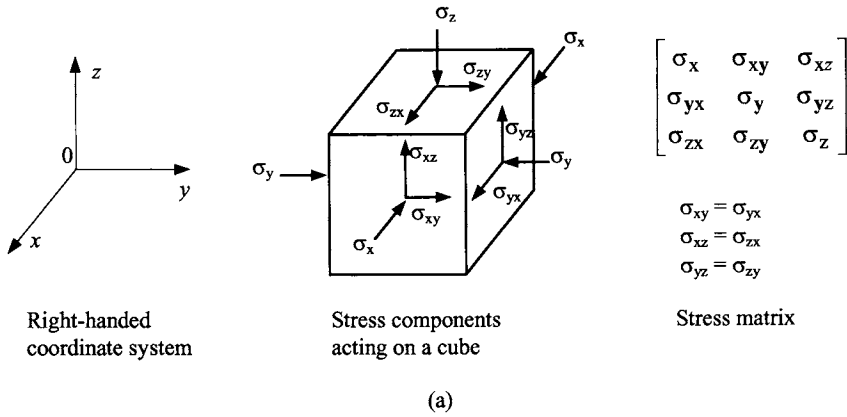


Fig. 2.1 (a) The components of the stress tensor acting on an infinitesimal cube within the rock mass; (b) Principal stress cube and principal stress matrix.

2.2 STRATEGY FOR ESTIMATING IN SITU ROCK STRESSES

An exact determination of in situ rock stresses is very difficult and for all practical purposes impossible because ‘the current stress state is the end product of a series of past geological events and is the superposition of stress components of several diverse types. Further, since rock masses are rarely homogeneous and continuous, stresses can be expected to vary from place to place in a rock mass. In situ stresses not only vary in space but also with time due to tectonic events, erosion, glaciation, etc. The problem is further complicated in that the present rock fabric may or may not be correlated at all with the current stress field (Terzaghi, 1962).’ (Amadei & Stephansson, 1997).

Because of the special nature of in situ rock stresses, they should be estimated using several methods and in a progressive process. The International Society of Rock Mechanics recommended an approach strategy to progressively build up a knowledge of the in situ rock stress tensor (Hudson et al., 2003). Table 2.2 lists the steps in the

progression. Combining various methods based on their respective attributes can help in obtaining a more reliable estimate of the in situ rock stresses. It is important to integrate the stress estimates from various methods. The integration should check if the simplifying assumptions associated with each method are met and take into account uncertainties in each estimate. The number of estimates for each corresponding method should also be considered with care to avoid giving any inappropriate weight to the more numerous data set.

In the following sections, the various methods for making preliminary estimation of in situ rock stresses will be presented, including empirical correlations or observations obtained from stress measurements made in the past and different analytical models. The reader can refer to Amadei and Stephansson (1997), Hudson and Harrison (1997) and the Rock Stress Estimation Special Issue of the International Journal of Rock Mechanics and Mining Sciences, 2003, Volume 40, Issue 7-8 for detailed description of the various measuring methods. It need be noted that the preliminary estimation of in situ rock stresses should no be considered a substitute for their measurement.

Table 2.2 Steps in developing a knowledge of the rock stress tensor components (after Hudson et al., 2003).

Use pre-existing information on the rock stress state at the site	
Consider whether the vertical direction is a principal stress direction (from topography, geological evidence and other information)	
Estimate the vertical stress component magnitude (from the rock density and overburden depth)	
Consider indications of the principal stress directions and the ratio of stress differences (from focal plane solutions inversion or seismic shear wave anisotropy)	
Establish the minimum principal stress orientation (whether actual or minimum horizontal stress) from hydraulic or drilling induced fractures and borehole breakout orientations	
Find components of the stress tensor using indirect methods on borehole core (such as the Kaiser effect and differential strain analysis)	
Establish the complete stress state at one or more locations by overcoring tests	Establish the minimum principal stress (from hydraulic fracturing tests in boreholes)
	Establish the maximum principal stress magnitude (from hydraulic fracturing tests in boreholes and from borehole failure analysis)
	Establish the complete state of stress at one or more locations [by hydraulic testing of pre-existing fractures (HTPF)]
Establish the variation of the stress state across the site due to different geological strata and fractures (as estimated through numerical analyses and further measurements)	

2.3 VARIATION OF IN SITU STRESSES WITH DEPTH

As a first estimation, it is often assumed that the three principal stresses of an in situ rock stress state are acting vertically and horizontally. The validity of this assumption has been checked by many researchers based on in situ stress measurements, including Bulin (1971), Worotnicki and Walton (1976), Klein and Brown (1983), Li (1986), Zoback et al. (1989), Myrvang (1993) and Stephansson (1993). With this assumption concerning orientations, the magnitudes of these principal stresses can be estimated using the correlations between vertical and horizontal stresses and depth presented in the following subsections.

2.3.1 Vertical stress

Hoek and Brown (1980a) analyzed worldwide data on measured in situ rock stresses and presented the graph shown in Fig. 2.2. For the measured vertical stresses shown in Fig. 2.2, the average trend with depth can be expressed as $\sigma_v = 0.027z$ MPa, where z is the depth below surface. Since the unit weight of rock masses is typically about 0.027 MN/m^3 , the vertical stresses can be simply estimated from the following relationship:

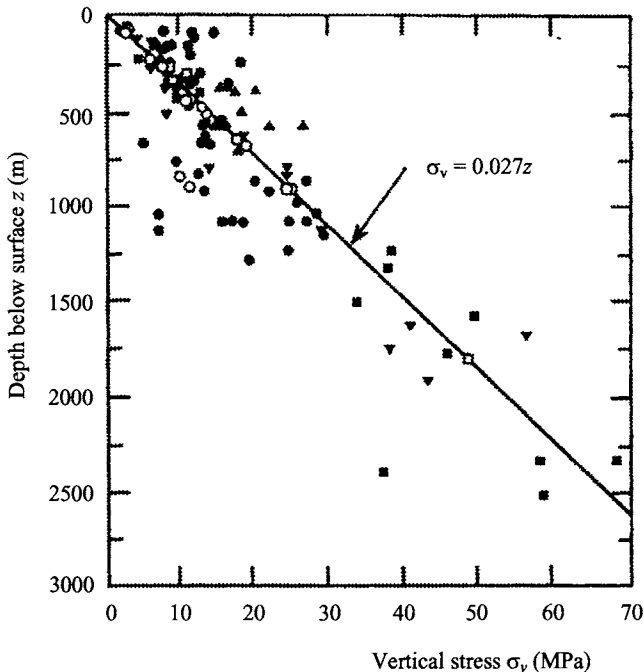


Fig. 2.2 Worldwide in situ rock stress data: vertical stress versus depth below surface (after Hoek & Brown, 1980a).

$$\sigma_v = \gamma z \quad (2.1)$$

where γ is the unit weight of the overlying rock mass; and z is the depth below surface.

It need be noted that equation (2.1) only provides a good estimate of the average stress from all the measured data. In some cases, the measured vertical stress may be dramatically different to the predicted one from equation (2.1). Table 2.3 lists different variation forms of vertical stress with depth.

2.3.2 Horizontal stresses

The horizontal stresses in rock are much more difficult to estimate than the vertical stress. In many cases, the horizontal stresses at the same location in a rock mass are different in different directions. The maximum horizontal stress σ_{hmax} and the minimum horizontal stress σ_{hmin} can be related to the vertical stress σ_v , as follows (see Fig. 2.3) (Anderson, 1951):

- $\sigma_v > \sigma_{hmax} > \sigma_{hmin}$ in normal fault area
- $\sigma_{hmax} > \sigma_{hmin} > \sigma_v$ in thrust fault area
- $\sigma_{hmax} > \sigma_v > \sigma_{hmin}$ in strike-slip fault area

Table 2.4 lists different variation forms of σ_{hmax} , σ_{hmin} and average horizontal stress σ_{have} with depth.

Table 2.3 Variation of vertical stress with depth (after Amadei & Stephansson, 1997; Yokoyam, 2003).

Reference	Variation of vertical stress σ_v (MPa) with depth z (m)	Location and depth range (m)
Herget (1974)	$(1.9 \pm 1.26) + (0.0266 \pm 0.0028)z$	World data (0–2,400)
Lindner & Halpern (1977)	$(0.942 \pm 1.1.31) + (0.0339 \pm 0.0067)z$	North American (0–1,500)
McGarr & Gay (1978)	0.0265z	World data (100–3,000)
Hoek & Brown (1980a)	0.027z	World data (0–3,000)
Herget (1987)	$(0.026 - 0.0324)z$	Canadian Shield (0–2,200)
Arjang (1989)	$(0.0266 \pm 0.008)z$	Canadian Shield (0–2,000)
Baumgärtner et al. (1993)	$(0.0275 - 0.0284)z$	KTP pilot hole (800–3,000)
Herget (1993)	0.0285z	Canadian Shield (0–2,300)
Sugawara & Obara (1993)	0.027z	Japanese Islands (0–1,200)
Te Kamp et al. (1995)	$(0.0275 - 0.0284)z$	KTP hole (0–9,000)
Lim and Lee (1995)	$0.233 + 0.024z$	South Korea (0–850)
Yokoyam, T. (2003)	0.0255z (Crystalline rock) 0.0249z (Sedimentary rock)	Japan (0–1,600)

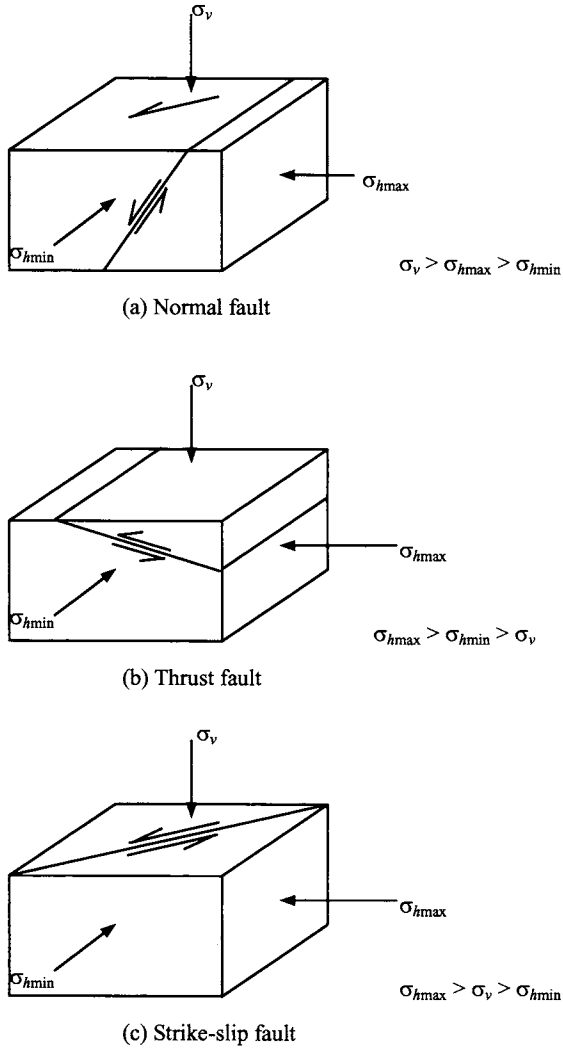


Fig. 2.3 Types of faults and state of in situ rock stresses (after Anderson, 1951).

Normally, the average horizontal stress is related to the vertical stress by the coefficient k such that:

$$\sigma_{have} = k\sigma_v = k\gamma z \tag{2.2}$$

Figure 2.4 shows the variation of in situ k values with depth from Jamison and Cook

Table 2.4 Variation of horizontal stress with depth (after Amadei & Stephansson, 1997; Rummel, 2002; Yokoyam, 2003).

Reference	Variation of σ_{have} , σ_{hmax} , σ_{hmin} (MPa) or k , k_{max} , k_{min} with depth z (m)	Location and depth range (m)
Voight (1966)	$\sigma_{have} = 8.0 + 0.043z$	World data (0–1,000)
Herget (1974)	$\sigma_{have} = (8.3 \pm 0.5) + (0.0407 \pm 0.0023)z$	World data (0–800)
Van Heerden (1976)	$k = 0.448 + 248/z$ ($r = 0.85$)	South Africa (0–2,500)
Worotnicki & Denham (1976)	$\sigma_{have} = 7.7 + (0.021 \pm 0.002)z$ ($r = 0.85$)	Australia (0–1,500)
Haimson (1977)	$\sigma_{hmax} = 4.6 + 0.025z$ $\sigma_{hmin} = 1.4 + 0.018z$ ($r = 0.95$)	Michigan Basin (0–5,000)
Lindner & Halpern (1977)	$\sigma_{have} = (4.36 \pm 0.815)$ $+ (0.039 \pm 0.0072)z$	North American (0–1,500)
Hoek & Brown (1980a)	$0.3 + 100/z < k < 0.5 + 1500/z$	World data (0–3,000)
Aytmatov (1986)	$5.0 + 0.058z < (\sigma_{hmax} + \sigma_{hmin}) <$ $9.5 + 0.075z$	World data (mostly former USSR) (0–1,000)
Li (1986)	$\sigma_{have} = 0.72 + 0.041z$ $0.3 + 100/z < k < 0.5 + 440/z$	China (0–500)
Rummel (1986)	$k_{max} = 0.98 + 250/z$ $k_{min} = 0.5 + 150/z$	World data (500–3,000)
Herget (1987)	$\sigma_{have} = 9.86 + 0.0371z$ $\sigma_{have} = 33.41 + 0.0111z$ $k = 1.25 + 267/z$ $k_{max} = 1.46 + 357/z$ $k_{min} = 1.10 + 167/z$	Canadian Shield (0–900) (990–2,200) (0–2,200)
Pine & Kwakwa (1989)	$\sigma_{hmax} = 15 + 0.028z$ $\sigma_{hmin} = 6 + 0.012z$	Carmmenellis granite Cornwall, UK (0–2,000)
Arjang (1989)	$\sigma_{hmax} = 8.8 + 0.0422z$ $\sigma_{hmin} = 3.64 + 0.0276z$ $\sigma_{have} = 5.91 + 0.0349z$	Canadian Shield (0–2,000)
Baumgärtner et al. (1993)	$\sigma_{hmax} = 30.4 + 0.023z$ $\sigma_{hmin} = 16.0 + 0.011z$ $\sigma_{hmin} = 1.75 + 0.0133z$	KTP pilot hole (800–3,000) Cajon pass hole (800–3,000)
Sugawara & Obara (1993)	$\sigma_{have} = 2.5 + 0.013z$	Japanese Islands (0–1,200)

Table 2.4 (Continued).

Reference	Variation of σ_{have} , σ_{hmax} , σ_{hmin} (MPa) or k , k_{max} , k_{min} with depth z (m)	Location and depth range (m)
Hast (in Stephansson, 1993)	$\sigma_{hmax} = 9.1 + 0.0724z$ ($r = 0.78$) $\sigma_{hmin} = 5.3 + 0.0542z$ ($r = 0.83$)	Fennoscandia, overcoring (0–1,000)
Stephansson (1993)	$\sigma_{hmax} = 10.4 + 0.0446z$ ($r = 0.61$) $\sigma_{hmin} = 5.0 + 0.0286z$ ($r = 0.58$)	Fennoscandia Leeman-Hiltscher overcoring (0–700)
	$\sigma_{hmax} = 6.7 + 0.0444z$ ($r = 0.61$) $\sigma_{hmin} = 0.8 + 0.0329z$ ($r = 0.91$)	Leeman-type overcoring (0–1,000)
	$\sigma_{hmax} = 2.8 + 0.0399z$ ($r = 0.79$) $\sigma_{hmin} = 2.2 + 0.0240z$ ($r = 0.81$)	Hydraulic fracturing (0–1,000)
Te Kamp et al. (1995)	$\sigma_{hmax} = 15.83 + 0.0303z$ $\sigma_{hmin} = 6.52 + 0.0157z$	KTP hole (0–9,000)
Lim and Lee (1995)	$\sigma_{have} = 1.858 + 0.018z$ ($r = 0.869$) $\sigma_{have} = 2.657 + 0.032z$ ($r = 0.606$)	South Korea overcoring (0–850) Hydraulic fracturing (0–500)
Rummel (2002)	$k_{max} = 1.30 + 110/z$ $k_{min} = 0.66 + 72/z$	Hong Kong (0–200)
Yokoyama, et al. (2003)	Crystalline rock: $\sigma_{hmax} = -21.9 + 0.0301z$ $\sigma_{hmin} = 33.7 + 0.0219z$ Sedimentary rock: $\sigma_{hmax} = 23.5 + 0.0340z$ $\sigma_{hmin} = 47.5 + 0.0281z$	Japan (0–1,600)

Notes: $k = \sigma_{have}/\sigma_v$; $k_{max} = \sigma_{hmax}/\sigma_v$; $k_{min} = \sigma_{hmin}/\sigma_v$; and r is the correlation coefficient.

(1979) with interpretation of faulting conditions. As would be expected, the values of σ_{have} in the normal fault areas are relatively low, the values of σ_{have} in the thrust fault areas are relatively high, and the values of σ_{have} in the strike-slip fault areas are intermediate.

Fig. 2.5 shows the worldwide in situ rock stress data compiled by Hoek and Brown (1980a). All the data can be enveloped by two formulae:

$$\frac{100}{z} + 0.3 < k < \frac{1500}{z} + 0.5 \tag{2.3}$$

Some other variation forms of k with depth are listed in Table 2.4.

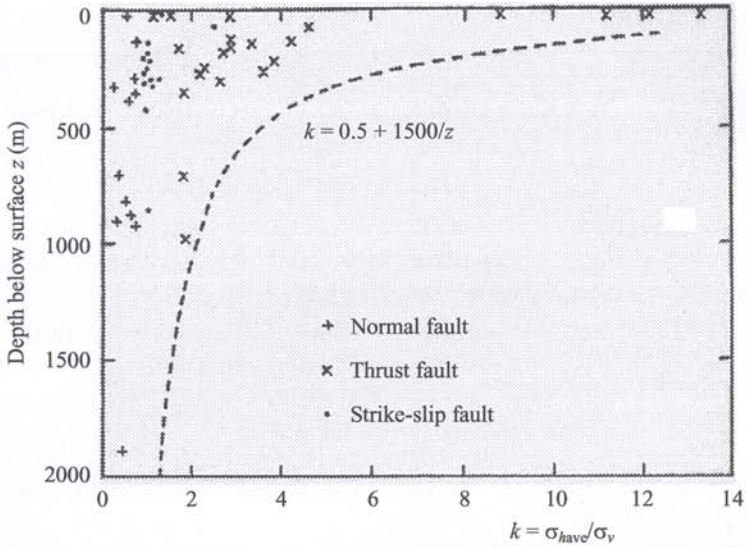


Fig. 2.4 Variation of average horizontal stress to vertical stress ratio versus depth with interpretation of faulting conditions (after Jamison & Cook, 1979).

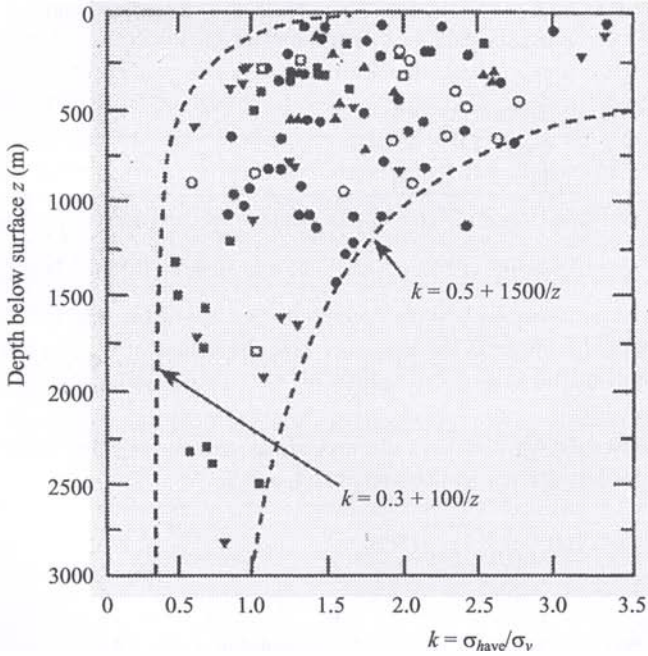


Fig. 2.5 Worldwide in situ rock stress data: Average horizontal stress to vertical stress ratio versus depth (after Hoek & Brown, 1980a).

Terzaghi and Richart (1952) suggested that, for a gravitationally loaded rock mass in which no lateral strain was permitted during formation of the overlying strata, the value of k is independent of depth and is given by

$$k = \frac{\nu}{1 - \nu} \quad (2.4)$$

where ν is the Poisson's ratio of the rock mass. For typical values of $\nu = 0.1 - 0.4$ for rock masses, equation (2.4) gives $k = 0.11 - 0.67$. Since the envelope formulae (2.3) tend towards $0.3 < k < 0.5$ as depth increases, equation (2.4) may provide a rough estimate of k at significant depths.

Sheorey (1994) developed an elasto-static thermal stress model of the earth. This model considers curvature of the crust and variation of elastic constants, density and thermal expansion coefficients through the crust and mantle. Sheorey (1994) presented the following simplified equation which can be used for estimating the average horizontal stress

$$\sigma_{have} = \frac{\nu}{1 - \nu} \gamma z + \frac{\beta E_h G}{1 - \nu} (z + 1000) \quad (2.5)$$

where ν is the Poisson's ratio of the rock; γ is the unit weight of the rock, in N/m^3 ; z is the depth below surface, in m; E_h is the average deformation modulus of the rock measured in the horizontal direction, in Pa; β is the coefficient of linear thermal expansion of the rock, in $1/^\circ\text{C}$; and G is the geothermal gradient of the rock, in $^\circ\text{C/m}$.

Table 2.5 lists the coefficient of linear thermal expansion of different rocks compiled by Sheorey et al. (2001). From this table, $\beta = 8 \times 10^{-6}/^\circ\text{C}$ can be chosen as a reasonable representative value for different rocks except for coal. The thermal gradient for crustal rocks can be taken as 0.024°C/m . Assuming the vertical stress $\sigma_v = \gamma z$ and taking the representative values of $\nu = 0.25$ and $\gamma = 2.7 \times 10^3 \text{ N/m}^3$, the average horizontal to vertical stress ratio k can be derived from equation (2.5) as

Table 2.5 Coefficient of linear thermal expansion β of some rocks (after Sheorey et al., 2001).

Rock	β ($\times 10^{-6}/^\circ\text{C}$)
Granite	6-9
Limestone	3.7-10.3
Marble	3-15
Sandstone	5-12
Schist	6-12
Dolomite	8.1
Conglomerate	9.1
Breccia	4.1-9.1
Coal	30

$$k = 0.33 + 9.5E_h \left(0.001 + \frac{1}{z} \right) \quad (2.6)$$

where E_h is in the unit of GPa.

A plot of equation (2.6) is given in Fig. 2.6 for a range of deformation moduli. The curves relating k with depth below surface z are similar to those based on in situ stress data shown in Fig. 2.5. Hence equation (2.6) provides a reasonable basis for estimating the value of k .

The average horizontal stress to vertical stress ratio k is, in general, greater than 1. High horizontal stresses are caused by different factors, including erosion, tectonics, rock anisotropy and rock discontinuities (Amadei & Stephansson, 1997; Hudson & Harrison, 1997). For detailed description of these factors, the reader can refer to the two references.

2.4 WORLD STRESS MAP

The World Stress Map (WSM) is a global database of contemporary tectonic stress of the Earth's crust. It was originally compiled by a research group headed by Mary Lou Zoback as part of the International Lithosphere Program. Since 1995, the WSM Project has been a research project of the Heidelberg Academy of Sciences and Humanities. (Reinecker et al., 2004).

Fig. 2.7 shows the 2004 version of the world stress map displaying the orientations of the maximum horizontal stress. The following four categories of stress indicators are used for determining the tectonic stress orientation (Reinecker et al., 2004):

- earthquake focal mechanisms
- well bore breakouts and drilling induced fractures
- in-situ stress measurements (overcoring, hydraulic fracturing, borehole slotter)
- young geologic data (from fault slip analysis and volcanic vent alignments)

The length of the stress symbols represents the data quality, with A as the best quality category. A-quality data are believed to record the orientation of the horizontal tectonic stress field to within $\pm 10^\circ$ - 15° , B-quality data to within $\pm 15^\circ$ - 20° and C-quality data to within $\pm 25^\circ$. D-quality data are considered to yield questionable tectonic stress orientations (Zoback, 1992; Sperner et al., 2003). The tectonic regimes are: NF for normal faulting, SS for strike-slip faulting, TF for thrust faulting and U for an unknown regime.

Stress maps of major continents and different countries are also available in Reinecker et al. (2004). These maps can be used for a first estimate of the orientations of the maximum horizontal stress.

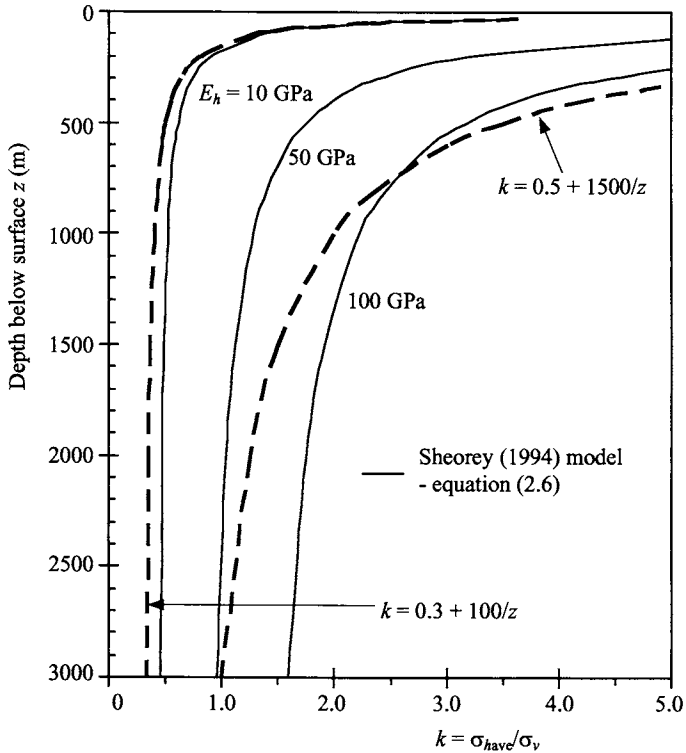


Fig. 2.6 Average horizontal stress to vertical stress ratio versus depth for different deformation moduli based on Sheorey (1994) model.

2.5 COMMENTS

The stress versus depth relationships and the world stress maps presented in the above two sections can be useful in estimating the in situ rock stresses. However, these relationships and maps should be used with caution and considering the important issues presented in the following.

The assumption that the principal stresses are vertical and horizontal with depth breaks down when the ground surface is not horizontal (Amadei & Stephansson, 1997). This can be clearly seen from Fig. 2.8 which shows a semi-infinite isotropic, homogeneous rock mass with a complex topography consisting of a series of hills and valleys and no surface loads. The rock mass is under gravity alone with no lateral displacements. Because of the traction-free boundary conditions, the principal stresses are parallel and normal to the ground surface. As depth increases, the principal stresses approach the same directions as when the ground surface is horizontal.

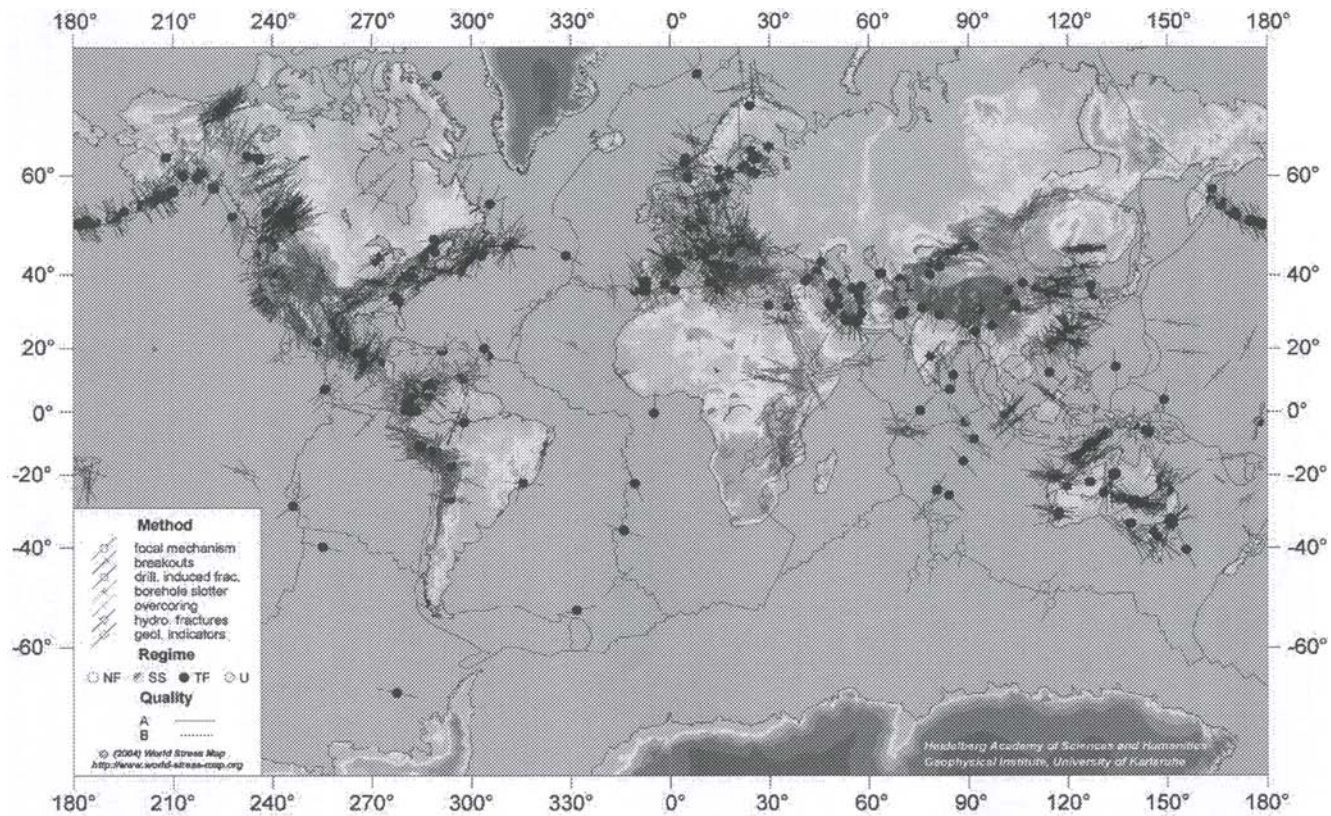


Fig. 2.7 World stress map displaying the orientations of the maximum horizontal stress (after Reinecker et al., 2004).

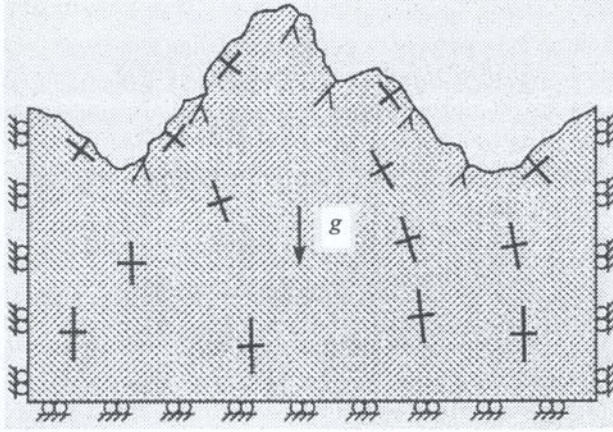


Fig. 2.8 Direction of principal stresses in a rock mass with a complex topography consisting of a series of hills and valleys (after Amadei & Stephansson, 1997).

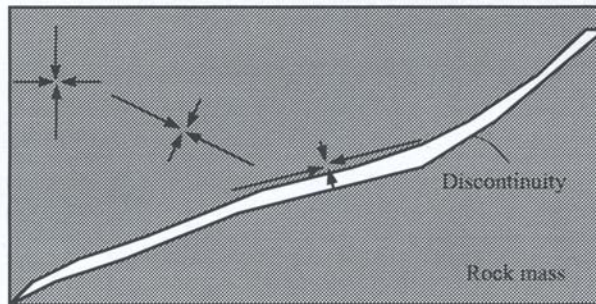


Fig. 2.9 An open discontinuity changes the stress field and causes the principal stresses to be locally parallel and perpendicular to the discontinuity plane (after Hudson et al., 2003).

Open discontinuities in the rock mass also change the directions and magnitudes of the principal stresses (see Fig. 2.9). Since no normal or shear stress can be sustained respectively perpendicular and parallel to the discontinuity surface, the discontinuity surface becomes a principal stress plane with zero principal stress value (Hudson et al., 2003).

The ordering of in situ stresses may change with depth. The hydraulic fracturing tests conducted by Haimson (1977) in an oil well near the center of the Michigan Basin revealed a change of the in situ stress ordering: $\sigma_{hmax} > \sigma_{hmin} > \sigma_v$ from 0 to 200 m, $\sigma_{hmax} > \sigma_v > \sigma_{hmin}$ from 200 to 4500 m, and $\sigma_v > \sigma_{hmax} > \sigma_{hmin}$ at depths larger than 4500

m. Dey and Brown (1986), Adams and Bell (1991) and Plumb (1994) also reported measurements showing the change of in situ stress ordering with depth.

The orientation of in situ stresses may also change with depth. Haimson and Rummel (1982) reported the variations in the orientation of the maximum horizontal stress of 60° over a distance of 500 m. Stephansson (1993) and Martin and Chandler (1993) also reported measurements showing the change of in situ stress orientations with depth.

3

Intact rock

3.1 INTRODUCTION

Intact rock refers to the unfractured blocks between discontinuities in a typical rock mass. These blocks may range from a few millimeters to several meters in size (Hock, 1994). The properties of intact rock are governed by the physical properties of the materials of which it is composed and the manner in which they are bonded to each other. The parameters which may be used in a description of intact rock include petrological name, color, texture, grain size, minor lithological characteristics, density, porosity, strength, hardness and deformability.

This chapter describes the classification of intact rocks and presents the typical values of and correlations between different index properties of them.

3.2 CLASSIFICATION OF INTACT ROCKS

Intact rocks may be classified from a geological or an engineering point of view. In the first case the mineral content of the rock is of prime importance, as is its texture and any change which has occurred since its formation. Although geological classifications of intact rocks usually have a genetic basis, they may provide little information relating to the engineering behavior of the rocks concerned since intact rocks of the same geological category may show a large scatter in strength and deformability, say of the order of 10 times. Therefore, engineering classifications of intact rocks are more related to the engineering properties of rocks.

3.2.1 *Geological classification*

(a) **Rock-forming minerals**

Rocks are composed of minerals, which are formed by the combination of naturally occurring elements. Although there are hundreds of recognized minerals, only a few are common. Table 3.1 summarizes the common rock-forming minerals and their properties. Moh's scale, used in the table, is a standard of ten minerals by which the hardness of a mineral may be determined. Hardness is defined as the ability of a mineral to scratch another. The scale is one for the softest mineral (talc) and ten for the hardest (diamond).

Table 3.1 Common rock-forming minerals and their properties.

Mineral	Hardness (Moh's scale, 1-10)	Relative Density	Fracture	Structure
Orthoclase feldspar	6	2.6	Good cleavage at right angles	Monoclinic. Commonly occurs as crystals
Plagioclase feldspar	6	2.7	Cleavage nearly at right angles – very marked	Triclinic. Showing distinct cleavage lamellae
Quartz	7	2.65	No cleavage; Choncooidal fracture	hexagonal
Muscovite	2.5	2.8	Perfect single cleavage into thin easily separated plates	Monoclinic. Exhibiting strong cleavage lamellae
Biotite	3	3	Perfect single cleavage into thin easily separated plates	Monoclinic. Exhibiting strong cleavage lamellae
Hornblende	5-6	3.05	Good cleavage at 120°	Hexagonal – normally in elongated prisms
Augite	5-6	3.05	Cleavage nearly at right angles	Monoclinic
Olivine	6-7	3.5	No cleavage	No distinctive structure
Calcite	3	2.7	Three perfect cleavages. Rhomboids formed	Hexagonal
Dolomite	4	2.8	Three perfect cleavages	Hexagonal
Kaolinite	1	2.6	No cleavage	No distinctive structure (altered feldspar)
Hematite	6	5	No cleavage	Hexagonal

(b) Elementary rock classification

Intact rocks are classified into three main groups according to the process by which they are formed: igneous, metamorphic and sedimentary.

Igneous rocks are formed by crystallization of molten magma. The mode of crystallization of the magma, at depth in the Earth's crust or by extrusion, and the rate of cooling affect the rock texture or crystal size. The igneous rocks are subdivided into plutonic, hypabyssal and extrusive (volcanic), according to their texture. They are further subdivided into acid, intermediate, basic and ultrabasic, according to their silica content. Table 3.2 shows a schematic classification of igneous rocks.

Metamorphic rocks are the result of metamorphism. Metamorphism is the solid-state conversion of pre-existing rocks by temperature, pressure and/or chemical changes. The great varieties of metamorphic rocks are characterized, classified and

Table 3.2 Geological classification of igneous rocks.

	Type			
	Acid > 65% silica	Intermediate 55–65% silica	Basic 45–55% silica	Ultrabasic < 45% silica
Plutonic	Granite Granodiorite	Diorite	Gabbro	Picrite Peridotite Serpentinite Dunite
Hypabyssal	Quartz Orthoclase porphyries	Plagioclase porphyries	Dolerite	Basic dolerites
Extrusive	Rhyolite Dacite	Pichstone Andesite	Basalt	Basic olivine basalts
Major mineral constituents	Quartz, orthoclase, sodium-plagioclase, muscovite, biotite, hornblende	Quartz, orthoclase, plagioclase, biotite, hornblende, augite	Calcium- plagioclase, augite, olivine, hornblende	Calcium- plagioclase, olivine, augite

Table 3.3 Classification of metamorphic rocks.

Classification	Rock	Description	Major mineral constituents
Massive	Hornfels	Micro-fine grained	Quartz
	Quartzite	Fined grained	Quartz
	Marble	Fine – coarse grained	Calcite or dolomite
Foliated	Slate	Micro-fine grained, laminated	Kaolinite, mica
	Phyllite	Soft, laminated	Mica, kaolinite
	Schist	Altered hypabyssal rocks, coarse grained	Feldspar, quartz, mica
	Gneiss	Altered granite	Hornblende

named according to their mineral assemblages and textures. Table 3.3 shows a classification of the metamorphic rocks according to their physical structure, i.e., massive or foliated.

Sedimentary rocks are formed from the consolidation of sediments. Sedimentary rocks cover three-quarters of the continental areas and most of the sea floor. In the process of erosion, rocks weather and are broken down into small particles or totally dissolved. These detritic particles may be carried away by water, wind or glaciers, and deposited far from their original position. When these sediments start to form thick deposits, they consolidate under their own weight and eventually turn into solid rock

Table 3.4 Classification of sedimentary rocks.

Method of formation	Classification	Rock	Description	Major mineral constituents
Mechanical	Rudaceous	Breccia	Large grains in clay matrix	Various
		Conglomerate		
	Arenaceous	Sandstone	Medium, round grains in calcite matrix	Quartz, calcite (sometimes feldspar, mica)
		Quartzite	Medium, round grains in silica matrix	Quartz
		Gritstone	Medium, angular grains in matrix	Quartz, calcite, various
		Breccia	Coarse, angular grains in matrix	Quartz, calcite, various
	Argillaceous	Claystone	Micro-fine-grained plastic texture	Kaolinite, quartz, mica
Shale		Harder-laminated	Kaolinite, quartz, mica	
Mudstone		compacted clay		
Organic	Calcareous	Limestone	Fossiliferous, coarse or fine grained	Calcite
	Carbonaceous (siliceous, ferruginous, phosphatic)	Coal		
Chemical	Ferruginous	Ironstone	Impregnated limestone or claystone (or precipitated)	Calcite, iron oxide
	Calcareous (siliceous, saline)	Dolomite limestone	Precipitated or replaced limestone, fine grained	Dolomite, calcite

through chemical or biochemical precipitation or organic process. As a result of this process, sedimentary rocks almost invariably possess a distinct stratified, or bedded, structure. Table 3.4 shows the classification of sedimentary rocks according to their formation process.

3.2.2 *Engineering classification*

The engineering classification of intact rocks is based on strength and/or deformation properties of the rock. Table 3.5 shows the classification system of the International Society of Rock Mechanics (ISRM, 1978c). The ISRM classification is also recommended in the *Canadian Foundation Engineering Manual* (CGS, 1985). In this classification, the rock may range from extremely weak to extremely strong depending on the unconfined compressive strength or the approximate field identification.

Table 3.5 Engineering classification of rock by strength (after ISRM, 1978c; CGS, 1985; Marinos & Hoek, 2001).

Grade	Classification	Field identification	Unconfined compressive strength (MPa)	Point Load Index (MPa)	Examples
R0	Extremely weak	Indented by thumbnail	< 1	- ¹⁾	Stiff fault gouge
R1	Very weak	Crumbles under firm blows of geological hammer; can be peeled with a pocket knife	1-5	- ¹⁾	Highly weathered or altered rock, shale
R2	Weak	Can be peeled with a pocket knife with difficulty; shallow indentations made by a firm blow with point of geological hammer	5-25	- ¹⁾	Chalk, claystone, potash, marl, siltstone, shale, rock salt
R3	Medium strong	Cannot be scraped or peeled with a pocket knife; specimen can be fractured with a single firm blow of geological hammer	25-50	1-2	Concrete, phyllite, schist, siltstone
R4	Strong	Specimen requires more than one blow of geological hammer to fracture	50-100	2-4	Limestone, marble, sandstone, schist
R5	Very strong	Specimen requires many blows of geological hammer to fracture	100-250	4-10	Amphibolite, sandstone, basalt, gabbro, gneiss, granodiorite, peridotite, rhyolite, tuff
R6	Extremely strong	Specimen can only be chipped with the geological hammer	> 250	> 10	Fresh basalt, chert, diabase, gneiss, granite, quartzite

1) Point load tests on rocks with unconfined compressive strength below 25 MPa are likely to yield highly ambiguous results.

Based on laboratory measurements of strength and deformation properties of rocks, Deere and Miller (1966) established a classification system based on the ultimate strength (unconfined compressive strength) and the tangent modulus E_t of elasticity at

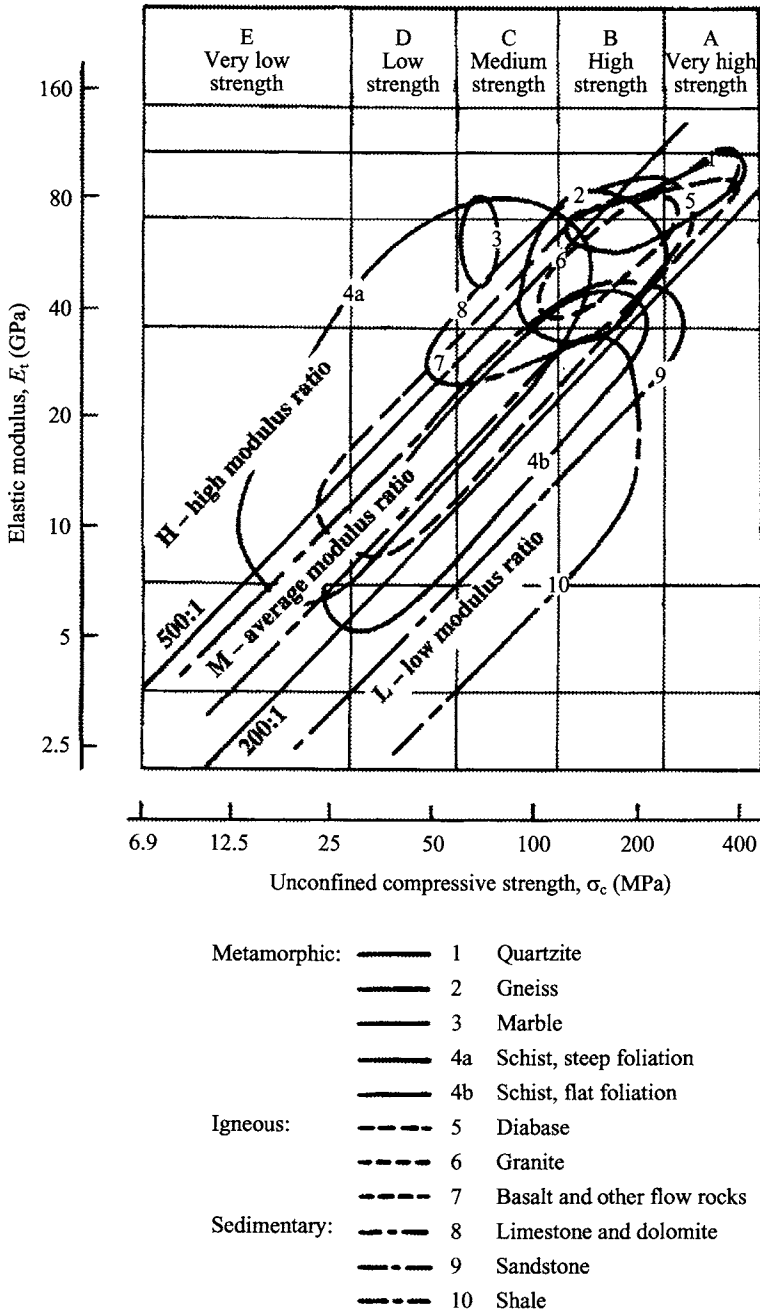


Fig. 3.1 Engineering classification of intact rocks (E_t is the tangent modulus at 50% ultimate strength) (after Deere & Miller, 1966).

50% of the ultimate strength. Fig. 3.1 summarizes the engineering classification of igneous, sedimentary and metamorphic rocks, respectively, as given in Deere and Miller (1966). The modulus ratio in these figures is that of the elastic modulus to the unconfined compressive strength. A rock may be classified as AM, BH, BL, etc. Voight (1968), however, argued that the elastic properties of intact rock could be omitted from practical classification since the elastic moduli as determined in the laboratory are seldom those required for engineering analysis.

3.3 INDEX PROPERTIES OF INTACT ROCKS

This section describes different index properties of intact rocks, lists their typical values, and presents the correlations between them. The index properties can help describe rocks quantitatively and can be used for estimating mechanical and hydraulic properties of rocks, as described in later chapters. It need be noted, however, that determination of index properties is not a substitute of detailed characterization of rocks.

3.3.1 Porosity

The porosity, n , is defined as the ratio of void or pore volume, V_v , to the total volume, V , of the rock,

$$n = \frac{V_v}{V} = \frac{V - V_s}{V} \quad (3.1)$$

where V_s is the volume of the grains or solid matrix substance. Porosity is dimensionless and given as a percentage or as a decimal fraction. The porosity of rocks can be determined using the method suggested by ISRM (1979c). Table 3.6 lists the typical values of porosity of different intact rocks.

Porosity is the result of various geological, physical and chemical processes and varies significantly for different rock types. Porosity changes significantly even for the same rock type due to different factors such as grain size distribution, grain shape, and depth and pressure. Fig. 3.2 shows the variation of porosity n with mean grain diameter d_{50} for Bentheim Sandstone (Schön, 1996).

Porosity generally decreases with increasing depth or pressure. Their relationship can be expressed by an exponential function or a logarithmic function (Schön, 1996)

$$n = n_0 e^{-Az} \quad (3.2)$$

$$n = n_0 - B \log z \quad (3.3)$$

where n_0 is the initial porosity at depth $z = 0$; and A and B are empirical factors

Table 3.6 Typical values of porosity of intact rocks (after Goodman, 1989).

Rock type	Age	Depth	Porosity (%)
Mount Simon sandstone	Cambrian	13,000 ft	0.7
Nugget sandstone (Utah)	Jurassic		1.9
Potsdam sandstone	Cambrian	Surface	11.0
Pottsville sandstone	Pennsylvanian		2.9
Berea sandstone	Mississippian	0-2,000 ft	14.0
Keuper sandstone (England)	Triassic	Surface	22.0
Navajo sandstone	Jurassic	Surface	15.5
Sandstone, Montana	Cretaceous	Surface	34.0
Beekmantown dolomite	Ordovician	10,500 ft	0.4
Black River limestone	Ordovician	Surface	0.46
Niagara dolomite	Silurian	Surface	2.9
Limestone, Great Britain	Carboniferous	Surface	5.7
Chalk, Great Britain	Cretaceous	Surface	28.8
Solenhofen limestone		Surface	4.8
Salem limestone	Mississippian	Surface	13.2
Bedford limestone	Mississippian	Surface	12.0
Bermuda limestone	Recent	Surface	43.0
Shale	Pre-Cambrian	Surface	1.6
Shale, Oklahoma	Pennsylvanian	1,000 ft	17.0
Shale, Oklahoma	Pennsylvanian	3,000 ft	7.0
Shale, Oklahoma	Pennsylvanian	5,000 ft	4.0
Shale	Cretaceous	600 ft	33.5
Shale	Cretaceous	2,500 ft	25.4
Shale	Cretaceous	3,500 ft	21.1
Shale	Cretaceous	6,100 ft	7.6
Mudstone, Japan	Upper Tertiary	Near surface	22-32
Granite, fresh		Surface	0-1
Granite, weathered			1-5
Decomposed granite (Saprolite)			20.0
Marble			0.3
Marble			1.1
Bedded tuff			40.0
Welded tuff			14.0
Cedar City tonalite			7.0
Frederick diabase			0.1
San Marcos gabbro			0.2

depending on the compressibility of rocks. Jelic (1984) derived the following relationship for sandstones with an initial porosity of $n_0 = 0.496$

$$n = 0.496e^{-0.556z} \quad (3.4)$$

in which z is given in km.

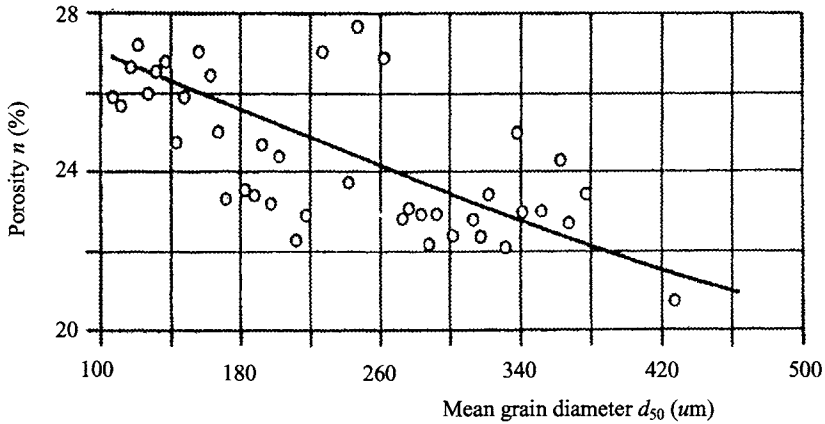


Fig. 3.2 Porosity n versus mean grain diameter d_{50} for Bentheim Sandstone (from Schön, 1996).

3.3.2 Density

The density is defined the mass per unit volume of a material. Since a rock contains both grains (solid matrix material) and voids, it is necessary to distinguish between different densities which are related to different parts or components of the rock, as defined in Table 3.7. The density of rocks can be determined using the method suggested by ISRM (1979c).

The density of rocks depends on the mineral composition, the porosity and the filling material in the voids. Table 3.8 lists the typical values of density for different intact rocks.

Table 3.7 Definition of various density terms (after Stacey et al., 1987).

Term	Definition	Remarks
Density (or bulk density)	$\rho = \frac{m}{V}$	Mass determined at natural water content
Dry density	$\rho_d = \frac{m_s}{V}$	Mass refers to solids only. All moistures dried out of the voids.
Saturated density	$\rho_{\text{sat}} = \frac{m_{\text{sat}}}{V}$	Mass refers to solids plus water which fills completely the voids.
Grain density (or solid density)	$\rho_s = \frac{m_s}{V_s}$	Both mass and volume refer to the grains (solids) only.

Notes: $m = m_s + m_w$ and $V = V_s + V_v$ in which m is the bulk sample mass, m_s is the mass of the grains (solids), m_w is the mass of water in the voids, V is the bulk sample volume, V_s is the volume of the grains (solids), and V_v is the volume of the voids.

Table 3.8 Typical values of density of intact rocks (after Lama & Vutukuri, 1978).

Rock type	Range of density (kg/m ³)	Mean density (kg/m ³)
<i>Igneous rocks</i>		
Granite	2516 – 2809	2667
Granodiorite	2668 – 2785	2716
Syenite	2630 – 2899	2757
Quartz diorite	2680 – 2960	2806
Diorite	2721 – 2960	2839
Norite	2720 – 3020	2984
Gabbro	2850 – 3120	2976
Diabase	2804 – 3110	2965
Peridotite	3152 – 3276	3234
Dunite	3204 – 3314	3277
Pyroxenite	3100 – 3318	3231
Anorthosite	2640 – 2920	2734
<i>Sedimentary rocks</i>		
Sandstone	2170 – 2700	–
Limestone	2370 – 2750	–
Dolomite	2750 – 2800	–
Chalk	2230	–
Marble	2750	–
Shale	2060 – 2660	–
Sand	1920 - 1930	–
<i>Metamorphic rocks</i>		
Gneiss	2590 – 3060	2703
Schist	2700 – 3030	2790
Slate	2720 – 2840	2810
Amphibolite	2790 – 3140	2990
Granulite	2630 – 3100	2830
Eclogite	3338 – 3452	3392

Note: The values listed in the table are for the bulk density determined at natural water content.

Since, as described earlier, the porosity decreases with increasing depth, the density of rocks increases with depth (see Fig. 3.3). Polak and Rapoport (1961) published the following simple relationship between depth and density

$$\rho = \rho_{z_0} + A \log \left(\frac{z}{z_0} \right) \quad (3.5)$$

where z is the depth; ρ_{z_0} is the density of the rock at depth z_0 ; and A is an empirical factor related to the compressibility of the rock.

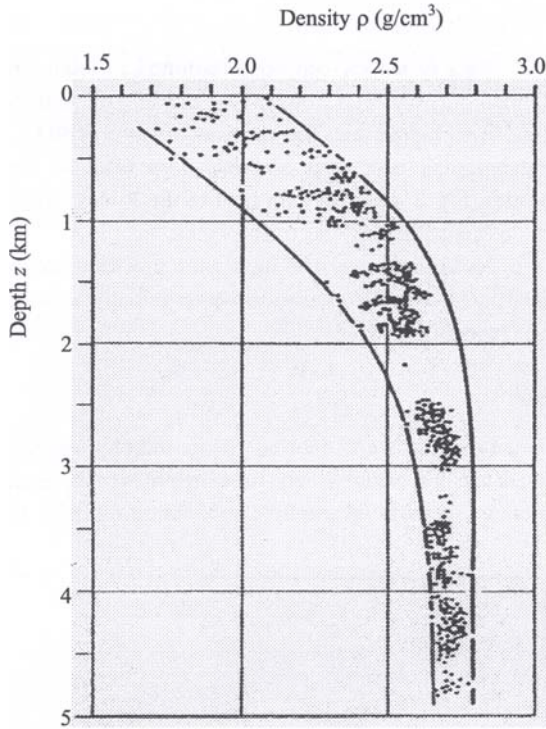


Fig. 3.3 Density ρ versus depth z for sedimentary rocks at the North German-Polish Basin (from Schön, 1996).

Stegena (1964) recommended the following relationship between depth and density

$$\begin{aligned}\rho &= \rho_{z_0} + (\rho_{z_m} - \rho_{z_0})(1 - e^{-Bz}) \\ &= \rho_{z_m} - (\rho_{z_m} - \rho_{z_0})e^{-Bz}\end{aligned}\quad (3.6)$$

where z is the depth; ρ_{z_0} is the density of the rock at depth z_0 ; ρ_{z_m} is the density of the rock at maximum depth z_m ; and B is an empirical factor related to the compressibility of the rock. This relation has an asymptotic value ρ_{z_m} when z reaches infinity. Jelic (1984) derived the following relationship for sandstones and siltstones

$$\rho = 2.72 - 1.244e^{-0.846z}\quad (3.7)$$

in which ρ is in g/cm^3 and z is given in km.

3.3.3 Wave velocity

The velocity of elastic waves in a rock can be determined in laboratory rock testing using one of the three methods: the high frequency ultrasonic pulse technique, the low frequency ultrasonic pulse technique and the resonant method (ISRM, 1978a). Wave velocity is closely related rock properties and has been used as one of the most important index properties. Fig. 3.4 shows the range of the P-wave velocity and the S-wave velocity for some of the commonly occurring rocks.

The wave velocity of rocks increases with increasing pressure due to the closing of voids or microcracks. The effect of pressure on wave velocity is smaller for denser rocks due to their lower reduction of voids.

3.3.4 Point load index

The point load index has often been reported as an indirect measure of the rock strength. The point load test has been widely used in practice because of its testing ease, simplicity of specimen preparation and field applications (ISRM, 1985).

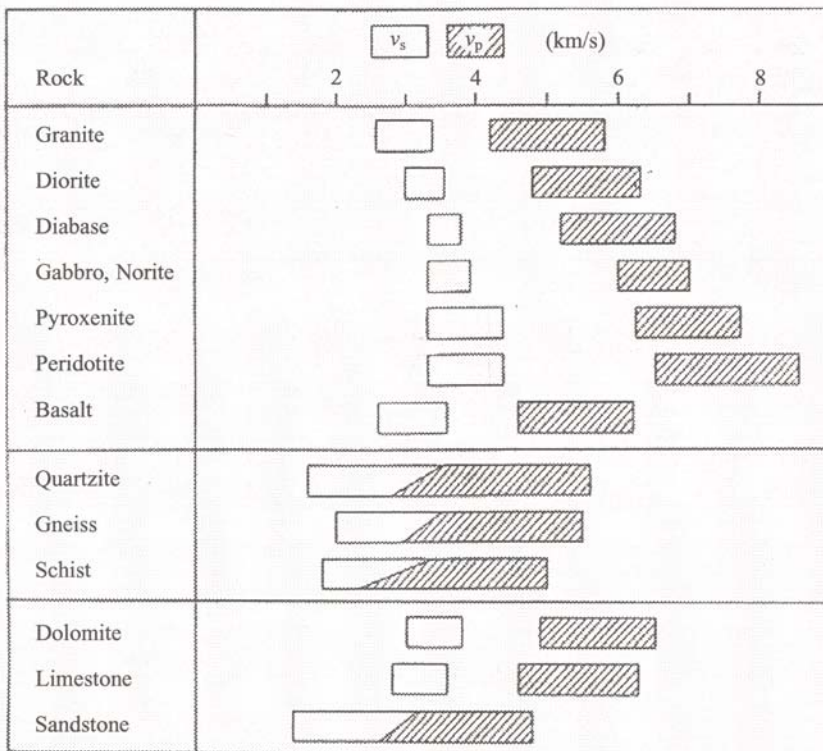


Fig. 3.4 Range of P-wave velocity v_p and S-wave velocity v_s of different rocks (from Schön, 1996).

For a point load test, a compressive load is applied through two conical platens, which causes the rock to break in tension between these two points. If the breaking load is P , the point load index, I_s , can then be determined by

$$I_s = \frac{P}{D^2} \quad (3.8)$$

where D is the diameter of the specimen if the load is applied in the diametric direction of a core. In other cases, $D = 2\sqrt{A/\pi}$, where A is the minimum cross-sectional area of the specimen for a plane through the platen contact points.

The size of the specimen affects the value of I_s which increases as D increases. To consider the size effect, it has been common to convert the measured I_s to that corresponding to $D = 50$ mm:

$$I_{s(50)} = I_s k_{\text{PLT}} \quad (3.9)$$

where k_{PLT} is the size correction factor, which can be determined by

$$k_{\text{PLT}} = \left(\frac{D}{50}\right)^{0.45} \quad (3.10)$$

One of the columns in Table 3.5 lists the typical range of the point load index for different rocks.

3.3.5 Schmidt hammer rebound number

The Schmidt rebound hammer has been used for testing the quality of concretes and rocks. Schmidt hammers are designed in different levels of impact energy, but the types of L and N are commonly adopted for rock property determinations. The L-type has an impact energy of 0.735 Nm which is only one third that of the N-type. ISRM (1978b) presented the detailed test procedure. Ayday and Göktan (1992) developed the following empirical correlation between L and N-type Schmidt hammer rebound numbers for the ISRM (1978b) test procedure

$$R_{n(N)} = 7.124 + 1.249R_{n(L)} \quad (r^2 = 0.882) \quad (3.11)$$

where $R_{n(L)}$ and $R_{n(N)}$ are, respectively, the L and N-type Schmidt hammer rebound numbers; and r^2 is the determination coefficient.

Table 3.9 lists the typical L-type Schmidt hammer rebound numbers $R_{n(L)}$ for some of the commonly occurring rocks.

Table 3.9 Typical L-type Schmidt hammer rebound numbers $R_{n(L)}$ for different rocks.

Rock	$R_{n(L)}$	Reference
Andesite	28-52	Dincer et al. (2004); Ayday & Goktan (1992)
Basalt	35-58	Stacey et al. (1987); Dincer et al. (2004)
Chalk	10-29	Bell et al. (1999)
Diabase	36-59	Stacey et al. (1987); Ayday & Goktan (1992)
Dolomite	40-60	Stacey et al. (1987); Sachpazis (1990)
Gabbro	49	Xu et al. (1990)
Gneiss	48	Stacey et al. (1987)
Granite	45-56	Stacey et al. (1987); Ayday & Goktan (1992)
gypsum	30-44	Yilmaz & Sendir (2002)
Limestone	16-59	Stacey et al. (1987)
Marble	31-47	Stacey et al. (1987); Ayday & Goktan (1992)
Marl	18-39	Ayday & Goktan (1992)
Mudstone	15	Xu et al. (1990)
Peridotite	45	Ayday & Goktan (1992)
Prasinite	41	Xu et al. (1990)
Quartzite	39	Stacey et al. (1987)
Rock salt	23	Stacey et al. (1987)
Sandstone	30-47	Stacey et al. (1987)
Schist	29-41	Stacey et al. (1987); Xu et al. (1990)
Serpentinite	45	Xu et al. (1990)
Siltstone	47	Stacey et al. (1987)
Tuff	13-40	Stacey et al. (1987); Ayday & Goktan (1992); Dincer et al. (2004)

3.3.6 *Slake durability index*

The slake durability index is used to describe the resistance of a rock material against breakdown or weathering with time. ISRM (1979c) proposed the test procedure for determining the slake durability index. Gamble (1971) tested representative shales and claystones and found the slake durability index to vary over the whole range from 0 to 100%. Based on his test results, Gamble proposed a classification of slake durability as shown in Table 3.10.

3.3.7 *Correlations between different index properties*

Index properties of rocks are closely related to each other and this section presents the correlations between some of them.

(a) **Density and porosity**

Density is closely related to porosity and their relationship can be expressed by the general function

Table 3.10 Slake durability classification (Gamble, 1971).

Group name	% retained after one 10-minute cycle (dry weight basis)	% retained after two 10-minute cycle (dry weight basis)
Very high durability	> 99	> 98
High durability	98-99	95-98
Medium high durability	95-98	85-95
Medium durability	85-95	60-85
Low durability	60-85	30-60
Very low durability	< 60	< 30

$$\rho = (1 - n)\rho_s + n[S_f\rho_f + (1 - S_f)\rho_g] \quad (3.12)$$

where ρ_s is the grain (or matrix) density; ρ_f and ρ_g are respectively the density of the fluid and gas in the voids; and S_f is the saturation (or degree of saturation) of the voids which is defined by

$$S_f = \frac{V_f}{V_v} \quad (3.13)$$

where V_f is the volume of the fluid in the voids; and V_v is the total volume of the voids.

For a saturated rock, $S_f = 1$ and equation (3.12) can be rewritten as

$$\rho = \rho_s - n(\rho_s - \rho_f) \quad (3.14)$$

Since the density of the fluid in the voids such as water is smaller than that of the grains, the density of rocks decreases with the porosity.

Tugrul and Zarif (1999) derived the following empirical relation between dry density ρ_d and porosity n for granitic rocks from Turkey

$$\rho_d = 2695 - 25.48n \quad (r^2 = 0.74) \quad (3.15)$$

Tugrul (2004) derived an empirical relation between dry density ρ_d and porosity n for sandstone, limestone, basalt and granodiorite from Turkey

$$\rho_d = 2765 - 33.64n \quad (r^2 = 0.94) \quad (3.16)$$

In both equations (3.15) and (3.16), ρ_d is in the unit of kg/m^3 and n is in %.

(b) P-wave velocity and porosity

The wave velocity of a rock is influenced by the matrix properties, the porosity and the properties of the fluid in the voids. Wyllie et al. (1956) derived the following general relation for saturated porous rock

$$\frac{1}{v_p} = \frac{1-n}{v_{ps}} + \frac{n}{v_{pf}} \quad (3.17)$$

where v_p , v_{ps} and v_{pf} are the P-wave velocity respectively of the rock, the grains and the fluid in the voids.

Raymer et al. (1980) derived the following empirical relation for consolidated rocks

$$v_p = (1-n)^2 v_{ps} + n v_{pf} \quad (3.18)$$

where v_p , v_{ps} and v_{pf} are the same as defined earlier.

Table 3.11 lists some of the empirical correlations between P-wave velocity v_p and porosity n based fitting analyses of test data.

Fig. 3.5 shows the variation of P-wave velocity with porosity for water saturated sandstone from Rotliegendes, Northern Germany.

(c) P-wave velocity and density

The P-wave velocity v_p increases with the density ρ of rocks. Fig. 3.6 shows the variation of v_p with ρ for igneous and metamorphic rocks. Many researchers have developed closed-form empirical correlations between wave velocity and density. Table 3.12 lists some of them.

(d) P-wave velocity and point load index

Fig. 3.7 shows the variation of point load index with the P-wave velocity for fresh and weathered crystalline rocks. In general, the point load index increases as the P-wave velocity increases.

Table 3.11 Empirical correlations between wave velocity v_p and porosity n .

Correlation	Rock Type	Reference
$v_p = 6.32n^{-0.016}$ ($r^2 = 0.76$)	Vesicular basalt	Al-Harhi et al. (1999)
$v_p = 6.52 - 0.36n$ ($r^2 = 0.66$)	Granitic rocks	Turgrul and Zarif (1999)
$v_p = 4.08n^{-0.42}$ ($r^2 = 0.79$)	Granites	Sousa et al. (2005)

Notes: v_p is in the unit of km/s and n is in %; and r^2 is the determination coefficient.

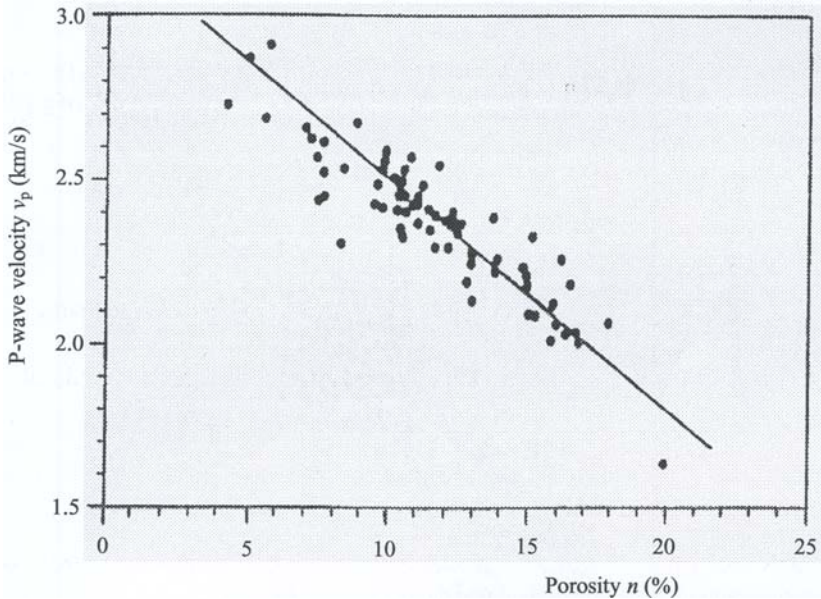


Fig. 3.5 Variation of P-wave velocity with porosity for water saturated sandstone from Rotliegendes, Northern Germany (from Schön, 1996).

Table 3.12 Correlations between P-wave velocity v_p and density ρ .

Correlation	Rock Type	Reference
$v_p = 2.76\rho - 0.98$	Igneous rocks	Birch (1961)
$v_p = 2.33 + 0.08\rho^{3.63}$	Basalts	Christensen & Salisbury (1975)
$v_p = 2.67\rho - 1.08$	Igneous rocks	Volarovich & Bajuk (1977)
$v_p = 3.10\rho - 2.98$	Plutonic rocks: granite, diorite, gabbro	Marle (1978) & Kopf (1977, 1980)
$v_p = 2.30\rho - 0.91$	Volcanic rocks: porphyrite, keratophyrite, diabase, basalt	Marle (1978) & Kopf (1977, 1980)
$v_p = 3.66\rho - 4.46$	Mudstone (Type I)	Gaviglio. (1989)
$v_p = 3.66\rho - 4.80$	Mudstone (Type III)	Gaviglio. (1989)
$v_p = 3.66\rho - 4.87$	Mudstone (Type IV)	Gaviglio. (1989)
$v_p = 3.66\rho - 4.11$	Wackestone (Type V)	Gaviglio. (1989)
$v_p = 2.61\rho - 1.0 \pm 0.4$	Mantle rocks	Henkel et al. (1990)
$v_p = 5.00\rho - 8.65$ ($r^2 = 0.55$)	Crystalline rocks	Starzec (1999)
$v_p = 4.32\rho - 7.51$ ($r^2 = 0.81$)	Carbonate rocks	Yasar & Erdogan (2004b)

Notes: v_p is in the unit of km/s and ρ is in the unit of g/cm^3 ; and r^2 is the determination coefficient.

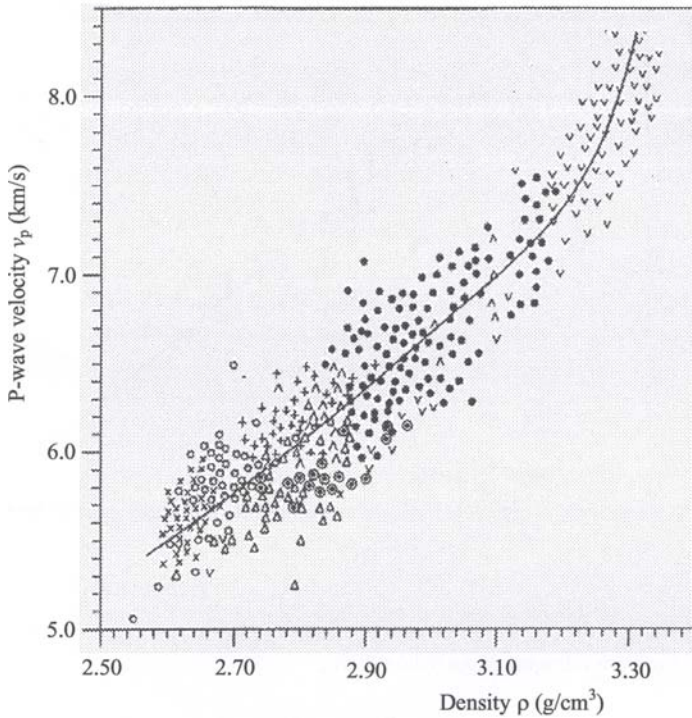


Fig. 3.6 Variation of P-wave velocity v_p with density ρ for igneous and metamorphic rocks (from Schön, 1996).

(e) Point load index and porosity

Fig. 3.8 shows the variation of point load index with porosity for fresh and weathered crystalline rocks. As the porosity increases, the point load index decreases. The relationship between point load index and porosity can be generalized as being negatively exponential (Gupta & Rao, 1998). The following is the empirical correlation between point load index $I_{s(50)}$ and porosity n derived by Palchik and Hatzor (2004) for porous chalks

$$I_{s(50)} = 7.74e^{-0.039n} \quad (r^2 = 0.84) \quad (3.19)$$

where $I_{s(50)}$ is in the unit of MPa and n is in %; and r^2 is the determination coefficient.

(f) Schmidt hammer rebound number and porosity

Schmidt hammer rebound number decreases as porosity increases. Yasar and Erdogan (2004a) derived the following empirical correlation between them based on the test

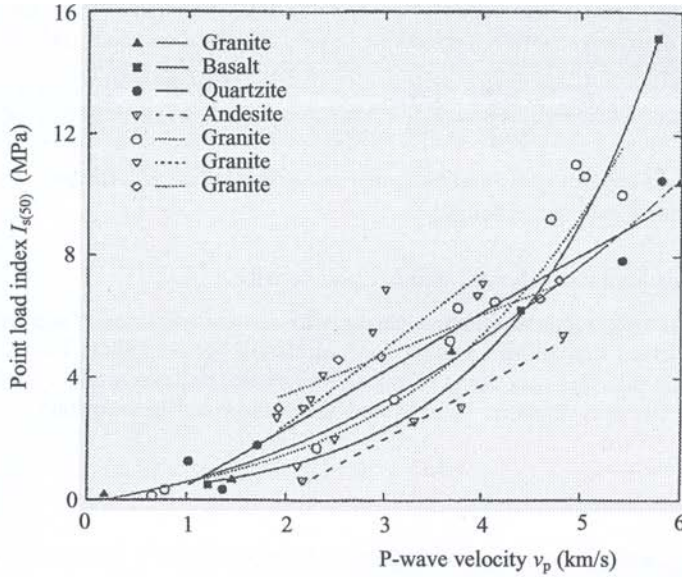


Fig. 3.7 Variation of point load index with P-wave velocity for fresh and weathered crystalline rock (from Gupta & Rao, 1998).

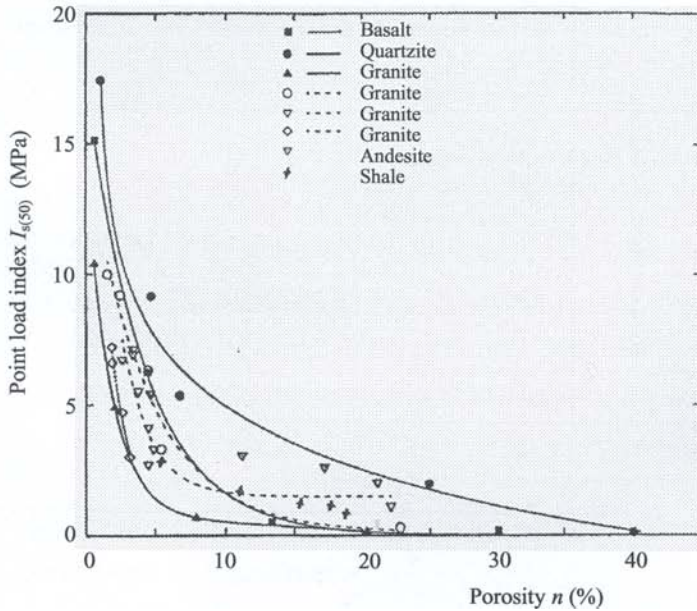


Fig. 3.8 Variation of point load index with porosity for fresh and weathered crystalline rock (from Gupta & Rao, 1998).

results of six different rock types – Ceyhan limestone, Barbaros marble, Antique Cream limestone, Osmaniye marble, Toprakkale Basalts and Handere sandstone

$$R_{n(L)} = 56.08 - 5.00n \quad (r^2 = 0.80) \quad (3.20)$$

where $R_{n(L)}$ is the L-type Schmidt hammer rebound number; n is the porosity in %; and r^2 is the determination coefficient.

(g) Schmidt hammer rebound number and density

Schmidt hammer rebound number increases as density increases. Yasar and Erdogan (2004a) derived the following empirical correlation between them based on the test results of six different rock types – Ceyhan limestone, Barbaros marble, Antique Cream limestone, Osmaniye marble, Toprakkale Basalts and Handere sandstone

$$R_{n(L)} = 3.0e^{1.066\rho} \quad (r^2 = 0.84) \quad (3.21)$$

where $R_{n(L)}$ is the L-type Schmidt hammer rebound number; ρ is the density in g/cm^3 ; and r^2 is the determination coefficient.

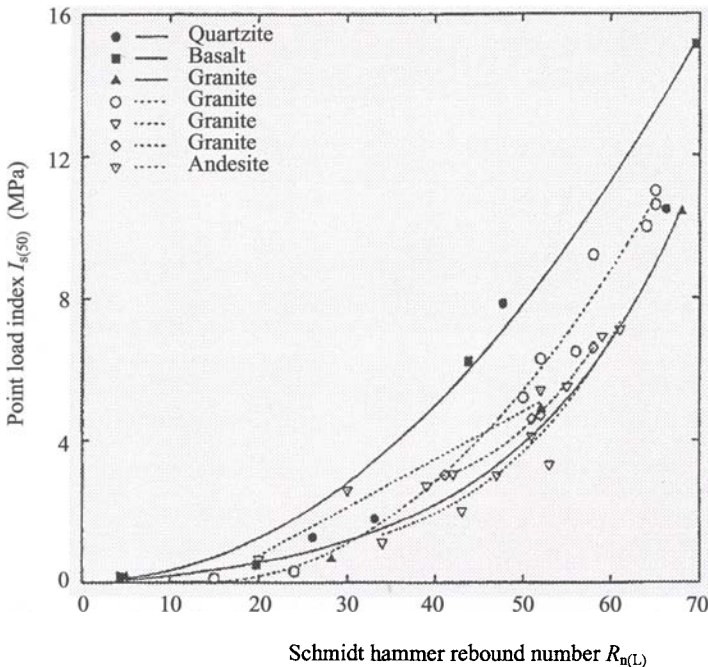


Fig. 3.9 Variation of point load index with Schmidt hammer rebound number for fresh and weathered crystalline rock (from Gupta & Rao, 1998).

(h) P-wave velocity and Schmidt hammer rebound number

Kahraman (2001a) derived the following empirical correlation between P-wave velocity v_p and the N-type Schmidt hammer rebound number $R_{n(N)}$

$$v_p = 0.11R_{n(N)} - 4.41 \quad (r^2 = 0.689) \quad (3.22)$$

where v_p is in the unit of km/s; and r^2 is the determination coefficient.

(g) Point load index and Schmidt hammer rebound number

Fig. 3.9 shows the variation of point load index with the L-type Schmidt hammer rebound number for fresh and weathered crystalline rocks. The point load index increases as the Schmidt hammer rebound number increases.

millimeters in the case of local faults. This fault thickness may contain weak materials such as fault gouge (clay), fault breccia (recemented), rock flour or angular fragments. The wall rock is frequently slickensided and may be coated with minerals such as graphite and chlorite which have low frictional strengths. The ground adjacent to the fault may be disturbed and weakened by associated discontinuities such as drag folds or secondary faults. These factors result in faults being zones of low shear strength on which slip may readily occur.

(b) Bedding planes

Bedding planes divide sedimentary rocks into beds or strata. They represent interruptions in the course of deposition of the rock mass. Bedding planes are generally highly persistent features, although sediments laid down rapidly from heavily laden wind or water currents may contain cross or discordant bedding. Bedding planes may contain parting material of different grain size from the sediments forming the rock mass, or may have been partially healed by low-order metamorphism. In either of these two cases, there would be some 'cohesion' between the beds; otherwise, shear resistance on bedding planes would be purely frictional. Arising from the depositional process, there may be a preferred orientation of particles in the rock, giving rise to planes of weakness parallel to the bedding planes.

(c) Joints

Joints are the most common and generally the most geotechnically significant discontinuities in rocks. Joints are breaks of geological origin along which there has been no visible relative displacement. A group of parallel or sub-parallel joints is called a joint set, and joint sets intersect to form a joint system. Joints may be open, filled or healed. Discontinuities frequently form parallel to bedding planes, foliations or slaty cleavage, and they may be termed bedding joints, foliation joints or cleavage joints. Sedimentary rocks often contain two sets of joints approximately orthogonal to each other and to the bedding planes. These joints sometimes end at bedding planes, but others, called master joints, may cross several bedding planes.

(d) Cleavage

There are two broad types of rock cleavage: fracture cleavage and flow cleavage. Fracture cleavage (also known as false cleavage and strain slip cleavage) is a term describing incipient, cemented or welded parallel discontinuities that are independent of any parallel alignment of minerals. Spencer (1969) lists six possible mechanisms for the formation of fracture cleavage. In each mechanism, lithology and stress conditions are assumed to have produced shearing, extension or compression, giving rise to numerous closely-spaced discontinuities separated by thin slivers of intact rock. Fracture cleavage is generally associated with other structural features such as faults, folds and kink bands. Flow cleavage, which can occur as slaty cleavage or schistosity,

is dependent upon the recrystallization and parallel alignment of platy minerals such as mica, producing inter-leaving or foliation structure. It is generally accepted that flow cleavage is produced by high temperatures and/or pressures associated with metamorphism in fine-grained rocks.

Although cleavage is usually clearly visible in slates, phyllites and schists, most cleavage planes possess significant tensile strength and do not, therefore, contribute to the discontinuity network. Cleavage can, however, create significant anisotropy in the deformability and strength of such rocks. Geological processes, such as folding and faulting, subsequent to the formation of the cleavage can exploit these planes of weakness and generate discontinuities along a proportion of the better developed cleavage planes. The decision as to whether a particular cleavage plane is a discontinuity presents one of the most challenging problems to those undertaking discontinuity surveys in cleaved rocks.

4.3 DESCRIPTION OF DISCONTINUITIES

The ISRM publication *Suggested methods for the quantitative description of discontinuities in rock masses* (ISRM, 1978c) defined ten parameters to describe the characteristics of discontinuities:

1. **Orientation:** The attitude of a discontinuity in space. It is described by the dip direction (azimuth) and dip of the line of steepest declination in the plane of the discontinuity.
2. **Spacing:** The perpendicular distance between adjacent discontinuities. It normally refers to the mean or modal spacing of a set of discontinuities.
3. **Persistence:** The discontinuity trace length as observed in an exposure. It may give a crude measure of the areal extent or penetration length of a discontinuity. Termination in solid rock or against other discontinuities reduces the persistence.
4. **Roughness:** The inherent surface roughness and waviness relative to the mean plane of a discontinuity. Both roughness and waviness contribute to the shear strength. Large scale waviness may also alter the dip locally.
5. **Wall strength:** The equivalent compressive strength of the adjacent rock walls of a discontinuity. It may be lower than rock block strength due to weathering or alteration of the walls. It is an important component of shear strength if rock walls are in contact.
6. **Aperture:** The perpendicular distance between adjacent rock walls of a discontinuity, in which the intervening space is air or water filled.
7. **Filling:** The material that separates the adjacent rock walls of a discontinuity and that is usually weaker than the parent rock. Typical filling materials are sand, silt, clay, breccia, gouge, mylonite. It also includes thin mineral coatings and healed discontinuities such as quartz and calcite veins.

8. **Seepage:** The water flow and free moisture visible in individual discontinuities or in the rock mass as a whole.
9. **Number of Sets:** The number of discontinuity sets comprising the intersecting discontinuity system. The rock mass may be further divided by individual discontinuities.
10. **Block Size:** The rock block dimensions resulting from the mutual orientation of intersecting discontinuity sets, and resulting from the spacing of the individual sets. Individual discontinuities may further influence the block size and shape.

The following sections describe the geometrical properties of discontinuities, including orientation, intensity, spacing, frequency, persistence, shape, size, roughness, aperture, discontinuity sets and block size.

4.4 DISCONTINUITY ORIENTATION

Orientation, or attitude of a discontinuity in space, is described by the dip of the line of maximum declination on the discontinuity surface measured from the horizontal, and the dip direction or azimuth of this line, measured clockwise from true north. Some geologists record the strike of the discontinuity rather than the dip direction. For rock mechanics purposes, it is usual to quote orientation data in the form of dip direction (three digits)/dip (two digits) such as $035^{\circ}/75^{\circ}$ and $290^{\circ}/30^{\circ}$. The orientation of discontinuities relative to an engineering structure largely controls the possibility of unstable conditions or excessive deformations developing. The importance of orientation increases when other conditions for deformation are present, such as low shear strength and a sufficient number of discontinuities for slip to occur. The mutual orientation of discontinuities will determine the shape of the individual blocks, beds or mosaics comprising the rock mass.

The orientation of discontinuities can be measured from cores or from exposures using one or two dimensional scanlines. The measured orientation data can be plotted on stereonets. Fig. 4.1 shows such a plot on a polar stereonet of the poles of 351 individual discontinuities whose orientations were measured at a particular field site (Hoek & Brown, 1980). Different symbols have been used for three different types of discontinuities – bedding planes, joints and a fault. The fault has a dip direction of 307° and a dip of 56° . Contours of pole concentrations may be drawn for the bedding planes and joints to give an indication of the preferred orientations of the various discontinuity sets present. Fig. 4.2 shows the contours of pole concentrations determined from the data shown in Fig. 4.1. The central orientations of the two major joint sets are $347^{\circ}/22^{\circ}$ and $352^{\circ}/83^{\circ}$, and that of the bedding planes is $232^{\circ}/81^{\circ}$.

Computer programs such as the one by Mahtab et al. (1972) are also available for plotting and contouring discontinuity orientation data. For a large number of discontinuities, it will be more convenient to use computer programs to plot and contour orientation data.

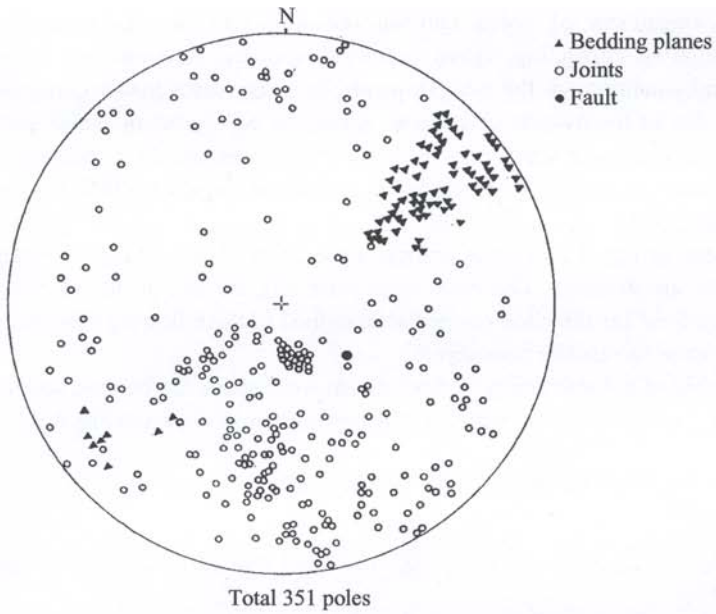


Fig. 4.1 Plot of poles of 351 discontinuities (after Hoek & Brown, 1980a).

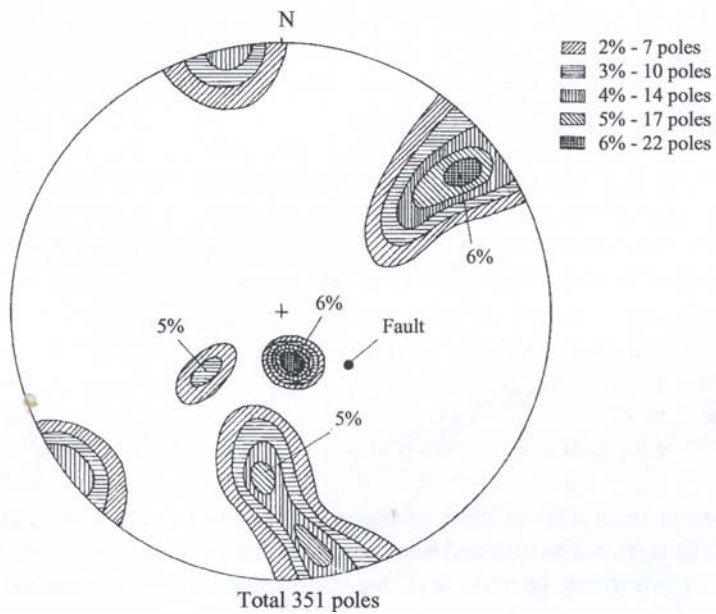


Fig. 4.2 Contours of pole concentrations for the data plotted in Fig. 4.1 (after Hoek & Brown, 1980a).

The assignment of poles into discontinuity sets is usually achieved by a combination of contouring, visual examination of the stereonet and knowledge of geological conditions at the site. However, in many cases visual clustering is very difficult due to the overlap of clusters. A number of algorithms which are based on statistical or fuzzy-set approaches are available for numerically clustering orientation data (Einstein et al., 1979; Miller, 1983; Mahtab & Yegulalp, 1984; Harrison, 1992; Kulatilake, 1993).

As seen in Fig. 4.1, there is scatter of the poles of discontinuities when they are plotted on the stereonet. The mean orientation of a number of discontinuities can be calculated from the direction cosines as described in the following. The sampling bias on orientation can also be considered.

The pole of a discontinuity in three-dimensional space can be represented by a unit vector (u_x, u_y, u_z) associated with the direction cosines as shown in Fig. 4.3:

$$u_x = \cos \alpha_n \cos \beta_n, \quad u_y = \sin \alpha_n \cos \beta_n, \quad u_z = \sin \beta_n \quad (4.1)$$

where α_n and β_n are respectively the trend and plunge of the pole, which can be obtained by

$$\alpha_n = \arctan\left(\frac{u_y}{u_x}\right) + Q \quad (4.2a)$$

$$\beta_n = \arctan\left(\frac{u_z}{\sqrt{u_x^2 + u_y^2}}\right) \quad (4.2b)$$

The parameter Q is an angle, in degrees, that ensures that α_n lies in the correct quadrant and in the range of 0 to 360° (see Table 4.1).

The dip direction and dip angle α/β of a discontinuity are related to the trend and plunge α_n/β_n of its normal by the following expressions:

$$\alpha_n = \alpha + 180^\circ \quad (\text{for } \alpha \leq 180^\circ) \quad (4.3a)$$

$$\alpha_n = \alpha - 180^\circ \quad (\text{for } \alpha \geq 180^\circ)$$

$$\beta_n = 90^\circ - \beta \quad (4.3b)$$

The mean orientation of a set of discontinuities intersecting a sampling line of trend/plunge α_s/β_s can be obtained using the procedure outlined below. This procedure corrects for orientation sampling bias through the introduction of weighted direction cosines.

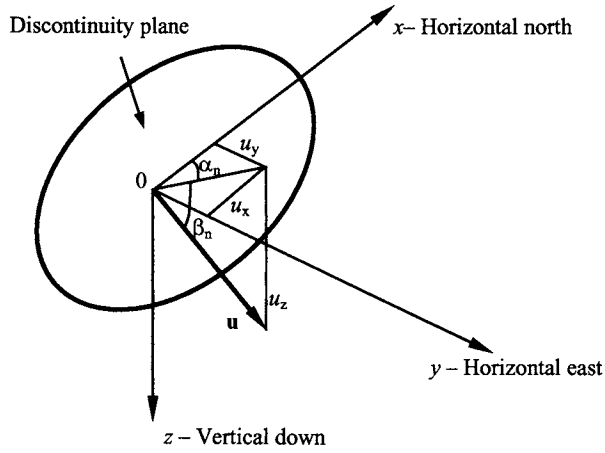


Fig. 4.3 Pole of a discontinuity represented by a unit vector u .

Table 4.1 The quadrant parameter Q in equation (4.2a).

u_x	u_y	Q
≥ 0	≥ 0	0
< 0	≥ 0	180°
< 0	< 0	180°
≥ 0	< 0	360°

1. For discontinuity i , calculate the angle δ_i between its normal and the sampling line:

$$\cos \delta_i = |u_{xi}u_{xs} + u_{yi}u_{ys} + u_{zi}u_{zs}| \quad (4.4)$$

where (u_{xi}, u_{yi}, u_{zi}) and (u_{xs}, u_{ys}, u_{zs}) are the direction cosines respectively of the normal to discontinuity i and the sampling line.

2. For discontinuity i , calculate the weighting factor w_i based on the angle δ_i obtained in step 1:

$$w_i = \frac{1}{\cos \delta_i} \quad (\delta_i < 90^\circ) \quad (4.5)$$

3. After the weighting factor for each discontinuity is obtained, calculate the total weighted sample size N_w for a sample of size N by

$$N_w = \sum_{i=1}^N w_i \quad (4.6)$$

4. Calculate the normalized weighting factor w_{ni} for each discontinuity by

$$w_{ni} = \frac{w_i N}{N_w} \quad (4.7)$$

5. Calculate the corrected direction cosines (n_{xi} , n_{yi} , n_{zi}) for the normal of each discontinuity by

$$(n_{xi}, n_{yi}, n_{zi}) = w_{ni}(u_{xi}, u_{yi}, u_{zi}) \quad (4.8)$$

6. Calculate the resultant vector (r_x , r_y , r_z) of the corrected normal vectors (n_{xi} , n_{yi} , n_{zi}), $i = 1$ to N :

$$r_x = \sum_{i=1}^N n_{xi}, \quad r_y = \sum_{i=1}^N n_{yi}, \quad r_z = \sum_{i=1}^N n_{zi} \quad (4.9)$$

7. The mean orientation of the N discontinuities is the orientation of the resultant vector whose trend and plunge can be found by replacing u_x , u_y and u_z by r_x , r_y and r_z in equation (4.2).

Several probability distributions have been suggested in the literature to represent the discontinuity orientations, including hemispherical uniform, hemispherical normal or Fisher, bivariate Fisher, Bingham, bivariate normal and bivariate lognormal. (Shanley & Mahtab, 1976; Zambak, 1977; Einstein et al., 1979; Kulatilake, 1985a, 1986). The best means to check if a certain distribution is applicable to represent the orientation of a discontinuity set is to perform goodness-of-fit tests. Shanley and Mahtab (1976) and Kulatilake (1985a, 1986) have presented χ^2 goodness-of-fit tests respectively for Bingham, hemispherical normal and bivariate normal distributions. Einstein et al. (1979) have tried all the aforementioned distributions to represent the statistical distributions for 22 data sets. They have reported that they could not find a probability distribution which satisfied χ^2 goodness-of-fit test at 5 percent significance level for 18 of these data sets. This shows clearly the inadequacy of the currently available analytical distributions in representing the discontinuity orientations. In the case that no analytical distribution can represent the discontinuity orientation data, empirical distributions can be used.

4.5 DISCONTINUITY INTENSITY

Discontinuity intensity is one of the most important parameters for describing discontinuities in a rock mass. Intensity can be expressed in terms of different measures in one, two or three dimensions, including discontinuity spacing, linear, areal and volumetric frequency, Rock Quality Designation (RQD), discontinuity trace length per unit area of rock exposure, and discontinuity area per unit volume of rock mass, as described in detail in the following subsections.

4.5.1 Discontinuity spacing and linear frequency

Discontinuity spacing is the distance between adjacent discontinuities measured along a sampling line. If the adjacent discontinuities are from a particular discontinuity set, the spacing is called the set spacing. When the sampling line is parallel to the mean normal to the discontinuity set, the set spacing is called the normal set spacing (Priest, 1993). Table 4.2 gives the terminology used by ISRM (1978c) for describing the magnitude of discontinuity spacing.

Discontinuity frequency is most commonly expressed in terms of the linear frequency λ defined as the number of discontinuities intersected by a unit length of sampling line. Linear frequency is the reciprocal of the mean spacing. Like the spacing, the frequency can be specified as set frequency or normal set frequency.

If the normal set frequency of a set of parallel discontinuities is λ_n , the set frequency λ_s along a sampling line that makes an acute angle θ to the set normal is

$$\lambda_s = \lambda_n \cos \theta \quad (4.10)$$

For a sampling line intersecting N sets of parallel discontinuities, the total discontinuity frequency λ is determined by

$$\lambda = \sum_{i=1}^N \lambda_{ni} \cos \theta_i \quad (4.11)$$

Table 4.2 Classification of discontinuity spacing (ISRM, 1978c).

Description	Spacing (mm)
Extremely close spacing	< 20
Very close spacing	20 – 60
Close spacing	60 – 200
Moderate spacing	200 – 600
Wide spacing	600 – 2000
Very wide spacing	2000 – 6000
Extremely wide spacing	> 6000

where λ_{ni} is the normal set frequency of the i th set; and θ_i is the acute angle between the sampling line and the normal to the i th set of discontinuities.

It is noted that the discontinuity frequency λ varies with the direction of the sampling line. Therefore, it is important to specify the corresponding direction when stating a discontinuity frequency value.

Like all other characteristics of rock masses, discontinuity spacings will not have uniquely defined values but, rather, will take a range of values, possibly according to some form of statistical distribution. The two major discontinuity spacing distribution forms used in the literature are negative exponential and lognormal (Rives et al., 1992). Priest and Hudson (1976) made measurements on a number of sedimentary rock masses in the United Kingdom and found that, in each case, the discontinuity spacing histogram gave a probability density distribution that could be approximated by the negative exponential distribution. The same conclusion has been reached by others, notably Wallis and King (1980) working on a Precambrian porphyritic granite, and Einstein and Baecher (1983) working on a variety of igneous, sedimentary and metamorphic rocks. Thus the frequency $f(s)$ of a given discontinuity spacing value s is given by the function

$$f(s) = \lambda e^{-\lambda s} \quad (4.12)$$

where $\lambda = 1/\bar{s}$ is the mean discontinuity frequency of a large discontinuity population and \bar{s} is the mean spacing.

Fig. 4.4 shows the discontinuity spacing histogram and the corresponding negative exponential distribution calculated from equation (4.12) for the Lower Chalk, Chinnor, Oxfordshire, UK (Priest & Hudson, 1976).

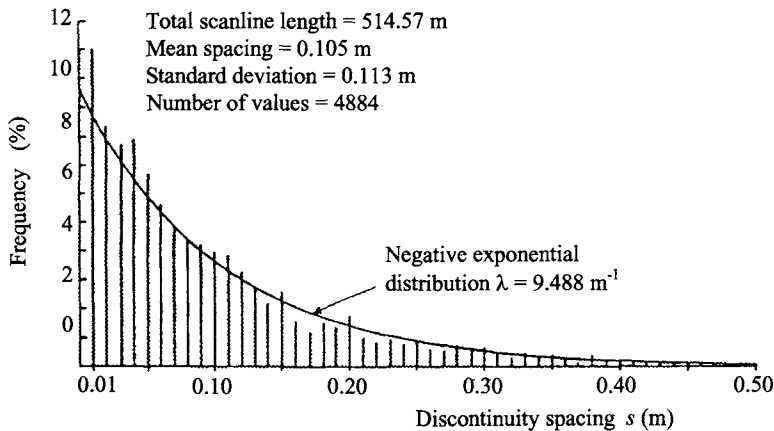


Fig. 4.4 Discontinuity spacing histogram, Lower Chalk, Chinnor, Oxfordshire, UK (after Priest & Hudson, 1976).

Seismic velocity measurements have been used for assessing the discontinuity frequency by different researchers (Savic et al., 1969; Sjögren et al., 1979; Idziak, 1981; Jamscikov et al., 1985; Palmström, 1995). Palmström (1995) presented the following two relationships between the linear discontinuity frequency λ and the P-wave velocity

$$\lambda = \frac{v_{p0}^{3.4}}{v_{pF}^{2.8}} \quad (4.13)$$

or

$$\lambda = 3 \left(\frac{v_{p0}}{v_{pF}} \right)^{v_{p0}/2} \quad (4.14)$$

where v_{p0} is the P-wave velocity of intact rock under the same conditions as in the field; and v_{pF} is the P-wave velocity of in situ rock mass. Both v_{p0} and v_{pF} are in the unit of km/s. Where v_{p0} is not known, it can be estimated from the value ranges shown in Fig. 3.4.

The following general equation was also used to fit the experimental data of linear discontinuity frequency λ and P-wave velocities (Schön, 1996)

$$v_{pF} = \frac{v_{p0}}{1 + a\lambda^m} \quad (4.15)$$

where a and m are empirical constants. For sedimentary rocks (limestone, dolomite) of the Uppersilesian Coal Basin, Poland, the following empirical relation is obtained (Idziak, 1981)

$$v_{pF} = \frac{7.67}{1 + 0.252\lambda^{3/2}} \quad (4.16)$$

Sjögren et al. (1979) and Palmström (1995) proposed the following hyperbolic expression for calculating the linear discontinuity frequency λ from measured P-wave velocities:

$$\lambda = \frac{v_{pN} - v_{pF}}{v_{pN} \times v_{pF} \times k_s} \quad (4.17)$$

where v_{pN} is the natural or maximum P-wave velocity of crack- and discontinuity-free rock; and k_s is a parameter taking into account the actual conditions of the in situ rock mass. v_{pN} and k_s can be determined using the procedure described in the following.

Since the rocks near the surface are seldom free from discontinuities, cracks and pores, it is seldom possible to find v_{pN} of rocks near the surface directly from seismic measurements. The best way to determine v_{pN} is conducting calculations when two sets of measured λ and v_{pF} data are available. From Sjögren et al. (1979) and Palmström (1995)

$$v_{pN} = \frac{v_{pF1} \times v_{pF2} (\lambda_2 - \lambda_1)}{\lambda_2 \times v_{pF2} - \lambda_1 \times v_{pF1}} \quad (4.18)$$

$$k_s = \frac{1}{\lambda_1} \left(\frac{1}{v_{pF1}} - \frac{1}{v_{pN}} \right) \quad (4.19)$$

where λ_1 , v_{pF1} and λ_2 , v_{pF2} are corresponding values of measured linear discontinuity frequency and in situ rock P-wave velocity, respectively, from two pairs of measurements.

Based on regression analysis of the data obtained for heavily fractured calcareous rock masses out-cropping in southern Italy (see Fig. 4.5), Budetta et al. (2001) obtained v_{pN} and k_s respectively as $v_{pN} = 6.33$ km/s and $k_s = 0.025$, i.e.

$$\lambda = \frac{6.33 - v_{pF}}{6.33 \times v_{pF} \times 0.025} \quad (4.20)$$

4.5.2 *Rock Quality Designation (RQD)*

Rock Quality Designation (RQD) was proposed by Deere (1964) as a measure of the quality of borehole core. The RQD is defined as the ratio (in percent) of the total length of sound core pieces that are 0.1 m (4 in.) or longer to the length of the core run. The value 0.1 m is referred to as the threshold value. RQD is perhaps the most commonly used method for characterizing the jointing in borehole cores, although this parameter may also implicitly include other rock mass features such as weathering and core loss.

For RQD determination, the International Society for Rock Mechanics (ISRM) recommends a core size of at least NX (size 54.7 mm) drilled with double-tube core barrel using a diamond bit. Artificial fractures can be identified by close fitting of cores and unstained surfaces. All the artificial fractures should be ignored while counting the core length for RQD. A slow rate of drilling will also give better RQD. The correct procedure for measuring RQD is shown in Fig. 4.6.

Correlations between RQD and linear discontinuity frequency λ have been derived for different discontinuity spacing distribution forms (Priest & Hudson, 1976; Sen & Kazi, 1984; Sen, 1993). For a negative exponential distribution of discontinuity

spacings, Priest and Hudson (1976) derived the following relationship between RQD and linear discontinuity frequency λ

$$\text{RQD} = 100e^{-\lambda t} (\lambda t + 1) \quad (4.21)$$

where t is the length threshold. For $t = 0.1$ m as for the conventional RQD defined earlier, equation (4.21) can be expressed as

$$\text{RQD} = 100e^{-0.1\lambda} (0.1\lambda + 1) \quad (4.22)$$

Fig. 4.7 shows the relations obtained by Priest and Hudson (1976) between measured values of RQD and λ , and the values calculated using equation (4.22).

For values of λ in the range 6 to 16 m^{-1} , a good approximation to measured RQD values was found to be given by the linear relation

$$\text{RQD} = 110.4 - 3.68\lambda \quad (4.23)$$

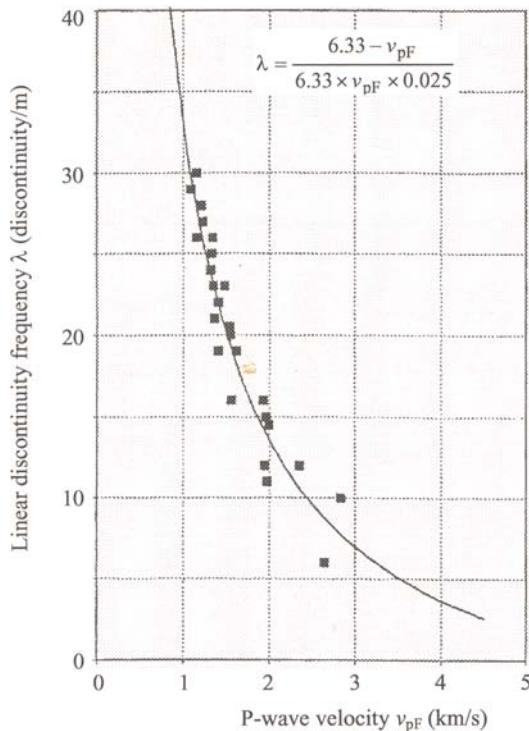


Fig. 4.5 Correlation between linear discontinuity frequency λ and P-wave velocity v_{pF} for heavily fractured calcareous rock in southern Italy (after Budetta et al., 2001).

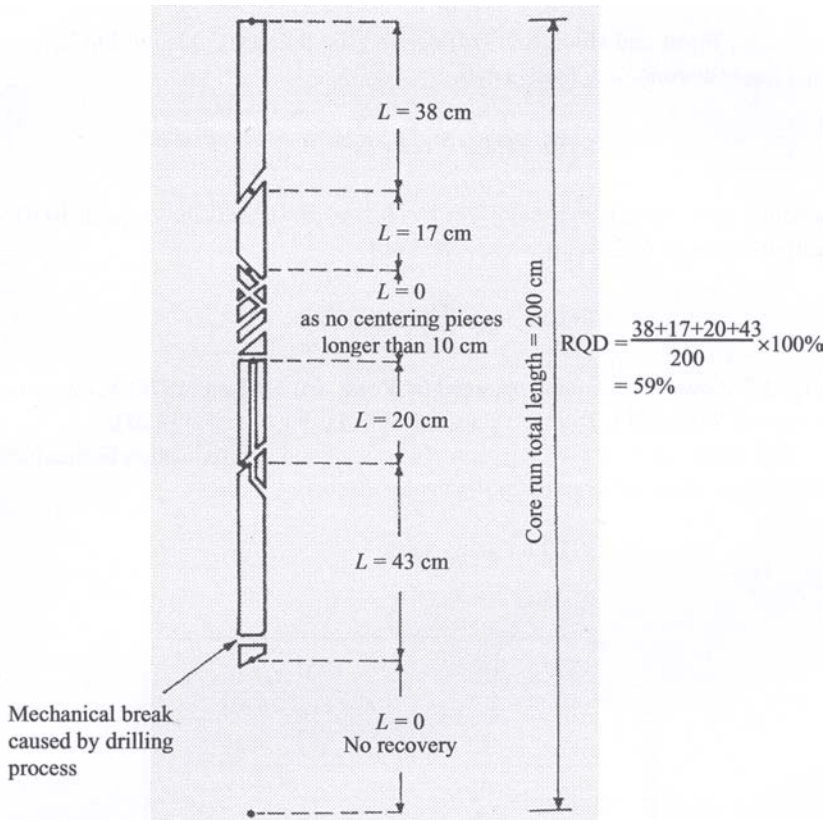


Fig. 4.6 Procedure for measurement and calculation of rock quality designation RQD (after Deere, 1989).

It is noted that equation (4.21) is derived with the assumption that the length of the sampling line L is large so that the term $e^{-\lambda L}$ is negligible. For a short sampling line of length L , Sen and Kazi (1984) derived the following expression for RQD with a length threshold t :

$$\text{RQD} = \frac{100}{1 - e^{-\lambda L} - \lambda L e^{-\lambda L}} [e^{-\lambda t} (\lambda t + 1) - e^{-\lambda L} (\lambda L + 1)] \quad (4.24)$$

Fig. 4.8 shows the variation of RQD with the length of the sampling line L for discontinuity frequency $\lambda = 10 \text{ m}^{-1}$ and length threshold $t = 0.1 \text{ m}$. It can be seen that when L is smaller than about 0.5 m or when $\lambda L < 5$, RQD increases significantly when L increases. When L is larger than 0.5 or when $\lambda L > 5$, RQD changes little with L . Therefore, it is important to use sampling lines that are long so that $\lambda L > 5$ and $e^{-\lambda L}$ is negligible.

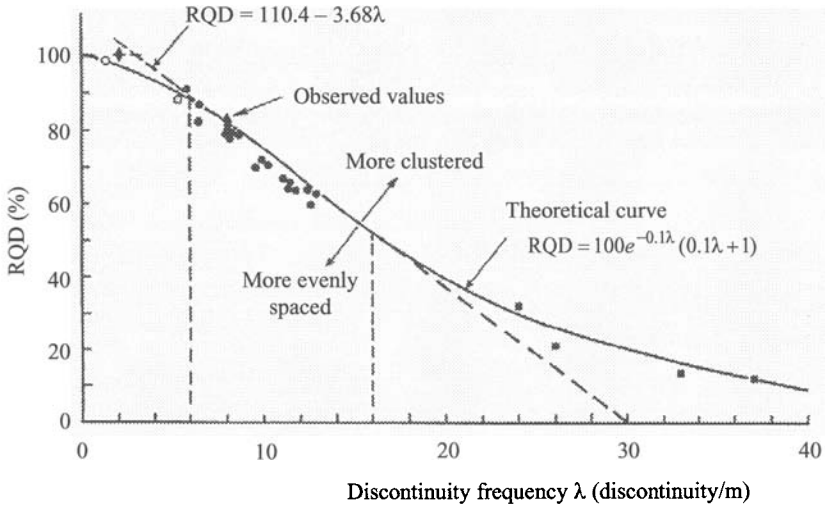


Fig. 4.7 Relationship between RQD and discontinuity frequency λ (after Priest & Hudson, 1976).

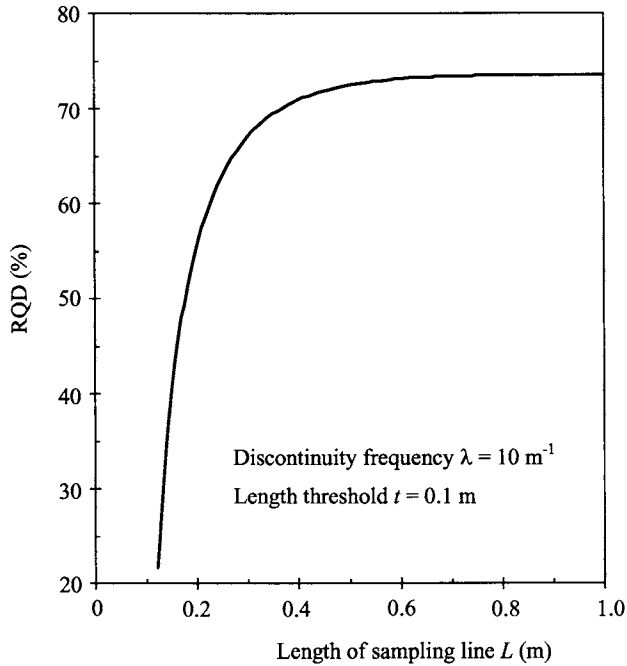


Fig. 4.8 Variation of RQD with the length of sample line L (after Sen & Kazi, 1984; Priest, 1993).

Because linear discontinuity frequency λ varies with direction, RQD will also vary with direction. It is, therefore, important to specify the corresponding direction when stating an RQD value.

Seismic velocity measurements have also been used to estimate RQD. By comparing the P-wave velocity of in situ rock mass with laboratory P-wave velocity of intact drill core obtained from the same rock mass, the RQD can be estimated by (Deere et al., 1967)

$$\text{RQD (\%)} = (v_{pF}/v_{p0})^2 \times 100 \quad (4.25)$$

where v_{pF} is the P-wave velocity of in situ rock mass; and v_{p0} is the P-wave velocity of the corresponding intact rock.

Based on the data of limestones, mudstones, marls and shales at a dam site in Wadi Mujib, Jordan, El-Naqa (1996) obtained the following empirical correlation between RQD and P-wave velocities:

$$\text{RQD (\%)} = 0.77 \times (v_{pF}/v_{p0})^{1.05} \times 100 \quad (r = 0.89) \quad (4.26)$$

where v_{pF} is the P-wave velocity of in situ rock mass; v_{p0} is the P-wave velocity of the corresponding intact rock; and r is the correlation coefficient.

Sjögren et al. (1979) and Palmström (1995) proposed the following hyperbolic correlation between RQD and P-wave velocities:

$$\text{RQD (\%)} = \frac{v_{pq} - v_{pF}}{v_{pq} \times v_{pF} \times k_q} \times 100 \quad (4.27)$$

where v_{pF} is the P-wave velocity of in situ rock mass; and v_{pq} is the P-wave velocity of a rock mass with RQD = 0; and k_q is a parameter taking into account the actual conditions of the in situ rock mass. Based on regression analysis of the data obtained for heavily fractured calcareous rock masses out-cropping in southern Italy (see Fig. 4.9), Budetta et al. (2001) obtained v_{pq} and k_q respectively as $v_{pq} = 1.22$ km/s and $k_q = -0.69$, i.e.

$$\text{RQD (\%)} = \frac{1.22 - v_{pF}}{1.22 \times v_{pF} \times (-0.69)} \times 100 \quad (4.27a)$$

4.5.3 *Areal and volumetric frequency*

Discontinuity intensity is also often expressed in terms of areal and/or volumetric frequency. Table 4.3 lists different discontinuity intensity measures defined by Dershowitz and Herda (1992). The areal frequency P_{20} (or λ_a) is the number of discontinuity traces per unit sampling area. Since the areal frequency λ_a is scale dependent for exposures or sampling planes at scales smaller than the maximum

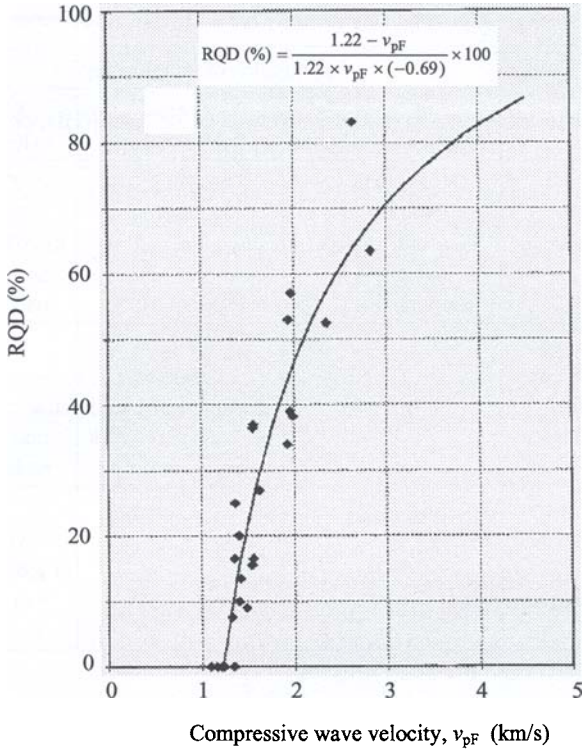


Fig. 4.9 Correlation between RQD and P-wave velocity v_{pF} for heavily fractured calcareous rock in southern Italy (after Budetta et al., 2001).

discontinuity trace length, the intensity measure P_{21} , the length of discontinuity traces per unit sampling area, can be used. Both λ_a and P_{21} are dependent on the relative orientation between the discontinuities and the sampling plane. P_{21} can be related to λ_a through the mean discontinuity trace length μ_l :

$$P_{21} = \lambda_a \mu_l \quad (4.28)$$

The mean discontinuity trace length can be determined as in Section 4.6.2.

Mauldon et al. (1999) derived a simple expression for estimating discontinuity intensity P_{21} from circular scanline sampling:

$$P_{21} = \frac{N}{4c} \quad (4.29)$$

where N is the number of traces intersecting the circular scanline; and c is the radius of the scanline circle (see Fig. 4.10). Circular scanline sampling measures only the traces

Table 4.3 Different measures for discontinuity intensity (after Dershowitz & Herda, 1992).

		Dimension of sampling region		
		1. Line (Scanline or borehole)	2. Area (Rock exposure)	3. Volume (Rock mass)
Measured parameter	Number of discontinuities	P_{10} or λ Number of discontinuities per unit length of sampling line [L^{-1}]	P_{20} or λ_a Number of discontinuities per unit area of rock exposure [L^{-2}]	P_{30} or λ_v Number of discontinuities per unit volume of rock mass [L^{-3}]
	Dimension one less than that of sampling region		P_{21} Length of discontinuity traces per unit area of rock exposure [L^{-1}]	P_{32} Area of discontinuities per unit volume of rock mass [L^{-1}]
	Dimension equal to that of sampling region			P_{33} Volume of discontinuities per unit volume of rock mass [-]

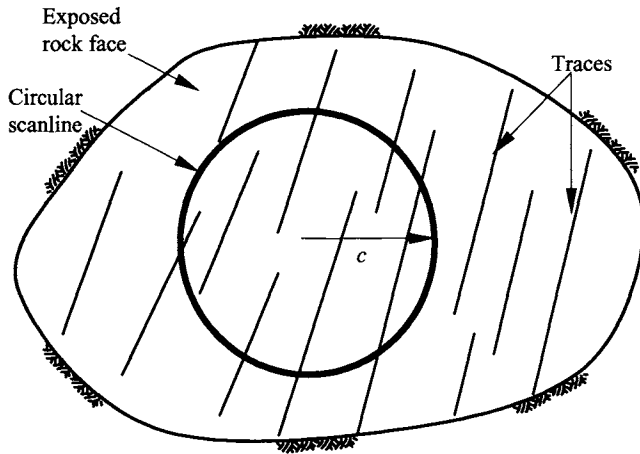


Fig. 4.10 Circular scanline sampling.

intersecting the line of the circle. One advantage of circular scanlines over straight scanlines is the elimination of directional bias. Circular scanlines have been used for discontinuity sampling at exposed rock faces by different researchers (Einstein et al., 1979; Titley et al., 1986; Davis & Reynolds, 1996; Mauldon et al., 1999).

The volume frequency P_{30} (or λ_v) is the number of discontinuities per unit volume of rock mass. Like λ_a , λ_v is scale dependent and changes with the size of the sampling region for regions at scales smaller than the maximum discontinuity size. Therefore, the intensity measure P_{32} , the area of discontinuities per unit volume of rock mass, can be used. P_{32} is related to λ_v through the mean area \bar{A} of the discontinuities:

$$P_{32} = \lambda_v \bar{A} \quad (4.30)$$

The mean area of the discontinuities can be determined as in Section 4.6.4.

The volumetric frequency λ_v can be determined from the discontinuity set spacings within a volume of rock mass as (Palmström, 1982)

$$\lambda_v = \frac{1}{s_1} + \frac{1}{s_2} + \frac{1}{s_3} + \dots \quad (4.31)$$

where s_1, s_2, s_3 are the mean discontinuity set spacings.

Random discontinuities in the rock mass can be considered by assuming a random spacing s_r for each of them. According to Palmström (2002), $s_r = 5$ m can be assumed. So the volumetric frequency λ_v can be generally expressed as

$$\lambda_v = \frac{1}{s_1} + \frac{1}{s_2} + \frac{1}{s_3} + \dots + \frac{N_r}{5} \quad (4.32)$$

where N_r is the number of random discontinuities.

The volumetric frequency λ_v can also be estimated from the areal frequency λ_a using the following empirical expression (Palmström, 2002)

$$\lambda_v = k_a \lambda_a \quad (4.33)$$

where k_a is the correlation factor, which varies mainly between 1 and 2.5 with an average value of 1.5. The highest value is where the sampling plane is parallel to the main discontinuity set.

The International Society for Rock Mechanics (ISRM, 1978c) presented the following approximate correlation between volumetric frequency λ_v and RQD

$$\text{RQD} = 115 - 3.3 \lambda_v \quad (4.34)$$

Here $\text{RQD} = 0$ for $\lambda_v > 35$, and $\text{RQD} = 100$ for $\lambda_v < 4.5$.

4.5.4 Block size

Block size is another important parameter for describing discontinuity intensity and rock mass behavior. Block dimensions are determined by discontinuity spacings, by the number of discontinuity sets and by the persistence of the discontinuities delineating potential blocks. Block shapes are determined by the number of sets and the orientations of the discontinuities delineating potential blocks. Where relatively regular jointing exists such as the jointing in sedimentary rocks, it may be possible to give adequate description of the block shapes. Fig. 4.11 shows the examples of block shapes presented by Dearman (1991). In most cases, however, the block shapes are irregular and can only be roughly described.

Where individual blocks can be observed in a surface, their volumes can be directly measured from relevant dimensions by selecting several representative blocks and measuring their average dimensions. Where three discontinuity sets occur, the block volume can be calculated as

$$V_b = \frac{s_1 s_2 s_3}{\sin \gamma_1 \sin \gamma_2 \sin \gamma_3} \quad (4.35)$$

where s_1, s_2, s_3 are the normal set spacings respectively of the three discontinuity sets; and $\gamma_1, \gamma_2, \gamma_3$ are the angles between the discontinuity sets. If the discontinuity sets intersect at right angles, the block volume can be simply calculated as

$$V_b = s_1 s_2 s_3 \quad (4.36)$$

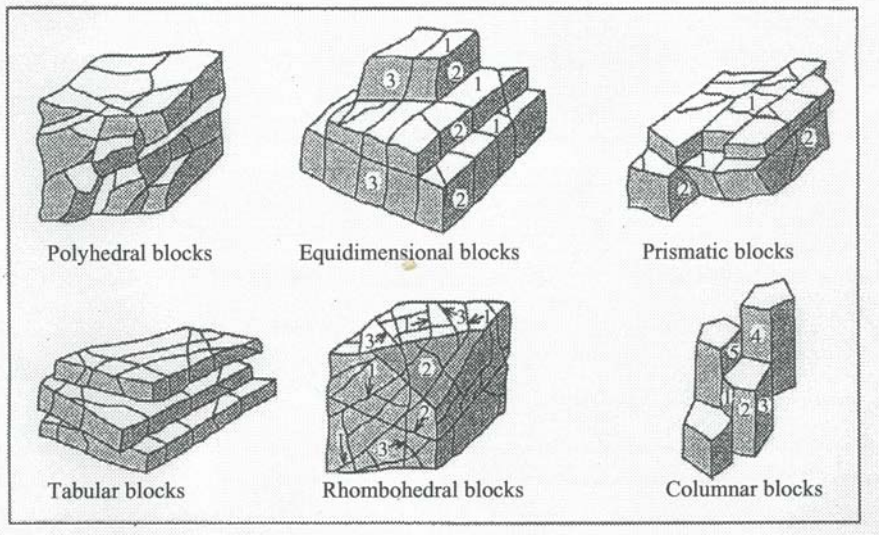


Fig. 4.11 Examples of block shapes (after Dearman, 1991).

The block size can also be described based on the volumetric discontinuity frequency λ_v using the terms in Table 4.4. To describe both the block size and shape, the adjectives listed in Table 4.5 can be used.

Fig. 4.12 shows the comparison of the possible ranges of RQD, volumetric frequency λ_v and block volume V_b from Palmström (2002). It can be seen that RQD covers only a limited part of the range of jointing.

Table 4.4 Terms for describing block size based on volumetric discontinuity frequency λ_v (after ISRM, 1978c).

Volumetric frequency λ_v (discontinuity/m ³)	Description
< 1	Very large blocks
1-3	Large blocks
3-10	Medium-sized blocks
10-30	Small blocks
> 30	Very small block

Table 4.5 Adjectives for describing block size and shape (after ISRM, 1978c).

Adjective	Description
Massive	Few discontinuities or very wide spacing
Blocky	Approximately equidimensional
Tabular	One dimension considerably smaller than the other two
Columnar	One dimension considerably larger than the other two
Irregular	Wide variations of block size and dimensions
Crushed	Heavily jointed to “sugar cube”

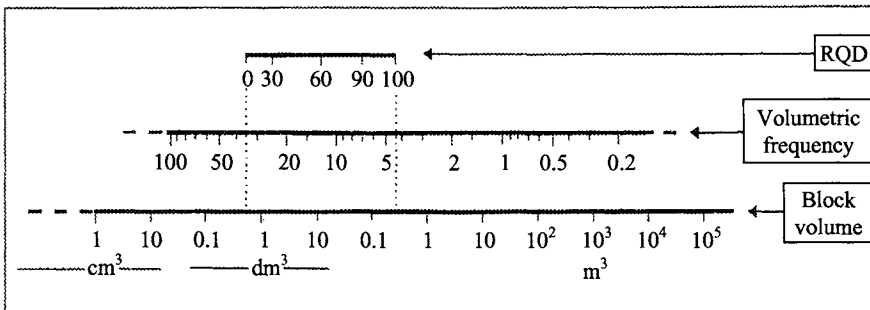


Fig. 4.12 Ranges of RQD, volumetric frequency λ_v and block volume V_b (after Palmström, 2002).

4.6 DISCONTINUITY PERSISTENCE, TRACE LENGTH AND SIZE

4.6.1 Discontinuity persistence

Persistence is a term used to describe the areal extent or size of a discontinuity within a plane. It can be crudely quantified by observing discontinuity trace lengths on exposed rock faces. ISRM (1978c) uses the most common or modal trace lengths of each set of discontinuities measured on exposed rock faces to classify persistence according to Table 4.6.

Discontinuity persistence is one of the most important rock mass parameters, but one of the most difficult to determine. The discontinuities of one particular set are often more continuous than those of the other sets. The minor sets tend to terminate against the primary features, or they may terminate in solid rock. The sets of discontinuities can be distinguished by terms of persistent, sub-persistent and non-persistent respectively. Fig. 4.13 shows a set of simple plane sketches and block diagrams used to help indicate the persistence of various sets of discontinuities in a rock mass. Clearly, the persistence of discontinuities has a major influence on the shear strength developed in the plane of the discontinuity.

Table 4.6 Classification of discontinuity persistence (ISRM, 1978c).

Description	Modal trace length (m)
Very low persistence	< 1
Low persistence	1 – 3
Medium persistence	3 – 10
High persistence	10 – 20
Very high persistence	> 20

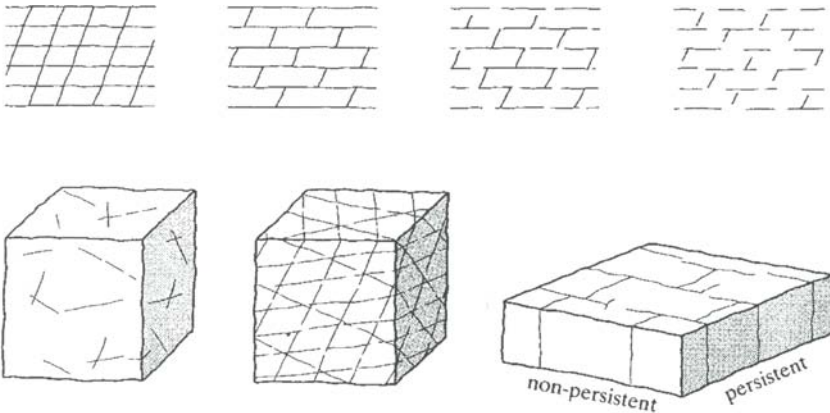


Fig. 4.13 Simple sketches and block diagrams indicating the persistence of various sets of discontinuities (after ISRM, 1978c).

Persistence ratio PR is often used to describe the persistence of discontinuities. In the literature, discontinuity persistence ratio PR is usually defined as

$$PR = \lim_{A_S \rightarrow \infty} \frac{\sum a_{S_i}}{A_S} \quad (4.37)$$

in which S is a region on the discontinuity plane with area A_S ; and a_{S_i} is the area of the i th discontinuity in S (see Fig. 4.14). The summation in equation (4.37) is over all discontinuities in S . Equivalently, discontinuity persistence ratio PR can be expressed as a limit length ratio along a given line on a discontinuity plane. In this case,

$$PR = \lim_{L_S \rightarrow \infty} \frac{\sum l_{S_i}}{L_S} \quad (4.38)$$

in which L_S is the length of a straight line segment S and l_{S_i} is the length of the i th discontinuity segment in S (see Fig 4.15). For a finite sampling length L_S , PR can be simply estimated by (see Fig. 4.16)

$$PR = \frac{\sum DL}{\sum DL + \sum RBL} \quad (4.39)$$

where $\sum DL$ is the sum of the length of all discontinuities; and $\sum RBL$ is the sum of the length of all rock bridges.

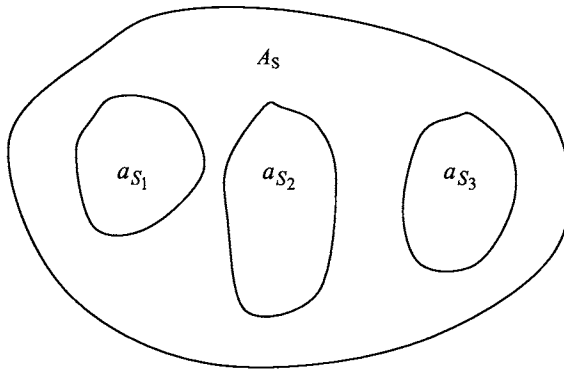


Fig. 4.14 Definition of PR as area ratio (after Einstein et al., 1983).

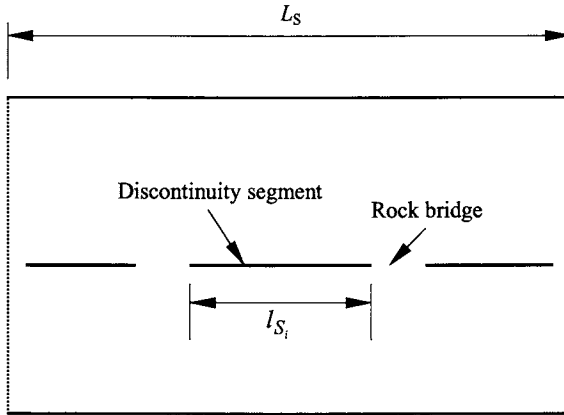
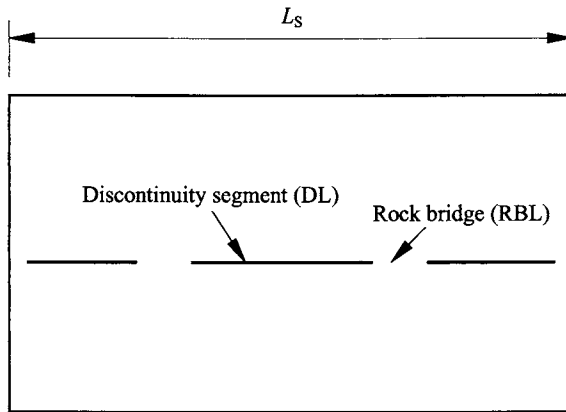


Fig. 4.15 Definition of PR as length ratio.



$$L_s = \Sigma DL + \Sigma RBL$$

Fig. 4.16 Estimation of PR for a finite sampling length.

The above definition of discontinuity persistence ratio PR considers only the discontinuities in the same plane. However, according to Einstein et al. (1983), when two discontinuities are at a low-angle transition ($\beta < \theta_t$, see Fig. 4.17), the rock bridge may fail by the same mechanism as the in-plane rock bridge (see Fig. 4.18), where θ_t is the angle of the tension cracks which can be obtained from Mohr's circle [see Fig. 4.18(a)]. For both the in-plane (Fig. 4.18) and the low-angle out-of-plane (Fig. 4.17) transitions, the intact-rock resistance R can be calculated by

$$R = \tau_a d \tag{4.40}$$

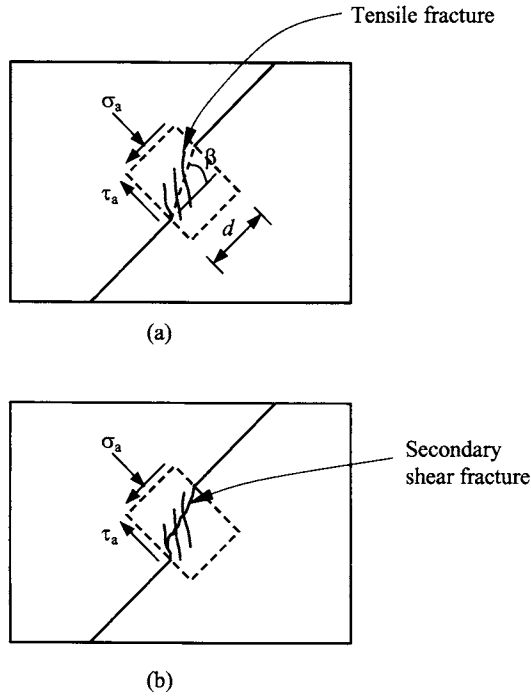


Fig. 4.17 Failure of “low-angle” transitions through intact rock: (a) Tensile fracture; and (b) Secondary shear fracture (after Einstein et al., 1983; Zhang, 1999).

where d is the “in-plane length” of the rock bridge; and τ_a is the peak shear stress mobilized in the direction of discontinuities which can be obtained by (Einstein et al., 1983)

$$\tau_a^2 = \sigma_t(\sigma_t - \sigma_a) \quad (4.41)$$

where σ_t is the tensile strength of the intact rock; and σ_a is the effective normal stress on the discontinuity plane.

Zhang (1999) proposed a definition of discontinuity persistence ratio PR that considers both in-plane and low-angle-transition discontinuities:

$$PR = \lim_{L_S \rightarrow \infty} \frac{\sum DL_i + \sum DL_1}{L_S} \quad (4.42)$$

in which L_S is the total sampling length along the direction of the discontinuity traces, DL_i is the length of the i th in-plane discontinuities and DL_1 is the length of the l th low-angle-transition discontinuities (see Fig. 4.19). For a finite sampling length, PR can be simply approximated by

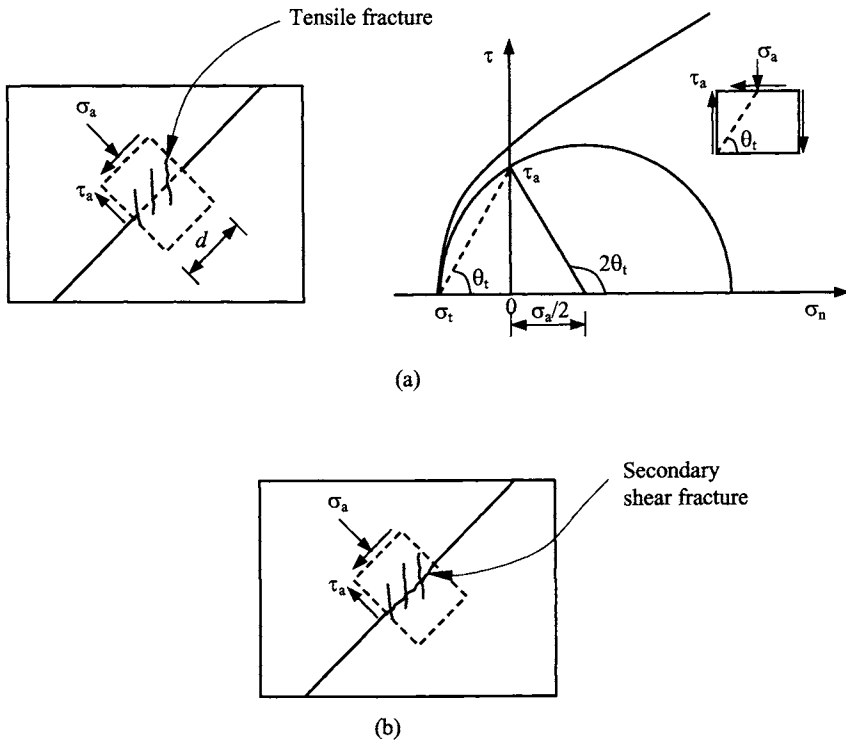


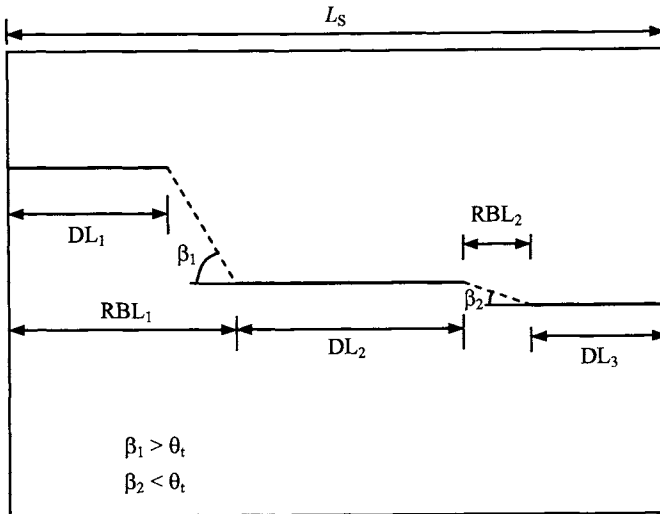
Fig. 4.18 In-plane failure of intact rock: (a) Tensile fracture and corresponding Mohr's circle; and (b) Secondary shear fracture (after Einstein et al., 1983; Zhang, 1999).

$$PR = \frac{\sum_{i=1}^m DL_i + \sum_{l=1}^n DL_l}{L_S} \quad (4.43)$$

where m and n are the numbers respectively of the in-plane and low-angle-transition ($\beta < \theta_t$) discontinuities within the sampling length L_S (see Fig. 4.19).

4.6.2 Discontinuity trace length

Discontinuity trace length is an important parameter for describing discontinuity size and persistence. When sampling trace lengths on exposed rock surfaces, errors can occur due to the following biases (Baecher & Lanney, 1978; Einstein et al., 1979; Priest & Hudson, 1981; Kulatilake & Wu, 1984c; Mauldon, 1998; Zhang & Einstein, 1998b, 2000):



For definition of PR considering only in-plane discontinuities, $PR = DL_2/L_s$

For definition of PR considering both in-plane and low-angle-transition discontinuities,

$$PR = (DL_2 + DL_3)/L_s$$

Fig. 4.19 Definition of PR considering both in-plane and low-angle-transition discontinuities (after Zhang, 1999).

- (1) Orientation bias: the probability of a discontinuity appearing at an exposed rock surface depends on the relative orientation between the rock face and the discontinuity.
- (2) Size bias: large discontinuities are more likely to be sampled than small discontinuities. This bias affects the results in two ways: (a) a larger discontinuity is more likely to appear at an exposed rock face than a smaller one; and (b) a longer trace is more likely to appear in a sampling area than a shorter one.
- (3) Truncation bias: Very small trace lengths are difficult or sometimes impossible to measure. Therefore, trace lengths below some known cutoff length are not recorded.
- (4) Censoring bias: Long discontinuity traces may extend beyond the visible exposure so that one end or both ends of the discontinuity traces can not be seen.

In inferring the trace length distribution on an infinite surface from the measured trace lengths on a finite size area on this surface, biases (2b), (3) and (4) should be considered. Biases (1) and (2a) are of interest only in three-dimensional simulations of

discontinuities, i.e., when inferring discontinuity size distributions as discussed in Section 4.6.4.

(a) Probability distribution of measured trace lengths

Many investigators have looked into the distribution of trace lengths (Table 4.7). Apart from Baecher et al. (1977), Cruden (1977), Einstein et al. (1979) and Kulatilake (1993) others have based their argument on inspection rather than on goodness-of-fit tests. It seems that only Baecher et al. (1977), Einstein et al. (1979) and Kulatilake (1993) have tried more than one distribution to find the best distribution to represent trace length data.

To find the suitable distribution for the measured trace lengths of each discontinuity set, the distribution forms in Table 4.7 can be checked by using χ^2 and Kolmogorov-Smirnov goodness-of-fit tests.

Table 4.7 Distribution forms of trace lengths.

Investigator	Distribution
Robertson (1970)	Exponential
McMahon (1974)	Lognormal
Bridges (1975)	Lognormal
Call et al. (1976)	Exponential
Barton (1977)	Lognormal
Cruden (1977)	Exponential
Baecher et al (1977)	Lognormal
Einstein et al. (1979)	Lognormal
Priest and Hudson (1981)	Exponential
Kulatilake (1993)	Exponential and Gamma (Gamma better)

(b) Corrected mean trace length

In inferring the corrected mean trace length (i.e., the mean trace length on an infinite surface), from the measured trace lengths on a finite exposure, biases (2b), (3) and (4) should be considered. Truncation bias (3) can be corrected using the method of Warburton (1980a). Decreasing the truncation level in discontinuity surveys can reduce the effects of truncation bias on trace length estimates. It is practically feasible to observe and measure trace lengths as low as 10 mm both in the field and from photographs (Priest & Hudson, 1981). Truncation at this level will have only a small effect on the data, particularly if the mean trace length is in the order of meters (Priest & Hudson, 1981; Einstein & Baecher, 1983). Therefore, the effect of truncation bias on trace length estimates can be ignored. However, biases (2b) and (4) are important (Kulatilake & Wu, 1984c) and need be considered.

Pahl (1981) suggested a technique to estimate the mean trace length on an infinite surface produced by a discontinuity set whose orientation has a single value, i.e., all discontinuities in the set have the same orientation. His technique is based on the categorization of randomly located discontinuities that intersect a vertical, rectangular planar rock face window of height h and width w , and whose traces make an angle ϕ with the vertical, as shown in Fig. 4.20. Discontinuities intersecting the sampling window can be divided into three classes: (1) discontinuities with both ends censored, (2) discontinuities with one end censored and one end observable, and (3) discontinuities with both ends observable. If the numbers of traces in each of the above three types are N_0 , N_1 and N_2 respectively, the total number of traces, N , will be

$$N = N_0 + N_1 + N_2 \quad (4.44)$$

Pahl (1981) has derived the following expression for mean trace length μ_l

$$\mu_l = \frac{wh(N + N_0 - N_2)}{(w \cos \phi + h \sin \phi)(N - N_0 + N_2)} \quad (4.45)$$

Although the approach in equation (4.45) is both rigorous and easy to implement, it relies on the discontinuities being grouped into a parallel or nearly parallel set. Kulatilake and Wu (1984c) extended Pahl's technique to discontinuities whose orientation is described by a probabilistic distribution. A major difficulty in applying the extended technique is to determine the probabilistic distribution function of the orientation of discontinuities.

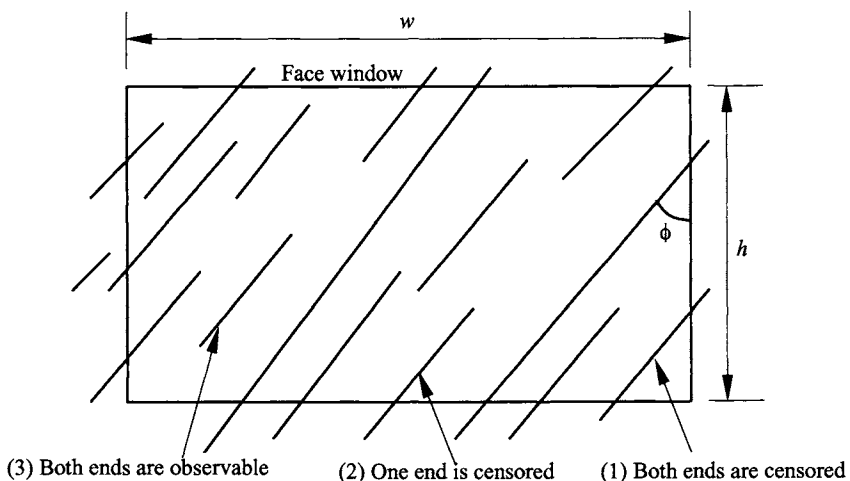


Fig. 4.20 Discontinuities intersecting a vertical rock face (after Pahl, 1981).

Using different methods, Mauldon (1998) and Zhang and Einstein (1998b) independently derived the following expression for estimating the mean trace length on an infinite surface, from the observed trace data in a finite circular window (see Fig. 4.21):

$$\mu_l = \frac{\pi(N + N_0 - N_2)}{2(N - N_0 + N_2)} c \quad (4.46)$$

where c is the radius of the circular sampling window. The major advantage of the method of Mauldon (1998) and Zhang and Einstein (1998b) over the methods of Pahl (1981) and Kulatilake and Wu (1984c) is that it does not need sampling data about the orientation of discontinuities, i.e., the method of Mauldon (1998) and Zhang and Einstein (1998b) is applicable to traces with arbitrary orientation distributions. Therefore, the method of Mauldon (1998) and Zhang and Einstein (1998b) can be used to estimate the mean trace length of more than one set of discontinuities. The orientation distribution-free nature of this method comes from the symmetric properties of the circular sampling windows.

Trace length measurements are not needed when using equations (4.45) and (4.46). In the derivation of equations (4.45) and (4.46), discontinuity trace length l can be anywhere between zero and infinity. Hence, μ_l obtained by equations (4.45) and (4.46) does not contain errors due to biases (2b) and (4) as described before.

μ_l in equations (4.45) and (4.46) is the population (thus correct or true) mean trace length, with N , N_0 and N_2 being respectively the expected total number of traces intersecting the window, the expected number of traces with both ends censored and the expected number of traces with both ends observable. In practice, the exact values of N , N_0 and N_2 are not known and thus μ_l has to be estimated using sampled data. From sampling in one rectangular or circular window, what we get is only one sample of N , N_0 and N_2 and from this sample only a point estimate of μ_l can be obtained. For example, for a sample of \hat{N} traces intersecting the sampling window, if \hat{N}_0 and \hat{N}_2 are respectively the numbers of discontinuities that appear on the window with both ends censored and both ends observable, the mean trace length of the sample, $\hat{\mu}_l$, can be obtained by

$$\hat{\mu}_l = \frac{wh(\hat{N} + \hat{N}_0 - \hat{N}_2)}{(w \cos \phi + h \sin \phi)(\hat{N} - \hat{N}_0 + \hat{N}_2)} \quad (\text{for rectangular window sampling}) \quad (4.47)$$

$$\hat{\mu}_l = \frac{\pi(\hat{N} + \hat{N}_0 - \hat{N}_2)}{2(\hat{N} - \hat{N}_0 + \hat{N}_2)} c \quad (\text{for circular window sampling}) \quad (4.48)$$

In other words, the $\hat{\mu}_l$ of several samples can be used to evaluate μ_l .

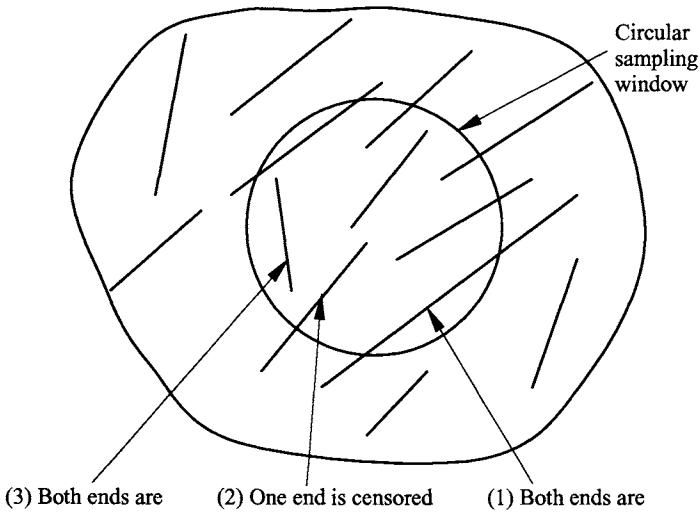


Fig. 4.21 Discontinuities intersecting a circular sampling window (after Zhang & Einstein, 1998).

When applying equation (4.47) or (4.48), the following two special cases may occur:

- (1) If $\hat{N}_o = \hat{N}$, then $\hat{\mu}_l \rightarrow \infty$. In this case, all the discontinuities intersecting the sampling window have both ends censored. This implies that the area of the window used for the discontinuity survey may be too small.
- (2) If $\hat{N}_2 = \hat{N}$, then $\hat{\mu}_l = 0$. In this case, all the discontinuities intersecting the sampling window have both ends observable. According to Pahl (1981), this results is due to violation of the assumption that the midpoints of traces are uniformly distributed in the two dimensional space.

These two special cases can be addressed by increasing the sampling window size and/or changing the sampling window position (Zhang, 1999). Another method to address these two special cases is to use multiple windows of the same size but at different locations and then use the total numbers from these windows to estimate $\hat{\mu}_l$ (Zhang & Einstein, 1998b).

(c) Trace length distribution on an infinite surface

Two probability density functions (*pdf*) can be defined for trace lengths as follows:

- (1) $f(l) = pdf$ of trace lengths on an infinite surface.

- (2) $g(l)$ = pdf of measured trace lengths on a finite exposure subjected to sampling biases.

It is necessary to obtain $f(l)$ from $g(l)$, because 3D size distribution of discontinuities is inferred from $f(l)$. Zhang and Einstein (2000) proposed the following procedure for obtaining $f(l)$:

- (1) Use the corrected mean trace length μ as the mean value of $f(l)$
- (2) Use the coefficient of variation (COV) value of $g(l)$ as the COV of $f(l)$
- (3) Find the distribution of $g(l)$ as discussed earlier and assume that $f(l)$ and $g(l)$ have the same distribution form

4.6.3 Discontinuity shape

The planar shape of discontinuities has a profound effect on the connectivity of discontinuities and on rock mass properties (Dershowitz et al., 1993; Petit et al., 1994). However, since a rock mass is usually inaccessible in three dimensions, the real discontinuity shape is rarely known. Information on discontinuity shape is limited and often open to more than one interpretation (Warburton, 1980a; Wathugala, 1991).

Discontinuities can be classified into two categories: unrestricted and restricted. Unrestricted discontinuities are blind and effectively isolated discontinuities whose growth has not been perturbed by adjacent geological structures such as faults and free surfaces. In general, the edge of unrestricted discontinuities is a closed convex curve. In many cases, the growth of discontinuities is limited by adjacent preexisting discontinuities and free surfaces. Such discontinuities are called restricted discontinuities. One way to represent restricted discontinuities is to use polygons, some of the polygon sides being those formed by intersections with the adjacent preexisting discontinuities and free surfaces.

Due to the mathematical convenience, many investigators assume that discontinuities are thin circular discs randomly located in space (Baecher et al., 1977; Warburton, 1980a; Chan, 1986; Villaescusa & Brown, 1992; Kulatilake, 1993). For circular discontinuities, the trace patterns in differently oriented sampling planes will be the same. In practice, however, the trace patterns may vary with the orientation of sampling planes (Warburton, 1980b). Therefore, Warburton (1980b) assumed that discontinuities in a set are parallelograms of various sizes. Dershowitz et al. (1993) used polygons to represent discontinuities in the FracMan discrete fracture code. The polygons are formed by inscribing a polygon in an ellipse. Ivanova (1998) and Meyer (1999) also used polygons to represent discontinuities in their discrete fracture code GeoFrac. It is noted that polygons can be used to effectively represent elliptical discontinuities when the number of polygon sides is large (say > 10) (Dershowitz et al., 1993). Zhang et al. (2002) assumed that discontinuities are elliptical and derived a general stereological relationship between trace length distributions and discontinuity size (expressed by the major axis length of the ellipse) distributions.

Many researchers infer the discontinuity shape from the study of trace lengths in both the strike and dip directions. Based on the fact that the average strike length of a discontinuity set is approximately equal to its average dip length, Robertson (1970) and Barton (1977) assumed that discontinuities are equidimensional (circular). However, the average strike length of a discontinuity set being the same as its average dip length does not necessarily mean that the discontinuities of such a set are equidimensional; instead, there exist the following three possibilities (Zhang et al., 2002):

1. The discontinuities are indeed equidimensional [see Fig. 4.22(a)].
2. The discontinuities are non-equidimensional such as elliptical or rectangular with long axes in a single (or deterministic) orientation. However, the discontinuities are oriented such that the strike length is approximately equal to the dip length [see Fig. 4.22(b)].
3. The discontinuities are non-equidimensional such as elliptical or rectangular with long axes randomly oriented. The random discontinuity orientation distribution makes the average strike length approximately equal to the average dip length [see Fig. 4.22(c)].

Therefore, the conclusion that discontinuities are equidimensional (circular) drawn from the fact that the average strike length of a discontinuity set is about equal to its average dip length is questionable. Investigators assume circular discontinuity shape possibly because of mathematical convenience.

Einstein et al. (1979) measured trace lengths of two sets of discontinuities on both the horizontal and vertical surfaces of excavations and found that discontinuities are non-equidimensional. Petit et al. (1994) presented results of a field study to determine the shape of discontinuities in sedimentary rocks. Pelites with isolated sandstone layers in the red Permian sandstones of the Lodeve Basin were studied. The exposed discontinuities (i.e., one of the discontinuity walls had been removed by erosion) appear as rough ellipses with a shape ratio L/H of about 2.0, where L and H are respectively the largest horizontal and vertical dimensions. For non-exposed discontinuities, the distributions of the dimensions of the horizontal and vertical traces were measured. The ratio of the mean L to the mean H of such traces is 1.9, which is very close to the L/H ratio of the observed individual discontinuity planes.

4.6.4 Discontinuity size

Zhang and Einstein (2000) presented a method for inferring the discontinuity size distribution from the corrected trace length distribution obtained from circular window sampling as described in Section 4.6.2, based on the stereological relationship between trace lengths and discontinuity diameter distributions for area sampling of discontinuities (Warburton, 1980a):

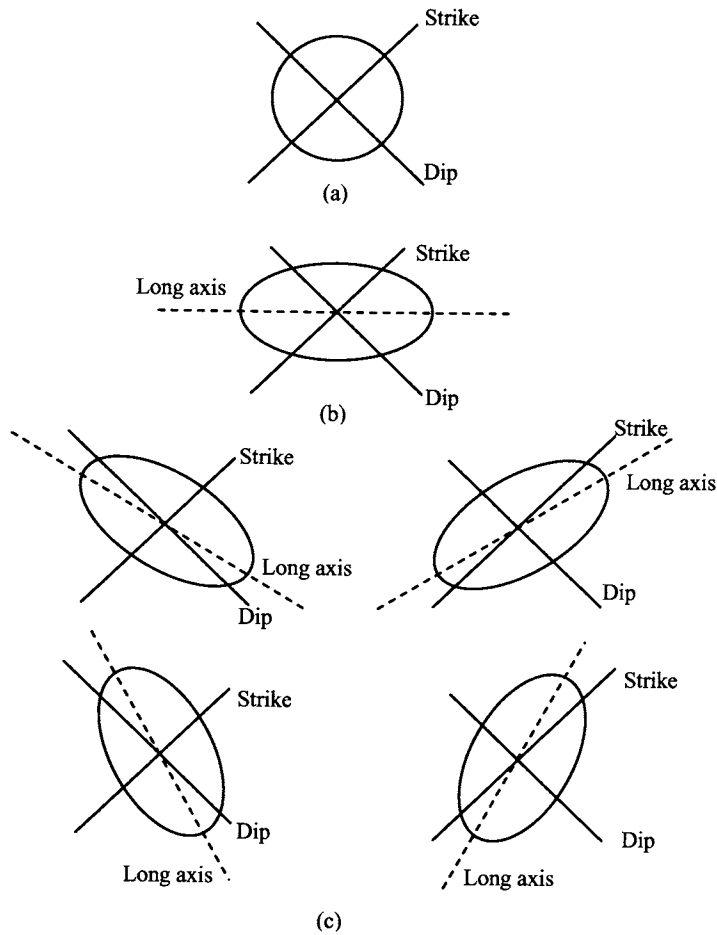


Fig. 4.22 Three possible cases for which the average strike length is about equal to the average dip length: (a) Discontinuities are equidimensional (circular); (b) Discontinuities are non-equidimensional (elliptical), with long axes in a single orientation. The discontinuities are oriented so that the strike length is about equal to the dip length; and (c) Discontinuities are non-equidimensional (elliptical), with long axes randomly orientated so that the average strike length is about equal to the average dip length (after Zhang et al., 2002).

$$f(l) = \frac{l}{\mu_D} \int_0^{\infty} \frac{g(D)}{\sqrt{D^2 - l^2}} dD \quad (4.49)$$

where D is the diameter of discontinuities; l is the trace length of discontinuities; $g(D)$ is the probability density function of the diameter of discontinuities; $f(l)$ is the probability density function of the trace length of discontinuities; and μ_D is the mean of the diameter of

discontinuities. Villaescusa and Brown (1992) presented a similar method for inferring the discontinuity size distribution from the corrected trace length distribution obtained from straight scanline sampling. They used the following stereological relationship between trace length and discontinuity diameter distributions for straight scanline sampling of discontinuities (Warburton, 1980a):

$$f(l) = \frac{4l^2}{\pi E(D^2)} \int_l^\infty \frac{g(D)}{\sqrt{D^2 - l^2}} dD \quad (4.50)$$

where $E(D^2)$ is the mean of D^2 .

Zhang et al. (2002) derived a general stereological relationship between trace length distributions and discontinuity size (expressed by the major axis length a of the ellipse) distributions for area (or window) sampling, following the methodology of Warburton (1980a, b):

$$f(l) = \frac{l}{M\mu_a} \int_{l/M}^\infty \frac{g(a)}{\sqrt{(Ma)^2 - l^2}} da \quad (l \leq aM) \quad (4.51)$$

where

$$M = \frac{\sqrt{\tan^2 \beta + 1}}{\sqrt{k^2 \tan^2 \beta + 1}} \quad (4.52)$$

in which k is the aspect ratio of the discontinuity, i.e., the length of the discontinuity minor axis is a/k (see Fig. 4.23); β is the angle between the discontinuity major axis and the trace line (note that β is measured in the discontinuity plane). Obviously, β will change for different sampling planes. For a specific sampling plane, however, there will be only one β value for a discontinuity set with a deterministic orientation.

When $k = 1$ (i.e., the discontinuities are circular), $M = 1$ and equation (4.51) reduces to equation (4.49).

Based on equation (4.51), Zhang et al. (2002) extended the method of Zhang and Einstein (2000) to elliptical discontinuities. Table 4.8 summarizes the expressions for determining the mean μ_a and standard deviation σ_a of discontinuity size a from the mean μ_l and standard deviation σ_l of trace length l , respectively for the lognormal, negative exponential and Gamma distribution of discontinuity size a . Conversely, with known μ_a and σ_a , and the distribution form of $g(a)$, μ_l and σ_l can also be obtained (see Table 4.9).

Consider a discontinuity set having a lognormal size distribution with $\mu_a = 8.0$ m and $\sigma_a = 4.0$ m (For other distribution forms, similar conclusions can be obtained). Fig. 4.24 shows the variation of the mean trace length and the standard deviation of trace

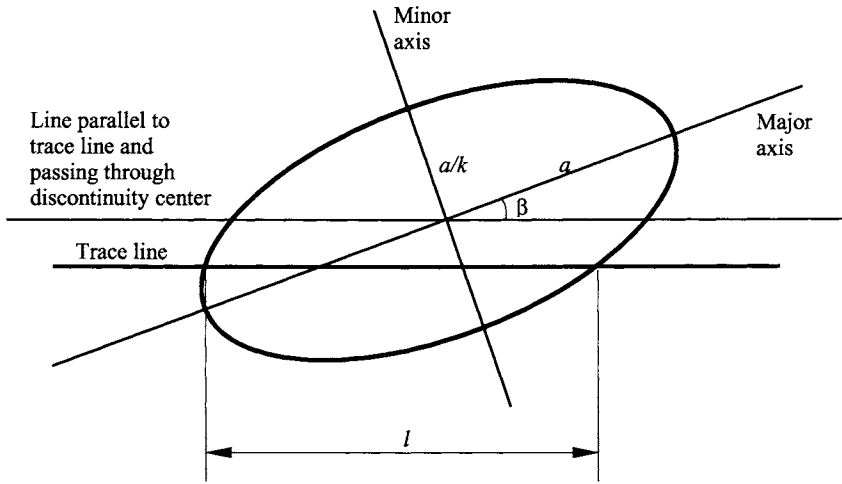


Fig. 4.23 Parameters used in the definition of an elliptical discontinuity (after Zhang et al., 2002).

Table 4.8 Expressions for determining μ_a and σ_a from μ_l and σ_l (after Zhang et al., 2002).

Distribution form of $g(a)$	μ_a	$(\sigma_a)^2$
Lognormal	$\frac{128(\mu_l)^3}{3\pi^3 M [(\mu_l)^2 + (\sigma_l)^2]}$	$\frac{1536\pi^2 [(\mu_l)^2 + (\sigma_l)^2] (\mu_l)^4 - 128^2 (\mu_l)^6}{9\pi^6 M^2 [(\mu_l)^2 + (\sigma_l)^2]^2}$
Negative exponential	$\frac{2}{\pi M} \mu_l$	$\left[\frac{2}{\pi M} \mu_l \right]^2$
Gamma	$\frac{64(\mu_l)^2 - 3\pi^2 [(\mu_l)^2 + (\sigma_l)^2]}{8\pi M \mu_l}$	$\frac{\{64(\mu_l)^2 - 3\pi^2 [(\mu_l)^2 + (\sigma_l)^2]\} \times \{3\pi^2 [(\mu_l)^2 + (\sigma_l)^2] - 32(\mu_l)^2\}}{64\pi^2 M^2 (\mu_l)^2}$

lengths with β . Since β is the angle between the trace line and the discontinuity major axis, it is related to the sampling plane orientation relative to the discontinuity. It can be seen that, despite the considerable difference between the maximum and the minimum, respectively, of the mean trace length and the standard deviation of trace lengths, there are extensive ranges of sampling plane orientations, reflected by β , over which both the mean trace length and the standard deviation of trace lengths show little variation, especially for large k values. The results in Fig. 4.24 could well explain why Bridges (1976), Einstein et al. (1979) and McMahon (Mostyn & Li, 1993) found different mean trace lengths on

Table 4.9 Expressions for determining μ_l and σ_l from μ_a and σ_a (after Zhang et al., 2002).

Distribution form of $g(a)$	μ_l	$(\sigma_l)^2$
Lognormal	$\frac{\pi M [(\mu_a)^2 + (\sigma_a)^2]}{4\mu_a}$	$\frac{32M^2 [(\mu_a)^2 + (\sigma_a)^2]^3 - 3\pi^2 M^2 (\mu_a)^2 [(\mu_a)^2 + (\sigma_a)^2]^2}{48(\mu_a)^4}$
Negative exponential	$\frac{\pi M}{2} \mu_a$	$\frac{(16 - \pi^2)M^2}{4} (\mu_a)^2$
Gamma	$\frac{\pi M [(\mu_a)^2 + (\sigma_a)^2]}{4\mu_a}$	$\frac{32M^2 [(\mu_a)^2 + (\sigma_a)^2] [(\mu_a)^2 + 2(\sigma_a)^2] - 3\pi^2 M^2 [(\mu_a)^2 + (\sigma_a)^2]^2}{48(\mu_a)^2}$

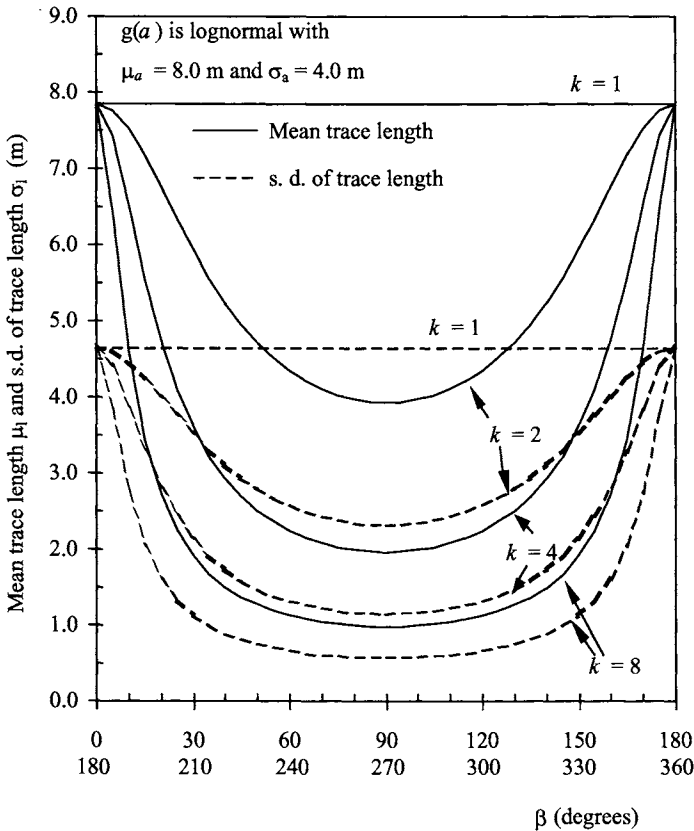


Fig. 4.24 Variation of mean trace length and standard deviation (s.d.) of trace length with β (after Zhang et al., 2002).

differently oriented sampling planes, whereas Robertson (1970) and Barton (1977) observed them to be approximately equal. In each of these papers or reports, the number of differently oriented sampling planes was very limited and, depending on the relative orientations of the sampling planes, the authors could observe either approximately equal mean trace lengths or significantly different mean trace lengths. For example, in Bridges (1976), Einstein et al. (1979) and McMahon (Mostyn & Li, 1993), the strike and dip sampling planes might be respectively in the $\beta = 0^\circ - 20^\circ$ (or $160^\circ - 180^\circ$) range and the $\beta = 40^\circ - 140^\circ$ range, or vice versa. From Fig. 4.24, this would result in very different mean trace lengths. On the other hand, in Robertson (1970) and Barton (1977), the strike and dip sampling planes might be both in the $\beta = 40^\circ - 140^\circ$ range (i.e., in the “flat” trace length part of Fig. 4.24) or respectively in some β ranges approximately symmetrical about $\beta = 90^\circ$. It should be noted that the comments above are assumptions because no information about the β values can be found in the original papers or reports.

The implications of Fig. 4.24 about field sampling are as follows:

If different sampling planes are used to collect trace (length) data, the sampling planes should be oriented such that significantly different mean trace lengths can be obtained from different planes. For example, if two sampling planes are used, one should be oriented in the $\beta = 0^\circ - 20^\circ$ (or $160^\circ - 180^\circ$) range and the other in the $\beta = 60^\circ - 120^\circ$ range.

It is noted that, with the same μ_l and σ_l , one can have different μ_a and σ_a if the assumed distribution form of $g(a)$ is different. This means that the estimation of discontinuity size distributions from the equations in Table 4.8 may not be robust. To overcome the problem of uniqueness, a relationship between the ratio of the 4th and 1st moments of the discontinuity size distribution and the 3rd moment of the trace length distribution is used to check the suitability of the assumed discontinuity size distribution form:

$$\frac{E(a^4)}{E(a)} = \frac{16E(l^3)}{3\pi M^3} \quad (4.53)$$

For the three distribution forms of $g(a)$ discussed above, equation (4.53) can be rewritten as:

(a) If $g(a)$ is lognormally distributed with mean μ_a and standard deviation σ_a ,

$$\frac{[(\mu_a)^2 + (\sigma_a)^2]^6}{(\mu_a)^9} = \frac{16E(l^3)}{3\pi M^3} \quad (4.54)$$

(b) If $g(a)$ has a negative exponential distribution with mean μ_a ,

$$24(\mu_a)^2 = \frac{16E(l^3)}{3\pi M^3} \quad (4.55)$$

(c) If $g(a)$ has a Gamma distribution with mean μ_a and standard deviation σ_a ,

$$\frac{[(\mu_a)^2 + (\sigma_a)^2][(\mu_a)^2 + 2(\sigma_a)^2][(\mu_a)^2 + 3(\sigma_a)^2]}{(\mu_a)^3} = \frac{16E(l^3)}{3\pi M^3} \quad (4.56)$$

The procedure for inferring the major axis orientation, aspect ratio k and size distribution $g(a)$ (probability density function of the major axis length a) of elliptical discontinuities from trace length sampling on different sampling windows is summarized as follows (The reader can refer to Zhang et al. 2002 for details):

1. Sampling

- (a) Trace length: Use two or more sampling windows at different orientations to conduct trace (length) sampling. The sampling windows (planes) should be oriented such that significantly different mean trace lengths can be obtained from different windows.
- (b) Orientation: Use exposed rock surface or borehole sampling so that the normal orientation of each discontinuity set can be obtained.
2. Conduct trace length analysis to estimate the true trace length distribution $f(l)$ on different sampling windows: μ_l , σ_l and form of $f(l)$.
3. Infer the major axis orientation, aspect ratio k and size distribution $g(a)$ of discontinuities from trace length sampling on different sampling windows:
 - (a) Assume a major axis orientation and compute the β (the angle between discontinuity major axis and trace line) value for each sampling window.
 - (b) For the assumed major axis orientation, compute μ_a and σ_a from μ_l and σ_l of each sampling window, by assuming aspect ratios $k = 1, 2, 4, 6, 8$ and lognormal, negative exponential and Gamma distribution forms of $g(a)$. The results are then used to draw the curves relating μ_a (and σ_a) to k , respectively, for the lognormal, negative exponential and Gamma distribution forms of $g(a)$.
 - (c) Repeat steps (a) and (b) until the curves relating μ_a (and σ_a) to k for different sampling windows intersect in one point. The major axis orientation for this case is the inferred actual major axis orientation. The k , μ_a and σ_a values at the intersection points are the corresponding possible characteristics of the discontinuities.
4. Find the best distribution form of $g(a)$ by checking the equality of equation (4.53). The k , μ_a and σ_a values found in Step (c) and corresponding to the best distribution form of $g(a)$ are the inferred characteristics of the discontinuity size.

4.7 FRACTURE TENSOR

Tensors have been used by several researchers to describe discontinuity geometry including intensity and orientation. Kachanov (1980) introduced a tensor α_{ij} to quantify the geometry of microcracks in rocks

$$\alpha_{ij} = \frac{1}{V} \sum_{k=1}^{m^{(V)}} [S^{(k)}]^{3/2} u_i^{(k)} u_j^{(k)} \quad (4.57)$$

where V is the volume of the rock mass considered; $S^{(k)}$ is the area of the k th discontinuity; $m^{(V)}$ is the number of discontinuities in volume V ; $u_i^{(k)}$ and $u_j^{(k)}$ ($i, j = x, y, z$) are components of the unit normal vector of the k th discontinuity with respect to orthogonal reference axes i and j ($i, j = x, y, z$) respectively (see Fig. 4.3 about the definition of the normal or pole direction of a discontinuity).

Oda (1982) also proposed a tensor F_{ij} (called the crack tensor) for describing discontinuity geometry

$$F_{ij} = \frac{1}{V} \sum_{k=1}^{m^{(V)}} S^{(k)} r^{(k)} u_i^{(k)} u_j^{(k)} \quad (4.58)$$

where $r^{(k)}$ is the radius of the k th discontinuity.

Kawamoto et al. (1988) regarded discontinuities as damages, and defined a tensor Ω_{ij} called the damage tensor

$$\Omega_{ij} = \frac{\bar{l}}{V} \sum_{k=1}^{m^{(V)}} S^{(k)} u_i^{(k)} u_j^{(k)} \quad (4.59)$$

where \bar{l} is a characteristic length for a given discontinuity system.

The tensors described above are non-dimensional due to some arbitrary operation included in their definitions: in equation (4.57) the area $S^{(k)}$ of a discontinuity is multiplied by the square root of $S^{(k)}$; in equation (4.58) the area $S^{(k)}$ of a discontinuity is multiplied by its radius $r^{(k)}$; and in equation (4.59) a characteristic length \bar{l} for a given discontinuity system is included. Because of the arbitrary operation, the physical meaning of the discontinuity intensity expressed by those definitions is not clear and thus a little confusing (e.g., what is the physical meaning of $[S^{(k)}]^{3/2}$?).

P_{32} , the mean area of discontinuities per unit volume of rock mass, as defined earlier, is the most useful measure of discontinuity intensity (Dershowitz & Herda, 1992; Mauldon, 1994). However, P_{32} does not include the effect of discontinuity orientations. Zhang (1999) and Zhang et al. (2002) introduced the fracture tensor F_{ij} , which is a combined measure of discontinuity intensity and orientation, defined as follows:

$$F_{ij} = \frac{1}{V} \sum_{k=1}^{m(V)} S^{(k)} u_i^{(k)} u_j^{(k)} \quad (4.60)$$

F_{ij} can be determined with the data obtained in the previous sections. Fracture tensor F_{ij} can also be written in a matrix form as follows

$$\mathbf{F}(F_{ij}) = \begin{bmatrix} F_{xx} & F_{xy} & F_{xz} \\ & F_{yy} & F_{yz} \\ \text{Sym.} & & F_{zz} \end{bmatrix} \quad (4.61)$$

F_{ij} has three principal values F_1 , F_2 and F_3 , which can be obtained by finding the eigenvalues of F_{ij} . The principal orientation of F_{ij} can be obtained by finding the eigenvectors corresponding to F_1 , F_2 and F_3 .

The first invariant of F_{ij} is just P_{32} , i.e.,

$$P_{32} = I_1^{(F)} = F_1 + F_2 + F_3 = F_{xx} + F_{yy} + F_{zz} \quad (4.62)$$

In contrast to the tensors proposed by Kachanov (1980), Oda (1982) and Kawamoto et al. (1988), the fracture tensor defined in equation (4.60) has a clear physical meaning. It represents the ratio of the total area of discontinuities and the volume of the rock mass considered. The fracture tensor defined in equation (4.60) keeps the advantage of P_{32} , i.e., P_{32} does not depend on the size of the sampled region as long as it is representative of the discontinuity network.

4.8 DISCONTINUITY ROUGHNESS

Roughness is a measure of the inherent surface unevenness and waviness of the discontinuity relative to its mean plane. The wall roughness of a discontinuity has an important influence on its shear strength, especially in the case of undisplaced and interlocked features such as unfilled joints. The importance of roughness declines with increasing aperture, filling thickness or previous shear displacement.

When the properties of discontinuities are being recorded from observations made on either boring cores or exposed faces, it is usual to distinguish between small-scale surface irregularity or unevenness and large-scale undulations or waviness of the surface (see Fig. 4.25). Each of these types of roughness may be quantified on an arbitrary scale of, say, one to five. Descriptive terms may also be used particularly in the preliminary stages of mapping. For example, ISRM (1978c) suggests that the terms listed in Table 4.10 and illustrated in Fig. 4.26 may be used to describe roughness on two scales – the small scale (several centimeters) and the intermediate scale (several

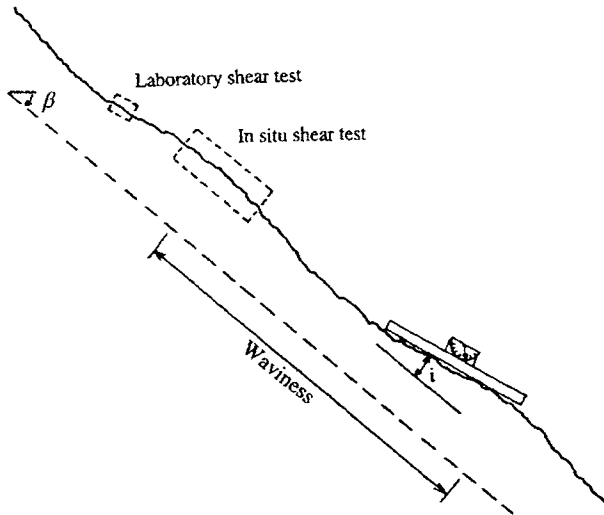


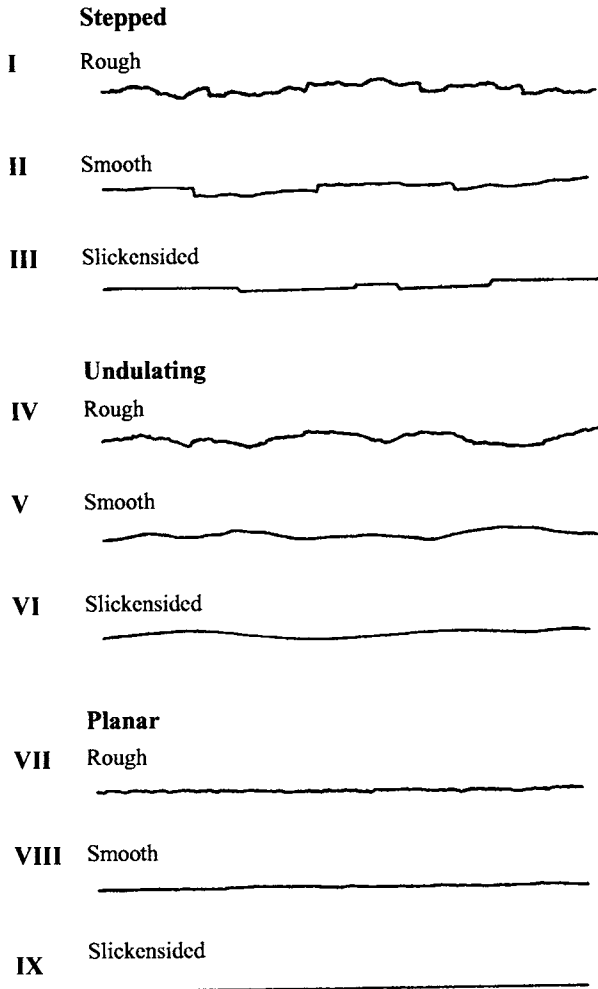
Fig. 4.25 Different scales of discontinuity roughness are sampled by different scales of test. Waviness can be characterized by the angle i (after ISRM, 1978c).

Table 4.10 Classification of discontinuity roughness (after ISRM, 1978c).

Class	Description
I	Rough or irregular, stepped
II	Smooth, stepped
III	Slickensided, stepped
IV	Rough or irregular, undulating
V	Smooth, undulating
VI	Slickensided, undulating
VII	Rough or irregular, planar
VIII	Smooth, planar
IX	Slickensided, planar

meters). Large-scale waviness may be superimposed on such small- and intermediate-scale roughness.

More detailed description of the methods for determining discontinuity roughness will be presented in Chapter 6.



4.26 Typical roughness profiles and suggested nomenclature. The length of each profile is in the range of 1 to 10 meters. The vertical and horizontal scales are equal (after ISRM, 1978c).

4.9 DISCONTINUITY APERTURE

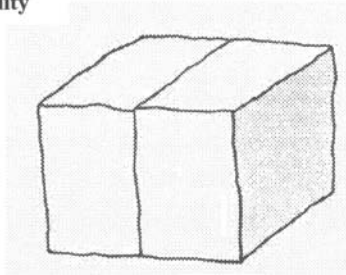
Aperture is the perpendicular distance separating the adjacent rock walls of an open discontinuity in which the intervening space is filled with air or water. Aperture is thereby distinguished from the width of a filled discontinuity (see Fig. 4.27). Large apertures can result from shear displacement of discontinuities having appreciable roughness, from outwash of filling materials (e.g. clay), from tensile opening, and/or from solution. In most subsurface rock masses, apertures are small, probably less than

half a millimeter. Table 4.11 lists terms describing aperture dimensions suggested by ISRM (1978c). Clearly, aperture and its areal variation will have an influence on the deformability, shear strength and hydraulic conductivity of discontinuities (see Chapters 6, 7 and 8 for details).

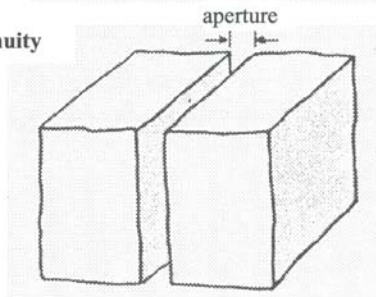
4.10 DISCONTINUITY FILLING

Filling is a term used to describe the material separating the adjacent rock walls of discontinuities, such as calcite, chlorite, clay, silt, fault gouge, breccia, quartz and pyrite. The perpendicular distance between the adjacent rock walls is termed the width of the filled discontinuity, as opposed to the aperture of a gapped or open discontinuity.

(a) Closed discontinuity



(b) Open discontinuity



(c) Filled discontinuity

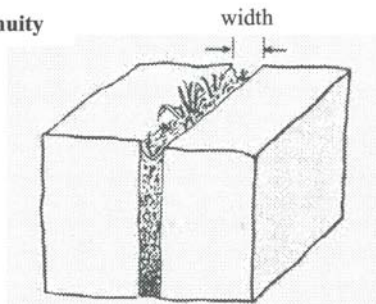


Fig. 4.27 Suggested definitions of the aperture of open discontinuities and the width of filled discontinuities (after ISRM, 1978c).

Table 4.11 Classification of discontinuity aperture (after ISRM, 1978c).

Description		Aperture (mm)
“Closed” features	Very tight	< 0.1
	Tight	0.1 – 0.25
	Partly open	0.25 – 0.5
“Gapped” features	Open	0.5 – 2.5
	Moderately wide	2.5 – 10
	Wide	> 10
“Open” features	Very wide	10 – 100
	Extremely wide	100 – 1000
	Cavernous	> 1000

Filling materials have a major influence on the shear strength of discontinuities. With the exception of discontinuities filled with strong vein materials (calcite, quartz, pyrite), filled discontinuities generally have lower shear strengths than comparable clean, closed discontinuities. The behavior of filled discontinuities depends on many factors of which the following are probably the most important:

- (1) Mineralogy of filling material
- (2) Grading or particle size
- (3) Over-consolidation ratio
- (4) Water content and permeability
- (5) Previous shear displacement
- (6) Wall roughness
- (7) Width

5

Rock masses

5.1 INTRODUCTION

The classification and index properties of intact rock and the characterization of rock discontinuities have been described respectively in Chapters 3 and 4. Field rock masses usually contain both intact rock and discontinuities. It is the properties of the rock mass (the combination of intact rock and discontinuities) that should be used in the design of a rock structure. This chapter describes different rock mass classification systems that are useful in the estimation of rock mass properties. The correlations between different classification indices are also presented. Finally, the classification of weathering of rocks is discussed in Section 5.4.

5.2 CLASSIFICATION OF ROCK MASSES

Numerous rock mass classification systems have been developed, including Terzaghi's Rock Load Height Classification (Terzaghi, 1946); Lauffer's Classification (Lauffer, 1958); Deere's Rock Quality Designation (RQD) (Deere, 1964); RSR Concept (Wickham et al., 1972); the Rock Mass Rating (RMR) system (Bieniawski, 1973, 1976, 1989); the Q-System (Barton et al., 1974); and the Geological Strength Index (GSI) system (Hoek & Brown, 1997). Most of these classification systems were primarily developed for the design of underground excavations. However, four of the above classification systems have been used extensively in the estimation of rock mass properties. These four classification systems are the RQD, the RMR, the Q-System, and the GSI.

5.2.1 *Rock quality designation (RQD)*

Rock Quality Designation (RQD) was introduced by Deere (1964) as an index assessing rock quality quantitatively. Table 5.1 shows the relationship between the RQD index and the rock mass quality. RQD can be determined directly by logging boring cores or indirectly by using different correlations such as the correlation between RQD and discontinuity frequency λ , and the correlation between RQD and seismic velocities. The different procedures for determining RQD have been discussed in detail in Chapter 4.

Table 5.1 Correlation between RQD and rock mass quality.

RQD (%)	Rock Mass Quality
< 25	Very poor
25 – 50	Poor
50 – 75	Fair
75 – 90	Good
90 – 100	Excellent

Although the RQD is a simple and inexpensive index, when considered alone it is not sufficient to provide an adequate description of a rock mass because it disregards discontinuity orientation, discontinuity condition, type of discontinuity filling and other features.

5.2.2 *Rock mass rating (RMR)*

The Rock Mass Rating (RMR) or the Geomechanics Classification System, proposed by Bieniawski (1973), was initially developed for tunnels. In recent years, it has been applied to the preliminary design of rock slopes and foundations as well as to the estimation of the in-situ deformation modulus and strength of rock masses. The RMR uses six parameters that are readily determined in the field (see Table 5.2):

- Unconfined compressive strength of the intact rock
- Rock Quality Designation (RQD)
- Spacing of discontinuities
- Condition of discontinuities
- Ground water conditions
- Orientation of discontinuities

All but the intact rock strength are normally determined in the standard geological investigations and are entered on an input data sheet. Table 5.3 shows the guidelines for assessing the discontinuity condition. The unconfined compressive strength of intact rock is determined in accordance with standard laboratory procedures but can be readily estimated in situ from the point-load strength index.

Rating adjustments for discontinuity orientation are summarized for underground excavations, foundations and slopes in Part B of Table 5.2. A more detailed explanation of these rating adjustments for dam foundations is given in Table 5.4, after ASCE (1996).

The six separate ratings are summed to give an overall RMR, with a higher RMR indicating better quality rock. Based on the observed RMR value, the rock mass is

Table 5.2 Geomechanics classification of jointed rock masses (after Bieniawski, 1989).

A. Classification parameters and their rating

Parameter		Range of values							
1	Strength of intact rock	Point-load strength index (MPa)	> 10	4-10	2-4	1-2	For this low range, unconfined compressive test is preferred		
		Unconfined compressive strength (MPa)	> 250	100-250	50-100	25-50	5-25	1-5	<1
	Rating	15	12	7	4	2	1	0	
2	Drill core quality RQD (%)		90-100	75-90	50-75	25-50	< 25		
	Rating		20	17	13	8	3		
3	Spacing of discontinuities (m)		> 2	0.6-2	0.2-0.6	0.06-0.2	< 0.06		
	Rating		20	15	10	8	5		
4	Conditions of discontinuities		Very rough surfaces, Not continuous, No separation, Unweathered wall rock	Slightly rough surfaces, separation < 1 mm, Slightly weathered walls	Slightly rough surfaces, separation < 1 mm, Highly weathered walls	Slickensided surfaces or Gouge < 5 mm thick or Separation 1-5 mm continuous	Soft gouge > 5 mm thick or Separation > 5 mm Continuous		
	Rating		30	25	20	10	0		
5	Ground water	Inflow per 10 m tunnel length (l/min)	None or	<10 or	10-25 or	25-125 or	>125 or		
		Ratio of joint water pressure to major principal stress	0 or	<0.1 or	0.1-0.2 or	0.2-0.5 or	>0.5 or		
		General conditions	Completely dry	Damp	Wet	Dripping	Flowing		
	Rating		15	10	7	4	0		

Table 5.2 (Continued).

B. Rating adjustment for joint orientations

Strike and dip orientations of discontinuities		Very favorable	Favorable	Fair	Unfavorable	Very Unfavorable
Ratings	Tunnels and mines	0	-2	-5	-10	-12
	Foundations	0	-2	-7	-15	-25
	Slopes	0	-5	-25	-50	-60

C. Rock mass classes and corresponding design parameters and engineering properties

Class No.	I	II	III	IV	V
RMR	100 - 81	80 - 61	60 - 41	40 - 21	< 20
Description	Very Good	Good	Fair	Poor	Very poor
Average stand-up time	20 years for 15 m span	1 year for 10 m span	1 week for 5 m span	10 hours for 2.5 m span	30 minutes for 1 m span
Cohesion of rock mass (MPa)	> 0.4	0.3 - 0.4	0.2 - 0.3	0.1 - 0.2	< 0.1
Internal friction angle of rock mass (°)	> 45	35 - 45	25 - 35	15 - 25	< 15
Deformation modulus (GPa) ^{a)}	> 56	56 - 18	18 - 5.6	5.6 - 1.8	< 1.8

^{a)} Deformation modulus values are from Serafim and Pereira (1983).

Table 5.3 Guidelines for classifying discontinuity condition (after Bieniawski, 1989).

Parameter		Range of values				
Discontinuity length (persistence/continuity)	Rating	6	4	2	1	0
	Measurement (m)	<1	1-3	3-10	10-20	>20
Separation (aperture)	Rating	6	5	4	1	0
	Measurement (mm)	None	<0.1	0.1-1	1-5	>5
Roughness	Rating	6	5	3	1	0
	Description	Very rough	Rough	Slight	Smooth	Slickensided
Infilling (gouge)	Rating	6	4	2	2	0
	Description and Measurement (mm)	None	Hard filling <5	Hard filling >5	Soft filling <5	Soft filling >5
Degree of weathering	Rating	6	5	3	1	0
	Description	None	Slight	Moderate	High	Decomposed

Note: Some conditions are mutually exclusive. For example, if infilling is present, it is irrelevant what the roughness may be, since its effect will be overshadowed by the influence of the gouge. In such cases, use Table 5.2 directly.

Table 5.4 Ratings for discontinuity orientations for dam foundations and tunneling (after ASCE, 1996).

A. Dam Foundations

Dip 0° – 10°	Dip 10° – 30°			
	Dip direction		Dip 30° – 60°	Dip 60° – 90°
	Upstream	Downstream		
Very favorable	Unfavorable	Fair	Favorable	Very unfavorable

B. Tunneling

Strike perpendicular to tunnel axis				Strike parallel to tunnel axis		Irrespective of strike
Drive with dip		Drive against dip		Dip 45° – 90°	Dip 20° – 45°	
Dip 45° – 90°	Dip 20° – 45°	Dip 45° – 90°	Dip 20° – 45°			
Very favorable	Favorable	Fair	Unfavorable	Very unfavorable	Fair	Fair

classified into five classes named as very good, good, fair, poor and very poor, as shown in Part C of Table 5.2. Also shown in Part C of Table 5.2 is an interpretation of these five classes in terms of roof stand-up time, cohesion, internal friction angle and deformation modulus for the rock mass.

Seismic velocity measurements can also be used to estimate RMR values. Based on the data of limestones, mudstones, marls and shales at a dam site in Wadi Mujib, Jordan, El-Naqa (1996) obtained the following empirical correlation between RMR and P-wave velocity:

$$\text{RMR} = 59.8 \times (v_{\text{pF}}/v_{\text{p0}})^{0.26} \quad (r = 0.84) \quad (5.1)$$

where v_{pF} is the P-wave velocity of the in situ rock mass; v_{p0} is the P-wave velocity of the corresponding intact rock; and r is the correlation coefficient.

Banks (2005) derived an empirical relation between the basic RMR and the slope angles in mature, natural rock outcrops:

$$\text{basic RMR} = 0.4S + 52 \quad (5.2)$$

where the basic RMR is the RMR without the adjustment to account for the influence that discontinuity orientations may have on the particular application; and S is the slope angle in mature, natural outcrops in degrees.

5.2.3 *Rock mass quality (Q)*

The Q-system, proposed by Barton et al. (1974), was developed specifically for the design of tunnel support systems. As the RMR system, the Q-system has been expanded to provide preliminary estimates of rock mass properties. The Q-system incorporates the following six parameters and the equation for obtaining rock mass quality Q:

- Rock Quality Designation (RQD)
- Number of discontinuity sets
- Roughness of the most unfavorable discontinuity
- Degree of alteration or filling along the weakest discontinuity
- Water inflow
- Stress condition

$$Q = \frac{\text{RQD}}{J_n} \times \frac{J_r}{J_a} \times \frac{J_w}{\text{SRF}} \quad (5.3)$$

where RQD = Rock Quality Designation; J_n = joint set number; J_r = joint roughness number; J_a = joint alteration number; J_w = joint water reduction number; and SRF = stress reduction number.

The meaning of the parameters used to determine the value of Q in equation (5.3) can be seen from the following comments by Barton et al. (1974):

The first quotient (RQD/J_n), representing the structure of the rock mass, is a crude measure of the block or particle size, with the two extreme values (100/0.5 and 10/20) differing by a factor of 400. If the quotient is interpreted in units of centimeters, the extreme 'particle sizes' of 200 to 0.5 cm are seen to be crude but fairly realistic approximations. Probably the largest blocks should be several times this size and the smallest fragments less than half the size. (Clay particles are of course excluded).

The second quotient (J_r/J_a) represents the roughness and frictional characteristics of the joint walls or filling materials. This quotient is weighted in favor of rough, unaltered joints in direct contact. It is to be expected that such surfaces will be close to peak strength, that they will dilate strongly when sheared, and they will therefore be especially favorable to tunnel stability.

When rock joints have thin clay mineral coatings and fillings, the strength is reduced significantly. Nevertheless, rock wall contact after small shear displacements have occurred may be a very important factor for preserving the excavation from ultimate failure.

Where no rock wall contact exists, the conditions are extremely unfavorable to tunnel stability. The 'friction angles' (given in Table 5.5) are a little below the residual strength values for most clays, and are possibly down-graded by the fact that these clay bands or fillings may tend to consolidate during shear, at least if normal consolidation or if softening and swelling has occurred. The swelling pressure of montmorillonite may also be a factor here.

The third quotient (J_w/SRF) consists of two stress parameters. SRF is a measure of: 1) loosening load in the case of an excavation through shear zones and clay bearing rock, 2) rock stress in competent rock, and 3) squeezing loads in plastic incompetent rocks. It can be regarded as a total stress parameter. The parameter J_w is a measure of water pressure, which has an adverse effect on the shear strength of joints due to a reduction in effective normal stress. Water may, in addition, cause softening and possible out-wash in the case of clay-filled joints. It has proved impossible to combine these two parameters in terms of inter-block effective stress, because paradoxically a high value of effective normal stress may sometimes signify less stable conditions than a low value, despite the higher shear strength. The quotient (J_w/SRF) is a complicated empirical factor describing the 'active stress'.

So the rock mass quality (Q) may be considered a function of three parameters which are approximate measures of:

- (i) Block size (RQD/J_n): It represents the overall structure of rock masses.
- (ii) Inter block shear strength (J_r/J_a): It represents the roughness and frictional characteristics of the joint walls or filling materials.
- (iii) Active stress (J_w/SRF): It is an empirical factor describing the active stress.

Table 5.5 provides the necessary guidance for assigning values to the six parameters. Depending on the six assigned parameter values reflecting the rock mass quality, Q can vary between 0.001 and 1000. Rock quality is divided into nine classes ranging from exceptionally poor (for Q from 0.001 to 0.01) to exceptionally good (for Q from 400 to 1000) as shown in Table 5.6.

Based on data from hard rock tunneling projects in several countries, Barton (1991) proposed a correlation between Q and P-wave velocity:

$$Q = 10^{v_p - 3.5} \quad (5.4)$$

where v_p is the P-wave velocity of the in situ rock mass in km/s.

Barton (2002) extended the above relation between Q and v_p to rocks that could be weaker or stronger than the assumed “hard” rock by introducing the normalized Q :

$$Q_c = Q \times \frac{\sigma_c}{100} \quad (5.5)$$

where Q_c is the normalized Q ; σ_c is the unconfined compressive strength of the intact rock; and 100 MPa is the σ_c assumed for the hard rock norm. The generalized $Q_c - v_p$ correlation is

$$Q_c = 10^{v_p - 3.5} \quad (5.6)$$

Based on the data of limestones, mudstones, marls and shales at a dam site in Wadi Mujib, Jordan, El-Naqa (1996) obtained the following empirical correlation between Q and P-wave velocity:

$$\ln Q = 2.61 \times (v_{pF}/v_{p0})^{0.97} \quad (r = 0.78) \quad (5.7)$$

where v_{pF} is the P-wave velocity of the in situ rock mass; v_{p0} is the P-wave velocity of the corresponding intact rock; and r is the correlation coefficient.

5.2.4 Geological strength index (GSI)

Hoek and Brown (1997) introduced the Geological Strength Index (GSI), both for hard and weak rock masses. Experienced field engineers and geologists generally show a liking for a simple, fast, yet reliable classification which is based on visual inspection of geological conditions. Hoek and Brown (1997) proposed such a practical classification for estimating GSI based on visual inspection alone (see Fig. 5.1). In this classification, there are five main qualitative classifications of rock mass structures:

Table 5.5 The Q-system and associated parameters RQD, J_n , J_r , J_a , SRF and J_w (after Barton et al., 1974).

Rock Quality Designation		
	RQD (%)	
Very poor	0 – 25	Note: (i) Where RQD is reported or measured to be <10 a nominal value of 10 is used to evaluate Q in equation (5.5) (ii) Take RQD to be nearest 5%
Poor	25 – 50	
Fair	50 – 75	
Good	75 – 90	
Excellent	90 – 100	
Joint Set Number		
	J_n	
Massive, none or few joints	0.5 – 1.0	Note: (i) For intersections use $(3.0 \times J_n)$ (ii) For portals use $(2.0 \times J_n)$
One joint set	2	
One joint set plus random	3	
Two joint sets	4	
Two joint sets plus random	6	
Three joint sets	9	
Three joint sets plus random	12	
Four or more joint sets, random, heavily jointed, 'sugar cube', etc	15	
Crushed rock, earthlike	20	
Joint Roughness Number		
	J_r	
(a) Rock wall contact and (b) Rock wall contact before 10 cm shear		Notes: (i) Add 1.0 if the mean spacing of the relevant joint set is greater than 3 m (ii) $J_r = 0.5$ can be used for planar slickensided joints having lineations, provided the lineations are favorably orientated
Discontinuous joint	4	
Rough or irregular, undulating	3	
Smooth, undulating	2	
Slickensided, undulating	1.5	
Rough and irregular, planar	1.5	
Smooth or irregular	1	
Slickensided, planar	0.5	
(c) No rock wall contact when sheared		
Zone containing clay minerals thick enough to prevent rock wall contact	1	
Sandy, gravelly or crushed zone thick enough to prevent rock wall contact	1	(nominal)
Joint Alternation Number		
	J_a	Approximate residual angle of friction (deg)
(a) Rock wall contact		
A. Tightly healed, hard, non-softening,	0.75	-

Table 5.5 (Continued).

impermeable filling, i.e. quartz or epidote		
B. Unaltered joint walls, surface staining only	1	25 – 35
C. Unaltered joint walls. Non-softening mineral coatings, sandy particles, clay-free disintegrated rock, etc.	2	25 – 30
D. Silty or sandy clay coatings, small clay fraction (non-softening)	3	20 – 25
E. Softening or low friction clay mineral coatings, i.e. kaolinite, mica. Also chlorite, talc, gypsum and graphite, etc, and small quantities of swelling clays (discontinuous coatings, 1 – 2 mm or less in thickness)	4	8 – 16
<i>(b) Rock wall contact before 10 cm shear</i>		
F. Sandy particles, clay free disintegrated rock, etc	4	25 – 30
G. Strongly over-consolidated, non-softening clay mineral fillings (continuous, < 5 mm in thickness)	6	16 – 24
H. Medium or low over-consolidation, softening, clay mineral fillings (continuous, < 5 mm in thickness)	8	12 – 16
J. Swelling clay fillings, i.e. montmorillonite (continuous, < 5 mm in thickness). Value of J_a depends on percentage of swelling clay-sized particles and access to water, etc	8 – 12	6 – 12
<i>(c) No rock wall contact when sheared</i>		
K. Zones or bands of disintegrated or crushed	6, 8 or 8 – 12	6 – 24

Table 5.5 (Continued).

	Joint Water Reduction Factor J_w	Approximate water pressure (kPa)
rock and clay (see G, H, J for description of clay condition)		
L. Zones or bands of silty or sandy clay, small clay fraction (non-softening)	5	-
M. Thick, continuous zones or bands of clay (see G, H, J for description of clay condition)	10, 13 or 13 – 20	6 – 24
A. Dry excavations or minor inflow, i.e. < 5 l/min locally	1	< 100
B. Medium inflow or pressure occasional outwash of joint fillings	0.66	100 – 250
C. Large inflow or high pressure in competent rock with unfilled joints	0.5	250 – 1000
D. Large inflow or high pressure, considerable occasional outwash of joint fillings	0.33	250 – 1000
E. Exceptionally high inflow or water pressure at blasting, decaying with time	0.1	> 1000
F. Exceptionally high inflow or water pressure continuing without decay	0.1 – 0.05	> 1000
Note:		
(i) Factors C-F are crude estimates. Increase J_w if drainage measures are installed		
(ii) Special problems caused by ice formation are not considered		
Stress Reduction Factor SRF		
(a) <i>Weakness zones intersecting excavation, which may cause loosening of rock mass when tunnel is excavated</i>		
A. Multiple occurrences of weakness zones containing clay or chemically disintegrated rock, very loose	10	Note: (i) Reduce these values by 25-50% if the relevant shear zones only influence but do not intersect the excavation

Table 5.5 (Continued).

surrounding rock (any depth)					
B. Single weakness zones containing clay or chemically disintegrated rock (depth of excavation < 50 m)			5		
C. Single weakness zones containing clay or chemically disintegrated rock (depth of excavation > 50 m)			2.5		
D. Multiple shear zones in competent rock (clay free), loose surrounding rock (any depth)			7.5		
E. Single shear zones in competent rock (clay free, depth of excavation < 50 m)			5		
F. Single shear zones in competent rock (clay free, depth of excavation > 50 m)			2.5		
G. Loose open joints, heavily jointed, or "sugar cube" etc (any depth)			5		
<i>(b) Competent rock, rock stress problems</i>					
	Strength/stress ratios				
	σ_c/σ_1	σ_t/σ_1			
H. Low stress, near surface	> 200	> 13	2.5	(ii)	If stress field is strongly anisotropic: when $5 < \sigma_1/\sigma_3 < 10$, reduce σ_c and σ_t to $0.8\sigma_c$ and $0.8\sigma_t$; when $\sigma_1/\sigma_3 > 10$, reduce σ_c and σ_t to $0.6\sigma_c$ and $0.6\sigma_t$. Where σ_c = unconfined compressive strength, σ_t = tensile strength, σ_1 and σ_3 = major and minor principal stresses.
J. Medium stress	200-10	13 - 0.66	1		
K. High stress, very tight structure (usually favorable to stability, maybe unfavorable to wall stability)	10 - 5	0.66 - 0.33	0.5 - 2.0		
L. Mild rock burst (massive rock)	5 - 2.5	0.33 - 0.16	5 - 10		
M. Heavy rock burst (massive rock)	< 2.5	< 0.16	10 - 20		
<i>(c) Swelling rock; chemical swelling activity depending on presence of water</i>					
P. Mild swelling rock pressure			5 - 10	(iii)	Few case records available where depth of crown below surface is less than span width. Suggest SRF increase from 2.5 to 5 for such cases (see H)
R. Heavy swelling rock pressure			10 - 15		

Table 5.6 Classification of rock mass based on Q-values (after Barton et al., 1974).

Group	Q	Classification
1	1000 – 400	Exceptionally good
	400 – 100	Extremely good
	100 – 40	Very good
	40 – 10	Good
2	10 – 4	Fair
	4 – 1	Poor
	1 – 0.1	Very poor
3	0.1 – 0.01	Extremely poor
	0.01 – 0.001	Exceptionally poor

- (i) Intact/Massive
- (ii) Blocky
- (iii) Very blocky
- (iv) Blocky/Disturbed
- (v) Disintegrated

Further, discontinuities are classified into 5 surface conditions which are similar to discontinuity conditions in RMR as described earlier:

- (i) Very good
- (ii) Good
- (iii) Fair
- (iv) Poor
- (v) Very poor

Based on the actual rock structure classification and the discontinuity surface condition, a block in the 5×5 matrix of Fig. 5.1 can be picked up and the corresponding GSI value can then be read from the figure. According to Hoek and Brown (1997), a range of values of GSI should be estimated in preference to a single value.

The GSI chart based on visual inspection has been commonly used by the rock mechanics community since it was developed. However, due to the lack of measurable parameters for describing the rock mass structures and the discontinuity surface conditions, it is possible for different persons to estimate different GSI values from the chart for the same rock mass, particularly for engineers with limited experience. Therefore, researchers have attempted to develop quantitative measures of the rock mass structures and the discontinuity surface conditions (Sonmez & Ulusay, 1999, 2002; Cai et al., 2003). Fig. 5.2 shows the quantitative GSI chart proposed by Sonmez and Ulusay (1999, 2002). The structure rating, SR, based on volumetric discontinuity frequency λ_v , is introduced to describe the rock mass structure. The surface condition rating, SCR, estimated from

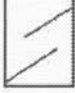




<p>Geological Strength Index (GSI)</p> <p>From the description of structure and surface conditions of the rock mass, pick an appropriate box in this chart. Estimate the average value of GSI from the contours. Do not attempt to be too precise. Quoting a range of GSI from 36 to 42 is more realistic than stating that GSI = 38.</p>		<p>Surface conditions</p> <p>Very good Very rough and fresh unweathered surfaces</p> <p>Good Rough, maybe slightly weathered or iron stained surfaces</p> <p>Fair Smooth and/or moderately weathered and altered surfaces</p> <p>Poor Slitkenisided or highly weathered surfaces or compact coatings with fillings of angular fragments</p> <p>Very poor Slitkenisided and highly weathered surfaces with soft clay coatings or fillings</p> <p>Decreasing surface quality ⇒</p>				
<p>Structure</p>		<p>⇒</p>				
	<p>Intact/Massive – Intact rock specimens or massive in-situ rock masses with very few widely spaced discontinuities</p>	90			N/A	N/A
	<p>Blocky – very well interlocked undisturbed rock mass consisting of cubical blocks formed by three orthogonal discontinuity sets</p>	80	70			
	<p>Very Blocky –interlocked, partially disturbed rock mass with multifaceted angular blocks formed by four or more discontinuity sets</p>		60	50		
	<p>Blocky/Disturbed – folded and/or faulted with angular blocks formed by many intersecting discontinuity sets</p>			40	30	
	<p>Disintegrated – poorly interlocked, heavily broken rock mass with a mixture of angular and rounded rock pieces</p>				20	10
<p>⇓</p>		<p>⇓</p>				

Fig. 5.1 Characterization of rock masses on the basis of interlocking and joint alteration (after Hoek & Brown, 1997).

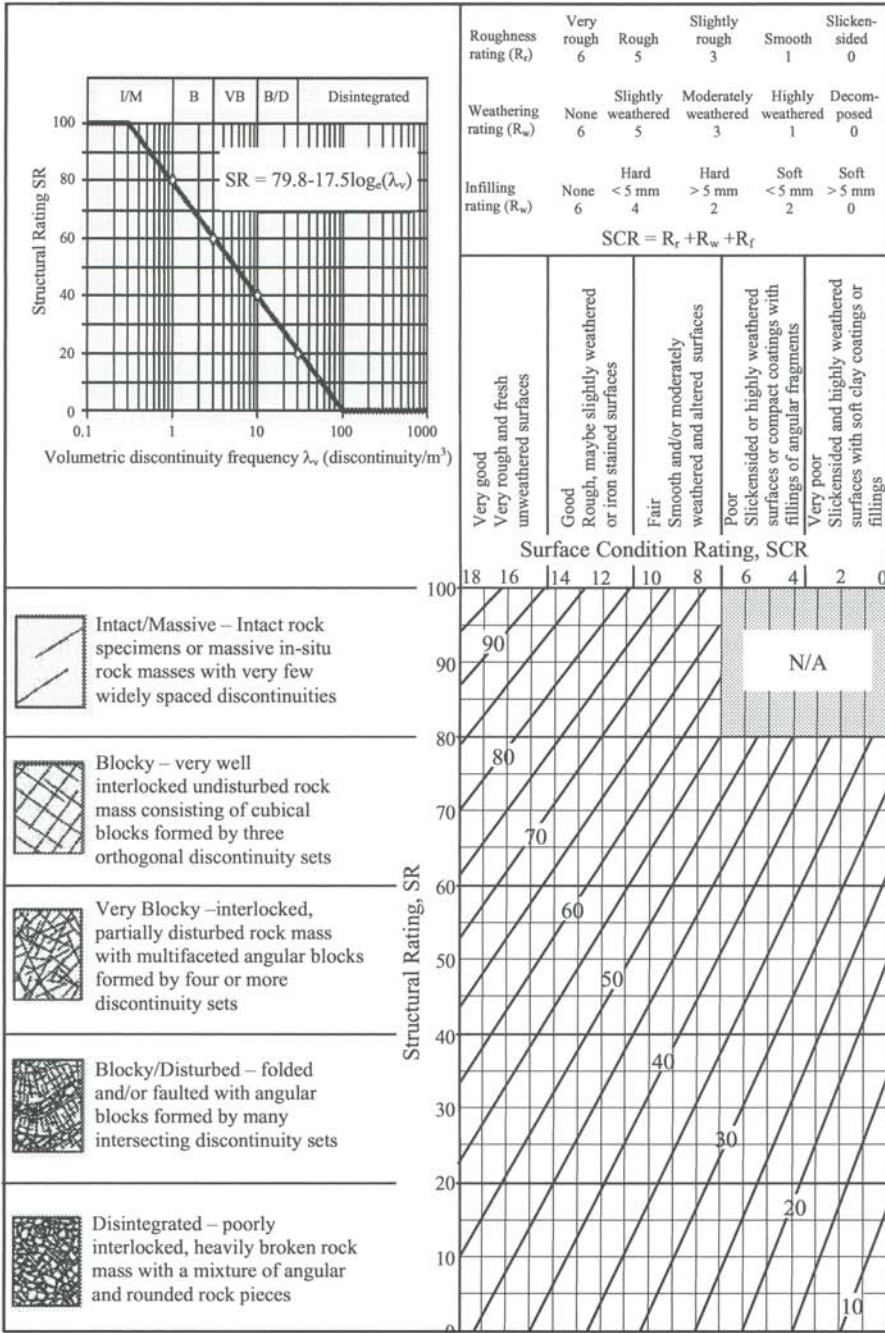


Fig. 5.2 Quantification of GSI chart by Sonmez and Ulusay (1999, 2002).

roughness, weathering and infilling conditions, is introduced to describe the discontinuity surface conditions. The volumetric discontinuity frequency λ_v and discontinuity roughness and infilling conditions can be evaluated as described in Chapter 4. The weathering condition can be evaluated using the methods presented in Section 5.4.

Cai et al. (2003) used quantitative block volume V_b and discontinuity condition factor J_c to describe, respectively, the rock mass structures and the discontinuity surface conditions. The block volume V_b can be estimated using the methods presented in Chapter 4. For the discontinuity condition factor J_c , Cai et al. (2003) presented a method for estimating it from the large-scale waviness, the small-scale smoothness and the joint alternation factor.

5.3 CORRELATIONS BETWEEN DIFFERENT CLASSIFICATION INDICES

Since the Q and RMR systems are based on much the same properties, they are highly correlated and can be predicted one from the other. Various researchers give relationships between Q and RMR in the following general form (Bieniaswki, 1976, 1989; Rutledge & Preston, 1978; Cameron-Clarke & Budavari, 1981; Abad et al., 1984; Goel et al., 1996):

$$\text{RMR} = A \ln Q + B \quad (5.8)$$

where A is typically in the range 5 – 15; and B in the range 40 – 60 (see Table 5.7).

Table 5.7 Empirical correlations between RMR and Q.

Correlation	Reference
$\text{RMR} = 9.0 \ln Q + 44$	Bieniaswki (1976), Jethwa et al. (1982)
$\text{RMR} = 5.9 \ln Q + 43$	Rutledge & Preston (1978)
$\text{RMR} = 5.4 \ln Q + 55$	Moreno (1980)
$\text{RMR} = 4.6 \ln Q + 56$ (Drill core)	Cameron-Clarke & Budavari (1981)
$\text{RMR} = 5.0 \ln Q + 61$ (In situ results)	
$\text{RMR} = 10.5 \ln Q + 42$	Abad et al. (1984)
$\text{RMR} = 8.7 \ln Q + 38$	Kaiser et al. (1986)
$\text{RMR} = 9.1 \ln Q + 45$	Trunk & Hömisch (1990)
$\text{RMR} = 7.0 \ln Q + 41$ (Bore cores)	El-Naqa (1994)
$\text{RMR} = 7.0 \ln Q + 44$ (Scanlines)	
$\text{RMR} = 15 \ln Q + 50$	Barton (1995)

Noting that the Q and RMR systems are not truly equivalent (e.g. the RMR system does not consider the stress condition of the rock mass, while the Q system does not consider discontinuity orientation and intact rock strength), Goel et al. (1996) developed a new type of empirical correlation between RMR and Q by introducing two new rock mass indices RCR and N :

$$\text{RCR} = 8 \ln N + 30 \quad (r = 0.92) \quad (5.9)$$

where RCR is the rock condition rating defined as RMR without rating for discontinuity orientation and intact rock strength; and N is the rock mass number defined as Q with SRF as 1.

GSI can also be estimated from RMR and Q (Hoek & Brown, 1997). When using Bieniawski's 1989 Rock Mass Rating (see Part A of Table 5.2) to estimate the value of GSI, the rock mass should be assumed to be completely dry and a rating of 15 assigned to the groundwater value. Very favorable discontinuity orientations should be assumed and the Adjustment for Discontinuity Orientation value set to zero. The minimum value which can be obtained for the 1989 classifications is 23. The estimated RMR is used to estimate the value of GSI as follows:

$$\text{GSI} = \text{RMR} - 5 \quad (5.10)$$

The Q value of Barton et al. (1974) can be used to estimate the value of GSI as follows:

$$\text{GSI} = 9 \ln Q + 44 \quad (5.11)$$

where Q is calculated from equation (5.3) by setting a value of 1 for both J_w (discontinuity water reduction factor) and SRF (stress reduction factor).

5.4 CLASSIFICATION OF WEATHERING OF ROCK

Weathering is the process of alteration of rock brought about by physical disintegration, chemical decomposition and biological activity. Weathering leads to change of the engineering properties of a rock at varying degrees depending on the stages of weathering. The early stages of weathering usually are represented by discoloration of the rock material, which increases from slightly to highly discolored as the degree of weathering increases. As weathering proceeds, the rock material becomes increasingly decomposed and/or disintegrated until a soil is formed. Various classification schemes have been proposed for classifying the weathering grades of rock masses, based on the presence or absence of discoloration in rock material, the rock to soil ratio, and the presence or absence of relict rock fabric in the groups which are predominantly soil (Bell, 1987). Classification of weathered rocks helps in better understanding their engineering behavior, allows samples to be grouped for description and for

geotechnical models to be developed, and ensures the best use of the geotechnical data determined in that index properties can be related to engineering properties (Anon, 1995)

There exist different classification schemes for classifying the weathering grades of rock masses. Table 5.8 shows the general weathering categories and grades suggested by ISRM (1978c), which may be modified to suit particular situations. Fig. 5.3 shows different classifications of weathering grades of rock masses. Some grades of weathering may not be seen in a given rock mass, and, in some cases, a particular grade may be present to a very small extent.

The classifications of weathering grades presented in Table 5.8 and Fig. 5.3 are qualitative only. Quantitative classifications of weathering grades using index properties are also developed by different researchers. Irfan and Dearman (1978) suggested that quick absorption, Schmidt hammer and point load strength tests could be used to determine a weathering index for granite as illustrated in Table 5.9.

Table 5.10 lists the measured total porosity and dry density of granitic rocks in the Northwest of Turkey at different weathering stages (Arel & Onalp, 2004).

Table 5.11 shows the relationship between weathering and RQD for rocks at the Gilgel Gibe hydropower project site located in the western part of Ethiopia (Ayalew et al., 2002).

Table 5.8 Weathering grade of rock mass (after ISRM, 1978c).

Term	Description	Grade
Fresh rock	No visible sign of rock material weathering; perhaps slight discoloration on major discontinuity surfaces.	I
Slightly weathered	Discoloration indicates weathering of rock material and discontinuity surfaces. All the rock material may be discolored by weathering and the external surface may be somewhat weaker than in its fresh condition.	II
Moderately weathered	Less than half of the rock material is decomposed and/or disintegrated to soil. Fresh or discolored rock is present either as continuous framework or as corestones.	III
Highly weathered	More than half of the rock material is decomposed and/or disintegrated to soil. Fresh or discolored rock is present either as discontinuous framework or as corestones.	IV
Completely weathered	All rock material is decomposed and/or disintegrated to soil. The original mass structure is still largely intact.	V
Residual soil	All rock material is converted to soil. The mass structure and material fabric are destroyed. There is a large change in volume, but the soil has not been significantly transported.	VI

	Love (1951) & Little (1961)	Vargas (1951)	Sowers (1954, 1963)	Chandler (1969)	Geological Soci. Eng. Group (1970)	Deere & Patton (1971)		
Schematic profile	Igneous rocks	Ignics, basaltics & sandstones	Igneous & metamorphic rocks	Marl & limolites	Igneous rocks	Igneous & metamorphic rocks		
	VI Soil	Residual soil	Upper zone	V Completely weathered	VI Residual soil	IA Horizon		
	V Completely weathered	Young residual soil	Intermediate zone		IV	V Completely weathered	Residual soil	IB Horizon
	IV Highly weathered	Disintegrated soil layers	Partially weathered zone		III		IV Highly weathered	Transition zone
	III Moderately weathered				II	III Moderately weathered		
	II Slightly weathered			II Weakly weathered				
	I Fresh rock	Fresh rock	Unweathered rock	I Unweathered rock	IB Softly weathered	Fresh rock		
					IA Fresh rock			

Fig. 5.3 Different classifications of weathering grades (after Oteo, 2002).

Table 5.9 Weathering indices for granite (after Irfan & Dearman, 1978).

Term	Quick absorption (%)	Bulk density (Mg/m^3)	Point load strength (MPa)	Unconfined compressive strength (MPa)
Fresh	< 0.2	2.61	> 10	> 250
Partially stained*	0.2-1.0	2.56-2.61	6-10	150-250
Completely stained*	1.0-2.0	2.51-2.56	4-6	100-150
Moderately weathered	2.0-10.0	2.05-2.51	0.1-4	2.5-100
Highly/completely weathered	> 10.0	< 2.05	< 0.1	< 2.5

* Slightly weathered

Table 5.10 Total porosity and dry density of granitic rocks at different weathering stages (after Arel & Onalp, 2004).

Grade	Term	Total porosity n (%)	Dry density ρ_d (Mg/m^3)
I	Fresh rock	3.48	2.63
II	Slightly weathered	3.57	2.59
III	Moderately weathered	4.65	2.46
IV	Highly weathered	5.42	2.38
V	Completely weathered	9.08	2.30
VI	Residual soil	15.5	2.00

Table 5.11 The relationship between weathering and RQD (after Ayalew et al., 2002).

Grade	Term	RQD (%)
I	Discolored (Fresh rock)	66-100
II	Slightly weathered	41-65
III	Moderately weathered	16-40
IV	Highly weathered	9-15
V	Decomposed (Completely weathered)	0-8

6

Deformability

6.1 INTRODUCTION

The deformation modulus of rock masses is used in the design of many structures in or on rock, from underground openings to foundations (Deere et al., 1967; Dershowitz et al., 1979; Bieniawski, 1978; Wyllie, 1999). Determination of rock mass deformation modulus is an important task in rock mechanics and rock engineering.

The presence of discontinuities has long been recognized as an important factor influencing the deformability of rock masses. Compared to intact rock, jointed rock masses show increased deformability. Therefore, determination of rock mass deformation modulus should consider not the deformability of the intact rock but also that of the discontinuities.

Since a rock mass seldom behaves as an ideal elastic material, its modulus is dependent upon the proportion of the stress-strain response considered. Fig 6.1 shows a stress-strain curve typical of an in-situ rock mass containing discontinuities with the various moduli that can be obtained. Although the curve, as shown, is representative of a jointed mass, it is also typical of intact rock except that the upper part of the curve tends to be concaved downward at stress levels approaching failure. As can be seen in Fig. 6.1 there are at least four portions of the stress-strain curve that can be used for determining in-situ rock mass moduli: the initial tangent modulus, the elastic modulus, the recovery modulus, and the deformation modulus (ASCE, 1996; ASTM, 2004):

- a. *Initial tangent modulus.* The initial tangent modulus is determined from the slope of a line constructed tangent to the initial concave upward section of the stress-strain curve (i.e. line 1 in Fig. 6.1). The initial curved section reflects the effects of discontinuity closure in in-situ tests and micro-crack closure in tests on small laboratory specimens.
- b. *Elastic modulus.* Upon closure of discontinuities/micro-cracks, the stress-strain curve becomes essentially linear. The elastic modulus, frequently referred to as the modulus of elasticity, is derived from the slope of this linear (or near linear) portion of the curve (i.e. line 2 in Fig. 6.1). In some cases, the elastic modulus is derived from the slope of a line constructed tangent to the stress-strain curve at some specified stress level. The stress level is usually specified as 50 percent of the maximum or peak stress.

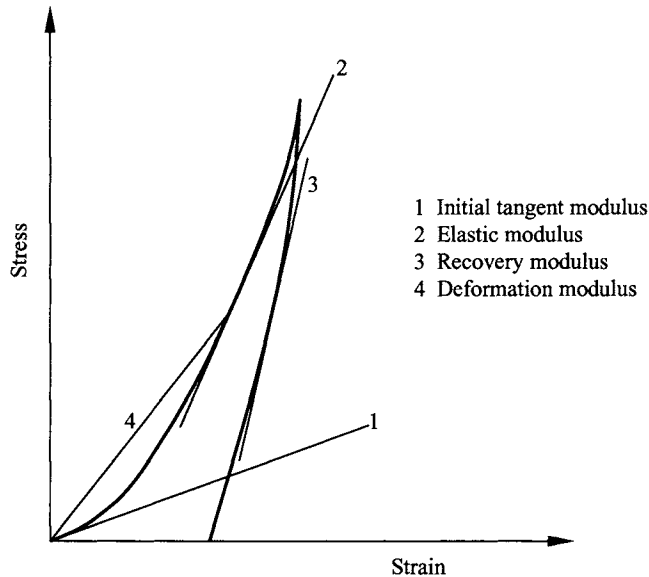


Fig. 6.1 Stress-strain curve typical of in-situ rock mass with various moduli that can be obtained (after ASCE, 1996; ASTM, 2004).

- c. Recovery modulus.* The recovery modulus is obtained from the slope of a line constructed tangent to the segment of the unloading stress-strain curve (i.e. line 3 in Fig. 6.1). As such, the recovery modulus is primarily derived from in-situ tests where test specimens are seldom stressed to failure.
- d. Deformation modulus or Secant modulus.* The deformation modulus is determined from the slope of the secant line established between zero and some specified stress level (i.e. line 4 in Fig. 6.1). The stress level is usually specified as 50 percent of the maximum or peak stress.

Since the actual jointed rock masses do not behave elastically, deformation modulus is usually used in practice.

6.2 DEFORMABILITY OF INTACT ROCK

Fig. 3.1 in Chapter 3 shows the range of the elastic modulus of different rocks. Tables 6.1 and 6.2 list the typical values of the elastic modulus and Poisson's ratio of different rocks.

The usual method for determining the elastic modulus of intact rock is to perform unconfined compression tests on pieces of rock core obtained from drilling using a diamond core barrel (ISRM, 1979a; ASTM, 2004). Since standard sample preparation is time consuming and expensive, indirect tests are also often conducted to estimate the

Table 6.1 Typical values of elastic modulus of intact rocks (after AASHTO, 1989).

Rock type	No. of values	No. of rock types	Elastic modulus (GPa)			Standard Deviation
			Maximum	Minimum	Mean	
Granite	26	26	100	6.41	52.7	24.5
Diorite	3	3	112	17.1	51.4	42.7
Gabbro	3	3	84.1	67.6	75.8	6.69
Diabase	7	7	104	69.0	88.3	12.3
Basalt	12	12	84.1	29.0	56.1	17.9
Quartzite	7	7	88.3	36.5	66.1	16.0
Marble	14	13	73.8	4.00	42.6	17.2
Gneiss	13	13	82.1	28.5	61.1	15.9
Slate	11	2	26.1	2.41	9.58	6.62
Schist	13	12	69.0	5.93	34.3	21.9
Phyllite	3	3	17.3	8.62	11.8	3.93
Sandstone	27	19	39.2	0.62	14.7	8.21
Siltstone	5	5	32.8	2.62	16.5	11.4
Shale	30	14	38.6	0.007	9.79	10.0
Limestone	30	30	89.6	4.48	39.3	25.7
Dolostone	17	16	78.6	5.72	29.1	23.7

Table 6.2 Typical values of Poisson's ratio of intact rocks (after AASHTO, 1989).

Rock type	No. of values	No. of rock types	Poisson's ratio			Standard Deviation
			Maximum	Minimum	Mean	
Granite	22	22	0.39	0.09	0.20	0.08
Gabbro	3	3	0.20	0.16	0.18	0.02
Diabase	6	6	0.38	0.20	0.29	0.06
Basalt	11	11	0.32	0.16	0.23	0.05
Quartzite	6	6	0.22	0.08	0.14	0.05
Marble	5	5	0.40	0.17	0.28	0.08
Gneiss	11	11	0.40	0.09	0.22	0.09
Schist	12	11	0.31	0.02	0.12	0.08
Sandstone	12	9	0.46	0.08	0.20	0.11
Siltstone	3	3	0.23	0.09	0.18	0.06
Shale	3	3	0.18	0.03	0.09	0.06
Limestone	19	19	0.33	0.12	0.23	0.06
Dolostone	5	5	0.35	0.14	0.29	0.08

elastic modulus by using empirical correlations. Table 6.3 lists a number of empirical correlations between the elastic modulus and the Schmidt hammer rebound number.

The propagation velocity of elastic waves measured on intact rock is usually used to calculate the *dynamic* elastic properties:

$$v_{\text{dyn}} = \frac{(v_p/v_s)^2 - 2}{2[(v_p/v_s)^2 - 1]} \quad (6.1)$$

$$E_{\text{dyn}} = \frac{\rho v_p^2 (1 - 2v_{\text{dyn}})(1 + v_{\text{dyn}})}{1 - v_{\text{dyn}}} \quad (6.2)$$

$$G_{\text{dyn}} = \rho v_s^2 \quad (6.3)$$

$$E_{\text{dyn}} = 2G_{\text{dyn}}(1 + v_{\text{dyn}}) \quad (6.4)$$

where v_{dyn} is the dynamic Poisson's ratio; v_p is the velocity of the P-wave; v_s is the velocity of the S-wave; G_{dyn} is the dynamic shear modulus; ρ is the density; and E_{dyn} is the dynamic elastic modulus.

Table 6.3 Correlations between elastic modulus E and Schmidt hammer rebound number R_n .

Correlation	r^2	Rock Type	Reference
$E = 0.6005\rho R_{n(L)} - 2.0276$		28 lithological units, 3 base rock types	Deere & Miller (1966)
$E = 0.0069 \times 10^{[1.0611\log(\rho R_{n(L)})+1.861]}$		25 lithological units	Aufmuth (1973)
$E = 0.192\rho^2 R_{n(L)} - 12.71$		20 lithological units	Beverly et al. (1979)
$E = 1.940R_{n(L)} - 33.92$	0.78	Marble, limestone, dolomite	Sachpazis (1990)
$E = e^{cR_{n(L)}+d}$ <i>c</i> and <i>d</i> are coefficients depending on rock type	0.77 0.92	Mica-schist, prasinite, to serpentinite, gabbro, mudstone	Xu et al. (1990)
$E = 0.00013R_{n(N)}^{3.09074}$	0.99	Chalk, limestone, sandstone, marble, syenite, granite	Katz et al. (2000)
$E = e^{0.054R_{n(L)}+1.146}$	0.90	Gypsum	Yilmaz & Sendir (2002)
$E = 0.47R_{n(L)} - 6.25$	0.85	Andesita, tuff, Basalt	Dincer et al. (2004)

Notes: E is in the unit of GPa; ρ is the rock density in g/cm^3 ; $R_{n(L)}$ and $R_{n(N)}$ are, respectively, the L- and N-type Schmidt hammer rebound numbers (see Chapter 3 for detailed description of Schmidt hammer rebound tests); and r^2 is the determination coefficient..

The dynamic elastic modulus calculated from equations (6.1) to (6.4) is usually larger than the static elastic modulus. Fig. 6.2 shows the ratio of dynamic elastic modulus to static elastic modulus compiled by Stacey et al. (1987). The ratio varies between about 1 and 3.

Table 6.4 lists some of the closed-form empirical correlations between static and dynamic moduli. It is noted that different correlations may give very different static

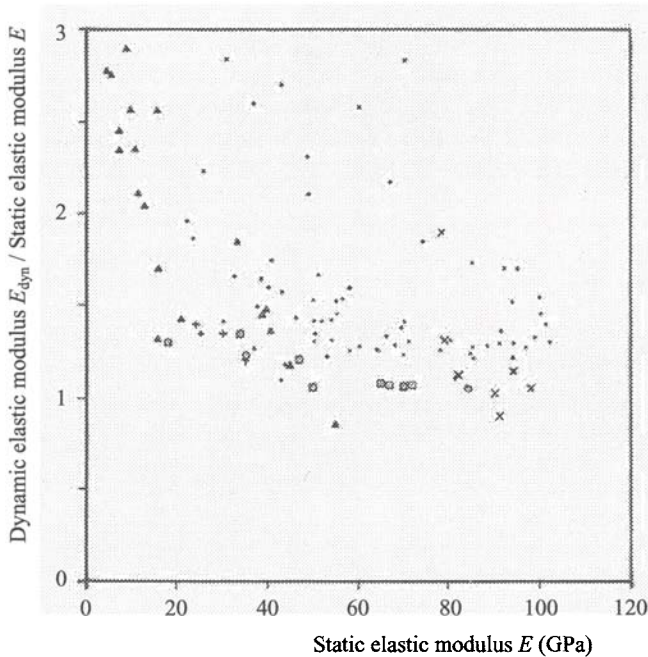


Fig. 6.2 Comparison of static and dynamic elastic modulus (after Stacey et al., 1987).

Table 6.4 Correlations between static modulus E and dynamic modulus E_{dyn} .

Correlation	Rock Type	Reference
$E = 1.137E_{\text{dyn}} - 9.685$	Granite	Belikov et al. (1970)
$E = 1.263E_{\text{dyn}} - 29.5$	Igneous & metamorphic rocks	King (1983)
$E = 0.64E_{\text{dyn}} - 0.32$	Different rocks	Eissa & Kazi (1988)
$E = 0.69E_{\text{dyn}} + 6.40$	Granite	McCann & Entwisle (1992)
$E = 0.48E_{\text{dyn}} - 3.26$ ($r^2 = 0.82$)	Crystalline rocks	McCann & Entwisle (1992)

Notes: Both E and E_{dyn} are in the unit of GPa; and r^2 is the determination coefficient.

modulus values. To obtain reliable results for a specific site, a series of tests need be carried out to calibrate the correlation to be used for the site.

Based on regression analysis of test data for dolomite, marble and limestone, Yasar and Erdogan (2004b) derived the following simple correlation between static elastic modulus and P-wave velocity:

$$E = 10.67v_p - 18.71 \quad (r^2 = 0.86) \quad (6.5)$$

where E is the static elastic modulus (GPa); v_p is the P-wave velocity (km/s); and r^2 is the determination coefficient.

The elastic modulus decreases as the porosity increases. Leite and Ferland (2001) derived a linear empirical correlation between elastic modulus E and porosity n based on test results of artificial porous rocks:

$$E = 10.10 - 0.109n \quad (r^2 = 0.74) \quad (6.6)$$

where E is in the unit of GPa and n is in %; and r^2 is the determination coefficient.

Lashkaripour (2002), however, derived a negative exponential relationship between elastic modulus E and porosity n based on test results of mudrocks including claystone, clay shale, mudstone, mud shale, siltstone and silt shale:

$$E = 37.9e^{-0.863n} \quad (r^2 = 0.68) \quad (6.7)$$

where E is in the unit of GPa and n is in %; and r^2 is the determination coefficient.

Fig 6.3 shows the variation of elastic modulus E with porosity n for dolomites and limestones (Palchik & Hatzor, 2002). The relationship between E and n can be described approximately by a negative exponential function.

Water content has a great effect on the deformability of intact rocks. The elastic modulus of intact rocks decreases as the water content increases. Fig. 6.4 shows the variation of the elastic modulus of two British sandstones at 50% ultimate stress with the water content (Hawkins & McConnell, 1992).

Based on best fitting analyses of laboratory test results, Vasarhelyi (2003, 2005) obtained the ratios of elastic modulus at saturated condition $E_{\text{saturated}}$ to that at dry condition E_{dry} respectively for British sandstones and Miocene limestones:

$$E_{\text{saturated}}/E_{\text{dry}} = 0.761 \quad \text{for British sandstones}$$

$$E_{\text{saturated}}/E_{\text{dry}} = 0.657 \quad \text{for Miocene limestones}$$

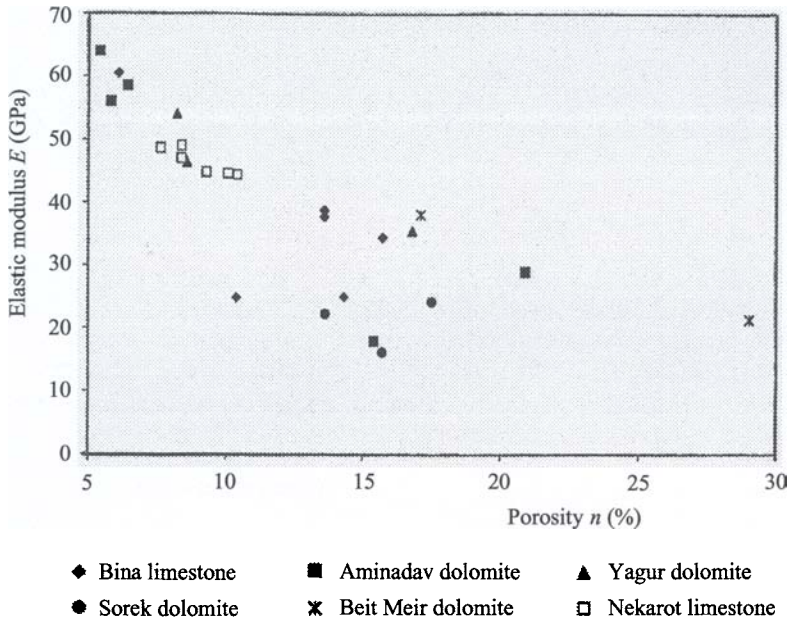


Fig. 6.3 Variation of elastic modulus E with porosity n for dolomites and limestones (after Palchik & Hatzor, 2002).

6.3 DEFORMABILITY OF ROCK DISCONTINUITIES

The behavior of jointed rock masses is dominated by the behavior of discontinuities in the rock mass. To consider the effects of discontinuities on the deformability of rock masses, the deformability of rock discontinuities should be known first.

The deformation properties of individual rock discontinuities can be described by normal stiffness k_n and shear stiffness k_s . These refer to the rate of change of normal stress σ_n and shear stress τ with respect to normal displacement u_n and shear displacement u_s . Details about the definition and determination of k_n and k_s are presented in the following.

6.3.1 Normal stiffness

If a compressive normal stress σ'_n is applied on a rock discontinuity, it would cause the discontinuity to close by a certain amount, say u_n . Fig. 6.5(a) shows a typical relationship between σ'_n and u_n . The slope of the curve in Fig. 6.5(a) gives the tangential normal stiffness k_n of the discontinuity and, at any stress level, is defined as

$$k_n = \frac{\Delta\sigma'_n}{\Delta u_n} \quad (6.8)$$

where Δ denotes an increment.

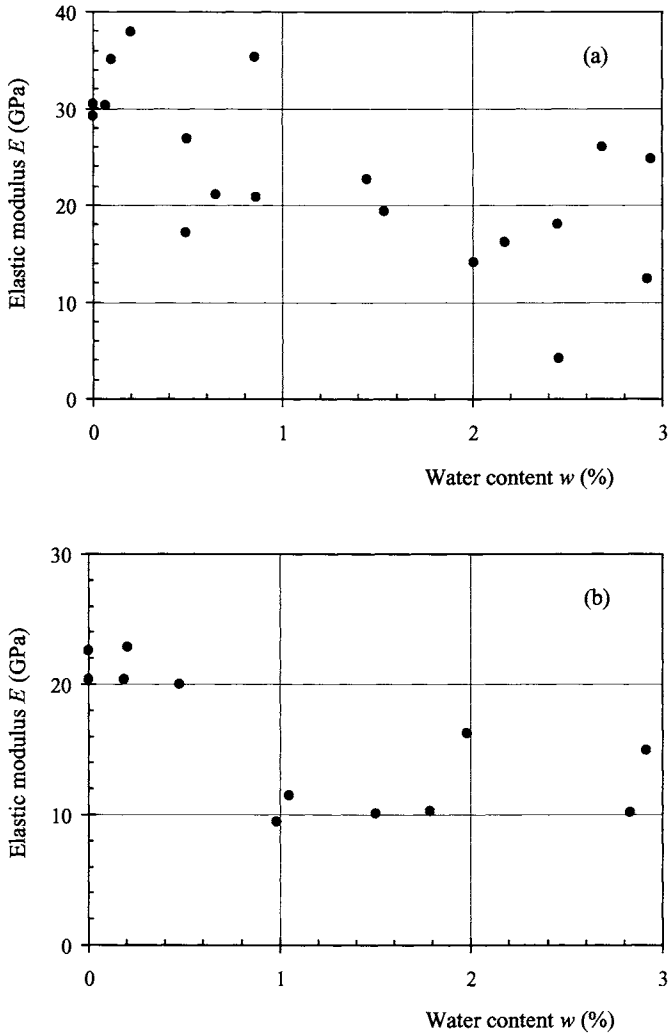


Fig. 6.4 Influence of water content w on elastic modulus E at 50% ultimate stress: (a) Lower Old Red Sandstone; and (b) Pennant - Type A (after Hawkins & McConnell, 1992).

It is noted that k_n is small when σ'_n is small but rapidly builds up as the discontinuity closes. There is actually a limit of discontinuity closure and $\sigma'_n \rightarrow \infty$ as this limit (u_{nc}) is reached. The relation between σ'_n and u_n can be expressed by the following hyperbolic function (Goodman et al., 1968; Bandis et al., 1983):

$$\sigma'_n = \frac{\alpha u_n}{u_{nc} - u_n} \quad (6.9)$$

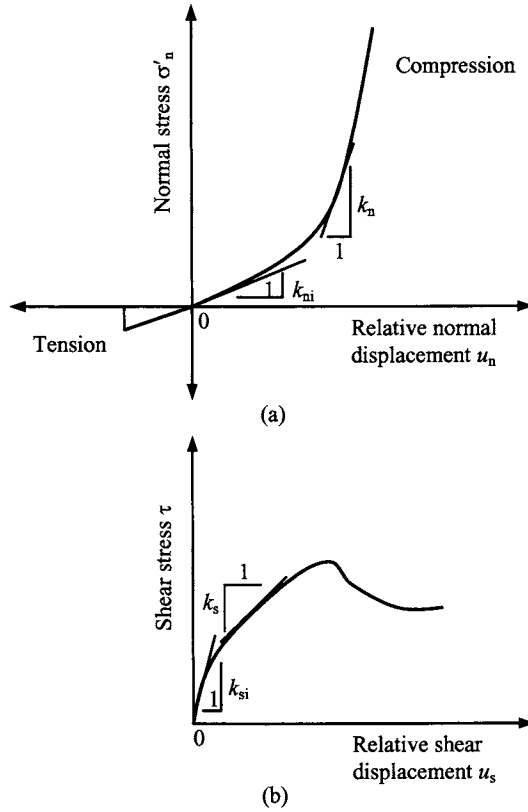


Fig. 6.5 Typical stress-relative displacement relationship: (a) σ'_n versus u_n ; and (b) τ versus u_s .

where α is an empirical constant; and u_{nc} is the limit of discontinuity closure.

Differentiating equation (6.9), the expression for k_n can be obtained as

$$k_n = \frac{d\sigma'_n}{du_n} = \frac{\alpha u_{nc}}{(u_{nc} - u_n)^2} \quad (6.10)$$

When $u_n = 0$, the initial tangential normal stiffness k_{ni} can be obtained as

$$k_{ni} = \frac{\alpha}{u_{nc}} \quad (6.11)$$

Combining equations (6.10) and (6.11) gives

$$k_n = k_{ni} \frac{u_{nc}^2}{(u_{nc} - u_n)^2} \quad (6.12)$$

Solving equation (6.9) for u_n and inserting it in equation (6.12) gives

$$k_n = k_{ni} \left(1 + \frac{\sigma'_n}{k_{ni} u_{nc}} \right)^2 \quad (6.13)$$

It is noted that equation (6.13) is valid for compressive normal stress only. It is usual to assume that discontinuities do not offer any resistance to tensile normal stresses implying $k_n = 0$ if σ'_n is tensile.

To determine the normal stiffness k_n at a normal stress σ'_n , one has to know the initial normal stiffness k_{ni} and the limit of discontinuity closure u_{nc} . According to Bandis et al. (1983), the initial normal stiffness k_{ni} in MPa/mm can be estimated from

$$k_{ni} \approx -7.15 + 1.75JRC + 0.02 \left(\frac{JCS}{e} \right) \quad (6.14)$$

where JRC is the discontinuity roughness coefficient; JCS is the discontinuity wall compressive strength in MPa; and e is the discontinuity aperture in mm at the beginning of loading which can be estimated from (Bandis et al., 1983)

$$e \approx JRC \left(\frac{0.04\sigma_c}{JCS} - 0.02 \right) \quad (6.15)$$

where σ_c is the unconfined compressive strength of the rock material. e is the mechanical aperture of the discontinuity and can also be estimated from the corresponding hydraulic aperture e_h of the discontinuity

$$e \approx \sqrt{e_h \cdot JRC^{2.5}} \quad (6.16)$$

The hydraulic aperture e_h will be described in detail in Chapter 8.

By analyzing experimental data for discontinuities with different values of JRC, Bandis et al (1983) obtained the following expression for determining the limit of discontinuity closure u_{nc}

$$u_{nc} \approx A + B(JRC) + C \left(\frac{JCS}{e} \right)^D \quad (6.17)$$

where JRC, JCS and e are the same as defined earlier; and A , B , C and D are empirical parameters which can be estimated from Table 6.5.

Equation (6.17) is only applicable to unfilled, interlocked discontinuities for which JRC is 5 to 15, JCS is 22 to 182 MPa, and e is 0.1 to 0.06 mm (Bandis et al., 1983; Priest, 1993). Bandis et al (1983) also obtained the following expression for determining u_{nc} without the data of JRC

$$u_{nc} \approx R \left(\frac{JCS}{e} \right)^S \quad (6.18)$$

where JCS and e are the same as defined earlier; and R and S are empirical parameters which can be estimated from Table 6.6.

The discontinuity roughness coefficient JRC provides an angular measure of the geometrical roughness of the discontinuity surface in the approximate range 0 (smooth) to 20 (very rough). The JRC can be estimated in a number of ways. Barton and Choubey (1977) presented a selection of scaled typical roughness profiles (Fig. 6.6), which facilitate the estimation of JRC for real discontinuities by visual matching. Barton (1987) published a table relating J_r (discontinuity roughness number in the Q classification system) to JRC (see Fig. 6.7). Barton and Bandis (1990) suggested that JRC could also be estimated from a simple tilt shear test in which a pair of matching discontinuity surfaces are tilted until one slides over the other. The JRC can be back-figured from the tilt angle α (Fig. 6.8) using the following equation:

Table 6.5 Empirical parameters A , B , C and D in equation (6.17) (after Bandis et al., 1983; Priest, 1993).

Parameter	Load cycle 1	Load cycle 2	Load cycle 3
A	-0.2960	-0.1005	-0.1032
B	-0.0056	-0.0073	-0.0074
C	2.2410	1.0082	1.1350
D	-0.2450	-0.2301	-0.2510

Table 6.6 Empirical parameters R and S in equation (6.18) (after Bandis et al., 1983; Priest, 1993).

Parameter	Load cycle 1	Load cycle 2	Load cycle 3
R	8.57	4.46	6.41
S	-0.68	-0.65	-0.72

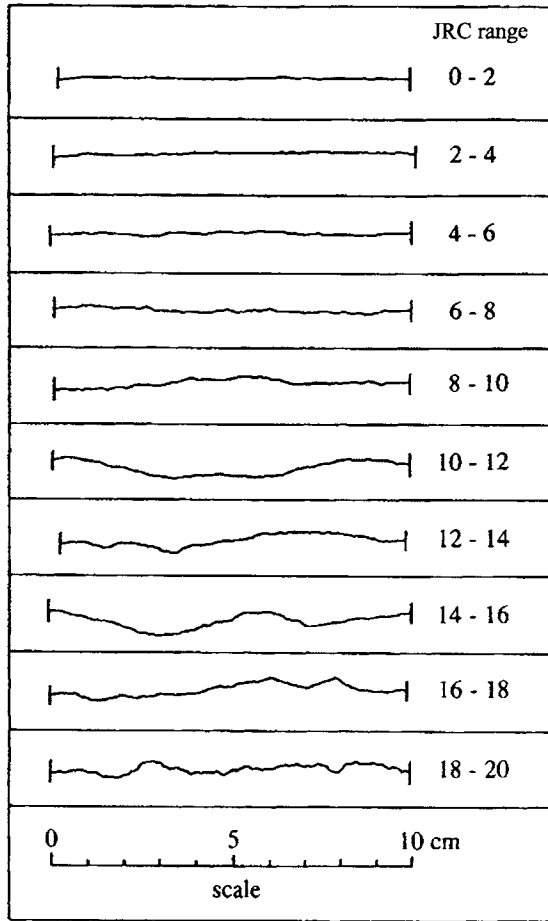


Fig. 6.6 Typical discontinuity roughness profiles and associated JRC values (after Barton & Choubey, 1977).

$$JRC = \frac{\alpha - \phi_r}{\log \left(\frac{JCS}{\sigma'_n} \right)} \quad (6.19)$$

where σ'_n is the normal stress on the discontinuity plane; and ϕ_r is the residual friction angle of the discontinuity which can be estimated from

$$\phi_r = (\phi_b - 20) + 20 \frac{R_{n(L),disc}}{R_{n(L),rock}} \quad (6.20)$$




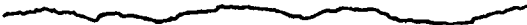





Profile	J_r	JRC (200 mm)	JRC (1 m)
Rough 	4	20	11
Smooth 	3	14	9
Slickensided 	2	11	8
Stepped			
Rough 	3	14	9
Smooth 	2	11	8
Slickensided 	1.5	7	6
Undulating			
Rough 	1.5	2.5	2.3
Smooth 	1.0	1.5	0.9
Slickensided 	0.5	0.5	0.4
Planar			

Fig. 6.7 Relationship between J_r in Q-system and JRC for 200 mm and 1 m samples (after Barton, 1987).

where ϕ_b is the basic friction angle of the rock material; and $R_{n(L),disc}$ and $R_{n(L),rock}$ are the rebound numbers from the L-type Schmidt hammer tests respectively on the discontinuity surface and the fresh rock surface. If the discontinuity surfaces are unweathered, ϕ_r can be simply taken equal to ϕ_b . The basic friction angle ϕ_b can be determined from direct shear tests or tilt tests on saw-cut rock surfaces. The values of ϕ_b depend on the rock type and water content. Table 6.7 lists the basic friction angles for different rocks from Barton and Choubey (1977).

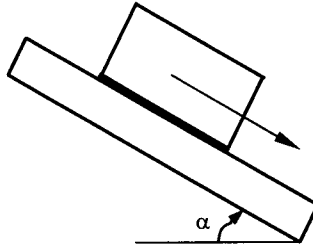


Fig. 6.8 Tilt test to measure the tilt angle α (after Barton & Bandis, 1990).

Table 6.7 Basic friction angles ϕ_b for different rocks (after Barton & Choubey, 1977).

Rock	ϕ_b dry (degrees)	ϕ_b wet (degrees)
Sandstone	26 - 35	25 - 34
Siltstone	31 - 33	27 - 31
Limestone	31 - 37	27 - 35
Basalt	35 - 38	31 - 36
Fine-grained granite	31 - 35	29 - 31
Coarse-grained granite	31 - 35	31 - 33
Gneiss	26 - 29	23 - 26
Slate	25 - 30	21
Dolerite	36	32
Porphyry	31	31
Shale		27
Chalk		30
Amphibolite	32	

The basic friction angle can also be estimated using tilt testing of diamond core samples (Stimpson, 1981). The tilt test involves attaching two pieces of core to a horizontal base, ensuring that the core samples are in contact with one another and are not free to slide. A third piece of core is then placed on top of the first two pieces and the base is rotated about a horizontal axis until sliding of the upper piece of core along the two line contacts with the lower pieces of core begins. The following equation can then be used to estimate the basic friction angle:

$$\phi_b = \arctan(1.155 \tan \alpha) \quad (6.21)$$

where ϕ_b is the basic friction angle for the upper piece of core; and α is the tilt angle at which sliding commences.

The nail brush is one of the simple methods to record surface profiles. Tse and Cruden (1979) present a method for estimating JRC based on digitization of the discontinuity surface into a total of M data points spaced at a constant small distance Δx along the profile. If y_i is the amplitude of the i th data point measured above (y_i^+) and below (y_i^-) the center line, the root mean square Z_2 of the first derivative of the roughness profile is given by

$$Z_2 = \sqrt{\frac{\sum_{i=1}^M (y_{i+1} - y_i)^2}{M(\Delta x)^2}} \quad (6.22)$$

By digitizing the ten typical roughness profiles presented in Fig. 6.6 and then conducting a series of regression analyses, Tse and Cruden (1979) found that there is a strong correlation between JRC and Z_2 . On this basis, they proposed the following expression for estimating JRC:

$$\text{JRC} \approx 32.2 + 32.47 \log Z_2 \quad (6.23)$$

The increasing availability of image analysis hardware and low-cost digitizing pads makes the method of Tse and Cruden (1979) a valuable objective alternative for the assessment of JRC. This approach should be used with caution, however, since Bandis et al. (1981) have shown that both JRC and JCS reduce with increasing scale. The idea of applying statistical and probabilistic analysis of surface profiles to the calculation of JRC has recently been examined and extended by several authors, notably McWilliams et al. (1990), Roberds et al. (1990), and Yu and Vayssade (1990). These last authors, noting that the value of JRC is dependent upon the sampling interval along the profile, propose the following extension to equation (6.23)

$$\text{JRC} \approx AZ_2 - B \quad (6.24)$$

where the constants A and B depend on the sampling interval Δx , taking values of 60.32 and 7.51, respectively, for an interval of 0.25 mm, 61.79 and 3.47 for an interval of 0.5 mm, and 64.22 and 2.31 for an interval of 1.0 mm. Lee et al. (1990), applying the concept of fractals to discontinuity surface profiles, obtained an empirical relation linking the fractal dimension D to the JRC value, as follows:

$$\text{JRC} = -0.87804 + 37.7844 \left(\frac{D-1}{0.015} \right) - 16.9304 \left(\frac{D-1}{0.015} \right)^2 \quad (6.25)$$

Unfortunately Lee et al. (1990) do not explain adequately how the fractal dimension D should be determined in practice. Odling (1994) proposed a method for determining the

fractal dimension D . In Odling's method, the roughness of a fracture surface is represented by the structure function S . For a discontinuity surface profile, S is defined as

$$S(\Delta x) = \frac{\sum_{i=1}^M (y_{i+1} - y_i)^2}{M} \quad (6.26)$$

where M is the number of data points at a sampling interval Δx , and y_i is the amplitude of the i th data point measured above (y_{i+}) and below (y_{i-}) the center line. The structure function is thus simply the mean square height difference of points on the profile at horizontal separations of Δx . The structure function is related to the Hurst exponent H (Voss, 1988; Poon et al., 1992):

$$S(\Delta x) = A(\Delta x)^{2H} \quad (6.27)$$

Thus, if a log-log plot of $S(\Delta x)$ versus Δx gives an acceptably straight line, the slope of this line gives $2H$. A is an amplitude parameter and is equivalent to the mean square height difference at a sampling interval of 1 unit, and is therefore dependent on the units of measurement. From H , the fractal dimension D can be determined from the following equation (Voss, 1988):

$$D = E - H \quad (6.28)$$

where E is the Euclidean dimension of embedding medium. $E = 2$ for surface profiles.

If the discontinuity is unweathered, JCS is equal to the unconfined compressive strength of the rock material σ_c , which can be determined using the correlations presented in Section 7.2. If there has been softening or other forms of weathering along the discontinuity, then JCS will be less than σ_c and must be estimated in some way. Suggested methods for estimating JCS are published by ISRM (1978c). Barton and Choubey (1977) explained how the Schmidt hammer rebound test can be used to estimate JCS from the following empirical expression

$$\log \text{JCS} \approx 0.88\gamma R_{n(L)} + 1.01 \quad (6.29)$$

where γ is the unit weight of the rock material (MN/m^3); $R_{n(L)}$ is the rebound number from the L-type Schmidt hammer test on the discontinuity surface; and JCS has the unit MPa in the range of 20 to 300 MPa. Although the Schmidt hammer is notoriously unreliable, particularly for heterogeneous materials, it is one of the few methods available for estimating the strength of a surface coating of material (see Chapter 3 for more detailed description of Schmidt hammer rebound tests).

6.3.2 Shear stiffness

If a shear stress τ is applied on the discontinuity, there will be a relative shear displacement u_s on the discontinuity. Fig. 6.5(b) shows a typical relationship between τ and u_s . It is now possible to define a tangential shear stiffness k_s exactly in the same way as for the normal stiffness k_n . Thus

$$k_s = \frac{\Delta\tau}{\Delta u_s} \quad (6.30)$$

The relation between shear stress τ and relative shear displacement u_s can be expressed by the following hyperbolic function (Duncan & Chang, 1970; Bandis et al., 1983; Priest, 1993):

$$\tau = \left(\frac{1}{k_{si} u_s} + \frac{R_f}{\tau_f} \right)^{-1} \quad (6.31)$$

where k_{si} and τ_f are respectively the initial tangent shear stiffness and the shear strength of the discontinuity; and R_f is the failure ratio given by τ_f/τ_{ult} in which τ_{ult} is the ultimate shear stress at large shear displacement.

Differentiating equation (6.31), the expression for k_s can be obtained as

$$k_s = \frac{d\tau}{du_s} = k_{si} \left(1 + \frac{R_f k_{si} u_s}{\tau_f} \right)^{-2} \quad (6.32)$$

Solving equation (6.31) for u_s and inserting it in equation (6.32) gives

$$k_s = k_{si} \left(1 - \frac{R_f \tau}{\tau_f} \right)^2 \quad (6.33)$$

To determine the shear stiffness k_s at a shear stress τ , one has to know the initial shear stiffness k_{si} , the shear strength τ_f and the failure ratio R_f . Bandis et al. (1983) found that the initial shear stiffness k_{si} increased with normal stress σ'_n and could be estimated from

$$k_{si} \approx k_j (\sigma'_n)^{n_j} \quad (6.34)$$

where k_j and n_j are empirical constants termed the stiffness number and the stiffness exponent respectively. Based on test results of dolerite, limestone, sandstone and slate at normal stresses from 0.23 to 2.36 MPa, Bandis et al. (1983) found that n_j was in the range of 0.615 to 1.118 MPa²/mm with an average of about 0.761 and R_f in the range of 0.652 to

0.887 with an average of about 0.783. The stiffness number k_j in MPa/mm was found to vary with JRC and could be estimated from

$$k_j \approx -17.19 + 3.86\text{JRC} \quad (\text{for } \text{JRC} > 4.5) \quad (6.35)$$

The shear strength τ_f of a discontinuity subject to a normal stress σ'_n can be determined by

$$\tau_f = \sigma'_n \tan \left[\text{JRC} \log \left(\frac{\text{JCS}}{\sigma'_n} \right) + \phi_r \right] \quad (6.36)$$

where JRC, JCS and ϕ_r are the same as defined earlier. For more detailed discussion of shear strength τ_f , the reader can refer to Chapter 7.

6.3.3 *Dilation of discontinuities*

It is noted that for discontinuities (especially rough discontinuities), an increment of a shear stress can produce an increment of relative displacement in the normal direction and vice versa an increment of a normal stress can produce an increment of relative displacement in the shear direction. This behavior is called dilation of discontinuities. If the relative shear displacement is broken into two components (along two perpendicular coordinate axes s and t on the discontinuity plane - see Fig. 6.9), the general constitutive relation for a discontinuity including the dilation behavior can be expressed as

$$\begin{Bmatrix} u_s \\ u_t \\ u_n \end{Bmatrix} = \begin{bmatrix} C_{ss} & C_{st} & C_{sn} \\ C_{ts} & C_{tt} & C_{tn} \\ C_{ns} & C_{nt} & C_{nn} \end{bmatrix} \begin{Bmatrix} \tau_s \\ \tau_t \\ \sigma'_n \end{Bmatrix} \quad (6.37)$$

where the subscripts 's' and 't' represent two orthogonal directions in the discontinuity plane; the subscript 'n' represents the direction normal to the discontinuity plane; u_s and u_t are the shear displacements respectively in directions s and t ; u_n is the closure displacement; τ_s and τ_t are the shear stresses respectively in directions s and t ; σ'_n is the normal stress; and $[C_{ij}]$ ($i, j = s, t, n$) is the compliance matrix of the discontinuity. Elements of the compliance matrix can be found experimentally by holding two of the stresses constant (for example at zero) and then monitoring the three relative displacement components associated with changes in the third stress component (Priest, 1993).

For simplicity, the following assumptions are often made for the behavior of a single discontinuity:

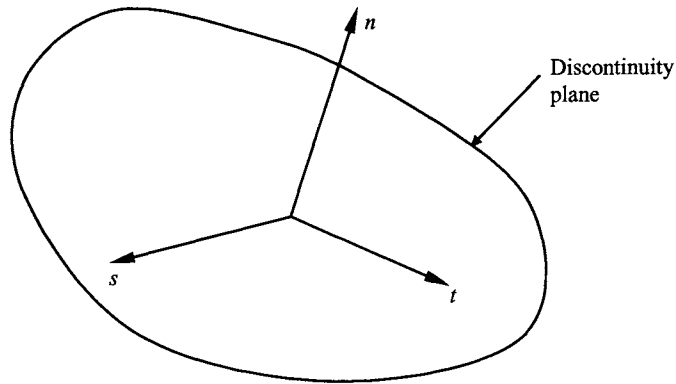


Fig. 6.9 A local coordinate system s, t, n .

- (1) Deformation behavior is the same in all directions in the discontinuity plane. Thus $C_{ss} = C_{tt}$, $C_{st} = C_{ts}$, $C_{sn} = C_{tn}$ and $C_{ns} = C_{nt}$.
- (2) The dilation (coupling) effect is neglected, i.e., C_{ij} ($i \neq j$) in equation (6.37) are zero.

With the above two assumptions, equation (6.37) can be simplified to

$$\begin{Bmatrix} u_s \\ u_t \\ u_n \end{Bmatrix} = \begin{bmatrix} C_{ss} & 0 & 0 \\ 0 & C_{ss} & 0 \\ 0 & 0 & C_{nn} \end{bmatrix} \begin{Bmatrix} \tau_s \\ \tau_t \\ \sigma'_n \end{Bmatrix} = \begin{bmatrix} \frac{1}{k_s} & 0 & 0 \\ 0 & \frac{1}{k_s} & 0 \\ 0 & 0 & \frac{1}{k_n} \end{bmatrix} \begin{Bmatrix} \tau_s \\ \tau_t \\ \sigma'_n \end{Bmatrix} \quad (6.38)$$

where k_s and k_n are respectively the discontinuity shear and normal stiffness as described in previous subsections.

6.4 DEFORMABILITY OF ROCK MASS

6.4.1 Empirical methods for estimating rock mass deformation modulus

A number of empirical methods have been developed that correlate various rock quality indices or classification systems to deformation modulus of rock masses. The commonly used include correlations between the deformation modulus and RQD, RMR, GSI and Q. The definition of RQD, RMR, GSI and Q and the methods for determining them have been discussed in Chapter 5.

(a) Methods relating deformation modulus with RQD

Based on field studies at Dworshak Dam, Deere et al. (1967) suggested that RQD be used for determining the rock mass deformation modulus. By adding further data from other sites, Coon and Merritt (1970) developed a relation between RQD and the modulus ratio E_m/E_r , where E_m and E_r are the deformation modulus respectively of the rock mass and the intact rock (see Fig. 6.10).

Gardner (1987) proposed the following relation for estimating the rock mass deformation modulus E_m from the intact rock modulus E_r by using a reduction factor α_E which accounts for frequency of discontinuities by RQD:

$$E_m = \alpha_E E_r \quad (6.39a)$$

$$\alpha_E = 0.0231(\text{RQD}) - 1.32 \geq 0.15 \quad (6.39b)$$

This method is adopted by the American Association of State Highway and Transportation Officials in the *Standard Specification for Highway Bridges* (AASHTO, 1989). For $\text{RQD} > 57\%$, equation (6.39) is the same as the relation of Coon and Merritt (1970). For $\text{RQD} < 57\%$, equation (6.39) gives $E_m/E_r = 0.15$.

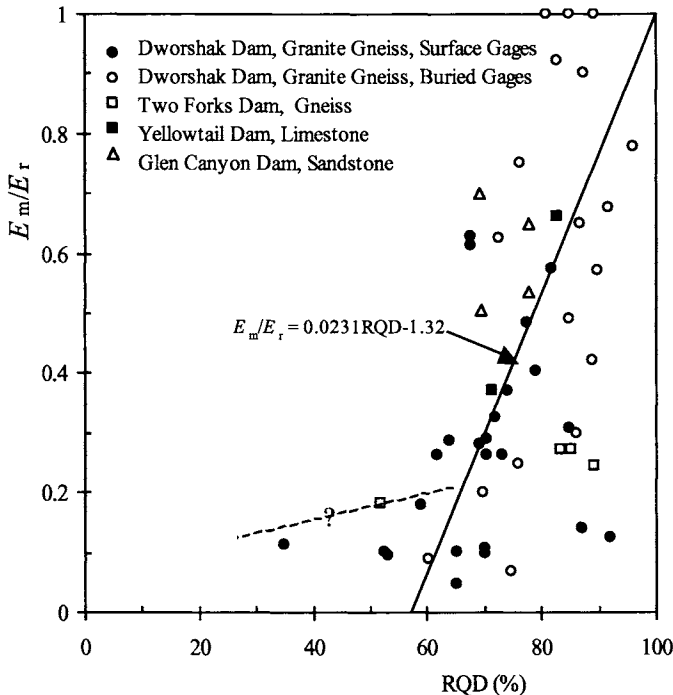


Fig. 6.10 Variation of E_m/E_r with RQD (after Coon & Merritt, 1970).

It is noted that the $RQD - E_m/E_r$ relations of Coon and Merritt (1970) and Gardner (1987) have the following limitations (Zhang & Einstein, 2004):

- (1) The range of $RQD < 60\%$ is not covered and only an arbitrary value of E_m/E_r can be selected in this range.
- (2) For $RQD = 100\%$, E_m is assumed to be equal to E_r . This is obviously unsafe in design practice because $RQD = 100\%$ does not mean that the rock is intact. There may be discontinuities in rock masses with $RQD = 100\%$ and thus E_m may be smaller than E_r even when $RQD = 100\%$.

Zhang and Einstein (2004) added further data collected from the published literature to cover the entire range $0 \leq RQD \leq 100\%$ (see Fig. 6.11). It can be seen that the data in Fig. 6.11 shows a large scatter, which may be caused by many different factors. The following discusses the most important four of them.

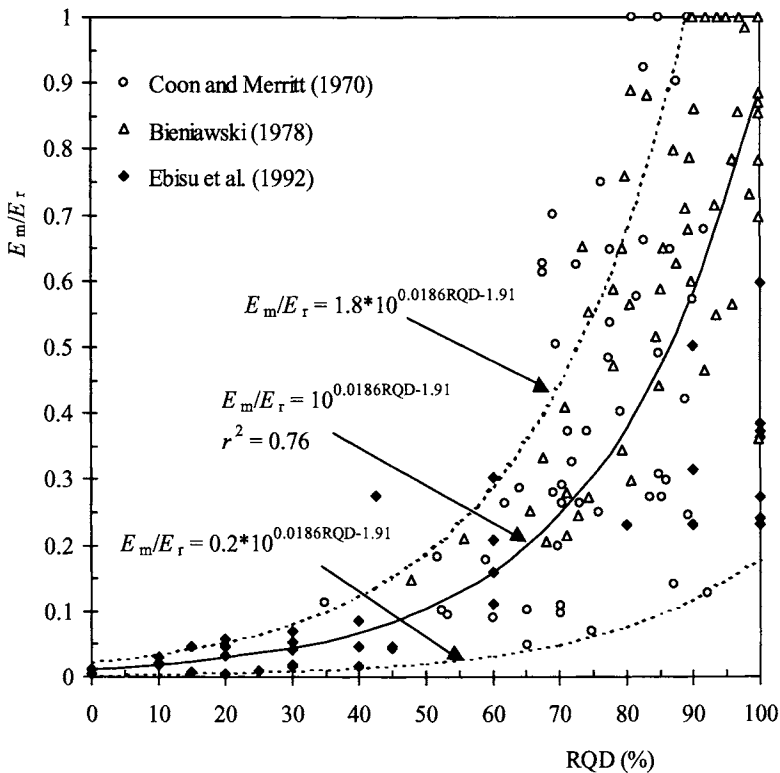


Fig. 6.11 $E_m/E_r - RQD$ data and proposed $E_m/E_r - RQD$ relations (after Zhang & Einstein, 2004).

(1) Testing Methods

The data in Fig. 6.11 were obtained with different testing methods. For example, Deere et al. (1967) used plate load tests while Ebisu et al. (1992) used borehole jacking tests. Different testing methods may give different values of deformation modulus even for the same rock mass. According to Bieniawski (1978), even a single testing method, such as the flat jack test, can lead to a wide scatter in the results even where the rock mass is very uniform.

(2) Directional Effect

Most rock masses are anisotropic and do not have a single deformation modulus. RQD also varies with direction through a fractured rock mass. The dependence of both RQD and deformation modulus on direction adds to the scatter of the data.

(3) Discontinuity Conditions

RQD does not consider the discontinuity conditions, such as the aperture and fillers. However, the discontinuity conditions have a great effect on the rock mass deformation modulus. Fig. 6.12 shows the variation of E_m/E_r with the average discontinuity spacing s for different values of k_n/E_r using the Kulhawy (1978) model (see Section 6.4.2). It can be seen that k_n/E_r which represents the discontinuity conditions has a great effect on the rock mass deformation modulus.

Kayabasi et al. (2003) derived the following relation from a database of 57 test values showing the influence of weathering of discontinuities on the rock mass deformation modulus:

$$E_m = 0.1423 \left[\frac{E_r(1 + 0.01\text{RQD})}{\text{WD}} \right]^{1.1747} \quad (6.40)$$

where WD is the weathering degree of discontinuities. By adding 58 new test values to the database of Kayabasi et al. (2003), Gokceoglu et al. (2003) derived the following relation based on regression analysis:

$$E_m = 0.001 \left[\frac{(E_r/\sigma_c)(1 + 0.01\text{RQD})}{\text{WD}} \right]^{1.5528} \quad (6.41)$$

The new relation considers the effect of the unconfined compressive strength of intact rock on the rock mass deformation modulus.

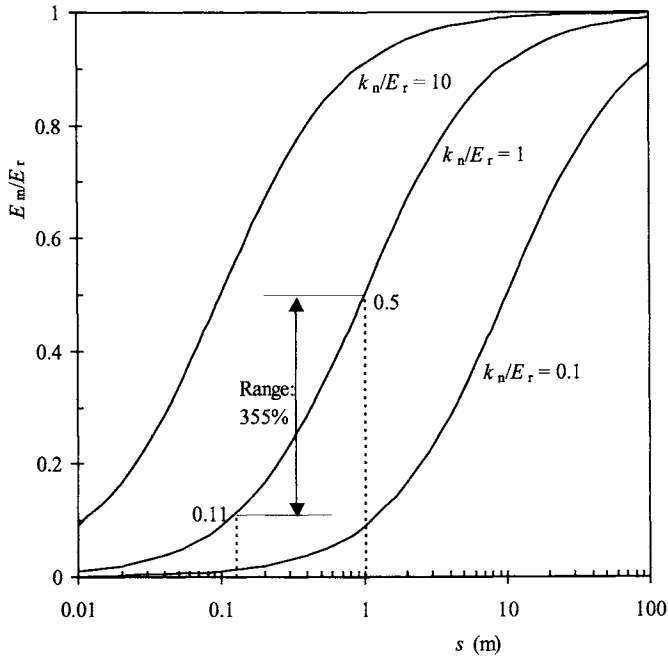


Fig. 6.12 Variation of E_m/E_r with average discontinuity spacing s for different values of k_n/E_r using Kulhawy (1978) model (after Zhang & Einstein, 2004).

(4) Insensitivity of RQD to Discontinuity Frequency

RQD used in Fig. 6.11 is defined in terms of the percentage of intact pieces of rock (or discontinuity spacings) greater than a threshold value t of 0.1 m. According to Harrison (1999), the adoption of a threshold value t of 0.1 m leads to the insensitivity of RQD to the change of discontinuity frequency λ or mean discontinuity spacing s . As discussed in Chapter 4, for a negative exponential distribution of discontinuity spacings, the theoretical RQD can be related to the discontinuity frequency λ by equation (4.21). Fig. 6.13 shows the variation of RQD with λ . It can be seen that, for a threshold value t of 0.1 m, when discontinuity frequency λ increases from 1 m^{-1} to 8 m^{-1} (i.e., the mean discontinuity spacing s decreases from 1 m to 0.125 m) RQD only decreases from 99.5% to 80.9%, which is a range of only 23%. However, when the mean discontinuity spacing s decreases from 1 m to 0.125 m, the rock mass deformation modulus will vary over a large range. As shown in Fig. 6.12, with $k_n/E_r = 1$, E_m/E_r changes from 0.5 to 0.11 when s decreases from 1 m to 0.125 m. Harrison (1999) showed that the sensitivity of RQD to the mean discontinuity spacing s is closely related to the adopted threshold value t . For example, if a threshold value t of 0.5 m is used, the corresponding RQD will change from 91.0% to 9.2% when λ increases from 1 m^{-1} to 8 m^{-1} (see Fig. 6.13).

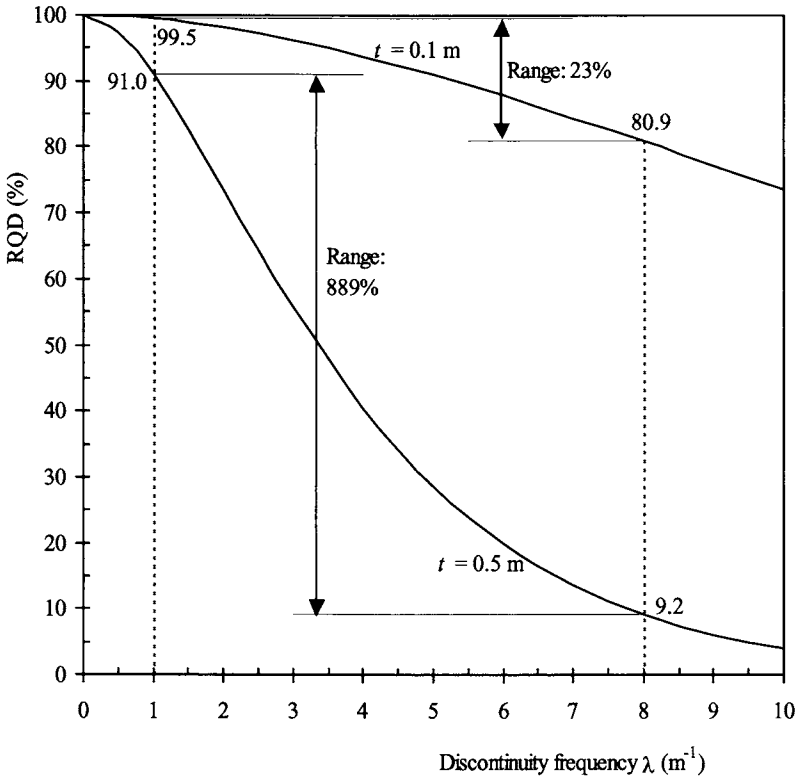


Fig. 6.13 RQD – discontinuity frequency relations for threshold values of 0.1 and 0.5 m (after Harrison, 1999 but with different threshold values)

Considering the data shown in Fig. 6.11, Zhang and Einstein (2004) proposed the following relations between the rock mass deformation modulus and RQD:

Lower bound:

$$E_m / E_r = 0.2 \times 10^{0.0186RQD - 1.91} \tag{6.42a}$$

Upper bound:

$$E_m / E_r = 1.8 \times 10^{0.0186RQD - 1.91} \tag{6.42b}$$

Mean:

$$E_m / E_r = 10^{0.0186RQD - 1.91} \tag{6.42c}$$

The mean relation between E_m/E_r and RQD was obtained by regression analysis of the data in Fig. 6.11. The coefficient of regression, r^2 , is 0.76. The upper bound could be put somewhat higher but it was selected to be conservative.

RQD is a directionally dependent parameter and its value may change significantly, depending on the borehole orientation. Therefore, it is important to know the borehole orientation when estimating the rock mass deformation modulus E_m using the E_m/E_r – RQD relationship. To reduce the directional dependence of RQD, equation (4.34) in Chapter 4 can be used to estimate RQD from the volumetric discontinuity frequency λ_v .

(b) Methods relating deformation modulus with RMR or GSI

Bieniawski (1978) studied seven projects and suggested the following correlation to predict rock mass deformation modulus E_m from RMR:

$$E_m = 2\text{RMR} - 100 \quad (\text{GPa}) \quad (6.43)$$

The obvious deficiency of this equation is that it does not give modulus values for RMR values less than 50. Additional studies carried out on rock masses with qualities ranging from poor to very good indicated that the rock mass deformation modulus E_m could be related to RMR by (Serafim & Pereira, 1983):

$$E_m = 10^{(\text{RMR}-10)/40} \quad (\text{GPa}) \quad (6.44)$$

Equation (6.44) has been found to work well for good quality rocks. However, for poor quality rocks it appears to predict deformation modulus values which are too high (Hoek & Brown, 1997). Based on practical observations and back analysis of excavation behavior in poor quality rock masses, Hoek and Brown (1997) modified equation (6.44) for unconfined compressive strength of intact rock $\sigma_c < 100$ MPa as follows:

$$E_m = \sqrt{\frac{\sigma_c}{100}} 10^{(\text{GSI}-10)/40} \quad (\text{GPa}) \quad (6.45)$$

Note that GSI (Geological Strength Index) has been substituted for RMR in equation (6.45).

Johnston et al. (1980) also found that equation (6.44) overestimates the rock mass deformation modulus for poor quality rocks. They reported that the results of various in situ load tests in moderately weathered Melbourne mudstone of σ_c in the range 2 to 3 MPa yielded a rock mass deformation modulus of about 0.5 GPa for estimated RMRs of about 70. If we use equation (6.45) with $\sigma_c = 2.5$ MPa and $\text{GSI} = \text{RMR} - 5 = 65$, we can obtain an E_m of 3.7 GPa which is much closer to the measured value of about 0.5 GPa than the value of 31.6 GPa calculated using equation (6.44).

Hoek (2004) presented the following simplified correlation for estimating the rock mass deformation modulus E_m from GSI:

$$E_m = 0.33e^{0.064GSI} \quad (\text{GPa}) \quad (6.46)$$

Using a database including 115 data values obtained from in situ plate loading and dilatometer tests, Gokceoglu et al. (2003) obtained the following correlations based on regression analyses:

$$E_m = 0.0736e^{0.0755RMR} \quad (\text{GPa}) \quad (6.47)$$

$$E_m = 0.1451e^{0.0654GSI} \quad (\text{GPa}) \quad (6.48)$$

Fig. 6.14 shows the comparison of the above correlations with the test data from different researchers.

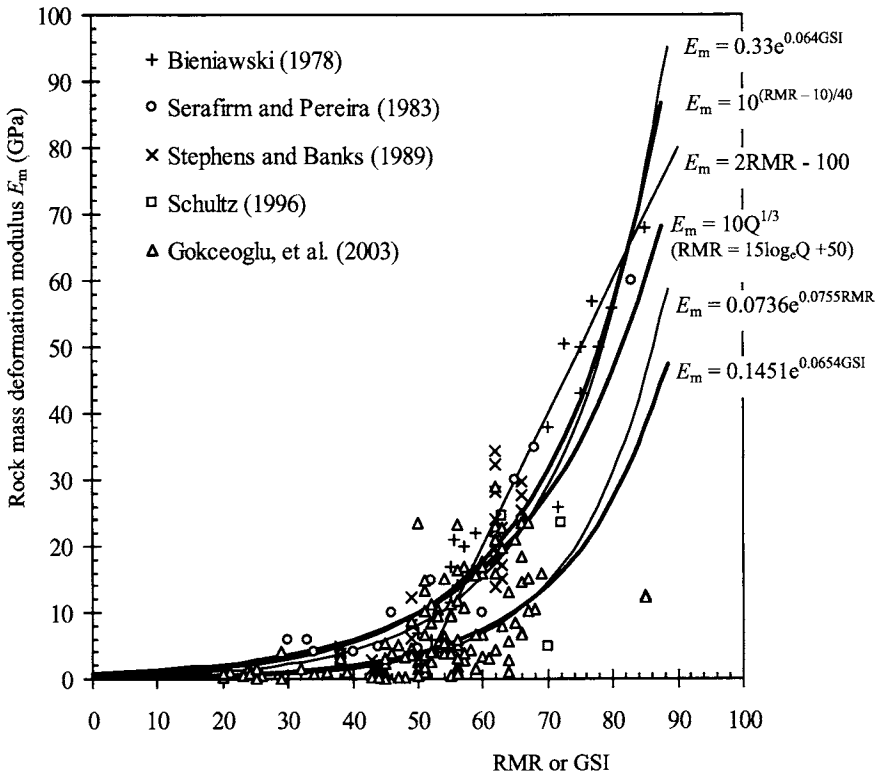


Fig. 6.14 Correlation between deformation modulus E_m and RMR or GSI.

There are also empirical correlations between the ratio of the rock mass deformation modulus E_m to the intact rock deformation modulus E_r and RMR. The following are two of them.

Nicholson and Bieniawski (1990):

$$\frac{E_m}{E_r} = 0.0028RMR^2 + 0.9e^{RMR/22.82} \quad (6.49)$$

Mitri et al. (1994):

$$\frac{E_m}{E_r} = \frac{1 - \cos(\pi \times RMR / 100)}{2} \quad (6.50)$$

(c) Methods relating deformation modulus with Q

Barton et al. (1980) suggested the following relationships between rock mass deformation modulus E_m and Q values:

Lower bound:

$$E_m = 10 \log Q \quad (\text{GPa}) \quad (6.51a)$$

Upper bound:

$$E_m = 40 \log Q \quad (\text{GPa}) \quad (6.51b)$$

Mean:

$$E_m = 25 \log Q \quad (\text{GPa}) \quad (6.51c)$$

where Q is the rock quality index as described in Chapter 5. The above relationships are only applicable to $Q > 1$ and generally hard rocks.

Barton (2002) suggested the following general relation for estimating the deformation modulus of rock masses

$$E_m = 10 \left(Q \frac{\sigma_c}{100} \right)^{1/3} \quad (\text{GPa}) \quad (6.52)$$

which is similar to equation (6.45) in that it considers the effect of the unconfined compressive strength of intact rock σ_c .

(d) Method relating deformation modulus with seismic P-wave velocity

Barton (2002) presented the following correlation for estimating the rock mass deformation modulus E_m from the seismic P-wave velocity

$$E_m = 10 \times 10^{(v_p - 3.5)/3} \text{ (GPa)} \quad (6.53)$$

where v_p is the seismic P-wave velocity of the rock mass in km/s.

(e) Method relating deformation modulus with unconfined compressive strength

Rowe and Armitage (1984) correlated the rock mass deformation modulus deduced from a large number of field tests of drilled shafts under axial loading with the average unconfined compressive strength σ_c of weak rock deposits in which the drilled shafts were founded as follows:

$$E_m \text{ (MPa)} = 215 \sqrt{\sigma_c} \quad (6.54)$$

Radhakrishnan and Leung (1989) found good agreement between the rock mass deformation moduli obtained from back analysis of load-settlement relationship of large diameter drilled shafts in weathered sedimentary rocks and those computed from equation (6.54).

(f) Comments

Although the empirical methods are most widely used in practice, there are some limitations:

1. The anisotropy of the rock mass caused by discontinuities is not considered.
2. Different empirical relations often give very different deformation modulus values of rock masses at the same site.

6.4.2 Equivalent continuum approach for estimating rock mass deformation modulus

Equivalent continuum approach treats jointed rock mass as an equivalent anisotropic continuum with deformability that reflects the deformation properties of the intact rock and those of the discontinuity sets.

(a) Rock mass with persistent discontinuities

For rock masses with persistent discontinuities, analytical expressions for their deformation properties have been derived by a number of authors, including Singh (1973), Kulhawy (1978), Gerrard (1982a, b, 1991), Amadei (1983), Oda et al. (1984), Fossum (1985), Yoshinaka and Yambe (1986), Oda (1988) and Amadei and Savage (1993). The basic idea

used by different authors to derive the expressions for deformation properties is essentially the same, i.e., the average stresses are assumed to distribute throughout the rock mass and the overall average strains of the rock mass are contributed by both the intact rock and the discontinuities. The only difference is the method for determining the additional deformation due to the discontinuities. Some of the typical results are presented in the following.

The three-dimensional equivalent continuum model presented by Kulhawy (1978) for a rock mass containing three orthogonal discontinuity sets is shown in Fig. 6.15. The intact rock material is defined by the Young's modulus E_r and Poisson's ratio ν_r , while the discontinuities are described by normal stiffness k_n , shear stiffness k_s , and mean discontinuity spacing s . For this model, the properties of the equivalent orthotropic elastic mass are given as

$$E_{mi} = \left(\frac{1}{E_r} + \frac{1}{s_i k_{ni}} \right)^{-1} \quad (6.55)$$

$$G_{mij} = \left(\frac{1}{G_r} + \frac{1}{s_i k_{si}} + \frac{1}{s_j k_{sj}} \right)^{-1} \quad (6.56)$$

$$\nu_{mij} = \nu_{mik} = \nu_r \frac{E_{mi}}{E_r} \quad (6.57)$$

for $i = x, y, z$ with $j = y, z, x$ and $k = z, x, y$. These equations describe the rock mass elastic properties completely. The single discontinuity model is a special case of the foregoing in which $s_x = s_y = \infty$. Singh (1973), Amadei (1983), Chen (1989) and Amadei and Savage (1993) obtained the same expressions as above for deformation properties of rock masses containing three orthogonal discontinuity sets.

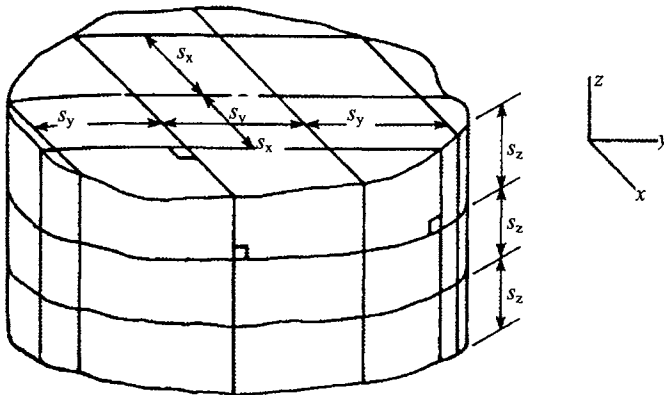


Fig. 6.15 Rock mass model of Kulhawy (1978).

For engineering convenience, it is useful to define a modulus reduction factor, α_E , which represents the ratio of the rock mass deformation modulus to the intact rock deformation modulus. This factor can be obtained by re-writing equation (6.55) as

$$\alpha_E = \frac{E_{mi}}{E_r} = \left(1 + \frac{E_r}{s_i k_{ni}} \right)^{-1} \quad (6.58)$$

The relationship is plotted in Fig. 6.16. This figure shows smaller values of α_E in rock masses with softer discontinuities (larger E_r/k_n values).

Unfortunately, the mean discontinuity spacing is not easy to obtain directly and, in normal practice, RQD values are determined instead. Using a physical model, the RQD can be correlated with the number of discontinuities per 1.5 meters (5 ft) core run, a common measure in practice. This relationship is shown in Fig. 6.17. Combining Figs. 6.16 and 6.17 yields Fig. 6.18, which relate α_E and RQD with E_r/k_n as an additional parameter.

Consider the jointed rock mass under uniaxial loading as shown in Fig. 6.19. The constitutive relation in the n, s, t coordinate system can be defined from the single discontinuity model of Kulhawy (1978). In the global coordinate system x, y, z , the constitutive relation can be determined using second tensor coordinate transformation rules. In matrix form this gives (Amadei & Savage, 1993)

$$(\varepsilon)_{xyz} = (A)_{xyz}(\sigma)_{xyz} \quad (6.59)$$

where $(\varepsilon)_{xyz}^t = (\varepsilon_x, \varepsilon_y, \varepsilon_z, \gamma_{xy}, \gamma_{yz}, \gamma_{zx})$ and $(\sigma)_{xyz}^t = (\sigma_x, \sigma_y, \sigma_z, \tau_{xy}, \tau_{yz}, \tau_{zx})$. The components $a_{ij} = a_{ji}$ ($i, j = 1 - 6$) of the compliance matrix $(A)_{xyz}$ depend on the dip angle θ as follows:

$$a_{11} = \frac{1}{E_r} + \frac{\sin^4 \theta}{k_n s} + \frac{\sin^2 \theta}{4k_s s} \quad (6.60a)$$

$$a_{12} = -\frac{\nu_r}{E_r} + \frac{\sin^2 2\theta}{4} \left(\frac{1}{k_n s} - \frac{1}{k_s s} \right) \quad (6.60b)$$

$$a_{13} = a_{23} = -\frac{\nu_r}{E_r} \quad (6.60c)$$

$$a_{22} = \frac{1}{E_r} + \frac{\cos^4 \theta}{k_n s} + \frac{\sin^2 \theta}{4k_s s} \quad (6.60d)$$

$$a_{33} = \frac{1}{E_r} \quad (6.60e)$$

$$a_{14} = \frac{\sin 2\theta \cos 2\theta}{2k_s s} + \frac{\sin^2 \theta \sin 2\theta}{k_n s} \quad (6.60f)$$

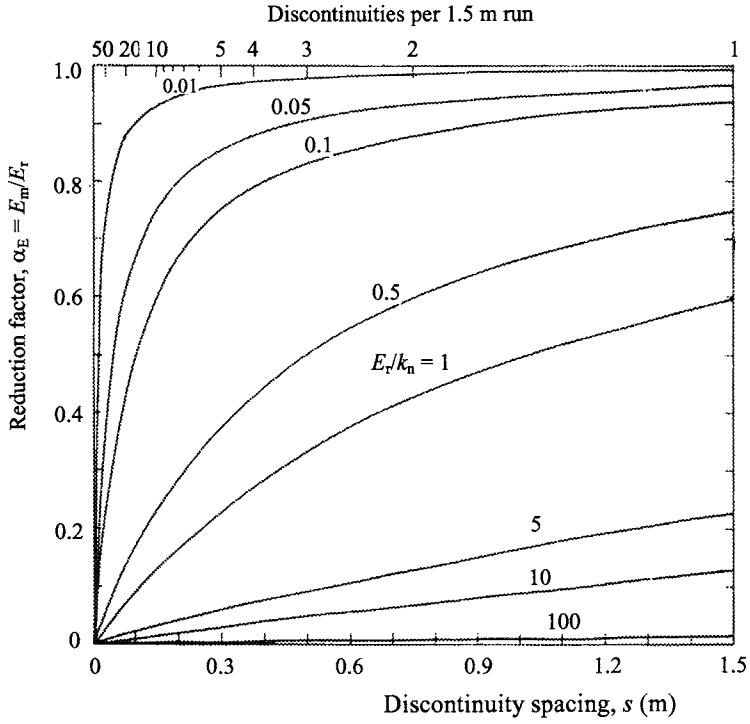


Fig. 6.16 Modulus reduction factor versus discontinuity spacing (after Kulhawy, 1978).

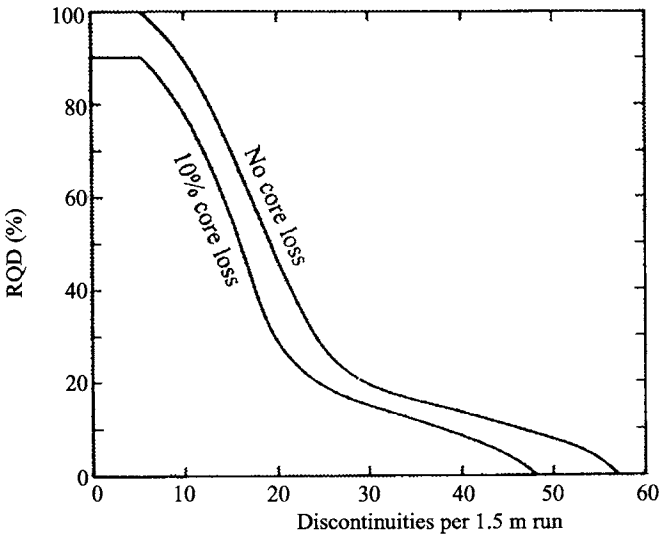


Fig. 6.17 RQD versus number of discontinuities per 1.5 m run (after Kulhawy, 1978)

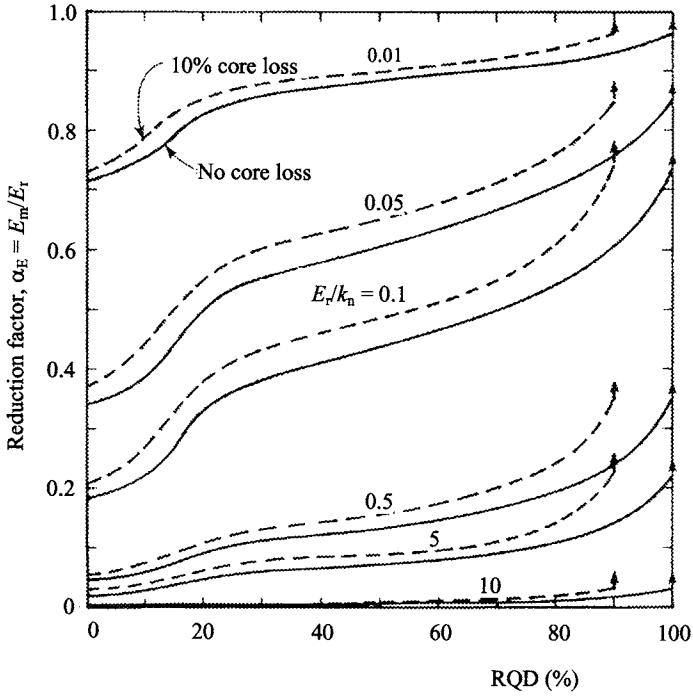


Fig. 6.18 Modulus reduction factor versus RQD (after Kulhawy, 1978)

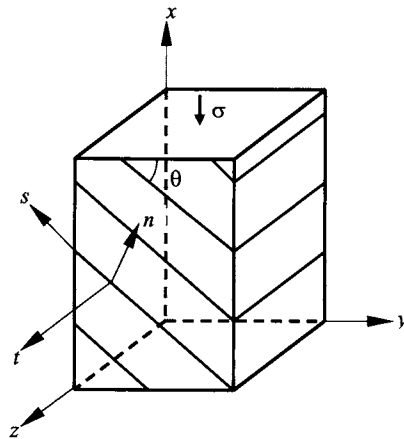


Fig. 6.19 Jointed rock mass under uniaxial loading (after Amadei & Savage, 1993).

$$a_{24} = -\frac{\sin 2\theta \cos 2\theta}{2k_s s} + \frac{\cos^2 \theta \sin 2\theta}{k_n s} \quad (6.60g)$$

$$a_{44} = \frac{1}{G_r} + \frac{\sin^2 2\theta}{k_n s} + \frac{\cos^2 2\theta}{k_s s} \quad (6.60h)$$

$$a_{55} = \frac{1}{G_r} + \frac{\cos^2 \theta}{k_s s} \quad (6.60i)$$

$$a_{56} = \frac{\sin 2\theta}{2k_s s} \quad (6.60j)$$

$$a_{66} = \frac{1}{G_r} + \frac{\sin^2 \theta}{k_s s} \quad (6.60k)$$

All other components a_{ij} vanish. Note that for the orientation of the discontinuities considered here, the jointed rock mass has a plane of elastic symmetry normal to the z -axis. If the discontinuity set is inclined with respect to x and z axes or if the rock sample under consideration has two or three orthogonal discontinuity sets, then new expressions must be derived.

Fossum (1985) derived a constitutive model for a rock mass that contains randomly oriented discontinuities with constant normal stiffness k_n and shear stiffness k_s . He assumed that if the discontinuities are randomly oriented, the mean discontinuity spacing would be the same in all directions taken through a representative sample of the rock mass. Arguing that the mechanical properties of the jointed rock mass would be isotropic, Fossum derived the following expressions for the bulk modulus K_m and shear modulus G_m of the equivalent elastic continuum:

$$K_m = \frac{E_r}{9} \left[\frac{3(1 + \nu_r)sk_n + 2E_r}{(1 + \nu_r)(1 - 2\nu_r)sk_n + (1 - \nu_r)E_r} \right] \quad (6.61)$$

$$G_m = \frac{E_r}{30(1 + \nu_r)} \left[\frac{9(1 + \nu_r)(1 - 2\nu_r)sk_n + (7 - 5\nu_r)E_r}{(1 + \nu_r)(1 - 2\nu_r)sk_n + (1 - \nu_r)E_r} \right] + \frac{2}{5} \left[\frac{E_r sk_s}{2(1 + \nu_r)sk_s + E_r} \right] \quad (6.62)$$

The equivalent Young's modulus and Poisson's ratio can then be obtained from

$$E_m = \frac{9K_m G_m}{3K_m + G_m} \quad (6.63)$$

$$\nu_m = \frac{3K_m - 2G_m}{2(3K_m + G_m)} \quad (6.64)$$

At large values of mean discontinuity spacing s the equivalent modulus E_m and Poisson's ratio ν_m approach the values E_r and ν_r for the intact rock material. At very small values of mean discontinuity spacing the equivalent modulus E_m and Poisson's ratio ν_m are given by the following expressions

$$E_m \rightarrow \frac{2E_r(7-5\nu_r)}{3(1-\nu_r)(9+5\nu_r)} \quad \text{as } s \rightarrow 0 \quad (6.65)$$

$$\nu_m \rightarrow \frac{(1+5\nu_r)}{(9+5\nu_r)} \quad \text{as } s \rightarrow 0 \quad (6.66)$$

Considering the fact that the available methods do not consider the statistical nature of jointed rock masses, Dershowitz et al. (1979) present a statistically based analytical model to examine the rock mass deformability. The statistical model is shown in Fig. 6.20. The rock mass is taken as a three dimensional circular cylinder. Deformation is assumed to accrue both from the elasticity of intact rock and from the displacement along discontinuities. Displacements along intersecting discontinuities are assumed to be independent. In this model compatibility of lateral displacements across jointed blocks is approximated by constraining springs. Inputs to the model include stiffness and deformation moduli, stress state, and discontinuity geometry. Intact rock deformability is expressed by Young's modulus E_r , set at 200,000 kg/cm², a typical value. Discontinuity stiffnesses are represented by normal stiffness k_n set at 1,000,000 kg/cm³, and shear stiffness k_s set at 200,000 kg/cm³. The stress state is described by vertical major principal stress σ_1 , and horizontal "confining" stress σ_3 . "Confining" stress σ_3 is determined from initial stress σ_{30} and a spring constant k_g as follows

$$\sigma_3 = \sigma_{30} + k_g \delta_y \quad (6.67)$$

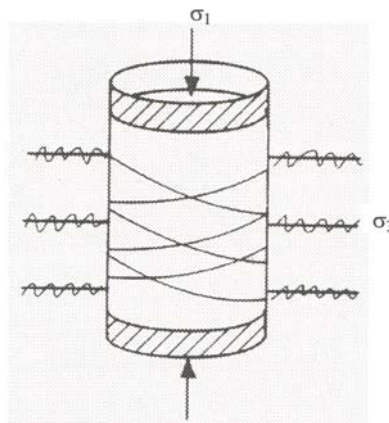


Fig. 6.20 Statistical model for jointed rock (after Dershowitz et al., 1979).

where δ_y is the calculated horizontal displacement; σ_{30} is set to 50 kg/cm²; and k_g is set at 2500 kg/cm³, a value chosen to maximize the increase of stress with lateral strain without causing rotation of principal planes.

Discontinuity geometry is described by three parameters: the mean spacing s_m , the mean orientation θ_m and the dispersion according to the Fisher model κ . Spacing is assumed to follow a negative exponential distribution and orientation a Fisher distribution (Table 6.8).

Some of the results are shown in Figs. 6.21 to 6.24. The results show that the proposed model is consistent with the data of Deere et al. (1967) and Coon and Merritt (1970) (see Fig. 6.10), to the extent that the relationships between deformation modulus and RQD are of similar form.

The model proposed by Dershowitz et al. (1979) has the following limitations:

- 1) The analysis applies only to “hard” rock. Shears and weathering can only be accommodated through changes in discontinuity stiffnesses, which is inadequate.
- 2) The analysis is for infinitesimal strains. Finite strains would violate the assumption of independence among discontinuity displacements.
- 3) The analysis is for a homogeneous deterministic stress field specified extraneous to the discontinuity pattern. Real rock masses may have complex stress distributions strongly influenced by the actual jointing pattern.
- 4) Boundary conditions are highly idealized.

(b) Rock mass with non-persistent discontinuities

For rock masses with non-persistent discontinuities, relationships between the deformation properties and the fracture tensor parameters in two and three dimensions have been derived by Kulatilake et al. (1992, 1993) and Wang (1992) from the discrete element method (DEM) analysis results of generated rock mass blocks. The procedure used to evaluate the effect of discontinuities and the obtained relationships between the deformation properties and the fracture tensor parameters in three dimensions are outlined in the following.

Table 6.8 Distribution assumptions for deformation model (after Dershowitz et al., 1979).

Discontinuity property	Distribution form
Spacing	Negative exponential: $\lambda e^{-\lambda s}$, $\lambda = (\text{mean spacing})^{-1}$
Size (Persistence)	Completely persistent
Orientation	Fisher: $\frac{\kappa e^{-\kappa \cos \alpha}}{4\pi \sinh \kappa}$, $\kappa = \text{dispersion}$; $\alpha = \text{angle from mean pole}$
Normal stiffness	Deterministic
Shear stiffness	Deterministic

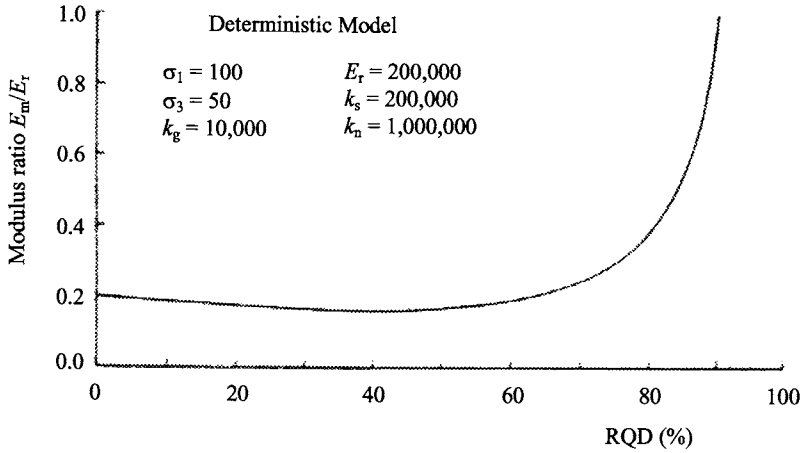


Fig. 6.21 Relationship between E_m/E_r and RQD, parallel discontinuities (after Dershowitz et al., 1979).

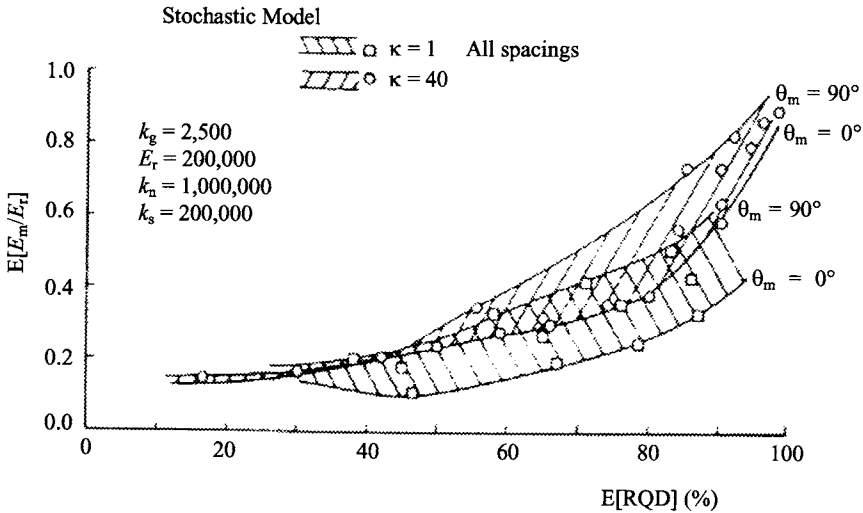


Fig. 6.22 Relationship between $E[E_m/E_r]$ and $E[RQD]$, subparallel discontinuities distributed according to Fisher (after Dershowitz et al., 1979).

The procedure for evaluating the effect of discontinuities on the deformability of rock masses is shown in Fig. 6.25. The first step is the generation of non-persistent discontinuities in 2 m cubical rock blocks. The discontinuities were generated in a systematic fashion as follows:

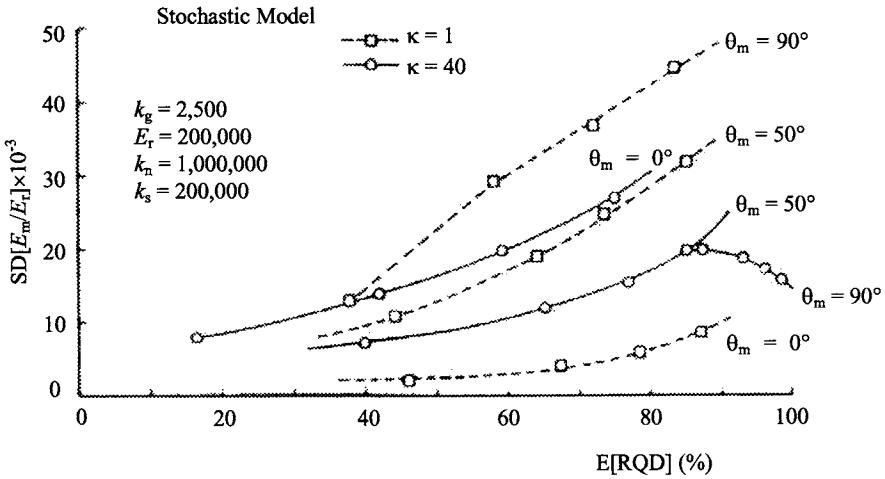


Fig. 6.23 Relationship between $SD[E_m/E_r]$ and $E[RQD]$, subparallel discontinuities distributed according to Fisher (after Dershowitz et al., 1979).

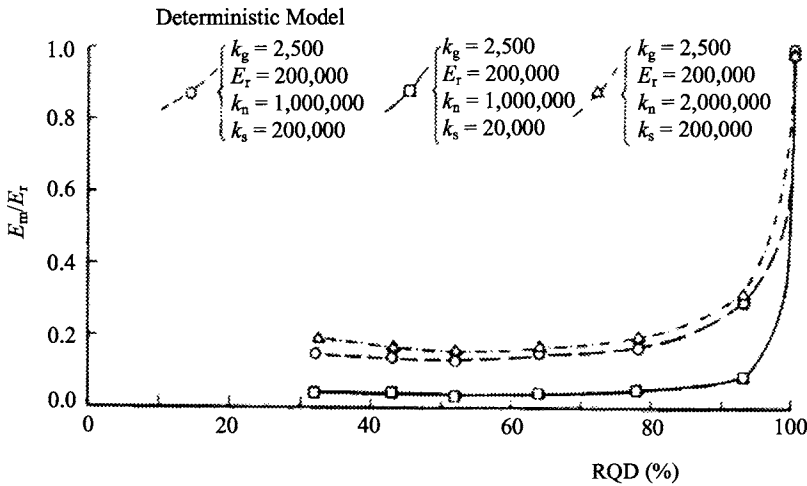


Fig. 6.24 Effect of stiffness values on modulus ratio E_m/E_r , parallel discontinuities (after Dershowitz et al., 1979).

- 1) In each rock block, a certain number of discontinuities having a selected orientation and a selected discontinuity size were placed to represent a discontinuity set.
- 2) Discontinuities were considered as 2D circular discs.

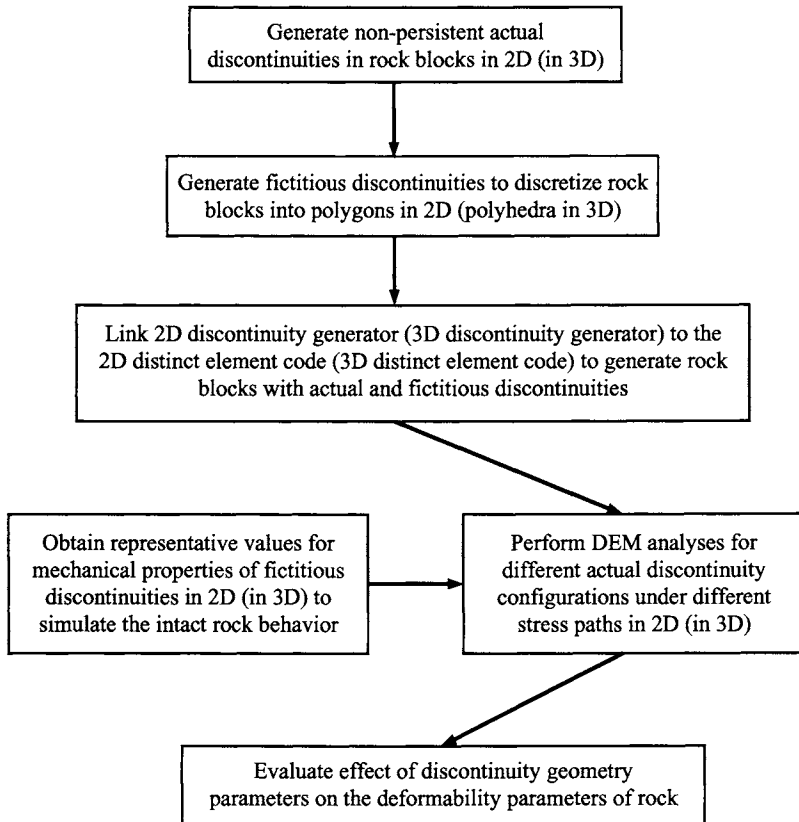


Fig. 6.25 Procedure for evaluating the effect of discontinuity geometry parameters on the deformability properties of jointed rock mass (after Kulatilake et al., 1993).

- 3) Discontinuity center locations were generated according to a uniform distribution.
- 4) Either a single discontinuity set or two discontinuity sets were included in each rock block.

The generated discontinuity networks in the rock blocks are given in Table 6.9.

The second step is the generation of fictitious discontinuities according to the actual non-persistent discontinuity network generated in the rock block. In order to use the DEM for 3D analyses of a generated rock block, the block should be discretized into polyhedra. Since a typical non-persistent discontinuity network in 3D may not discretize the block into polyhedra, it is necessary to create some type of fictitious discontinuities so that when they are combined with actual discontinuities, the block was discretized into polyhedra. Before the generation of fictitious discontinuities, the actual disc-shaped discontinuities are converted into square-shaped ones having the same area. In order for the fictitious

Table 6.9 Generated discontinuity networks of actual discontinuities in the rock block for 3D DEM analysis (after Kulatilake et al., 1992, 1993).

# of discontinuity sets	Orientation α/β	Discontinuity size/ block size	# of discontinuities	Discontinuity location
One set	60°/45°	0.1 – 0.9 with step 0.1	5, 10, 20, 30	Uniform distribution
	94.42°/37.89°	0.3, 0.5, 0.6, 0.7, 0.9	5, 10, 20, 30	
	30°/45°	0.3, 0.5, 0.6, 0.7, 0.8, 0.9	5, 10, 20,	
	90°/45°	0.3, 0.5, 0.6, 0.7, 0.8, 0.9	5, 10, 20	
	68.2°/72.2°	0.3, 0.6, 0.7, 0.8	5, 10, 20, 30	
	248.9°/79.8°	0.3, 0.6, 0.7, 0.8	5, 10, 20, 30	
Two sets	60°/45°	0.1, 0.2, 0.3, 0.5, 0.6, 0.7	10	
	240°/60°		10	

discontinuities to simulate the intact rock behavior, an appropriate constitutive model and associated parameter values for the fictitious discontinuities have to be found. From the investigation performed on 2D rock blocks, Kulatilake et al. (1992) found that by choosing the mechanical properties of the fictitious discontinuities in the way given below, it is possible to make the fictitious discontinuities behave as the intact rock:

- (a) The strength parameters of the fictitious discontinuities are the same as those of the intact rock.
- (b) $G_r/k_s = 0.008 - 0.012$.
- (c) $k_r/k_s = 2 - 3$, with the most appropriate value being E_r/G_r .

For the intact rock (granitic gneiss) studied by Kulatilake et al. (1992, 1993) and Wang (1992), the approximate parameters of the fictitious discontinuities are shown in Table 6.10. The mechanical parameters of the actual discontinuities used by them are also shown in this table. The constitutive models used for the intact rock and discontinuities (both actual and fictitious) are shown in Figs. 6.26 and 6.27, respectively.

The third step is the DEM analysis of the rock block (using the 3D distinct element code 3DEC) under different stress paths and the evaluation of the effect of discontinuities on the deformation parameters of the rock mass. In order to estimate different property values of the jointed rock block, Kulatilake et al. (1993) and Wang (1992) used the following stress paths:

- 1) The rock block was first subjected to an isotropic compressive stress of 5 MPa in three perpendicular directions (x , y , z); then, for each of the three directions, e.g. the z -direction, the compressive stress σ_z was increased, while keeping the confining

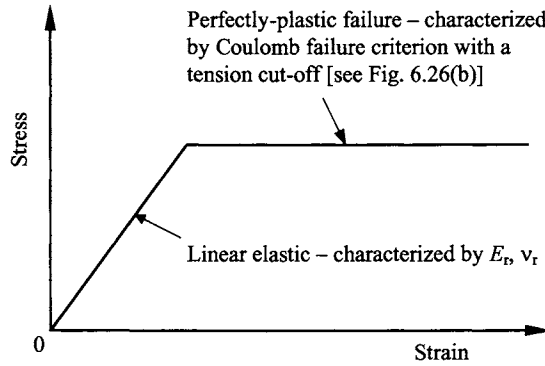
stresses in the other two directions (σ_x and σ_y) the same, until the failure of the rock occurred (see Fig. 6.28). From these analysis results, it is possible to estimate the deformation modulus of the rock block in each of the three directions and the related Poisson's ratios.

- 2) The rock block was first subjected to an isotropic compressive stress of 5 MPa in three perpendicular directions (x, y, z); then, on each of the three perpendicular planes, e.g. the x - y plane, the rock was subjected to an increasing shear stress as shown in Fig. 6.29. These analysis results can be used to estimate the shear modulus of the rock block on each of the three perpendicular planes.

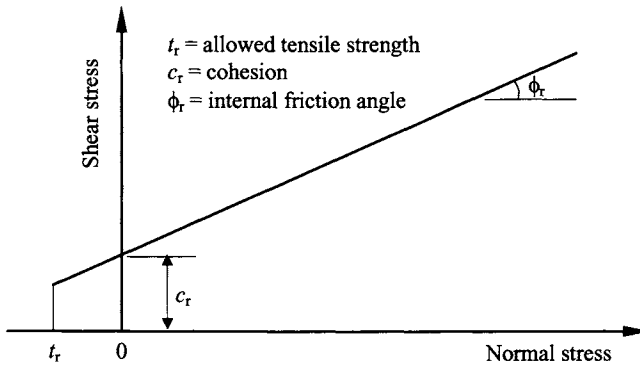
In the DEM analysis, during the loading process, displacements were recorded simultaneously on each block face in the direction(s) needed to calculate the required block strains. On each block face, five points were selected to record the displacement. The average value of these five displacements was considered as the mean displacement of this face for block strain calculations. To make it possible to estimate the deformation properties of the rock block from the DEM analysis results, Kulatilake et al. (1993) and Wang (1992) assumed that the rock block was orthotropic in the x, y, z directions, regardless of the actual orientations of the discontinuities, i.e.,

Table 6.10 Values for the mechanical parameters of intact rock, actual and fictitious discontinuities used by Kulatilake et al. (1992, 1993) and Wang (1992).

Intact rock or Discontinuities	Parameter	Assigned value
Intact rock	Young's modulus E_r	60 GPa
	Poisson's ratio ν_r	0.25
	Cohesion c_r	50 MPa
	Tensile strength t_r	10 MPa
	Friction coefficient $\tan\phi_r$	0.839
Fictitious discontinuities	Normal stiffness k_n	5000 GPa/m
	Shear stiffness k_s	2000 GPa/m
	Cohesion c_j	50 MPa
	Dilation coefficient d_j	0
	Tensile strength t_j	10 MPa
	Friction coefficient $\tan\phi_j$	0.839
Actual discontinuities	Normal stiffness k_n	67.2 GPa/m
	Shear stiffness k_s	2.7 GPa/m
	Cohesion c_j	0.4 MPa
	Tensile strength t_j	0
	Friction coefficient $\tan\phi_j$	0.654



(a)



(b)

Fig. 6.26 Constitutive model assumed for intact rock: (a) stress versus strain; (b) Coulomb failure criterion with a tension cut-off (after Kulatilake et al., 1993).

$$\begin{Bmatrix} \Delta \varepsilon_x \\ \Delta \varepsilon_y \\ \Delta \varepsilon_z \\ \Delta \varepsilon_{xy} \\ \Delta \varepsilon_{xz} \\ \Delta \varepsilon_{yz} \end{Bmatrix} = \begin{bmatrix} \frac{1}{E_x} & -\frac{\nu_{yx}}{E_y} & -\frac{\nu_{zx}}{E_z} & 0 & 0 & 0 \\ & \frac{1}{E_y} & -\frac{\nu_{zy}}{E_z} & 0 & 0 & 0 \\ & & \frac{1}{E_3} & 0 & 0 & 0 \\ & & & \frac{1}{G_{xy}} & 0 & 0 \\ & \text{Sym.} & & & \frac{1}{G_{xz}} & 0 \\ & & & & & \frac{1}{G_{yz}} \end{bmatrix} \begin{Bmatrix} \Delta \sigma_x \\ \Delta \sigma_y \\ \Delta \sigma_z \\ \Delta \sigma_{xy} \\ \Delta \sigma_{xz} \\ \Delta \sigma_{yz} \end{Bmatrix} \quad (6.68)$$

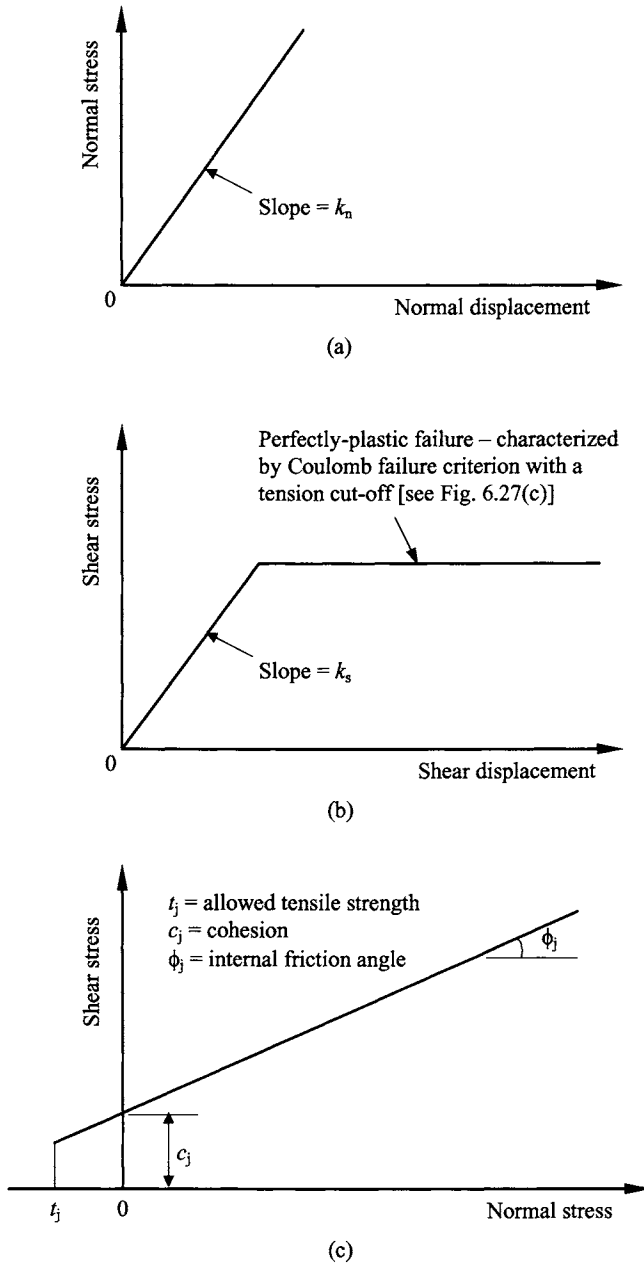


Fig. 6.27 Constitutive model assumed for joints: (a) normal stress versus normal displacement; (b) shear stress versus shear displacement; and (c) Coulomb failure criterion with a tension cut-off (after Kulatilake et al., 1993).

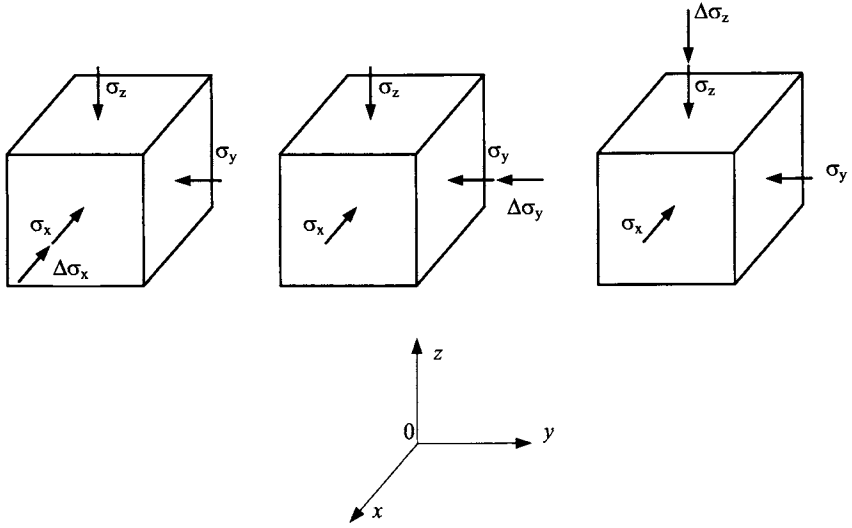


Fig. 6.28 Stress paths of first type used to perform DEM analysis of generated rock blocks (after Kulatilake et al., 1993).

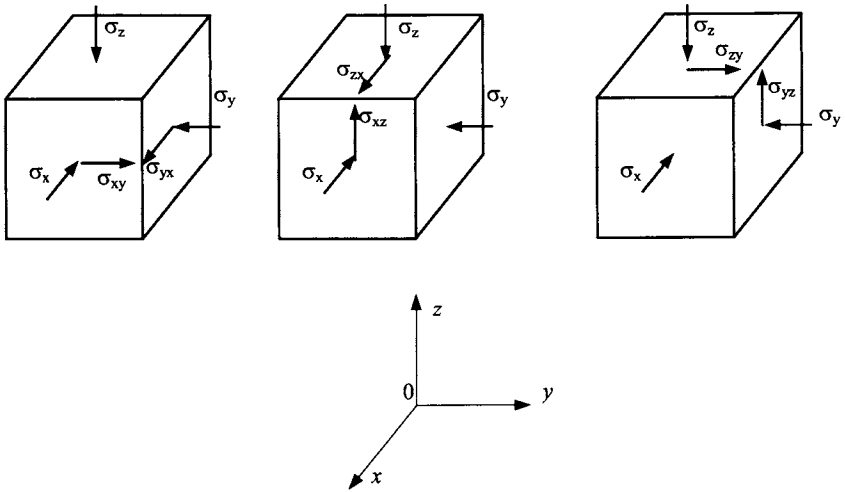


Fig. 6.29 Stress paths of second type used to perform DEM analysis of generated rock blocks (after Kulatilake et al., 1993).

With the above constitutive model, the deformation moduli E_x , E_y , E_z and Poisson's ratios ν_{xy} , ν_{xz} , ν_{yx} , ν_{yz} , ν_{zx} , ν_{zy} can be estimated from the DEM analysis results of rock blocks under stress path 1 (Fig. 6.28). The shear moduli G_{xy} , G_{xz} and G_{yz} can be estimated from the DEM analysis results of rock blocks under stress path 2 (Fig. 6.29).

To reflect the effect of discontinuity geometry parameters on the deformation properties, Kulatilake et al. (1993) and Wang (1992) used the fracture tensor defined by Oda (1982) as an overall measure of the discontinuity parameters – discontinuity density, orientation, size and the number of discontinuity sets. For thin circular discontinuities, the general form of the fracture tensor at the 3D level for the k th discontinuity set can be expressed as (see also Chapter 4 about the discussion of fracture tensors)

$$F_{ij}^{(k)} = 2\pi\rho \int_0^\infty \iint_{\Omega/2} r^3 n_i n_j f(\mathbf{n}, r) d\Omega dr \quad (6.69)$$

where ρ is the average number of discontinuities per unit volume (discontinuity density), r is the radius of the circular discontinuity (discontinuity size), \mathbf{n} is the unit vector normal to the discontinuity plane, $f(\mathbf{n}, r)$ is the discontinuity probability density function of \mathbf{n} and r , $\Omega/2$ is a solid angle corresponding to the surface of a unit hemisphere, and n_i and n_j ($i, j = x, y, z$) are the components of vector \mathbf{n} in the rectangular coordinate system considered (see Fig. 6.30). The solid angle $d\Omega$ is also shown in Fig. 6.30. If the distributions of the size and the orientation of the discontinuities are independent of each other, equation (6.69) can be rewritten as follows

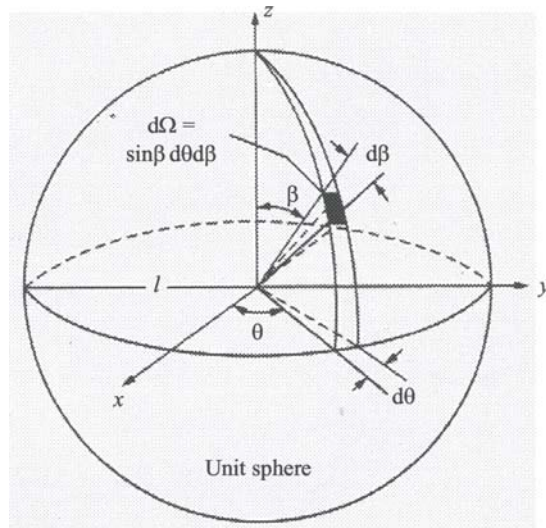


Fig. 6.30 Unit sphere used to define the solid angle $d\Omega$ (after Oda, 1982).

$$F_{ij}^{(k)} = 2\pi\rho \int_0^\infty r^3 f(r) dr \iint_{\Omega/2} n_i n_j f(\mathbf{n}) d\Omega \quad (6.70)$$

where $f(\mathbf{n})$ and $f(r)$ are the probability density functions of the unit normal vector \mathbf{n} and size r , respectively. If there are more than one discontinuity set in the rock mass, the fracture tensor for the rock mass can be obtained by

$$F_{ij} = \sum_{k=1}^N F_{ij}^{(k)} \quad (6.71)$$

where N is the number of discontinuity sets in the rock mass. Fracture tensor F_{ij} can also be written in matrix form as follows

$$\mathbf{F}(F_{ij}) = \begin{bmatrix} F_{xx} & F_{xy} & F_{xz} \\ & F_{yy} & F_{yz} \\ \text{Sym.} & & F_{zz} \end{bmatrix} \quad (6.72)$$

Since the diagonal components of the fracture tensor F_{xx} , F_{yy} and F_{zz} express the combined effect of discontinuity density and discontinuity size in the x , y and z directions, respectively, Kulatilake, et al. (1993) and Wang (1992) showed the obtained deformation properties as in Figs. 6.31 and 6.32. Putting the data in Figs. 6.31(a)–(c) and Figs. 6.32(a)–(c) respectively together, Figs. 6.33 and 6.34 were obtained, which show that the deformation properties of jointed rock masses are related to the corresponding components of the fracture tensor. As for the Poisson's ratios of the generated rock blocks, Kulatilake, et al. (1993) and Wang (1992) found that they were between 50 and 190% of the intact rock Poisson's ratio.

(c) Comments

In the equivalent continuum approach, the elastic properties of the equivalent material are essentially derived by examining the behavior of two rock blocks having the same volume and by using an averaging process. One volume is a representative sample of the rock mass whereas the second volume is cut from the equivalent continuum and is subject to homogeneous (average) stresses and strains. Therefore, the equivalent continuum approach requires that the representative sample of the rock mass be large enough to contain a large number of discontinuities. On the other hand, the corresponding equivalent continuum volume must also be sufficiently small to make negligible stress and strain variations across it. This leads to a dilemma which is typical in modeling continuous or discontinuous composite media.

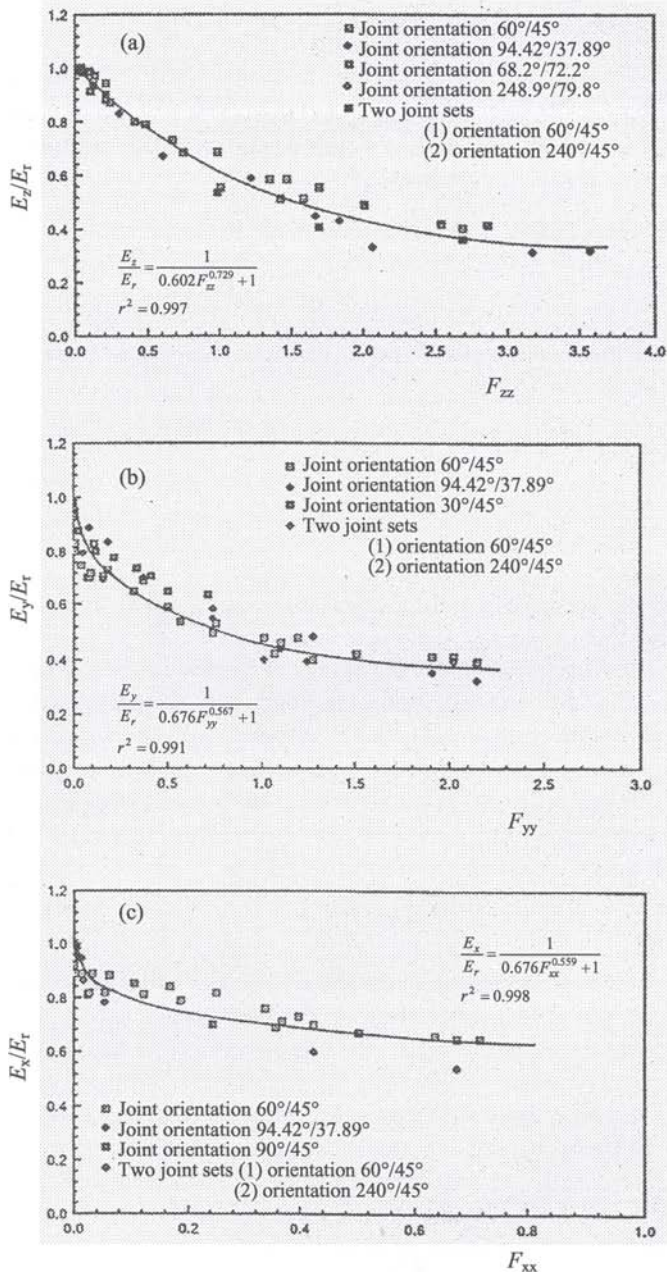


Fig. 6.31 Relations between rock block deformation moduli and fracture tensor components for different discontinuity networks: (a) E_z/E_r vs F_{zz} ; (b) E_y/E_r vs F_{yy} ; and (c) E_x/E_r vs F_{xx} (after Kulatilake et al., 1993).

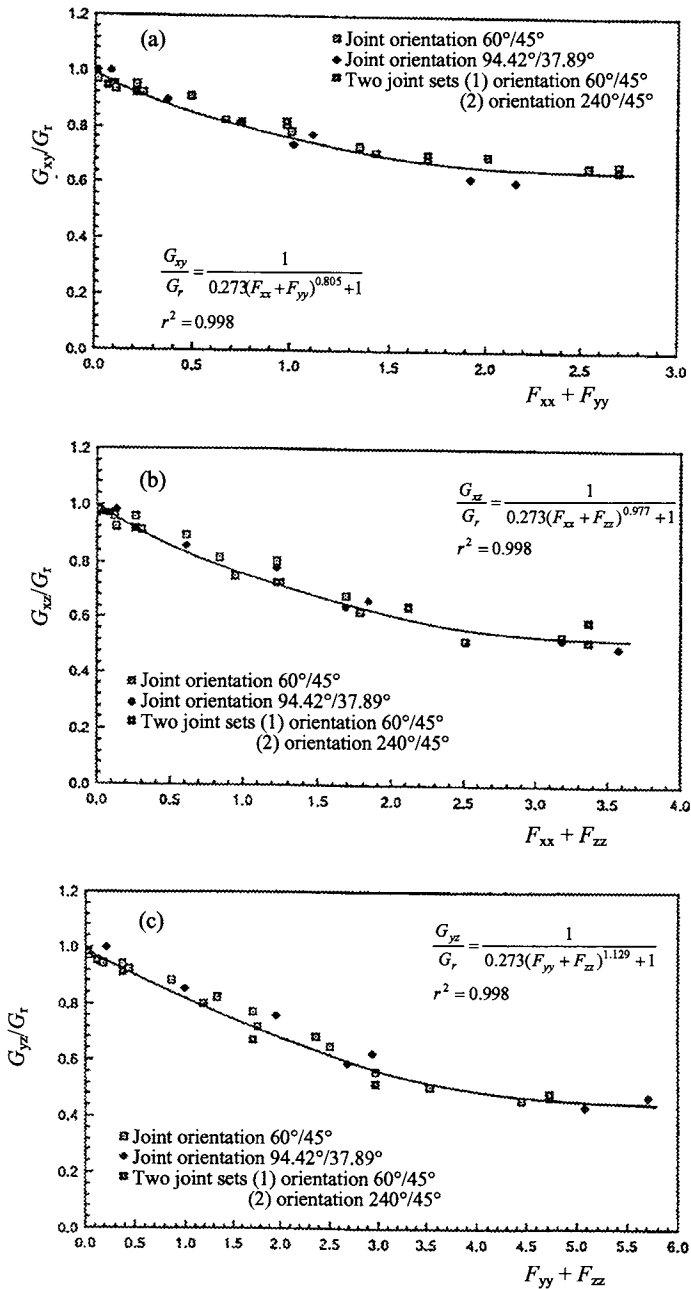


Fig. 6.32 Relations between rock block shear moduli and summation of corresponding fracture tensor components for different discontinuity networks: (a) G_{xy}/G_r vs $(F_{xx} + F_{yy})$; (b) G_{xz}/G_r vs $(F_{xx} + F_{zz})$; and (c) G_{yz}/G_r vs $(F_{yy} + F_{zz})$ (after Kulatilake et al., 1993).

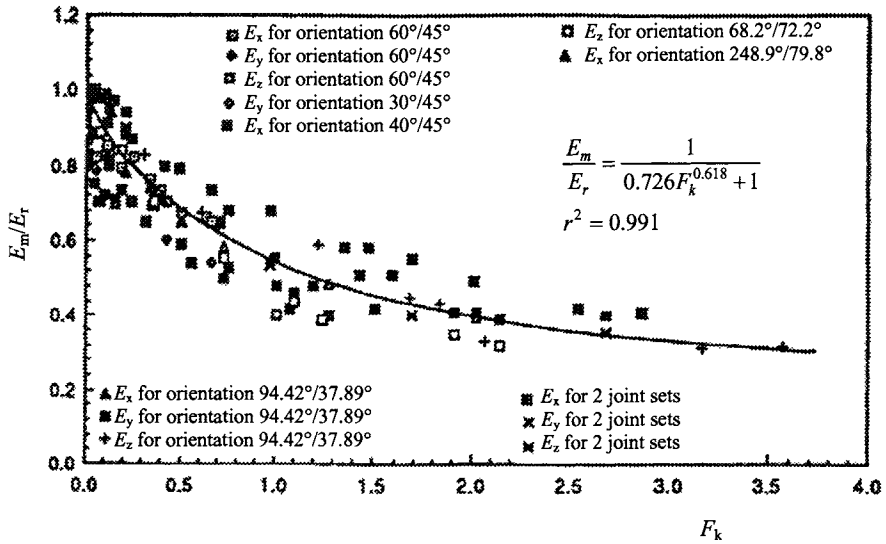


Fig. 6.33 Relations between rock block deformation modulus in any direction E_m and the fracture tensor components in the same direction (after Kulatilake et al., 1993).

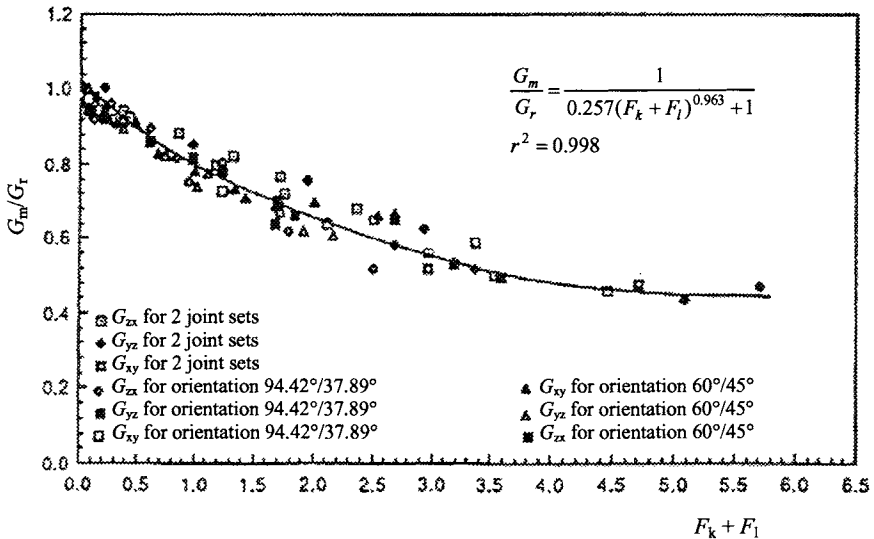


Fig. 6.34 Relations between rock block shear modulus on any plane G_m and the summation of fracture tensor components on that plane (after Kulatilake et al., 1993).

Numerous authors have used the equivalent continuum approach and derived the expressions for the equivalent continuum deformation properties. Most of these expressions are based on the assumption that the discontinuities are persistent. This is a conservative assumption since, in reality, most of the discontinuities are non-persistent with finite size.

For a rock mass containing non-persistent discontinuities, Kulatilake et al. (1992, 1993) and Wang (1992) derived relationships between the deformation properties and the fracture tensor parameters from the DEM analysis results of generated rock mass blocks. However, there exist limitations for the method they used and thus for the relationships they derived as follows:

1. The generated rock mass block is assumed to be orthotropic in the x , y , z directions, regardless of the actual orientations of the discontinuities. The appropriateness of this assumption is questionable. For example, the two blocks shown in Fig. 6.35 have the same fracture tensor F_{ij} , block 1 containing three orthogonal discontinuity sets while block 2 containing one discontinuity set. It is appropriate to assume that block 1 is orthotropic in the x , y , z directions. However, it is obviously inappropriate to assume that block 2 is orthotropic in the x , y , z directions.
2. To do DEM analysis on the generated rock mass block, fictitious discontinuities are introduced so that when they are combined with actual discontinuities, the block is discretized into polyhedra. To make the fictitious discontinuities behave as the intact rock, appropriate mechanical properties have to be assigned to the fictitious discontinuities. From the investigation performed on 2D rock blocks, Kulatilake et al. (1992) found a relationship between the mechanical properties of the fictitious discontinuities and those of the intact rock. However, even if the mechanical properties of the fictitious discontinuities are chosen from this relationship, the fictitious discontinuities can only approximately behave as the intact rock. So the introduction of fictitious discontinuities brings further errors to the final analysis results.
3. Discontinuity persistence ratio PR (defined as the ratio of the actual area of a discontinuity to the cross-section area of the discontinuity plane with the rock block) should have a great effect on the deformability of rock masses. However, the relationships derived by Kulatilake et al. (1992, 1993) and Wang (1992) does not show any effect of PR on the deformability of jointed rock masses.
4. The conclusion that E_i/E_r ($i = x, y, z$) is related only to F_{ii} ($i = x, y, z$) is questionable. This can be clearly seen from the two rock blocks shown in Fig. 6.36. The two blocks have the same fracture tensor component F_{zz} . From Fig. 6.33, the two blocks will have the same deformation modulus in the z -direction. However, block 2 is obviously more deformable than block 1 in the z -direction.

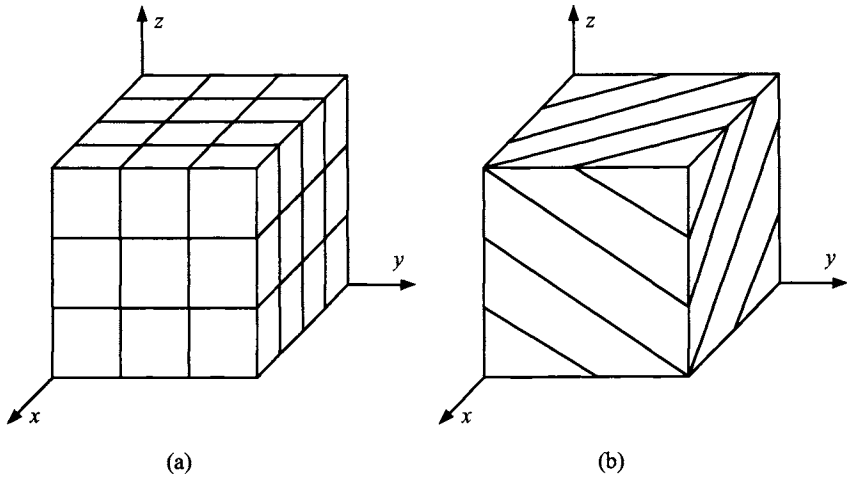


Fig. 6.35 Two rock blocks having the same fracture tensor but different discontinuity sets: (a) Rock block with three orthogonal discontinuity sets; and (b) Rock block with one discontinuity set.

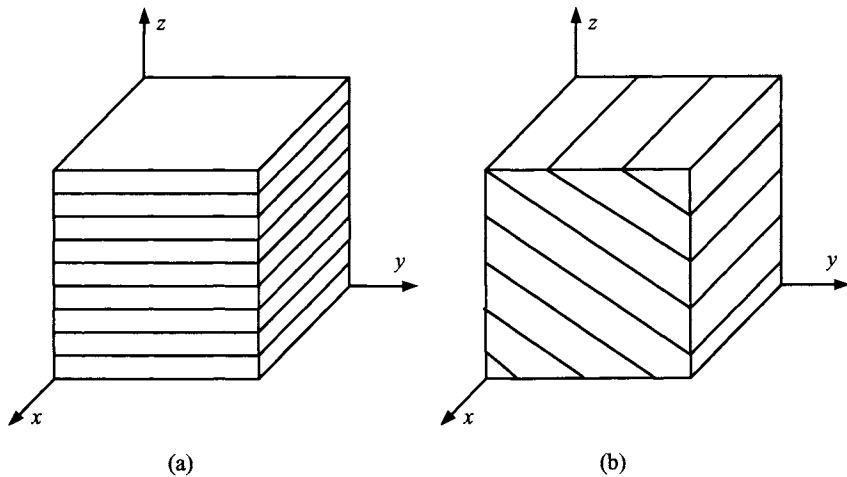


Fig. 6.36 Two rock blocks having the same fracture tensor component in z -direction but different discontinuity orientations: (a) Rock block with discontinuity normal parallel to z -axis; and (b) Rock block with discontinuity normal inclined from z -axis.

6.5 SCALE EFFECT ON ROCK DEFORMABILITY

Research results (see, e.g., Heuze, 1980; Hoek & Brown, 1980; Lo et al., 1987; Medhurst & Brown, 1996) indicate that rock masses show strong scale dependent mechanical properties. The scale effect on the deformability of rock masses can be seen

from the difference of rock mass deformation modulus measured in the field and intact rock modulus measured in the laboratory. Heuze (1980) concluded that the rock mass deformation modulus measured in the field ranges between 20 and 60% of the intact rock modulus measured in the laboratory. Fig. 6.37 shows the variation of measured dynamic modulus (E_{dyn}) with the test volume of rock. The static moduli of the intact rock (E_r) and of the rock mass (E_m) are also shown in this figure. One simple and apparent explanation to the reduction of rock mass deformation modulus is that the effect of discontinuities is included in the rock masses.

6.6 EFFECT OF CONFINING STRESS ON ROCK DEFORMABILITY

Although the effect of confining stress on rock deformability is not considered in many rock mechanics problems, research results have shown that rock deformation modulus increases significantly with the confining stress (Gustkiewicz, 1985; Arora, 1987; Zimmerman, 1991; Verman et al., 1997; Asef & Reddish, 2002). Arora (1987) undertook comprehensive experimental studies of the effect of confining stress on the deformation modulus of jointed rock masses. He conducted triaxial tests on three types of rocks: plaster of Paris, Jamrani sandstone and Agra sandstone with σ_c respectively of 11.3, 55 and 110 MPa. The test specimens contain clean and rough-broken discontinuities created at various inclination ranging from 0 to 90°. Using the axial stress versus strain plot, the deformation modulus was calculated at 50% of the maximum stress. Fig. 6.38 shows the normalized deformation modulus against the normalized unconfined strength of the jointed rock mass, leading to the development of the following expression:

$$\frac{E_{m(\sigma_3=0)}}{E_{m(\sigma_3)}} = 1 - \exp\left(-0.1 \frac{\sigma_{\text{cm}}}{\sigma_3}\right) \quad (6.73)$$

where $E_{m(\sigma_3=0)}$ is the deformation modulus of the jointed rock mass at unconfined stress state; $E_{m(\sigma_3)}$ is the deformation modulus of the jointed rock mass at triaxial stress state with $\sigma_2 = \sigma_3$; and σ_{cm} is the unconfined compressive strength of the jointed rock mass. The equation can be used for intact rock deformation modulus E_r if σ_{cm} is substituted by σ_c .

Verman et al. (1997) obtained an empirical expression showing the variation of the deformation modulus of rock masses with depth:

$$E_m = 0.4H^\alpha 10^{\frac{\text{RMR}-20}{38}} \quad (6.74)$$

where α is a variable depending on RMR ($\alpha = 0.3$ and 0.16 respectively at RMR = 68 and 31); and H is the depth in meters.

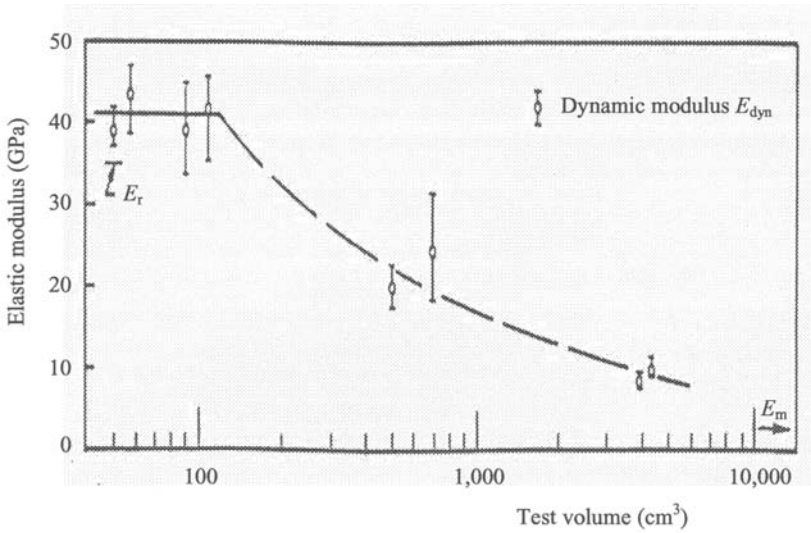


Fig. 6.37 Effect of test volume on the elastic modulus of rock (after Lo et al., 1987).

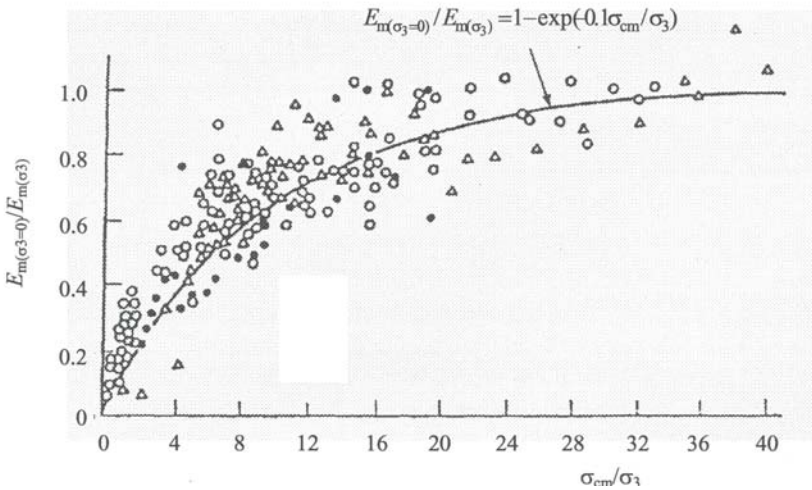


Fig. 6.38 Variation of $E_{m(\sigma_3=0)}/E_{m(\sigma_3)}$ with σ_{cm}/σ_3 (after Arora, 1987).

Asef and Reddish (2002) showed that equation (6.73) significantly overestimates the deformation modulus at a given confining stress when compared with equation (6.74). By re-analyzing Arora’s original data, Asef and Reddish (2002) derived the following empirical equation:

$$\frac{E_{m(\sigma_3)}}{E_{m(\sigma_3=0)}} = \frac{200 \frac{\sigma_3}{\sigma_{cm}} + b}{\frac{\sigma_3}{\sigma_{cm}} + b} \quad (6.75)$$

where $b = 15 + \exp(-0.18\sigma_c)$, $E_{m(\sigma_3=0)}$ is the deformation modulus of the jointed rock mass at unconfined stress state; $E_{m(\sigma_3)}$ is the deformation modulus of the jointed rock mass at triaxial stress state with $\sigma_2 = \sigma_3$; σ_{cm} is the unconfined compressive strength of the jointed rock mass; and σ_c is the unconfined compressive strength of the intact rock. The equation can also be used for intact rock deformation modulus E_r if σ_{cm} is substituted by σ_c . Fig. 6.39 is the comparison of equation (6.75) with new test data of Asef and Reddish (2002).

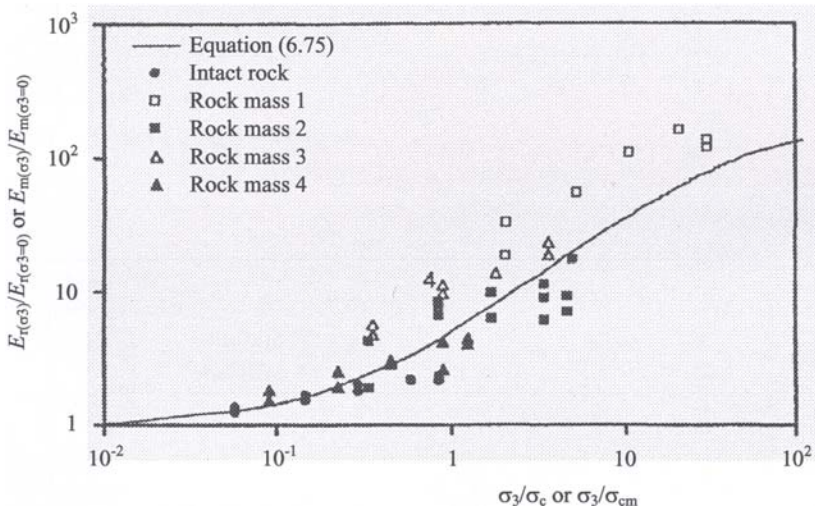
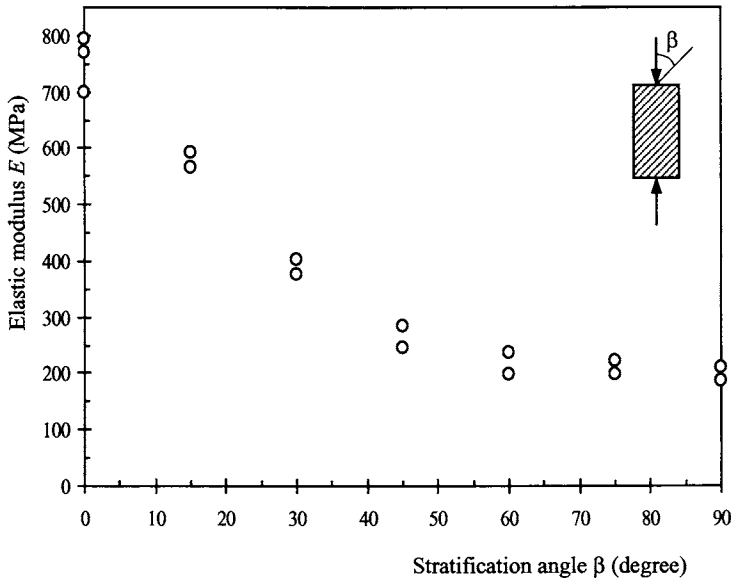


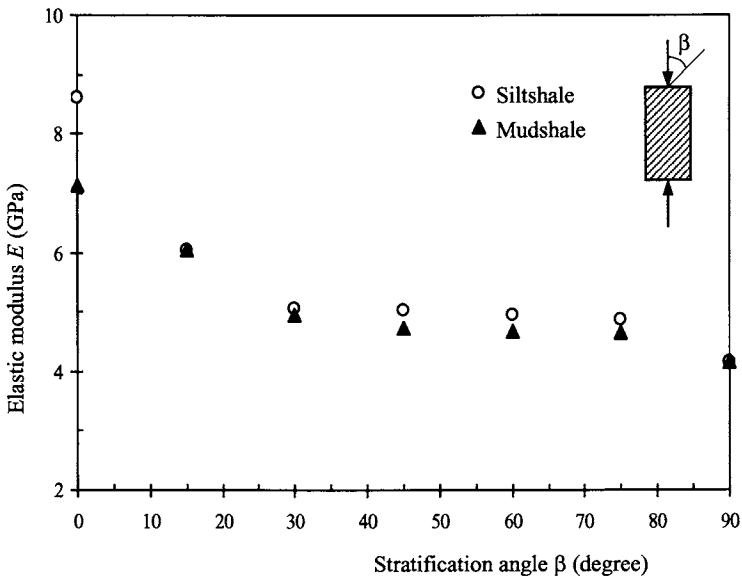
Fig. 6.39 Variation of $E_{r(\sigma_3)}/E_{r(\sigma_3=0)}$ or $E_{m(\sigma_3)}/E_{m(\sigma_3=0)}$ with σ_3/σ_c or σ_3/σ_{cm} (after Asef & Reddish, 2002).

6.7 ANISOTROPY OF ROCK DEFORMABILITY

Anisotropy is one of the key aspects of rock properties. Some intact rocks, such as sandstone, shale, limestone, schist, slate and gneiss belonging to sedimentary and metamorphic groups, show strong deformability anisotropy. Fig. 6.40 shows the anisotropy of elastic modulus for diatomite, siltshale and mudshale under conditions of unconfined compression. The highest and lowest values of the elastic modulus correspond, respectively, to the directions parallel and perpendicular to the stratification plane. The



(a)



(b)

Fig. 6.40 Anisotropy of elastic modulus of intact rocks: (a) Montagne d'Andance diatomite (after Alliot & Boehler, 1979); and (b) Siltshale and mudshale (after Ajalloeian & Lashkaripour, 2000)

degree of deformability anisotropy can be quantified by the deformability anisotropy ratio R_E defined as

$$R_E = \frac{E_{\max}}{E_{\min}} \quad (6.76)$$

where E_{\max} and E_{\min} are, respectively, the maximum (usually in the direction parallel to the stratification plane, i.e., $\beta = 0^\circ$) and minimum (usually in the direction perpendicular to the stratification plane, i.e., $\beta = 90^\circ$) elastic moduli. Table 6.11 lists the values of R_E for different rocks.

Rock masses containing discontinuities also display deformability anisotropy. The equivalent continuum models presented in Section 6.4.2 clearly show the anisotropy of rock mass deformability due to the presence of discontinuities.

Table 6.11 Deformability anisotropy ratio R_E for different rocks.

Rock	Anisotropy ratio R_E	Reference
Cedillo slate	7.10	Peres Rodrigues (1979)
Rothbach sandstone	5.31	Louis et al. (2005)
Diatomite	3.81	Allirot & Boehler (1979)
Siltshale	2.06	Ajalloeian & Lashkaripour (2000)
Mudshale	1.72	Ajalloeian & Lashkaripour (2000)
Carboniferous mudstone	1.52	King et al. (1994)
Marble	1.50	Lepper (1949)
Bentheim sandstone	1.45	Louis et al. (2005)
Hast Schist	1.44	Read et al. (1987)
Hornfel	1.31	Chang & Haimson (2005)
Metapelite	1.29	Chang & Haimson (2005)
Adamswiller sandstone	1.26	Gatelier et al., 2002
Sandstone	1.23	Müller (1930)

7

Strength

7.1 INTRODUCTION

Estimating the strength of rock masses is one of the major problems confronting designers of engineering structures on or in rock. The strength of a rock mass depends not only on the nature of the rock material (intact rock), but also on the discontinuities that separate the intact rock blocks. Because of the discontinuities, a rock mass almost always has significantly lower strength than the corresponding intact rock.

Unconfined compressive strength is the most generally used measurement of rock strength. Tensile strength is also used as a measurement of rock strength in many cases. Different correlations for estimating the unconfined compressive strength and the tensile strength of rocks will be presented in Sections 7.2 and 7.4 respectively for intact rocks and rock masses. Since rocks are seldom naturally loaded in only one direction, empirical strength criteria considering the effect of minor principal stresses will also be presented.

In many cases, the behavior of a rock mass is controlled by sliding along discontinuities. To analyze the stability of a rock mass, it is necessary to know the shear strength of discontinuities. In Section 7.3, several shear strength models for rock discontinuities will be presented.

Rocks show strong scale dependent and anisotropic strength properties. The scale effect on and anisotropy of rock strength will be briefly discussed respectively in Sections 7.5 and 7.6.

7.2 STRENGTH OF INTACT ROCK

7.2.1 Unconfined compressive strength of intact rock

The typical range of the unconfined compressive strength of different rocks is listed in Table 7.1. The procedure for measuring the unconfined compressive strength has been standardized by both the American Society for Testing and Materials (ASTM) and the International Society for Rock Mechanics (ISRM). Although the method is relatively simple, it is time consuming and expensive; also, it requires well-prepared rock cores, which is often difficult for weak rocks and especially for shales. Therefore, indirect tests are often conducted to estimate the unconfined compressive strength by using

Table 7.1 Typical range of unconfined compressive strength of intact rocks (AASHTO, 1989).

Rock category	General description	Rock	Unconfined compressive strength, σ_c ⁽¹⁾ (MPa)
A	Carbonate rocks with well-developed crystal cleavage	Dolostone	33 – 310
		Limestone	24 – 290
		Carbonatite	38 – 69
		Marble	38 – 241
		Tactite-Skarn	131 – 338
B	Lithified argillaceous rock	Argillite	29 – 145
		Claystone	1 – 8
		Marlstone	52 – 193
		Phyllite	24 – 241
		Siltstone	10 – 117
		Shale ⁽²⁾	7 – 35
		Slate	145 – 207
C	Arenaceous rocks with strong crystals and poor cleavage	Conglomerate	33 – 221
		Sandstone	67 – 172
		Quartzite	62 – 379
D	Fine-grained igneous crystalline rock	Andesite	97 – 179
		Diabase	21 – 572
E	Coarse-grained igneous and metamorphic crystalline rock	Amphibolite	117 – 276
		Gabbro	124 – 310
		Gneiss	24 – 310
		Granite	14 – 338
		Quartz diorite	10 – 97
		Quartz monozonite	131 – 159
		Schist	10 – 145
Syenite	179 – 427		

⁽¹⁾Range of unconfined compressive strength reported by various investigators.

⁽²⁾Not including oil shale.

empirical correlations, such as point load, Schmidt hammer, cone indenter and sound velocity tests.

(a) Point load index versus unconfined compressive strength

The point load index is an indirect measure of the rock strength. The point load test has been briefly described in Chapter 3.

There exist different empirical correlations between the unconfined compressive strength σ_c and the point load index $I_{s(50)}$. Table 7.2 lists some of them. The ratio of σ_c to $I_{s(50)}$ varies widely. To obtain reliable results for a specific site, a series of unconfined compression tests need be carried out to calibrate the point load tests.

Table 7.2 Correlations between unconfined compressive strength σ_c and point load index $I_{s(50)}$.

Correlation	Reference
$\sigma_c = 15.3I_{s(50)} + 16.3$	D'Andrea et al. (1965)
$\sigma_c = 20.7I_{s(50)} + 29.6$	Deer & Miller (1966)
$\sigma_c = 24I_{s(50)}$	Broch & Franklin (1972)
$\sigma_c = 23I_{s(50)}$	Bieniawski (1975)
$\sigma_c = (10 \text{ to } 29)I_{s(50)}$	Al Jassar & Hawkins (1979)
$\sigma_c = 29I_{s(50)}$	Hassani et al. (1980)
$\sigma_c = 16I_{s(50)}$ for sedimentary rocks	Read et al. (1980)
$\sigma_c = 20I_{s(50)}$ for basalts	
$\sigma_c = 18.7I_{s(50)} - 13.2$	Singh (1981)
$\sigma_c = 14.5I_{s(50)}$	Forster (1983)
$\sigma_c = 16.5I_{s(50)} + 51.0$	Gunsallus & Kulhawy (1984)
$\sigma_c = (20 \text{ to } 25)I_{s(50)}$	ISRM (1985)
$\sigma_c = (9 \text{ to } 27)I_{s(50)}$	Hawkins & Olver (1986)
$\sigma_c = (8 \text{ to } 54)I_{s(50)}$	Norbury (1986)
$\sigma_c = (8.6 \text{ to } 16)I_{s(50)}$	Vallejo et al. (1989)
$\sigma_c = 23I_{s(50)} + 13$	Chargill & Shakoor (1990)
$\sigma_c = (14 \text{ to } 82)I_{s(50)}$	Tsidzi (1991)
$\sigma_c = 16I_{s(50)}$	Ghosh & Srivastava (1991)
$\sigma_c = 9.3I_{s(50)} + 20.0$	Grasso et al. (1992)
$\sigma_c = 25.67I_{s(50)}^{0.57}$	
$\sigma_c = 23.37I_{s(50)}$ ($r^2 = 0.96$) for quartzite rocks	Singh & Singh (1993)
$\sigma_c = 19I_{s(50)} + 12.7$ ($r^2 = 0.81$) for sandstones	Ulusay et al. (1994)
$\sigma_c = 12.5I_{s(50)}$ ($r^2 = 0.53$) for granite & tuff	Chau & Wong (1996)
$\sigma_c = 14.3I_{s(50)}$	Smith (1997)
$\sigma_c = 15.25I_{s(50)}$ ($r^2 = 0.96$) for granitic rocks	Tugrul & Zarif (1999)
$\sigma_c = (14.5 \text{ to } 27)I_{s(50)}$ for limestones	Romana (1999)
$\sigma_c = (12 \text{ to } 24)I_{s(50)}$ for sandstones	
$\sigma_c = (10 \text{ to } 15)I_{s(50)}$ for siltstones & mudstones	
$\sigma_c = (5 \text{ to } 10)I_{s(50)}$ for chalk & porous limestones	
$\sigma_c = 23.6I_{s(50)} - 2.7$ for coal measure rocks	Kahraman (2001b)
$\sigma_c = 8.4I_{s(50)} + 9.5$ for 22 different rocks	
$\sigma_c = 21.4I_{s(50)}$ ($r^2 = 0.85$) for mudrocks	Lashkaripour (2002)
$\sigma_c = 24.4I_{s(50)}$ for strong rocks	Quane & Russel (2003)
$\sigma_c = 3.86I_{s(50)}^2 + 5.65 I_{s(50)}$ for weak rocks	
$\sigma_c = 10.3I_{s(50)} + 28.1$ ($r^2 = 0.76$) for sandstones	Zorlu et al. (2004)

Table 7.2 *Continued.*

Correlation	Reference
$\sigma_c = (8 \text{ to } 18)I_{s(50)}$	Palchik & Hatzor (2004)
$\sigma_c = 23I_{s(50)}$ ($r^2 = 0.75$) for limestones, marlstones $\sigma_c = 7.3I_{s(50)}^{1.71}$ ($r^2 = 0.82$) and sandstones	Tsiambaos & Sabatakakis (2004)
$\sigma_c = 10.9I_{s(50)} + 27.4$ ($r^2 = 0.61$) for all rocks	Kahraman et al. (2005)
$\sigma_c = 24.8I_{s(50)} - 39.6$ ($r^2 = 0.72$) for rocks with $n < 1\%$	
$\sigma_c = 10.2I_{s(50)} + 23.4$ ($r^2 = 0.75$) for rocks with $n > 1\%$	

Note: Both σ_c and $I_{s(50)}$ are in the unit of MPa; r^2 is the determination coefficient; and n is the porosity.

Palchik and Hatzor (2004) investigated the influence of porosity on the relation between σ_c and $I_{s(50)}$ for porous chalks. They showed that the ratio of $\sigma_c/I_{s(50)}$ is not constant (range 8 to 18), but is porosity dependent. An increase in porosity from 18% to 40% leads to a decrease in $\sigma_c/I_{s(50)}$ from 18 to 8. Kahraman et al. (2005) also investigated the influence of porosity on the relation between σ_c and $I_{s(50)}$ for different rock types (igneous, sedimentary and metamorphic). There is a significant correlation between σ_c and $I_{s(50)}$ for all rock types, but it is not strong. When the rocks were divided into two groups according to porosity values ($n < 1\%$ and $n > 1\%$), strong correlations were obtained. The slope of the regression line of the rocks having porosity values lower than 1% is much greater than that of the rocks having porosity values higher than 1% (see Table 7.2).

(b) Schmidt hammer rebound number versus unconfined compressive strength

The Schmidt hammer rebound test has been briefly described in Chapter 3. Various empirical correlations have been proposed for calculating the unconfined compressive strength of rocks from the Schmidt hammer rebound number (Sheorey et al., 1984; Haramy & DeMarco, 1985; Sachpazis, 1990; Kahraman, 2001b). Fig. 7.1 shows a series of empirically determined curves relating the L-type Schmidt hammer rebound number at different orientations to the unconfined compressive strength.

Table 7.3 lists a number of closed-form empirical correlations for estimating the unconfined compressive strength from the Schmidt hammer rebound number. It is noted that different correlations may give very different unconfined compressive strength values. To obtain reliable results for a specific site, a series of unconfined compression tests need be carried out to calibrate the Schmidt hammer rebound tests. It is also important to specify the hammer type (L or N).

(c) Shore Sclerscope hardness versus unconfined compressive strength

The Shore Sclerscope hardness was originally designed for use on metals. It measures the relative rebound of a diamond-tipped hammer that drops freely from a fixed height

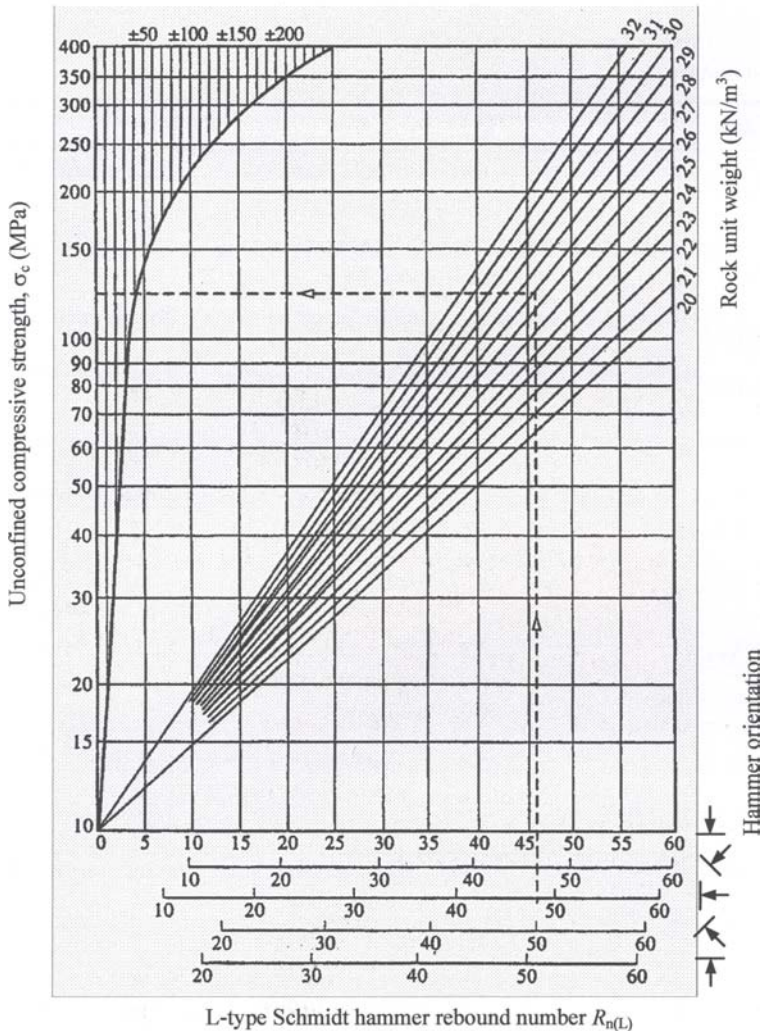


Fig. 7.1 L-type Schmidt hammer rebound number $R_{n(L)}$ versus unconfined compressive strength σ_c (after Deere & Miller, 1966).

onto the surface of a specimen. ISRM (1978b) details the method for Shore Scleroscope hardness testing of rocks using model C-2. The specimen surface should be smooth to within 0.02 mm, and preferably the volume should be at least 40 cm³ and 50 mm thick. Each test should be on a fresh site on the prepared rock surface as the hammer makes a small indentation on impact. 50 readings are recommended, with the highest five and lowest five being discarded before calculating the average rebound height, H , the Shore Scleroscope hardness.

Table 7.3 Correlations between unconfined compressive strength σ_c and Schmidt hammer rebound number R_n .

Correlation	r^2	Rock Type	Reference
$\sigma_c = 6.9 \times 10^{[0.0087\rho R_{n(L)} + 0.16]}$	0.94	28 lithological units, 3 base rock types	Deere & Miller (1966)
$\sigma_c = 6.9 \times 10^{[1.3481\log(\rho R_{n(L)}) - 1.325]}$		25 lithological units	Aufmuth (1973)
$\sigma_c = 12.74e^{0.185\rho R_{n(L)}}$		20 lithological units	Beverly et al. (1979)
$\sigma_c = 0.447e^{(0.045R_{n(L)} + \rho)}$		Different rock types in Northern Silesia	Kidybinski (1980)
$\sigma_c = 0.994R_{n(L)} - 0.383$	0.70	10 lithological units	Haramy & DeParco (1985)
$\sigma_c = 0.043\rho_d R_{n(L)} + 1.2$		Sandstone	Cargill & Shakoor (1990)
$\sigma_c = 0.018\rho_d R_{n(L)} + 2.9$		Carbonate	
$\sigma_c = 4.29R_{n(L)} - 67.5$	0.92	Marble, limestone, dolomite)	Sachpazis (1990)
$\sigma_c = e^{aR_{n(L)} + b}$	0.83	Mica-schist, prasinite, to serpentinite, gabbro,	Xu et al. (1990)
<i>a</i> and <i>b</i> are coefficients depending on rock type	0.90	mudstone	
$\sigma_c = 8.36R_{n(L)} - 416$	0.76	Granitic rocks	Tugrul & Zarif (1999)
$\sigma_c = e^{0.059R_{n(L)} + 0.818}$	0.96	Gypsum	Yilmaz & Sendir (2002)
$\sigma_c = e^{0.053R_{n(L)} + 1.332}$	0.88	Limestone, claystone, siltstone, sandstone, marl, marlstone, basalt, calcarenite, ophite	Morales et al. (2004)
$\sigma_c = 4 \times 10^{-6} R_{n(L)}^{4.2917}$	0.80	Limestone, marble, sandstone, basalt	Yasar & Erdogan (2004a)
$\sigma_c = 2.75R_{n(L)} - 35.83$	0.95	Basalt, andesite, tuff	Dincer et al. (2004)
$\sigma_c = 2.208e^{0.067R_{n(N)}}$	0.96	Chalk, limestone, sandstone, marble, syenite, granite	Katz et al. (2000)
$\sigma_c = 6.97e^{0.014\rho R_{n(N)}}$	0.78	Dolomite, sandstone, limestone, marl, diabase, serpentine, hematite	Kahraman (2001b)

Notes: σ_c is in the unit of MPa; ρ is the rock density in g/cm^3 ; $R_{n(L)}$ and $R_{n(N)}$ are respectively the L- and N-type Schmidt hammer rebound numbers (see Chapter 3 for detailed description of Schmidt hammer rebound test); and r^2 is the determination coefficient.

Various empirical correlations have been proposed for calculating the unconfined compressive strength of rocks from the Shore Sclerscope hardness (Wuerker, 1953; Atkinson, 1993; Brook, 1993; Koncagiul & Santi, 1999; Yasar & Erdođan, 2004a). Table 7.4 lists some of them.

(d) Cone indenter number versus unconfined compressive strength

The cone indenter test was developed by the National Coal Board (now “British Coal Corporation”) as a method for estimating the strength of rocks which may be excavated by roadheading equipment (Szlavin, 1974; Brook, 1993). In a cone indenter test, a sharp tungsten carbide conical point is pressed into the rock under a standard force of 40 N, the force being measured by the deflection of a steel strip, and the total travel of the point, enabling the penetration to be calculated, is measured by a micrometer. Small pieces of rock, up to 25×25×6 mm, are used, either natural chippings in the field, or saw cut thin pieces. This is a modification of the metal hardness tests such as Brinel and Rockwell hardness, such that easily measured penetration occurs and a very flat surface is not essential. The penetration of the cone into the rock specimen, P_s in mm, is compared to the standard spring deflection of 0.635 mm, to give the 40 N force and the standard cone indenter number

$$I_s = \frac{0.635}{P_s} \quad (7.1)$$

This procedure is repeated on a fresh piece or part of rock and the average of 10 measurements are used to calculate the I_s value. The unconfined compressive strength σ_c can be estimated from I_s as follows (Szlavin, 1974; Brook, 1993)

$$\sigma_c = 24.8I_s \quad (\text{MPa}) \quad (7.2)$$

Table 7.4 Correlations between unconfined compressive strength σ_c and Shore Sclerscope hardness H .

Correlation		Reference
$\sigma_c = 2.1H$	Lower limit	Wuerker (1953)
$\sigma_c = 2.8H$	Average	
$\sigma_c = 3.4H$	Upper limit	
$\sigma_c = 3.54(H - 12)$		Atkinson (1993); Brook (1993)
$\sigma_c = 0.895H + 41.98$	$(r^2 = 0.32)$	Koncagiul & Santi (1999)
$\sigma_c = H^{5.555} \times 10^{-8}$	$(r^2 = 0.83)$	Yasar & Erdođan (2004a)

Note: σ_c is in the unit of MPa; and r^2 is the determination coefficient.

For some very strong rocks, the penetration of the 40 N force indenter is very small, say less than 0.12 mm. For such rocks, a modified method is suggested in which the applied force is raised to 110 N with spring deflection 1.27 mm. The modified cone indenter number with the penetration P_m is then

$$I_m = \frac{1.27}{P_m} \quad (7.3)$$

The unconfined compressive strength σ_c can be estimated from I_m as follows (Szlavin, 1974; Brook, 1993)

$$\sigma_c = 35.8I_m \quad (\text{MPa}) \quad (7.4)$$

Some very weak rocks may be broken by the point when a 40 N force is applied. For such rocks, a modified method is suggested in which the applied force is reduced to 12 N with spring deflection 0.23 mm. The cone indenter number with the penetration P_w is then

$$I_w = \frac{0.23}{P_w} \quad (7.5)$$

The unconfined compressive strength σ_c can be estimated from I_w as follows (Szlavin, 1974; Brook, 1993)

$$\sigma_c = 16.5I_w \quad (\text{MPa}) \quad (7.6)$$

(e) Seismic wave velocity versus unconfined compressive strength

Seismic wave velocity has been used to estimate the unconfined compressive strength of rocks by different researchers. Table 7.5 lists a number of empirical correlations for estimating the unconfined compressive strength σ_c from the P-wave velocity v_p . It is noted that different correlations may give very different unconfined compressive strength values. Fig. 7.2 clearly shows the wide range of the unconfined compressive strength values for different rocks at the same P-wave velocity.

(f) Porosity versus unconfined compressive strength

Porosity has a great effect on the strength of intact rocks. The unconfined compressive strength of intact rocks decreases as the porosity increases. Rshewski and Novik (1978) recommended the following relationship between them

$$\sigma_c = \alpha(1 - \beta n)^2 \quad (7.7)$$

Table 7.5 Correlations between unconfined compressive strength σ_c and P-wave velocity v_p .

Correlation	Rock Type	Reference
$\sigma_c = 35.0v_p - 31.5$	Sandstone	Freyburg (1972)
$\sigma_c = 2.45v_p^{1.82}$	Limestone	Militzer & Stoll (1973)
$\log \sigma_c = 0.358v_p + 0.283$	Limestone	Golubev & Rabinovich (1976)
$\log \sigma_c = 0.444v_p + 0.003$	Schist	Golubev & Rabinovich (1976)
$\sigma_c = -0.98v_p + 0.68v_p^2 + 0.98$	Sandy and shaly rocks	Gorjainov & Ljachovickij (1979)
$\sigma_c = kp v_p^2 + A$	Soft rocks	Inoue & Ohomi (1981)
$\sigma_c = 1277e^{(-11.2/v_p)}$	Sandstone	McNally (1987)
$\sigma_c = 36.0v_p - 31.2$	Coal measure rocks	Göktan (1988)
$\sigma_c = 35.54v_p - 55$ ($r^2 = 0.64$)	Granitic rocks	Tugrul & Zarif (1999)
$\sigma_c = 9.95v_p^{1.21}$ ($r^2 = 0.69$)	Dolomite, sandstone, limestone, marl, diabase, serpentine, hematite	Kahraman (2001b)
$\sigma_c = 31.5v_p - 63.7$ ($r^2 = 0.80$)	Dolomite, marble and limestone	Yasar & Erdogan (2004b)
$\sigma_c = 22.03v_p^{1.247}$ ($r^2 = 0.72$)	Granites	Sousa et al. (2005)

Notes: σ_c is the unconfined compressive strength in MPa; ρ is the rock density in g/cm^3 ; v_p is the P-wave velocity in km/s; and r^2 is the determination coefficient.

where n is the porosity; and α and β are constants which can be obtained by fitting analysis of test results. For limestone, they found $\alpha = 277$ MPa and β between 2 and 5.

Tugrul and Zarif (1999) derived the following simple empirical relation between unconfined compressive strength σ_c and porosity n for granitic rocks from Turkey

$$\sigma_c = 183 - 16.55n \quad (r^2 = 0.69) \quad (7.8)$$

where σ_c is in the unit of MPa; n is in %; and r^2 is the determination coefficient.

According to Palchik and Hatzor (2004), the relationship between unconfined compressive strength and porosity can be described by the following negative exponential function

$$\sigma_c = ae^{-bn} \quad (7.9)$$

where n is the porosity; and a and b are constants which can be obtained by fitting analysis of test results. Table 7.6 shows the values of a and b for different rocks.

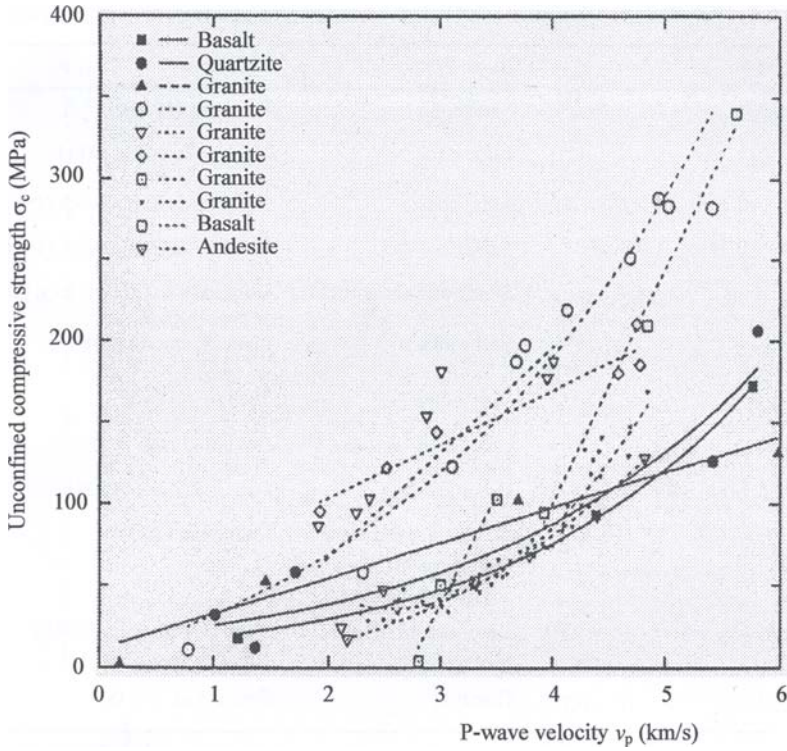


Fig. 7.2 Variation of unconfined compressive strength σ_c with P-wave velocity v_p for fresh and weathered crystalline rocks (after Gupta & Rao, 1998).

Table 7.6 Values of a and b in equation (7.9) for different rocks.

a	b	r^2	Rock Type	Reference
74.4	0.048	0.79	Sandstone	Palchik (1999)
210.1	0.821	0.67	Mudrocks: claystone, clay shale, mudstone, mud shale, siltstone and silt shale	Lashkaripour (2002)
273.1	0.076	0.87	Chalk	Palchik & Hatzor (2004)
195.0	0.210	0.79	Sandstone, limestone, basalt and granodiorite	Tugrul (2004)

Notes: For the values of a and b listed in the table, the unconfined compressive strength σ_c is in the unit of MPa and the porosity n is in %. r^2 is the determination coefficient.

Fig. 7.3 shows the variation of unconfined compressive strength with porosity for various geomaterials from polluted sludge to hard rock (Adachi & Yoshida, 2002).

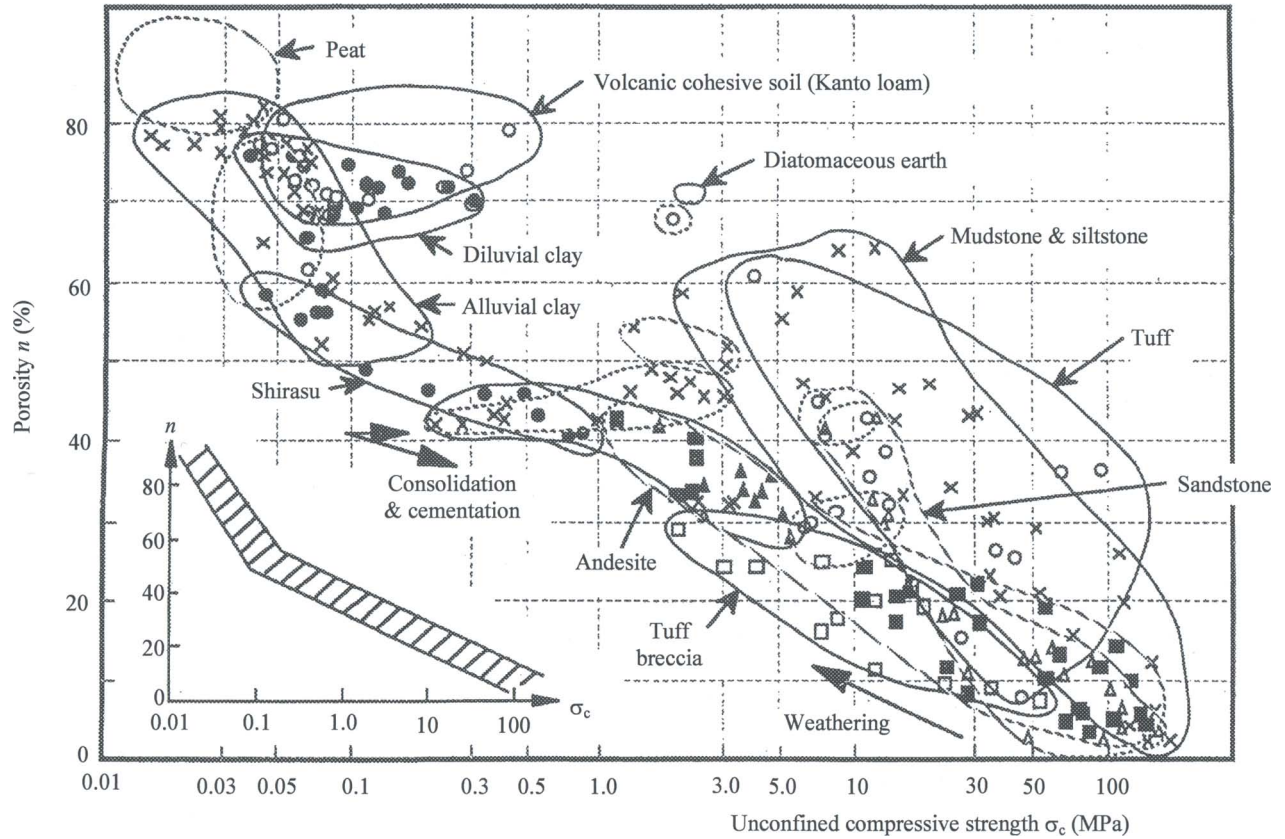


Fig. 7.3 Variation of unconfined compressive strength σ_c with porosity n for various geomaterials (after Adachi & Yoshida, 2002).

(g) Density versus unconfined compressive strength

Since density is closely related to the degree of porosity, it also affects the strength of intact rocks. The unconfined compressive strength of intact rocks increases as the density increases. Turgrul and Zarif (1999) derived the following simple empirical relation between unconfined compressive strength σ_c and dry density ρ_d for granitic rocks from Turkey

$$\sigma_c = 0.566 \rho_d - 1347 \quad (r^2 = 0.67) \quad (7.10)$$

where σ_c is in the unit of MPa; ρ_d is in the unit of kg/m^3 ; and r^2 is the determination coefficient.

According to Smorodinov et al. (1970) and Vasarhelyi (2005), the relationship between unconfined compressive strength σ_c and density ρ can be described by the exponential function

$$\sigma_c = ae^{b\rho} \quad (7.11)$$

where a and b are constants which can be obtained by fitting analysis of test results.

Fig. 7.4 shows the data and trend line of unconfined compressive strength σ_c versus dry density ρ_d for chalks from different locations (Bowden et al., 2002).

(h) Effect of water content on unconfined compressive strength

Researchers have studied the effect of water content on the strength of intact rocks. The unconfined compressive strength of intact rocks decreases as the water content increases and their relationship can be described by the following negative exponential function (Hawkins & McConnell, 1992):

$$\sigma_c = ae^{-bw} + c \quad (7.12)$$

where w is the water content and a , b , and c are constants. Hawkins and McConnell (1992) tested 35 British sandstones from 21 locations with water content ranging from 0.75 to 26.7% and obtained the following values of a , b and c , based on fitting analyses of the tests results:

$$a = 4.16 \text{ to } 84.01; \quad b = 0.0752 \text{ to } 6.4167; \quad \text{and } c = 2.97 \text{ to } 230.98$$

Based on the tests on three types of Coal Measures mudrock (clayshale, mudstone and mudshale) from northern England, Lashkaripour (2002) obtained the following values of a , b , and c :

$$a = 83.59; \quad b = 0.4433; \quad \text{and } c = 0$$

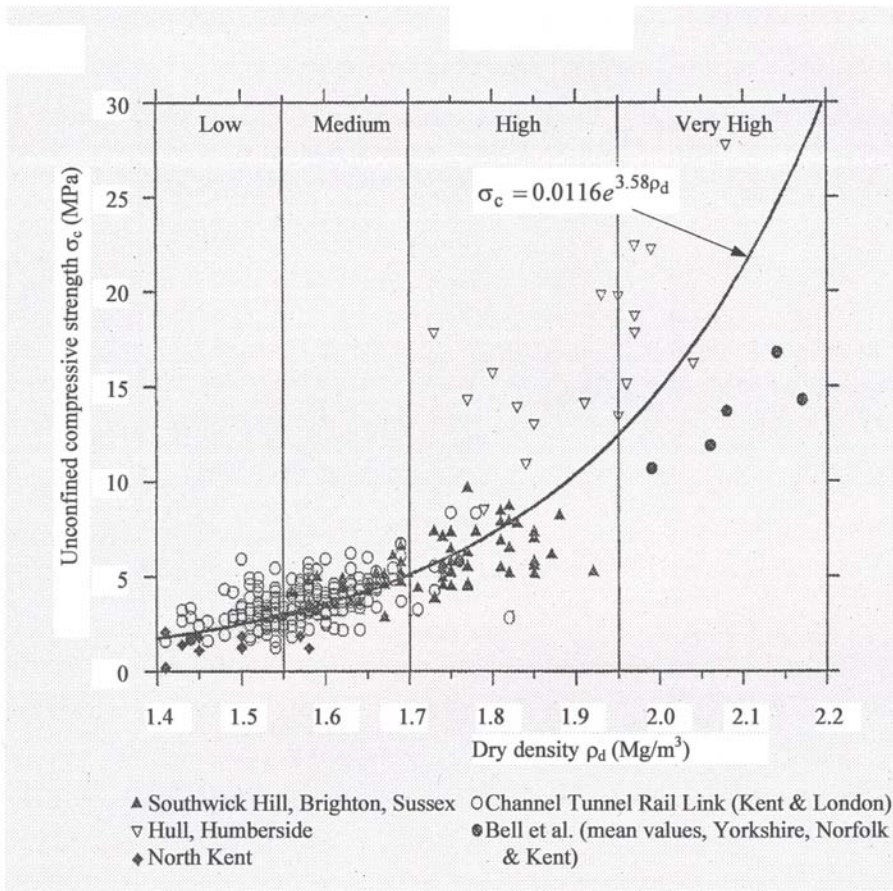


Fig. 7.4 Unconfined compressive strength σ_c versus dry density ρ_d for chalks (after Bowden et al., 2002).

Fig. 7.5 shows the variation of unconfined compressive strength σ_c with water content w for porous chalks. It is noticed that σ_c in the direction parallel to bedding is larger than that in the direction perpendicular to bedding.

Table 7.7 lists the ratio of unconfined compressive strength at saturated condition $\sigma_{c(\text{saturated})}$ to that at dry condition $\sigma_{c(\text{dry})}$ for different rocks. In general, the unconfined compressive strength at saturated condition is about 50 to 80% of that at dry condition.

7.2.2 Tensile strength of intact rock

There is a strong correlation between the tensile strength and the unconfined compressive strength. The following simple correlation is usually used as a first estimate of the tensile strength from the unconfined compressive strength

$$\sigma_t = -\frac{\sigma_c}{10} \quad (7.13)$$

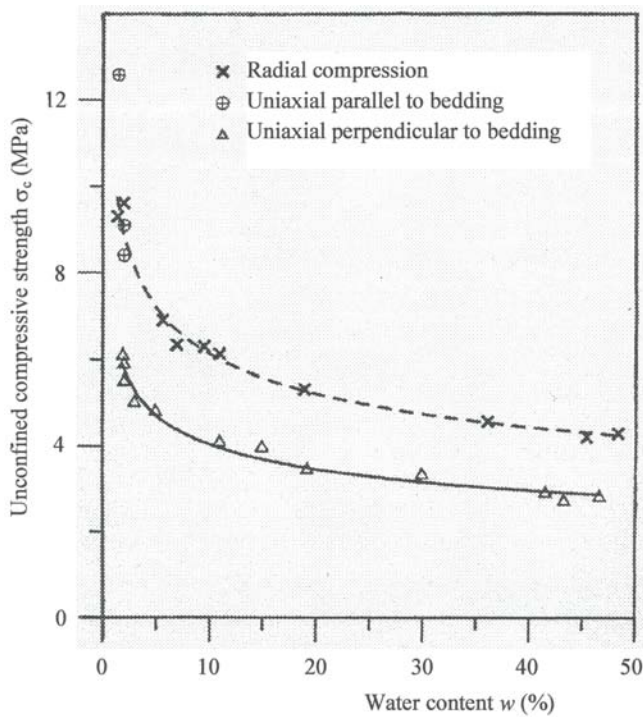


Fig. 7.5 Variation of unconfined compressive strength σ_c with water content w for porous chalks (after Talesnick et al., 2001).

Table 7.7 Ratio of unconfined compressive strength at saturated condition $\sigma_{c(\text{saturated})}$ to that at dry condition $\sigma_{c(\text{dry})}$ for different rocks.

$\sigma_{c(\text{saturated})}/\sigma_{c(\text{dry})}$	Rock	Reference
0.50	Shale and Quartzitic sandstone	Colback & Wild (1965)
0.76	Penrith sandstone	Dyke & Dobereiner (1991)
0.75	Bunter sandstone	Dyke & Dobereiner (1991)
0.66	Waterstone	Dyke & Dobereiner (1991)
0.97	Oolitic limestone	Lashkaripour & Ghafoori (2002)
0.62	Sandstone and sandy limestone	Lashkaripour & Ghafoori (2002)
0.81	Oolitic limestone and limy sandstone	Lashkaripour & Ghafoori (2002)
0.52	Shale	Lashkaripour & Ghafoori (2002)
0.76	British sandstone	Vasarhelyi (2003)
0.66	Miocene limestone	Vasarhelyi (2005)

Because of the strong correlation between the tensile strength and the unconfined compressive strength, the methods for estimating the unconfined compressive strength can also be used to estimate the tensile strength. For example, the point load index $I_{s(50)}$ can be used to estimate the tensile strength

$$\sigma_t = -1.5I_{s(50)} \quad (7.14)$$

The strength criteria to be described in Section 7.2.3 can also be used to determine the tensile strength of an intact rock. For example, with the Hoek-Brown strength criterion for intact rocks, the tensile strength can be estimated from

$$\sigma_t = 0.5\sigma_c[m_i - (m_i^2 + 4)^{0.5}] \quad (7.15)$$

where m_i is a material constant for the intact rock, which depends only upon the rock type (texture and mineralogy) as tabulated in Table 7.8. This equation shows that the ratio of σ_t/σ_c varies with rock types. For the possible range of m_i from 4 to 33 (see Table 7.8),

$$\sigma_t = -(0.03 \text{ to } 0.24)\sigma_c \quad (7.16)$$

Lade (1993) presented the following general relation between σ_t and σ_c for all rock types:

$$\sigma_t = Tp_a \left(\frac{\sigma_c}{p_a} \right)^t \quad (7.17)$$

where p_a is the atmospheric pressure in the same units as those of σ_t and σ_c ; and T and t are dimensionless numbers which vary with rock types. Figs. 7.6(a), (b) and (c) show the data of σ_t and σ_c collected by Lade (1993) respectively for igneous, metamorphic and sedimentary rocks. Based on fitting analysis of the data, Lade (1993) obtained the values of T and t for these three types of rocks as follows:

Igneous rocks:	$T = -0.435,$	$t = 0.740$
Metamorphic rocks:	$T = -0.0518,$	$t = 1.017$
Sedimentary rocks:	$T = -0.316,$	$t = 0.770$
All rocks:	$T = -0.219,$	$t = 0.825$

In addition to the best fitting lines for each type of rocks, the lines of $|\sigma_t/\sigma_c| = 1/5, 1/10, 1/20$ and $1/50$ are also drawn in the figures. It can be seen that the data are widely scattered and $\sigma_t/\sigma_c = -1/10$ [equation (7.13)] is approximately an average of the whole data.

Table 7.8 Values of parameter m_i for different rocks (after Hoek & Brown, 1997; Marinos & Hoek, 2001).

Rock type	Class	Group	Texture			
			Coarse	Medium	Fine	Very fine
Sedimentary	Clastic		Conglomerate (21±3) ^a Breccia (19±5)	Sandstone 17±4	Siltstone 7±2 Greywacke (18±3)	Claystone 4±2 Shale (6±2) Marl (7±2)
		Carbonate				
	Non-Clastic	Evaporite		Gypsum 8±2	Anhydrite 12±2	
		Organic				Chalk 7±2
Metamorphic	Non-foliated		Marble 9±3	Hornfels (19±4) Metasandstone (19±3)	Quartzite 20±3	
	Slightly foliated		Migmatite (29±3)	Amphibolite 26±6	Gneiss 28±5	
	Foliated ^b			Schist 12±3	Phyllite (7±3)	Slate 7±4
Igneous	Plutonic	Light	Granite 32±3 Granodiorite (29±3)	Diorite 25±5		
		Dark	Gabbro 27±3 Norite 20±5	Dolerite (16±5)		
	Hypabyssal		Porphyrie (20±5)		Diabase (15±5)	Peridotite (25±5)
	Volcanic	Lava		Rhyolite (25±5) Andesite 25±5	Dacite (25±3) Basalt (25±5)	Obsidian (19±3)
		Pyroclastic	Agglomerate (19±3)	Breccia (19±5)	Tuff (13±5)	

^a Values in parenthesis are estimates.

^b These values are for intact rock specimen tests normal to bedding or foliation. The value of m_i will be significantly different if failure occurs along a weakness plane.

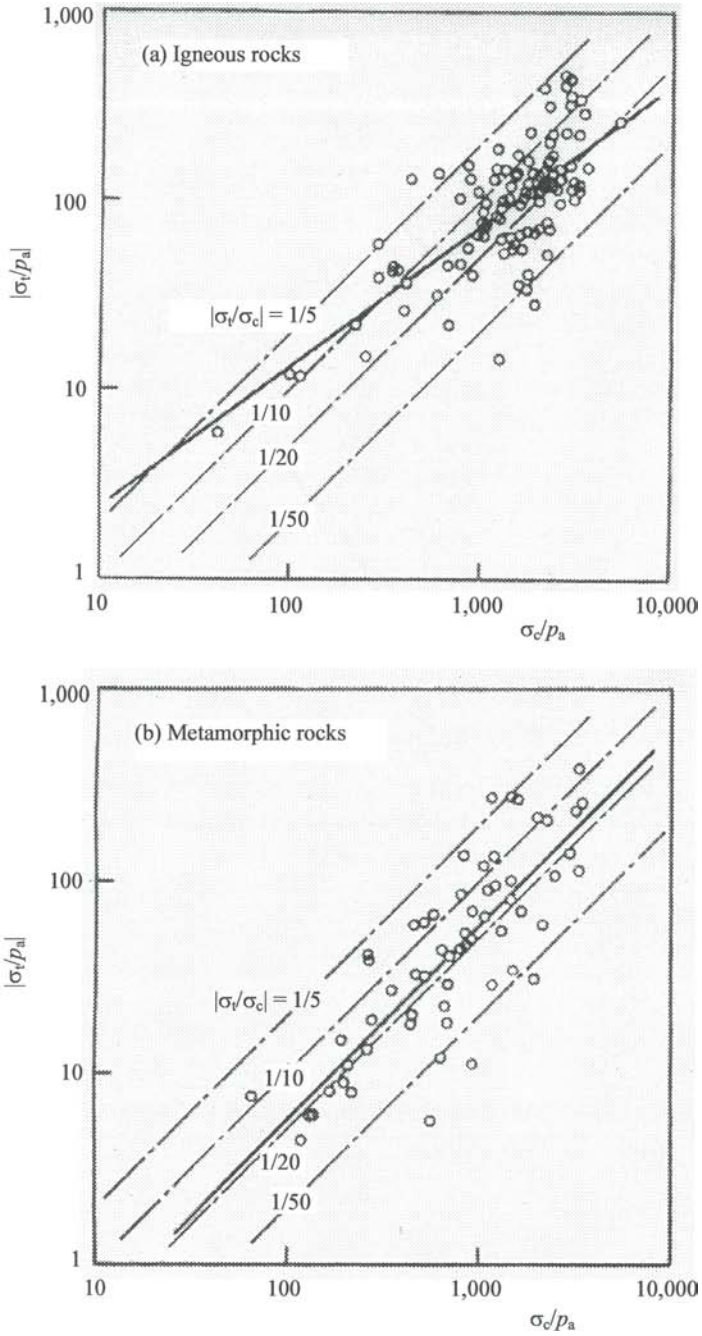
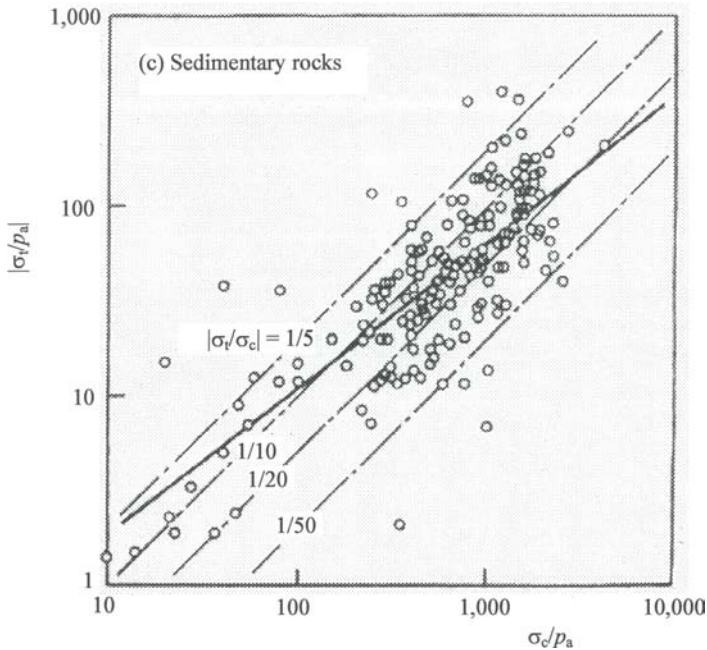


Fig. 7.6 Relation between tensile strength and unconfined compressive strength for (a) Igneous rocks; (b) Metamorphic rocks; and (c) Sedimentary rocks (after Lade, 1993).

Fig. 7.6 *Continued.*

The tensile strength of intact rocks also decreases as water content increases. According to Vasarhelyi (2004), the reduction percentage for the tensile strength of a rock from dry condition to saturated condition is about the same as that for the unconfined compressive strength of the same rock. Fig. 7.7 shows the variation of tensile strength σ_t with water content w for porous chalks.

7.2.3 Empirical strength criteria of intact rock

Various empirical strength criteria of intact rock have been developed by different researchers (e.g., Bieniawski, 1974; Hoek & Brown, 1980; Johnston, 1985; Lade, 1993; Wang & Lmeny, 1995; Chang & Haimson, 2000; Al-Ajmi & Zimmerman, 2005). Some of them are presented in this subsection.

(a) Hoek-Brown criterion

For intact rock, the Hoek-Brown criterion may be expressed in the following form

$$\sigma'_1 = \sigma'_3 + \sigma_c \left(m_i \frac{\sigma'_3}{\sigma_c} + 1 \right)^{0.5} \quad (7.18)$$

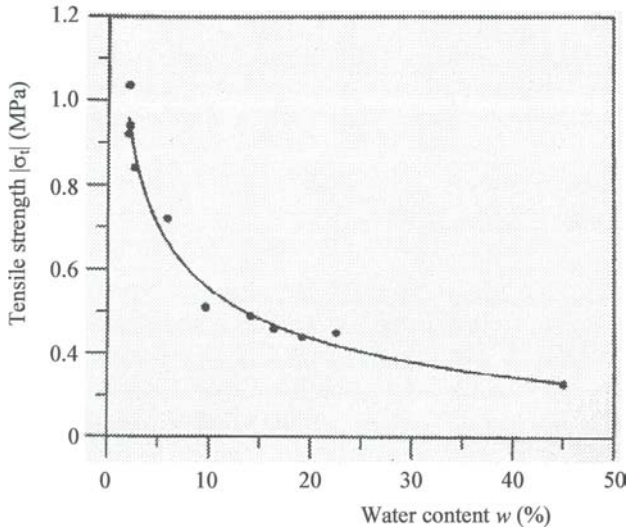


Fig. 7.7 Variation of tensile strength σ_t with water content w for porous chalks (after Talesnick et al., 2001).

where σ_c is the unconfined compressive strength of the intact rock; σ'_1 and σ'_3 are respectively the major and minor effective principal stresses; and m_i is a material constant for the intact rock. m_i depends only upon the rock type (texture and mineralogy) as tabulated in Table 7.8.

(b) Bieniawski-Yudhbir criterion

Bieniawski (1974) proposed a strength criterion for intact rock as follows

$$\frac{\sigma'_1}{\sigma_c} = 1 + b \left(\frac{\sigma'_3}{\sigma_c} \right)^{0.65} \quad (7.19)$$

where b is a parameter which can be determined from Table 7.9.

(c) Johnston criterion

Based on experimental data of a wide range of geotechnical material, from lightly overconsolidated clays through hard rocks, Johnston (1985) proposed the following strength criterion for intact rock

$$\sigma'_{1n} = \left(\frac{M}{B} \sigma'_{3n} + 1 \right)^B \quad (7.20)$$

Table 7.9 Parameter b in the Bieniawski-Yudhbir criterion (Yudhbir et al., 1983).

Rock Type	b
Tuff, Shale, Limestone	2
Siltstone, mudstone	3
Quartzite, Sandstone, Dolerite	4
Norite, Granite, Quartz diorite, Chert	5

where σ'_{1n} and σ'_{3n} are the normalized effective principal stresses at failure, obtained by dividing the effective principal stresses, σ'_1 and σ'_3 , by the relevant unconfined compressive strength, σ_c ; and B and M are intact material constants. By placing $\sigma'_{3n} = 0$, the unconfined compressive strength is correctly modeled with the right-hand side of equation (7.20) becoming one.

By putting $B = 1$, the criterion simplifies to

$$\sigma'_{1n} = M\sigma'_{3n} + 1 \quad (7.21)$$

which for

$$M = \frac{1 + \sin \phi'}{1 - \sin \phi'} \quad (7.22)$$

is identical to the normalized Mohr-Coulomb criterion.

The parameter B , which describes the nonlinearity of a failure envelope, is essentially independent of the material type, and is a function of unconfined compressive strength:

$$B = 1 - 0.0172(\log \sigma_c)^2 \quad (7.23)$$

The parameter M , which describes the slope of a failure envelope at $\sigma'_{3n} = 0$, is found to be a function of both the unconfined compressive strength and the material type. For the material types shown in Table 7.10, M can be estimated by (no result is obtained for type D material because of lack of data):

$$\text{Type A,} \quad M = 2.065 + 0.170(\log \sigma_c)^2 \quad (7.24a)$$

$$\text{Type B,} \quad M = 2.065 + 0.231(\log \sigma_c)^2 \quad (7.24b)$$

$$\text{Type C,} \quad M = 2.065 + 0.270(\log \sigma_c)^2 \quad (7.24c)$$

$$\text{Type E,} \quad M = 2.065 + 0.659(\log \sigma_c)^2 \quad (7.24d)$$

Table 7.10 A range of rock types (after Hoek & Brown, 1980).

Type	General Rock Type	Examples
A	Carbonate rocks with well developed crystal cleavage	Dolomite, limestone, marble
B	Lithified argillaceous rocks	Mudstone, siltstone, shale, slate
C	Arenaceous rocks with strong crystals and poorly-developed crystal cleavage	Sandstone, quartzite
D	Fine grained polyminerallic igneous crystalline rocks	Andesite, dolerite, diabase, rhyolite
E	Coarse grained polyminerallic igneous and metamorphic crystalline rocks	Amphibolite, gabbro, gneiss, granite, norite, quartz diorite

(d) Ramamurthy Criterion

Ramamurthy and his coworkers (Ramamurthy et al., 1985; Ramamurthy, 1986; Ramamurthy, 1993) modified the Coulomb theory to represent the nonlinear shear strength behavior of rocks. For intact rock, the strength criterion is in the following form

$$\frac{\sigma'_1 - \sigma'_3}{\sigma'_3} = B_r \left(\frac{\sigma_c}{\sigma'_3} \right)^{\alpha_r} \quad (7.25)$$

where σ'_1 and σ'_3 are the major and minor principal effective stresses; σ_c is the unconfined compressive strength; α_r is the slope of the curve between $(\sigma'_1 - \sigma'_3)/\sigma'_3$ and σ_c/σ'_3 , with a mean value of 0.8 for most intact rocks; and B_r is a material constant of intact rock, equal to $(\sigma'_1 - \sigma'_3)/\sigma'_3$ when $\sigma_c/\sigma'_3 = 1$. The values of B_r vary from 1.8 to 3.0 depending on the type of rock (see Table 7.11).

The values of α_r and B_r can be estimated by conducting a minimum of two triaxial tests at confining pressures greater than 5% of σ_c for the rock. The above expression is applicable in the ductile region and in most of the brittle region. It underestimates the strength when σ'_3 is less than 5% of σ_c and also ignores the tensile strength of the rock. To account for the tensile strength, the following expression can be used

$$\frac{\sigma'_1 - \sigma'_3}{\sigma'_3 + \sigma_t} = B \left(\frac{\sigma_c}{\sigma'_3 + \sigma_t} \right)^\alpha \quad (7.26)$$

where σ_t is the tensile strength of rock preferably obtained from Brazilian tests; $\alpha = 0.67$ for most rocks; and B is a material constant. The values of α and B in equation (7.26) can be obtained by two triaxial tests conducted at convenient confining pressures greater than 5% of σ_c for the rock. In the absence of these tests, the value of B can be estimated as $1.3(\sigma_c/\sigma_t)^{1/3}$.

Table 7.11 Mean values of parameter B_f for different rocks (after Ramamurthy, 1993).

Rock type	Metamorphic and sedimentary rocks						Igneous rocks	
	Argillaceous		Arenaceous		Chemical			
Siltstone	Shales	Sandstone	Quartzite	Limestone	Marble	Andesite	Granite	
Clays	Slates			Anhydrite	Dolomite	Diorite	Charnockite	
Tuffs	Mudstone			Rock salt		Norite		
Loess	Claystone					Liparite		
						Basalt		
B_f	1.8	2.2	2.2	2.6	2.4	2.8	2.6	3.0
Mean value	2.0		2.4		2.6		2.8	

7.2.4 Mohr-Coulomb parameters of intact rock

Since the Mohr-Coulomb failure criterion is often used in the analyses of rock mechanics problems, it is necessary to estimate the cohesion and friction parameters of the intact rock:

$$\tau_f = c_i + \sigma'_n \tan \phi_i \quad (7.27)$$

where τ_f is the shear strength of the intact rock; c_i and ϕ_i are respectively the cohesion and internal friction angle of the intact rock; and σ'_n is the effective normal stress on the sliding plane.

Table 7.12 lists the representative peak values of c_i and ϕ_i for different rocks (Goodman, 1989). Robertson (1970), while recognizing that there is considerable variation, has suggested that the peak cohesion be about 16% of the unconfined compressive strength. If the Mohr-Coulomb criterion is used to represent the residual strength (the minimum strength reached by the rock subjected to deformation beyond the peak), the subscript r may be used with the cohesion and friction angle terms in equation (7.27). The residual cohesion will approach zero and the residual internal friction angle will lie between zero and the peak internal friction angle.

7.3 STRENGTH OF ROCK DISCONTINUITIES

Discontinuities usually have negligible tensile strength and a shear strength that is, under most circumstances, significantly smaller than that of the surrounding intact rock material. The following describes several shear strength models for rock discontinuities.

7.3.1 Mohr-Coulomb model

The simplest shear strength model of discontinuities is the Mohr-Coulomb failure criterion, which can be expressed by

Table 7.12 Typical peak cohesion c_i and internal friction angle ϕ_i for different rocks (after Goodman, 1989).

Rock	Porosity (%)	c_i (MPa)	ϕ_i (°)	Range of confining pressure (MPa)
Berea sandstone	18.2	27.2	27.8	0 – 200
Bartlesville sandstone		8.0	37.2	0 – 203
Pottsville sandstone	14.0	14.9	45.2	0 – 68.9
Repetto siltstone	5.6	34.7	32.1	0 – 200
Muddy shale	4.7	38.4	14.4	0 – 200
Stockton shale		0.34	22.0	0.8 – 4.1
Edmonton bentonitic shale (water content 30%)	44.0	0.3	7.5	0.1 – 3.1
Sioux quartzite		70.6	48.0	0 – 203
Texas slate; loaded 30° to cleavage		26.2	21.0	34.5 – 276
90° to cleavage		70.3	26.9	34.5 – 276
Georgia marble	0.3	21.2	25.3	5.6 – 68.9
Wolf Camp limestone		23.6	34.8	0 – 203
Indiana limestone	19.4	6.7	42.0	0 – 9.6
Hasmark dolomite	3.5	22.8	35.5	0.8 – 5.9
Chalk	40.0	0	31.5	10 – 90
Blaine anhydrite		43.4	29.4	0 – 203
Inada biotite granite	0.4	55.2	47.7	0.1 – 98
Stone Mountain granite	0.2	55.1	51.0	0 – 68.9
Nevada Test Site basalt	4.6	66.2	31.0	3.4 – 34.5
Schistose gneiss 30° to schistosity	0.5	46.9	28.0	0 – 69
90° to schistosity	1.9	14.8	27.6	0 – 69

$$\tau_f = c_j + \sigma'_n \tan \phi_j \quad (7.28)$$

where τ_f is the shear strength of the discontinuity; c_j and ϕ_j are respectively the cohesion and internal friction angle of the discontinuity; and σ'_n is the effective normal stress on the

discontinuity plane. It need be noted that the “primes” for c_j and ϕ_j have been omitted for brevity although they are for the effective stress conditions. The Mohr-Coulomb model can be used for planar, clean (no filling) discontinuities.

7.3.2 Bilinear shear strength model

Natural discontinuities contain undulations and asperities and their shear strength-normal stress relation is usually non-linear. Patton (1966) addressed this problem by formulating the bilinear model as shown in Fig. 7.8. At normal stresses less than or equal to σ'_0 the shear strength is given by

$$\tau_f = \sigma'_n \tan(\phi_b + i) \tag{7.29}$$

where ϕ_b is the basic friction angle for an apparently smooth surface of the rock material; and i is the effective roughness angle. Table 6.7 lists the typical values of ϕ_b for different rocks.

At normal stresses greater than or equal to σ'_0 the shear strength is given by

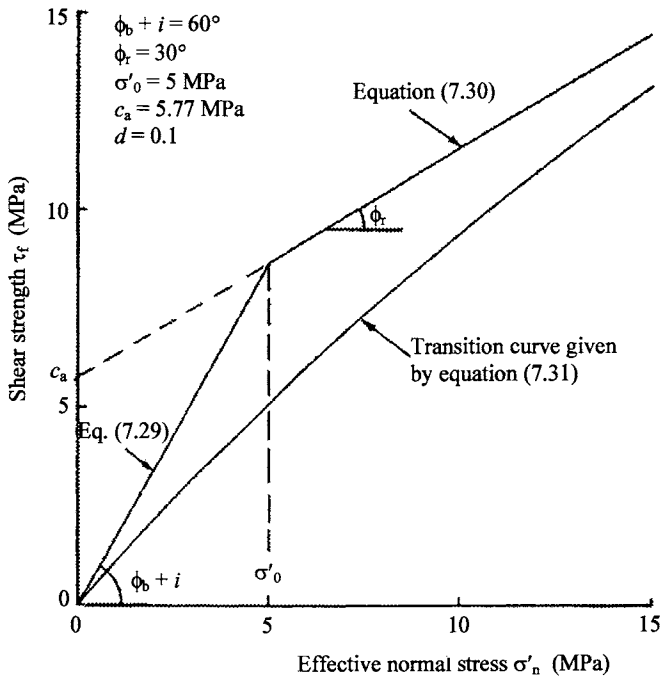


Fig. 7.8 Bilinear shear strength model (equations 7.29 and 7.30) with empirical transition curve (equation 7.31).

$$\tau_f = c_a + \sigma'_n \tan \phi_r \quad (7.30)$$

where c_a is the apparent cohesion derived from the asperities; and ϕ_r is the residual friction angle of the rock material forming the asperities.

Jaeger (1971) proposed the following shear strength model to provide a curved transition between the straight lines of the Patton model

$$\tau_f = c_a(1 - e^{-d\sigma'_n}) + \sigma'_n \tan \phi_r \quad (7.31)$$

where d is an experimentally determined empirical parameter which controls the shape of the transition curve.

7.3.3 Barton model

A direct, practical approach to predicting the shear strength of discontinuities on the basis of relatively simple measurements was developed by Barton and his coworkers (Barton, 1976; Barton & Choubey, 1977; Barton & Bandis, 1990). According to the Barton model, the shear strength τ_f of a discontinuity subjected to a normal stress σ'_n in a rock material is given by

$$\tau_f = \sigma'_n \tan \left[\text{JRC} \log \left(\frac{\text{JCS}}{\sigma'_n} \right) + \phi_r \right] \quad (7.32)$$

where JRC, JCS and ϕ_r are respectively the discontinuity roughness coefficient, the discontinuity wall compressive strength and the residual friction angle of the discontinuity which can be estimated using the methods presented in Section 6.3.

Equation (7.32) suggests that there are three factors which control the shear strength of rock discontinuities: the residual friction angle ϕ_r (or the basic friction angle ϕ_b), a geometrical component JRC, and an asperity failure component controlled by the ratio JCS/σ'_n . Research results show that both JRC (geometrical component) and JCS (asperity failure component) decrease with increasing scale (Bandis, 1990; Barton & Bandis, 1982) (see Fig. 7.9). Based on extensive testing of discontinuities, discontinuity replicas, and a review of literature, Barton and Bandis (1982) proposed the scale corrections for JRC and JCS:

$$\text{JRC}_n = \text{JRC}_0 \left[\frac{L_n}{L_0} \right]^{-0.02\text{JRC}_0} \quad (7.33a)$$

$$\text{JCS}_n = \text{JCS}_0 \left[\frac{L_n}{L_0} \right]^{-0.03\text{JCS}_0} \quad (7.33b)$$

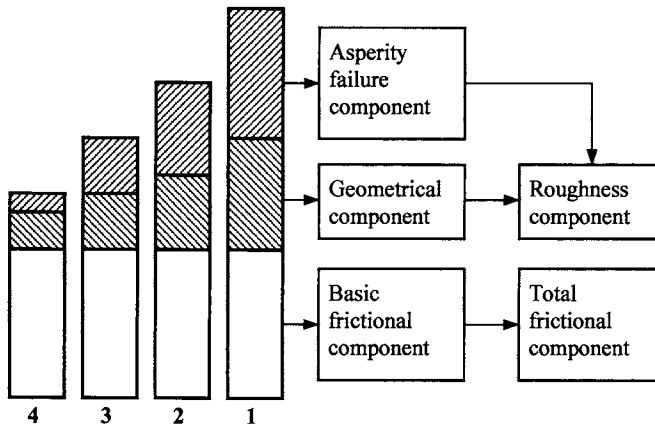
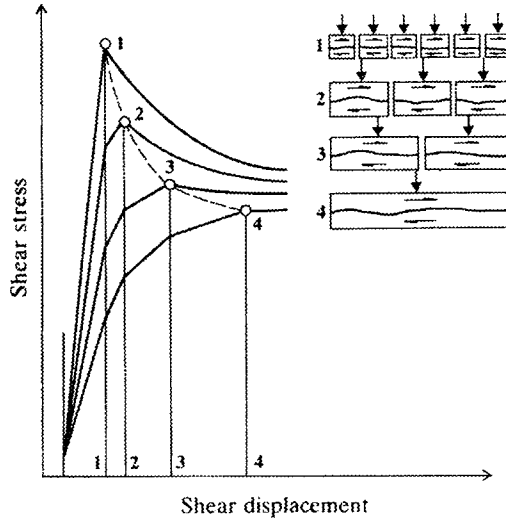


Fig. 7.9 Influence of scale on the three components of the shear strength of a rough discontinuity (after Bandis, 1990; Barton & Bandis, 1990).

where JRC_0 , JCS_0 and L_0 (length) refer to 100 mm laboratory scale samples and JRC_n , JCS_n and L_n refer to in situ block sizes.

It is worth noting two important limitations on the use of Barton model for estimating the shear strength of discontinuities. Barton and Choubey (1977) suggest that the curves should be truncated such that the maximum allowable shear strength for design purposes is given by $\arctan(\tau/\sigma'_n) = 70^\circ$. For example, curve 1 in Fig. 7.10 has a linear “cut-off”

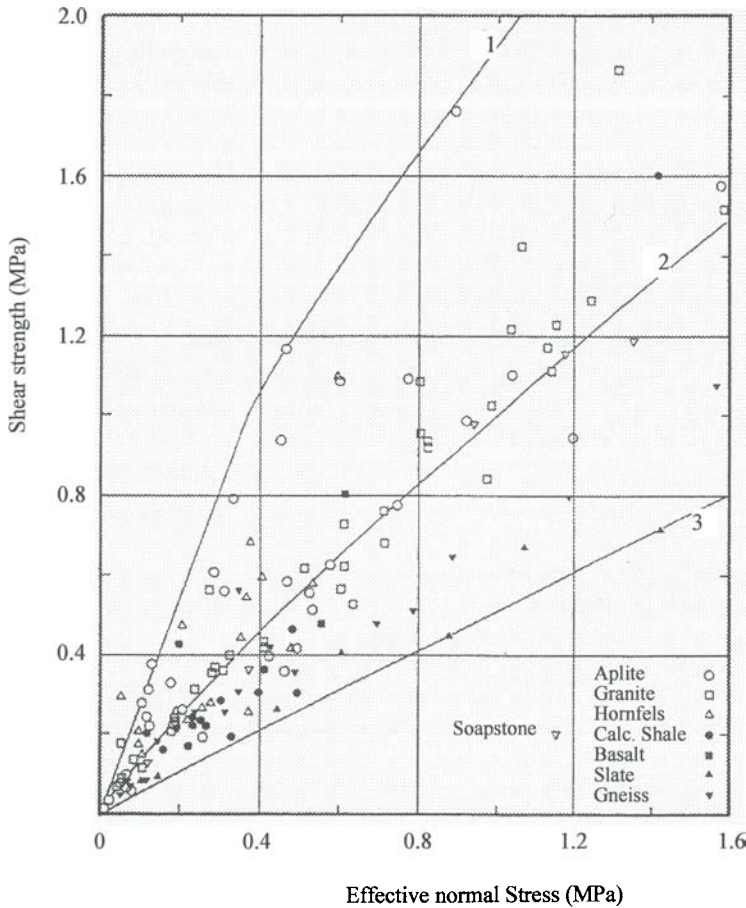


Fig. 7.10 Range of peak shear strength for 136 joints representing eight different rock types. Curves 1, 2 and 3 are evaluated using equation (7.32) (after Barton & Choubey, 1977).

representing the maximum suggested design value of 70° for the total frictional angle. Barton (1976) cautioned that when the effective normal stress exceeds the unconfined compressive strength of the rock material, the measured shear strength is always appreciably higher than that predicted by equation (7.32). Noting that this discrepancy was probably due to the effect of confining stresses increasing the strength of asperities, Barton proposed that a high stress version of equation (7.32) could be obtained by replacing JCS by $(\sigma'_1 - \sigma'_3)$, i.e.,

$$\tau = \sigma'_n \tan \left[\text{JRC} \log \left(\frac{\sigma'_1 - \sigma'_3}{\sigma'_n} \right) + \phi_r \right] \quad (7.34)$$

where σ'_1 is the effective axial stress required to yield the rock material under an effective confining stress σ'_3 . The failure stress σ'_1 can either be determined experimentally or can be estimated from an appropriate yield criterion such as the Hoek-Brown criterion.

7.3.4 Shear strength of filled discontinuities

The previous sections deal with the shear strength of discontinuities in which rock wall contact occurs over the entire length of the surface under consideration. If a discontinuity contains a filling material such as clay gouge, the shear strength of the discontinuity will be influenced by the thickness and properties of the filling material. If the thickness of the filling material is more than about 25 to 50 percent of the amplitude of the asperities, there will be little or no rock-to-rock contact and the shear strength of the discontinuity will be controlled by the shear strength properties of the filling material (Goodman, 1970). The peak and residual shear strength of filled discontinuities can be expressed by the Mohr-Coulomb model [equation (7.28)]. Table 7.13 lists the shear strength parameters of filled discontinuities and filling materials summarized by Hoek and Bray (1981).

7.4 STRENGTH OF ROCK MASS

7.4.1 Unconfined compressive strength of rock mass

Because of discontinuities, jointed rock mass will have a much lower unconfined compressive strength than intact rock. It is difficult to determine the unconfined compressive strength of jointed rock masses in the laboratory because the samples need to be undisturbed and sufficiently large to be representative of the discontinuity conditions. To estimate the unconfined compressive strength of rock masses, empirical correlations considering the discontinuity characteristics are usually used. Table 7.14 lists some of the empirical correlations for estimating the rock mass unconfined compressive strength σ_{cm} . Fig. 7.11 shows a comparison of some of the correlations with the in situ test data of Aydan and Dalgic (1998).

Some of the correlations in Table 7.14 are derived from their corresponding strength criteria. As an example, the following shows the derivation of the Hoek (1994) and Hoek et al. (1995) correlation. With the Hoek-Brown strength criterion for rock masses [equation (7.40)], the unconfined compressive strength can be expressed as

$$\sigma_{cm} = \sqrt{s}\sigma_c \quad (7.35)$$

where s is a constant that depends on the characteristics of the rock mass, which can be estimated from RMR or GSI (see Section 7.4.3 for details). If equation (7.44b) is used to estimate s , equation (7.35) is changed to

Table 7.13 Shear strength of filled discontinuities and filling materials (after Hoek & Bray, 1981).

Rock	Description	Peak c_j (MPa)	Peak ϕ_j (°)	Residual c_j (MPa)	Residual ϕ_j (°)
Basalt	Clayey basaltic breccia, wide variation from clay to basalt content	0.24	42		
Bentonite	Bentonite seam in chalk	0.015	7.5		
	Thin layers	0.09-0.12	12-17		
	Triaxial tests	0.06-0.1	9-13		
Bentonitic shale	Triaxial tests	0-0.27	8.5-29		
	Direct shear tests			0.03	8.5
Clays	Over-consolidated, slips, joints and minor shears	0-0.18	12-18.5	0-0.003	10.5-16
Clay shale	Triaxial tests	0.06	32		
	Stratification surfaces			0	19-25
Coal measure rocks	Clay mylonite seams, 10 to 25 mm	0.012	16	0	11-11.5
Dolomite	Altered shale bed, \pm 150 mm thick	0.04	14.5	0.02	17
Diorite, granodiorite and porphyry	Clay gouge (2% clay, PI = 17%)	0	26.5		
Granite	Clay filled faults	0-0.1	24-25		
	Sandy loam fault filling	0.05	40		
	Tectonic shear zone, schistose and broken granites, disintegrated rock and gouge	0.24	42		
Greywacke	1-2 mm clay in bedding planes			0	21
Limestone	6 mm clay layer			0	13
	10-20 mm clay fillings	0.1	13-14		
	<1 mm clay filling	0.05-0.2	17-21		
Limestone, marl and lignites	Interbedded lignite layers	0.08	38		
	Lignite/marl contact	0.1	10		
Limestone	Marlaceous joints, 20 mm thick	0	25	0	15-24
Lignite	Layer between lignite and clay	0.014-0.03	15-17.5		
Montmorillonite	80 mm seams of bentonite (montmorillonite) clay in chalk	0.36	14	0.08	11
Bentonite clay		0.016-0.02	7.5-11.5		
Schists, quartzites and siliceous schists	100-150 mm thick clay filling	0.03-0.08	32		
	Stratification with thin clay	0.61-0.74	41		
	Stratification with thick clay	0.38	31		
Slates	Finely laminated and altered	0.05	33		
Quartz / kaolin / pyrolusite	Remolded triaxial tests	0.042-0.09	36-38		

Table 7.14 Empirical correlations for estimating rock mass unconfined compressive strength σ_{cm} .

Reference	Correlation
Yudhbir et al. (1983)	$\frac{\sigma_{cm}}{\sigma_c} = e^{\frac{7.65(RMR-100)}{100}}$
Laubscher (1984) and Singh & Goel (1999)	$\frac{\sigma_{cm}}{\sigma_c} = \frac{RMR - \text{Rating for } \sigma_c}{106}$
Ramamurthy et al. (1985) and Ramamurthy (1986, 1993)	$\frac{\sigma_{cm}}{\sigma_c} = e^{\frac{RMR-100}{18.75}}$
Trueman (1988) and Asef et al. (2000)	$\sigma_{cm} = 0.5e^{0.06RMR} \quad (\text{MPa})$
Kalamaras & Bieniawski (1993)	$\frac{\sigma_{cm}}{\sigma_c} = e^{\frac{RMR-100}{24}}$
Hoek (1994) and Hoek et al. (1995)	$\frac{\sigma_{cm}}{\sigma_c} = e^{\frac{GSI-100}{18}}$
Grimstad & Bhasin (1995) and Singh & Goel (1999)	$\sigma_{cm} = 7\gamma f_c Q^{1/3} \quad (\text{MPa})$ where $f_c = \sigma_v/100$ for $Q > 10$ and $\sigma_c > 100$ MPa, otherwise $f_c = 1$; and γ is the unit weight of the rock mass in g/cm^3 .
Sheorey (1997)	$\frac{\sigma_{cm}}{\sigma_c} = e^{\frac{RMR-100}{20}}$
Aydan & Dalgic (1998)	$\frac{\sigma_{cm}}{\sigma_c} = \frac{RMR}{RMR + 6(100 - RMR)}$
Barton (2002)	$\sigma_{cm} = 5\gamma(Q\sigma_c/100)^{1/3} \quad (\text{MPa})$ where γ is the unit weight of the rock mass in g/cm^3 .
Hoek (2004)	$\frac{\sigma_{cm}}{\sigma_c} = 0.036e^{\frac{GSI}{30}}$

$$\frac{\sigma_{cm}}{\sigma_c} = e^{\frac{GSI-100}{18}} \quad (7.36)$$

which is what shown in Table 7.14.

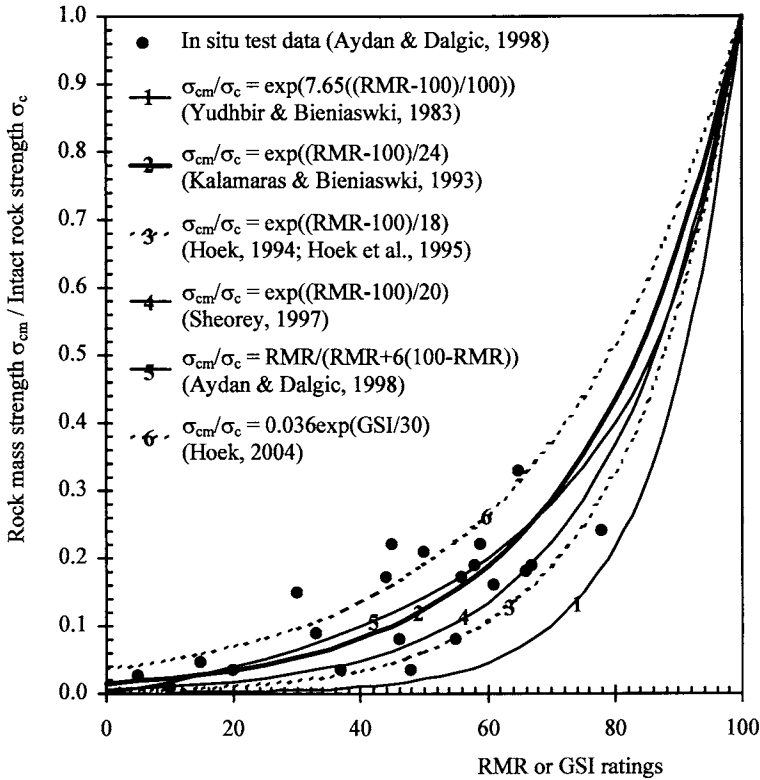


Fig. 7.11 Variation of ratio of rock mass unconfined compressive strength σ_{cm} to intact rock unconfined compressive strength σ_c with RMR or GSI ratings (modified from Hoek, 2004).

7.4.2 Tensile strength of rock mass

The tensile strength of a rock mass can be obtained by (Singh & Goel, 1999)

$$\sigma_{tm} = -0.029\gamma f_c Q^{0.3} \quad (\text{MPa}) \quad (7.37)$$

where $f_c = \sigma_c/100$ for $Q > 10$ and $\sigma_c > 100$ MPa, otherwise $f_c = 1$; and γ is the unit weight of the rock mass in g/cm^3 .

The strength criteria described in Section 7.4.3 can also be used to obtain the tensile strength of a rock mass. For example, with the Hoek-Brown strength criterion for rock masses [equation (7.40)], the tensile strength can be determined by

$$\sigma_{tm} = 0.5\sigma_c [m_b - (m_b^2 + 4s)^{0.5}] \quad (7.38)$$

where m_b is the material constant for the rock mass; and s is a constant that depends on the characteristics of the rock mass.

7.4.3 Empirical strength criteria of rock mass

There are different empirical strength criteria of rock masses. The four empirical strength criteria of rock masses, corresponding to those of intact rock presented in Section 7.2.3, are discussed in this section.

(a) Hoek-Brown criterion

For jointed rock masses, the most general form of the Hoek-Brown criterion, which incorporates both the original and the modified form, is given by

$$\sigma'_1 = \sigma'_3 + \sigma_c \left(m_b \frac{\sigma'_3}{\sigma_c} + s \right)^a \quad (7.39)$$

where m_b is the material constant for the rock mass; and s and a are constants that depend on the characteristics of the rock mass.

The original criterion has been found to work well for most rocks of good to reasonable quality in which the rock mass strength is controlled by tightly interlocking angular rock pieces. The failure of such rock masses can be defined by setting $a = 0.5$ in equation (7.39), giving

$$\sigma'_1 = \sigma'_3 + \sigma_c \left(m_b \frac{\sigma'_3}{\sigma_c} + s \right)^{0.5} \quad (7.40)$$

For poor quality rock masses in which the tight interlocking has been partially destroyed by shearing or weathering, the rock mass has no tensile strength or 'cohesion' and specimens will fall apart without confinement. For such rock masses the following modified criterion is more appropriate and it is obtained by putting $s = 0$ in equation (7.39):

$$\sigma'_1 = \sigma'_3 + \sigma_c \left(m_b \frac{\sigma'_3}{\sigma_c} \right)^a \quad (7.41)$$

Equations (7.39) to (7.41) are of no practical value unless the values of the material constants m_b , s and a can be estimated in some way. Hoek and Brown (1988) proposed a set of relations between the parameters m_b , s and a and the 1976 version of Bieniawski's Rock Mass Rating (RMR), assuming completely dry conditions and a very favorable (according to the RMR rating system) discontinuity orientation:

- (i) disturbed rock masses

$$m_b = \exp\left(\frac{\text{RMR} - 100}{14}\right) m_i \quad (7.42a)$$

$$s = \exp\left(\frac{\text{RMR} - 100}{6}\right) \quad (7.42b)$$

$$a = 0.5 \quad (7.42c)$$

(ii) undisturbed or interlocking rock masses

$$m_b = \exp\left(\frac{\text{RMR} - 100}{28}\right) m_i \quad (7.43a)$$

$$s = \exp\left(\frac{\text{RMR} - 100}{9}\right) \quad (7.43b)$$

$$a = 0.5 \quad (7.43c)$$

Equations (7.42) and (7.43) are acceptable for rock masses with RMR values of more than about 25, but they do not work for very poor rock masses since the minimum value which RMR can assume is 18 for the 1976 RMR system and 23 for the 1989 RMR system (see Chapter 5 for details). In order to overcome this limitation, Hoek (1994) and Hoek et al. (1995) introduced the Geological Strength Index (GSI). The relationships between m_b , s and a and the Geological Strength Index (GSI) are as follows:

(i) For $\text{GSI} > 25$, i.e. rock masses of good to reasonable quality

$$m_b = \exp\left(\frac{\text{GSI} - 100}{28}\right) m_i \quad (7.44a)$$

$$s = \exp\left(\frac{\text{GSI} - 100}{9}\right) \quad (7.44b)$$

$$a = 0.5 \quad (7.44c)$$

(ii) For $\text{GSI} < 25$, i.e. rock masses of very poor quality

$$m_b = \exp\left(\frac{\text{GSI} - 100}{28}\right) m_i \quad (7.45a)$$

$$s = 0 \quad (7.45b)$$

$$a = 0.65 - \frac{\text{GSI}}{200} \quad (7.45c)$$

It is noted that the distinction between disturbed and undisturbed rock masses is dropped in evaluating the parameters m_b , s and a from GSI. This is based on the fact that disturbance is

generally induced by engineering activities and should be allowed by downgrading the values of GSI. The methods for determining RMR and GSI have been discussed in Chapter 5.

Water has a great effect on the strength of rock masses. Many rocks show a significant strength decrease with increasing moisture content. Therefore, it is important to conduct laboratory tests at moisture contents which are as close as possible to those which occur in the field. A more important effect of water is the strength reduction which occurs as a result of water pressures in the pore spaces in the rock. This is why the effective not the total stresses are used in the Hoek-Brown strength criterion.

The Hoek-Brown strength criterion was originally developed for intact rock and then extended to rock masses. The process used by Hoek and Brown in deriving their strength criterion for intact rock (equation 7.18) was one of pure trial and error (Hoek et al., 1995). Apart from the conceptual starting point provided by the Griffith theory, there is no fundamental relationship between the empirical constants included in the criterion and any physical characteristics of the rock. The justification for choosing this particular criterion (equation 7.18) over the numerous alternatives lies in the adequacy of its predictions of the observed rock fracture behavior, and the convenience of its application to a range of typical engineering problems (Hoek, 1983). The material constants m_i is derived based upon analyses of published triaxial test results on intact rock (Hoek, 1983; Doruk, 1991; Hoek et al., 1992). The strength criterion for rock masses is just an empirical extension of the criterion for intact rock. Since it is practically impossible to determine the material constants m_b and s using triaxial tests on rock masses, empirical relations are suggested to estimate these constants from RMR or GSI. The RMR and the GSI rating systems are also empirical. For these reasons the Hoek-Brown empirical rock mass strength criterion must be used with extreme care. In discussing the limitations in the use of their strength criterion, Hoek and Brown (1988) emphasize that it is not applicable to anisotropic rocks nor to elements of rock masses that behave anisotropically by virtue of containing only a few discontinuities. Alternative empirical approaches and further developments of the Hoek-Brown criterion which seek to account for some of its limitations are given by Amadei (1988), Pan and Hudson (1988), Ramamurthy and Arora (1991), Amadei and Savage (1993), and Ramamurthy (1993).

(b) Bieniawski-Yudhbir criterion

Based on tests of jointed gypsum-celite specimens, Yudhbir et al. (1983) changed the strength criterion for intact rock [equation (7.19)] to the form

$$\frac{\sigma'_1}{\sigma_c} = a + b \left(\frac{\sigma'_3}{\sigma_c} \right)^{0.65} \quad (7.46)$$

to fit rock masses. Yudhbir et al. (1983) recommended that parameter a be determined from

$$a = 0.0176Q^{0.65} \quad \text{or} \quad a = \exp\left[7.65\left(\frac{\text{RMR} - 100}{100}\right)\right] \quad (7.47)$$

where Q is the classification index of Barton et al. (1974), and RMR is Bieniawski's 1976 Rock Mass Rating (Bieniawski, 1976). Parameter b is determined from Table 7.9.

Kalamaras and Bieniawski (1993) suggested that both a and b should be varied with RMR for better results. They proposed the criterion of Table 7.15 specifically for coal seams.

(c) Johnston criterion

For rock masses, Johnston (1985) proposed the following strength criterion

$$\sigma'_{1n} = \left(\frac{M}{B} \sigma'_{3n} + s\right)^B \quad (7.48)$$

where σ'_{1n} and σ'_{3n} are the normalized effective principal stresses at failure, obtained by dividing the effective principal stresses, σ'_1 and σ'_3 , by the relevant unconfined compressive strength, σ_c ; B and M are intact material constants as described in Section 7.2.3; and s is a constant to account for the strength of discontinuous soil and rock masses in a manner similar to that proposed by Hoek and Brown (1980).

(d) Ramamurthy Criterion

For rock masses, the strength criterion has the same form as for intact rock (Ramamurthy et al., 1985; Ramamurthy, 1986; Ramamurthy, 1993), i.e.

$$\frac{\sigma'_1 - \sigma'_3}{\sigma'_3} = B_m \left(\frac{\sigma_{cm}}{\sigma'_3}\right)^{\alpha_m} \quad (7.49)$$

where σ_{cm} is the rock mass strength in unconfined compression; B_m is a material constant for rock masses; and α_m is the slope of the plot between $(\sigma'_1 - \sigma'_3)/\sigma'_3$ and σ_{cm}/σ'_3 , which can be assumed to be 0.8 for rock masses as well. σ_{cm} and B_m can be obtained by

Table 7.15 Rock mass criterion for coal seams by Kalamaras and Bieniawski (1993).

Equation	Parameters
$\frac{\sigma'_1}{\sigma_c} = a + 4\left(\frac{\sigma'_3}{\sigma_c}\right)^{0.6}$	$a = \exp\left(\frac{\text{RMR} - 100}{14}\right)$
$\frac{\sigma'_1}{\sigma_c} = a + b\left(\frac{\sigma'_3}{\sigma_c}\right)^{0.6}$	$a = \exp\left(\frac{\text{RMR} - 100}{12}\right), \quad b = \exp\left(\frac{\text{RMR} + 20}{52}\right)$

$$\sigma_{cm} = \sigma_c \exp\left(\frac{\text{RMR} - 100}{18.75}\right) \quad (7.50)$$

$$B_m = B_r \exp\left(\frac{\text{RMR} - 100}{75.5}\right) \quad (7.51)$$

in which σ_c is the unconfined compressive strength of intact rock; and B_r is a material constant for intact rock, as in equation (7.25).

(e) Comments

In addition to the four empirical strength criteria of rock masses described above, there are many other criteria. All these criteria are purely empirical and thus it is impossible to say which one is correct or which one is not. However, the Hoek-Brown strength criterion is the most widely referred and used. Since its advent in 1980, considerable application experience has been gained by its authors as well as by others. As a result, this criterion has been modified several times to meet the needs of users who have applied it to conditions which were not visualized when it was originally developed.

It is noted that all the empirical strength criteria described above for rock masses have the following limitations:

1. The influence of the intermediate principal stress, which in some cases is important, is not considered.
2. The criteria are not applicable to anisotropic rock masses. So they can be used only when the rock masses are approximately isotropic, i.e. when the discontinuity orientation does not have a dominant effect on failure.

7.4.4 *Mohr-Coulomb parameters of rock mass*

Since many of the numerical models and limit equilibrium analyses used in rock mechanics and rock engineering are expressed in terms of the Mohr-Coulomb failure criterion, it is necessary to estimate the cohesion and friction angle parameters of rock masses:

$$\tau_f = c_m + \sigma'_n \tan \phi_m \quad (7.52)$$

where τ_f is the shear strength of the rock mass; c_m and ϕ_m are respectively the cohesion and internal friction angle of the rock mass; and σ'_n is the effective normal stress on the sliding plane.

Estimation of c_m and ϕ_m can be done using one of the empirical strength criteria presented in Section 7.4.3 and based on the solution published by Balmer (1952) in which the normal and shear stresses are expressed in terms of the corresponding principal stresses as follows:

$$\sigma'_n = \sigma'_3 + \frac{\sigma'_1 - \sigma'_3}{\frac{\partial \sigma'_1}{\partial \sigma'_3} + 1} \quad (7.53)$$

$$\tau_f = (\sigma'_n - \sigma'_3) \sqrt{\frac{\partial \sigma'_1}{\partial \sigma'_3}} \quad (7.54)$$

For example, for the Hoek-Brown strength criterion, one can have:

For GSI > 25, when $a = 0.5$:

$$\frac{\partial \sigma'_1}{\partial \sigma'_3} = 1 + \frac{m_b \sigma_c}{2(\sigma'_1 - \sigma'_3)} \quad (7.55)$$

For GSI < 25, when $s = 0$:

$$\frac{\partial \sigma'_1}{\partial \sigma'_3} = 1 + am_b^a \left(m_b \frac{\sigma'_3}{\sigma_c} \right)^{a-1} \quad (7.56)$$

Once a set of (σ'_n, τ_f) values have been calculated from equations (7.53) and (7.54), the equivalent Mohr envelope defined by the following expression can be used to fit the (σ'_n, τ_f) data:

$$\tau_f = A \sigma_c \left(\frac{\sigma'_n - \sigma_{tm}}{\sigma_c} \right)^B \quad (7.57)$$

where A and B are material constants which can be determined by fitting analysis; σ'_n is the effective normal stress; and σ_{tm} is the tensile strength of the rock mass which can be determined from equation (7.38).

After A and B are determined, the friction angle at a specified effective normal stress can be obtained by

$$\phi_m = \arctan \left[AB \left(\frac{\sigma'_n - \sigma_{tm}}{\sigma_c} \right)^{B-1} \right] \quad (7.58)$$

and the corresponding cohesion is given by

$$c_m = \tau_f - \sigma'_n \tan \phi_m \quad (7.59)$$

The cohesion c_m given by equation (7.59) is an upper bound value and need be reduced to about 75% of the calculated value for practical applications (Hoek, 1999).

The values of c_m and ϕ_m obtained from the above method are very sensitive to the range of the minor principal stress σ'_3 used to generate the (σ'_n, τ_f) data sets. According to Hoek (2000), the most consistent results can be obtained when 8 equally spaced values of σ'_3 are used in the range $0 < \sigma'_3 < \sigma_c$. Fig. 7.12 shows the cohesive strength and friction angles of rock masses for different GSI and m_i values from Hoek (2000).

7.4.5 *Equivalent continuum approach for estimating rock mass strength*

The equivalent continuum approach treats the jointed rock mass as an equivalent anisotropic continuum with strength properties that are directional and reflect the properties of intact rock and those of the discontinuities. The discontinuities are characterized without reference to their specific locations. Jaeger (1960) and Jaeger and Cook (1979) presented an equilibrium continuum strength model for jointed rock masses under axisymmetric loading condition. In their model, the strength of both the intact rock and the discontinuities are described by the Mohr-Coulomb criterion. Since the effect of the intermediate principal stress is not considered in the model of Jaeger (1960) and Jaeger and Cook (1979), Amadei (1988) and Amadei and Savage (1989, 1993) derived solutions for the strength of a jointed rock mass under a variety of multiaxial states of stress. As in the model of Jaeger (1960) and Jaeger and Cook (1979), the modeled rock mass is cut by a single discontinuity set. In the formulations of Amadei (1988) and Amadei and Savage (1989, 1993), however, the intact rock strength is described by the Hoek-Brown strength criterion and the discontinuity strength is modeled using a Mohr-Coulomb criterion with a zero tensile strength cut-off.

(a) **Model of Jaeger (1960) and Jaeger and Cook (1979)**

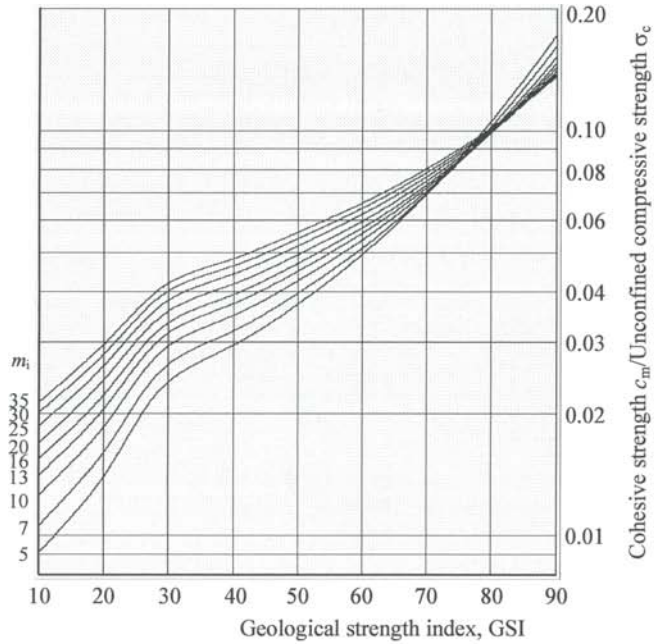
Fig. 7.13(a) shows a cylindrical rock mass specimen subjected to an axial major principal stress σ'_1 and a lateral minor principal stress σ'_3 . The rock mass is cut by well-defined parallel discontinuities inclined at an angle β to the major principal stress σ'_1 . The strength of both the intact rock and the discontinuities are described by the Mohr-Coulomb criterion, i.e.

$$\tau_i = c_i + \sigma'_n \tan \phi_i \quad (7.60)$$

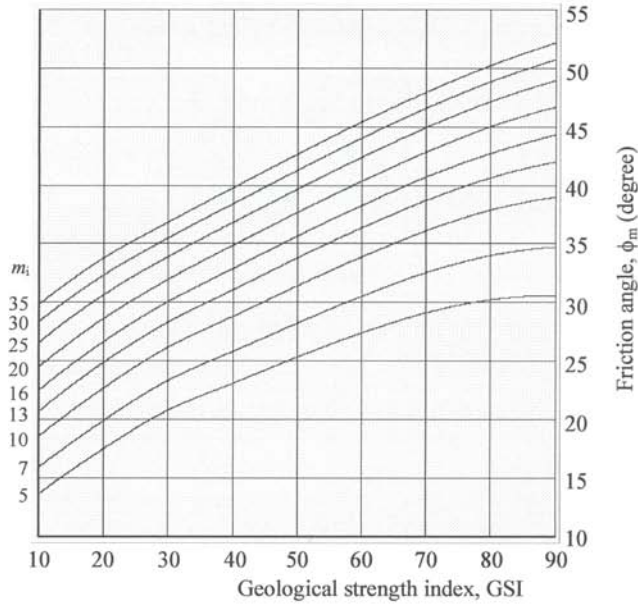
$$\tau_j = c_j + \sigma'_n \tan \phi_j \quad (7.61)$$

where τ_i and τ_j are respectively the shear strength of the intact rock and the discontinuities; c_i and ϕ_i are respectively the cohesion and internal friction angle of the intact rock; c_j and ϕ_j are respectively the cohesion and internal friction angle of the discontinuities; and σ'_n is the effective normal stress on the shear plane.

For the applied stresses on the rock mass cylinder, the effective normal stress σ'_n and the shear stress τ on a plane which makes an angle β' to the σ'_1 axis are respectively given by



(a)



(b)

Fig. 7.12 (a) Cohesive strength c_m ; and (b) Friction angle ϕ_m for different GSI and m_i values (after Hoek, 2000).

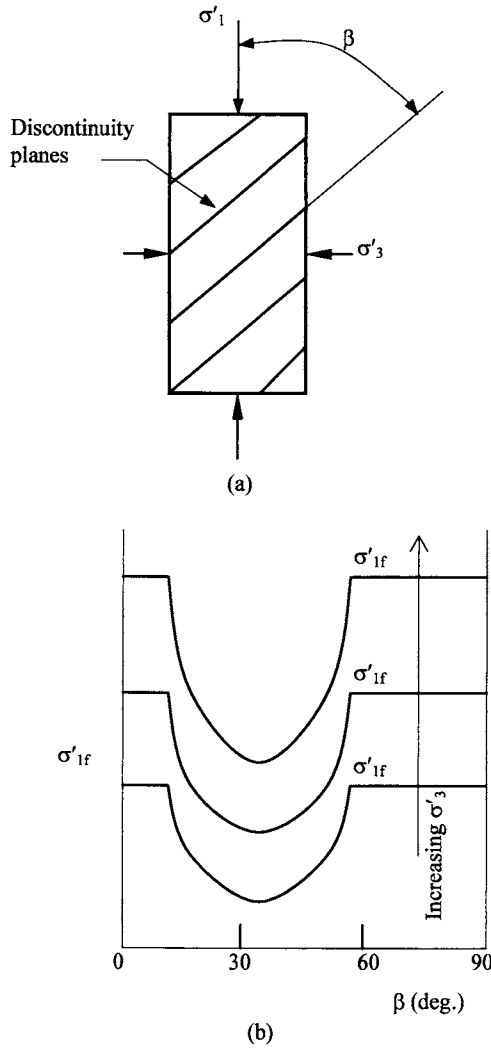


Fig. 7.13 Variation of compressive strength with angle β of the discontinuity plane (after Jaeger & Cook, 1979).

$$\sigma'_n = \frac{1}{2}(\sigma'_1 + \sigma'_3) - \frac{1}{2}(\sigma'_1 - \sigma'_3) \cos 2\beta' \tag{7.62}$$

$$\tau = \frac{1}{2}(\sigma'_1 - \sigma'_3) \sin 2\beta' \tag{7.63}$$

If shear failure occurs on the discontinuity plane, the effective normal stress σ'_n and the shear stress τ on the discontinuity plane can be obtained by replacing β' in equations

(7.62) and (7.63) by β . Adopting the obtained stresses on the discontinuity plane to substitute for σ'_n and τ_j in equation (7.61) and then rearranging, we can obtain the effective major principal stress required to cause shear failure along the discontinuity as follows

$$\sigma'_{1f} = \sigma'_3 + \frac{2(c_j + \sigma'_3 \tan \phi_j)}{\sin 2\beta(1 - \tan \phi_j \tan \beta)} \quad (7.64)$$

If shear failure occurs in the intact rock, the minimum effective major principal stress can be obtained by

$$\sigma'_{1f} = 2c_i \tan \left(\frac{\pi}{4} + \frac{\phi_i}{2} \right) + \sigma'_3 \tan^2 \left(\frac{\pi}{4} + \frac{\phi_i}{2} \right) \quad (7.65)$$

The model of Jaeger (1960) and Jaeger and Cook (1979) assumes that failure during compressive loading of a rock mass cylinder subject to a lateral stress σ'_3 [see Fig. 7.13(a)] will occur when σ'_1 exceeds the smaller of the σ'_{1f} values given by equations (7.64) and (7.65). Fig. 7.13(b) shows the variation of σ'_{1f} with β , from which we can clearly see the anisotropy of the rock mass strength caused by the discontinuities.

(b) Model of Amadei (1988) and Amadei and Savage (1989, 1993)

The principle used by Amadei (1988) and Amadei and Savage (1989, 1993) to derive the expressions of the jointed rock mass strength is the same as that used by Jaeger (1960) and Jaeger and Cook (1979). However, since the effect of the intermediate principal stress is included and since the nonlinear Hoek-Brown strength criterion is used, the derivation process and the final results are much more complicated. For reasons of space, only some of the typical results of Amadei and Savage (1989, 1993) are shown here.

Consider a jointed rock mass cube under a triaxial state of stress σ'_x , σ'_y and σ'_z . The orientation of the discontinuity plane is defined by two angles β and Ψ with respect to the xyz coordinate system (see Fig. 7.14). Let nst be another coordinate system attached to the discontinuity plane such that the n -axis is along the discontinuity upward normal and the s - and t -axes are in the discontinuity plane. The t -axis is in the xz plane. The upward unit vector \mathbf{n} has direction cosines

$$\bar{x} = \sin \psi \cos \beta; \quad \bar{y} = \cos \psi; \quad \bar{z} = \sin \psi \sin \beta \quad (7.66)$$

Defining $m = \sigma'_y/\sigma'_x$ and $n = \sigma'_z/\sigma'_x$ and introducing two functions

$$F_f = \tau^2 - \sigma_n'^2 \tan^2 \phi_j^2 \quad \text{and} \quad F_n = \sigma_n' \quad (7.67)$$

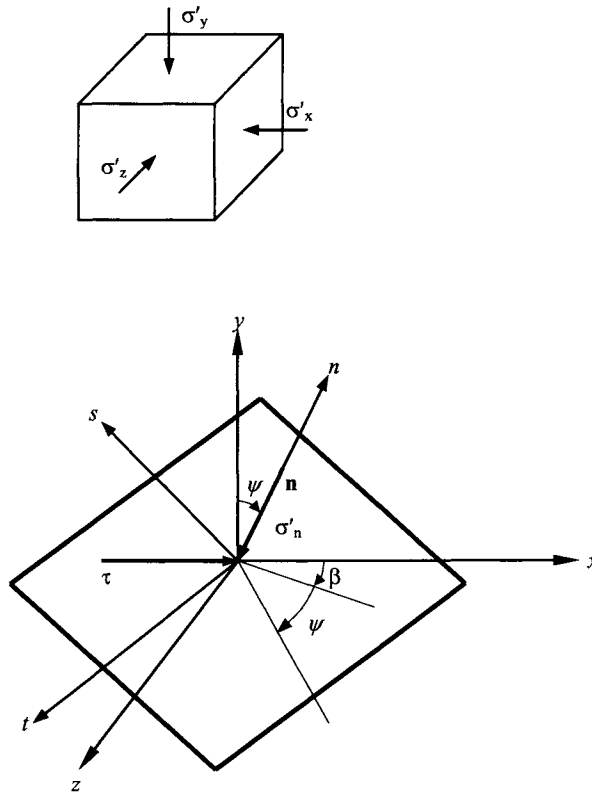


Fig. 7.14 Discontinuity plane in a triaxial stress field (after Amadei & Savage, 1993).

where σ'_n and τ are respectively the normal and shear stresses acting across the discontinuity; and ϕ_j is the friction angle of the discontinuity, the limiting equilibrium (incipient slip) condition of the discontinuity can be derived as

$$\begin{aligned}
 F_f = & \sigma'_x \{ [\bar{x}^2 - \bar{x}^4 (1 + \tan^2 \phi_j)] + m^2 [\bar{y}^2 - \bar{y}^4 (1 + \tan^2 \phi_j)] \\
 & + m^2 [\bar{z}^2 - \bar{z}^4 (1 + \tan^2 \phi_j)] - 2m\bar{x}^2 \bar{y}^2 (1 + \tan^2 \phi_j) \\
 & - 2m\bar{x}^2 \bar{z}^2 (1 + \tan^2 \phi_j) - 2mn\bar{y}^2 \bar{z}^2 (1 + \tan^2 \phi_j) \} = 0
 \end{aligned} \tag{7.68}$$

The nonnegative normal stress condition of the discontinuity is

$$F_n = \sigma'_x (\bar{x}^2 + m\bar{y}^2 + n\bar{z}^2) \geq 0 \tag{7.69}$$

So for a discontinuity with orientation angles β and ψ , the condition $F_f = 0$ corresponds to impending slip. No slip takes place when F_f is negative. Fig. 7.15 shows a typical set of failure surfaces $F_f(m, n) = 0$ for ψ equal to 40° or 80° and β ranging between 0° and 90° . In this figure the ranges $F_f(m, n) > 0$ are shaded and $F_n = 0$ is represented as a dashed straight line. The positive normal stress condition ($F_n > 0$) is shown as the region on either side of the line $F_n = 0$ depending on the sign of σ_x .

Depending on the ordering of σ'_x , σ'_y and σ'_z , the Hoek-Brown strength criterion for intact rock [equation (7.18)] assumes six possible forms as shown in Table 7.16. Using $m_i = 7$ and $\sigma_c = 42$ MPa, the intact rock failure surfaces for different values of σ'_x/σ_c can be obtained as shown in Fig. 7.16.

The failure surfaces of the jointed rock masses can be obtained by superposition of the discontinuity failure surfaces and the intact rock failure surfaces. Fig. 7.17 is obtained by superposition of the failure surfaces in Figs. 7.15 and 7.16. The following remarks can be made about the diagrams shown in Fig. 7.17:

1. In general, for a given value of σ'_x/σ_c , the size of the stable domain enclosed by the intact rock failure surface is reduced because of the discontinuities. The symmetry of the intact rock failure surface with respect to the $m = n$ axis in the m, n space (Fig. 7.17) is lost. The strength of the jointed rock mass is clearly anisotropic.
2. The strength reduction associated with the discontinuities is more pronounced for discontinuities with orientation angles β and ψ for which the discontinuity failure surface in the m, n space is ellipse than when it is an hyperbola or a parabola.
3. Despite the zero discontinuity tensile strength and the strength reduction associated with the discontinuities, jointed rock masses can be stable under a wide variety of states of stress $\sigma'_x, \sigma'_y = m\sigma'_x, \sigma'_z = n\sigma'_x$. These states of stress depend on the values of discontinuity orientation angles β and ψ and the stress ratio σ'_x/σ_c .

(c) Comments

In Subsection (a), a rock mass with one discontinuity set is considered. If we apply the model of Jaeger (1960) and Jaeger and Cook (1979) to a rock mass with several

Table 7.16 Forms of equation (7.18) for different orderings of σ'_x, σ'_y and σ'_z .

Principal stress ordering	Major stress σ'_1	Minor stress σ'_3	Forms of equation (7.18)
$\sigma'_x > \sigma'_y > \sigma'_z$	σ'_x	σ'_z	$\sigma'_x = \sigma'_z + \sigma_c \sqrt{m_i \sigma'_z / \sigma_c + 1}$
$\sigma'_x > \sigma'_z > \sigma'_y$	σ'_x	σ'_y	$\sigma'_x = \sigma'_y + \sigma_c \sqrt{m_i \sigma'_y / \sigma_c + 1}$
$\sigma'_y > \sigma'_x > \sigma'_z$	σ'_y	σ'_z	$\sigma'_y = \sigma'_z + \sigma_c \sqrt{m_i \sigma'_z / \sigma_c + 1}$
$\sigma'_y > \sigma'_z > \sigma'_x$	σ'_y	σ'_x	$\sigma'_y = \sigma'_x + \sigma_c \sqrt{m_i \sigma'_x / \sigma_c + 1}$
$\sigma'_z > \sigma'_x > \sigma'_y$	σ'_z	σ'_y	$\sigma'_z = \sigma'_y + \sigma_c \sqrt{m_i \sigma'_y / \sigma_c + 1}$
$\sigma'_z > \sigma'_y > \sigma'_x$	σ'_z	σ'_x	$\sigma'_z = \sigma'_x + \sigma_c \sqrt{m_i \sigma'_x / \sigma_c + 1}$

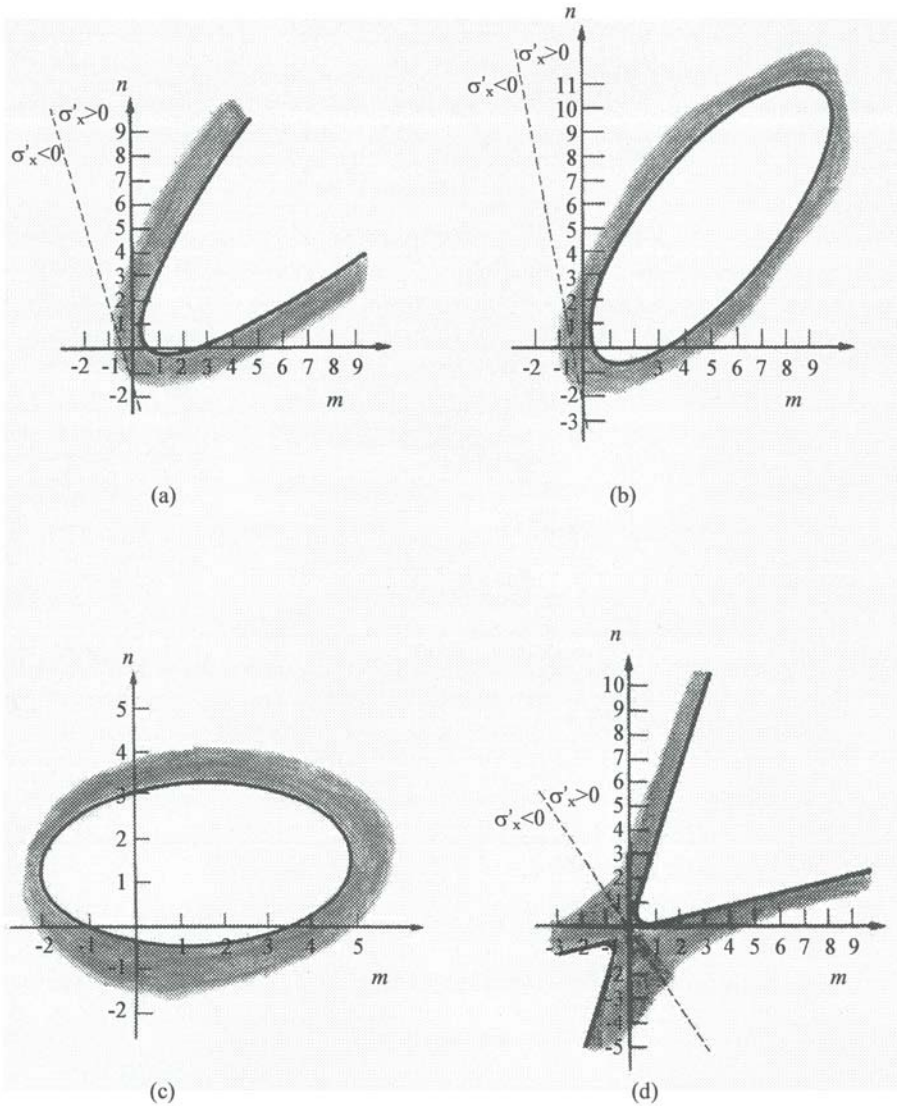


Fig. 7.15 Shape of the failure surface $F_f(m, n) = 0$ in the $m = \sigma'_x/\sigma'_{x0}$, $n = \sigma'_z/\sigma'_x$ space for (a) $\beta = 38.935^\circ$, $\psi = 40^\circ$; (b) $\beta = 30^\circ$, $\psi = 40^\circ$; (c) $\beta = 20^\circ$, $\psi = 80^\circ$; and (d) $\beta = 70^\circ$, $\psi = 40^\circ$. The region $F_n > 0$ is above the dashed line $F_n = 0$ when σ'_x is compressive and below that line when σ'_x is tensile. Friction angle $\phi_f = 30^\circ$ (after Amadei & Savage, 1993).

discontinuity sets, the strength of the rock mass can be obtained by considering the effect of each discontinuity set. For example, consider a simple case of two discontinuity sets A and B [see Fig. 7.18(a)], the angle between them being α . The

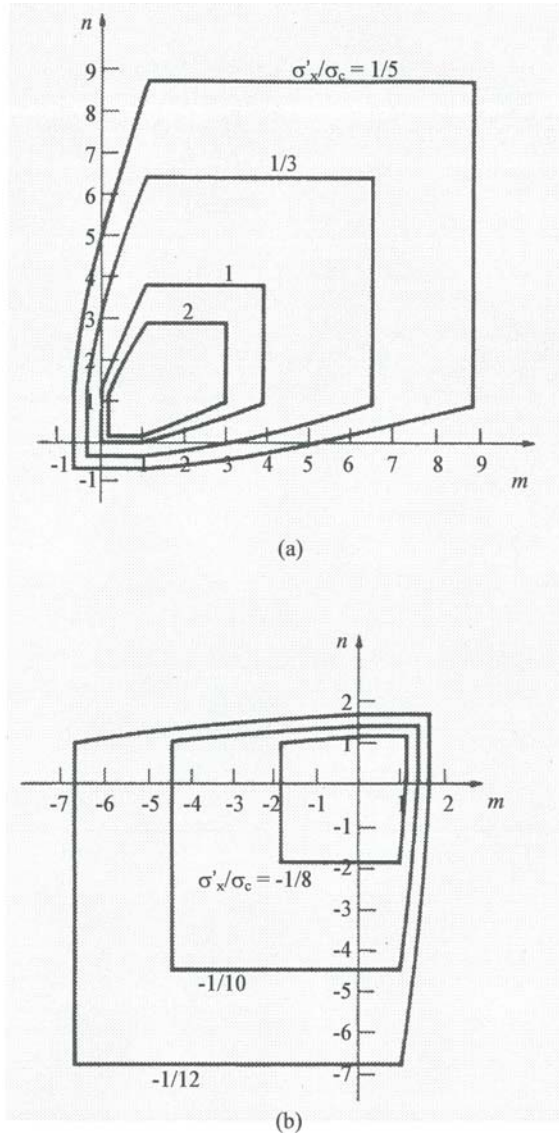


Fig. 7.16 Geometrical representation of the Hoek-Brown failure surface for intact rock in the $m = \sigma'_y/\sigma'_x$, $n = \sigma'_z/\sigma'_x$ space for different values of σ'_x/σ_c with $m_1 = 7$ and $\sigma_c = 42$ MPa. (a) σ'_x is compressive; and (b) σ'_x is tensile (after Amadei & Savage, 1993).

corresponding variation of the compressive strength $\sigma'_{1\beta}$, if the two discontinuity sets are present singly, is shown in Fig. 7.18(b). As the angle β_a of discontinuity set A is changed from 0 to 90°, the angle β_b of discontinuity set B with the major stress

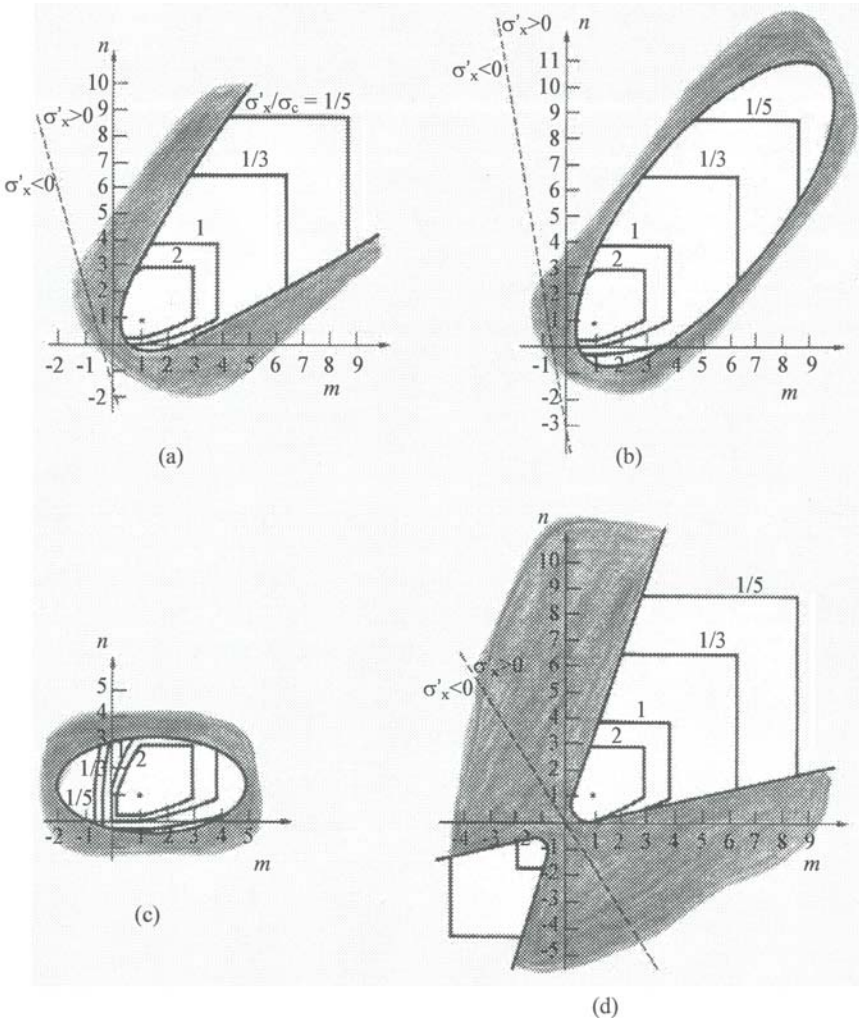


Fig. 7.17 Superposition of the joint failure surface with $\phi_j = 30^\circ$ and the intact rock failure surface with $m_i = 7$ and $\sigma_c = 42$ MPa in the $m = \sigma'_y/\sigma'_x$, $n = \sigma'_z/\sigma'_x$ space for (a) $\beta = 38.935^\circ$, $\psi = 40^\circ$; (b) $\beta = 30^\circ$, $\psi = 40^\circ$; (c) $\beta = 20^\circ$, $\psi = 80^\circ$; and (d) $\beta = 70^\circ$, $\psi = 40^\circ$ (after Amadei & Savage, 1993).

direction will be

$$\beta_b = |\alpha - \beta_a| \quad \text{for } \alpha \leq 90^\circ \tag{7.70}$$

When β_a is varied from 0 to 90° , the resultant strength variation for $\alpha = 60$ and 90°

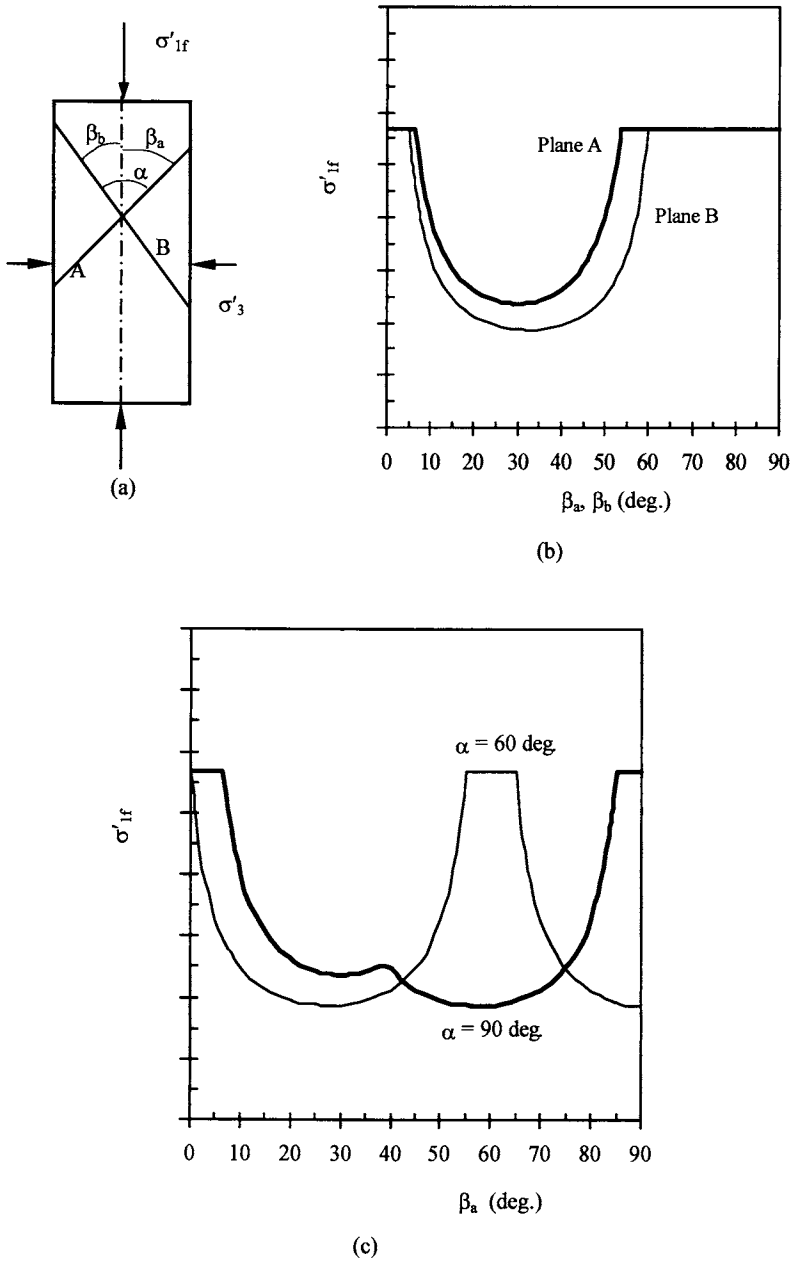


Fig. 7.18 (a) Rock mass with two discontinuity sets A and B; (b) Strength variation with β if the discontinuity sets are present singly; and (c) Strength variation when both discontinuity sets are present.

will be as in Fig. 7.18(c), choosing the minimum of the two values $\sigma'_{1\beta a}$ and the corresponding $\sigma'_{1\beta b}$ from the curves in Fig. 7.18(b).

Hoek and Brown (1980) have shown that with three or more discontinuity sets, all sets having identical strength characteristics, the rock mass will exhibit an almost flat strength variation (see Fig. 7.19), concluding that in highly jointed rock masses, it is possible to adopt one of the empirical isotropic rock mass failure criteria presented in Section 7.4.3.

It should be noted that, in the models of the equivalent continuum approach, discontinuities are assumed to be persistent and all discontinuities in one set have the same orientation. In reality, however, discontinuities are usually non-persistent and the discontinuities in one set have orientation distributions.

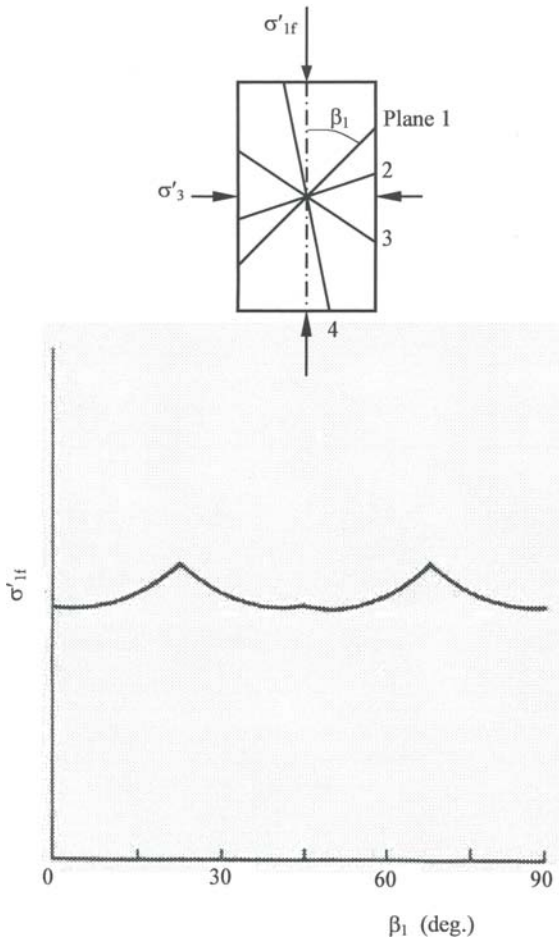


Fig. 7.19 Strength variation with angle β_1 of discontinuity plane 1 in the presence of 4 discontinuity sets, the angle between two adjoining planes being 45° (after Hoek & Brown, 1980).

7.5 SCALE EFFECT ON ROCK STRENGTH

Research results (see, e.g., Heuze, 1980; Hoek & Brown, 1980; Medhurst & Brown, 1996) indicate that rock masses show strong scale dependent mechanical properties. In the following, the scale effect on the strength of rock masses is briefly discussed.

Experimental results show that rock strength decreases significantly with increasing sample size. Based upon analyses of published data, Hoek and Brown (1980) suggested that the unconfined compressive strength σ_{cd} of a rock specimen with a diameter of d mm is related to the unconfined compressive strength σ_{c50} of a 50 mm diameter specimen by

$$\sigma_{cd} = \sigma_{c50} \left(\frac{50}{d} \right)^{0.18} \quad (7.71)$$

This relationship, together with the data upon which it was based, is illustrated in Fig. 7.20. Hoek and Brown (1997) suggested that the reduction in strength is due to the greater opportunity for failure through and around grains, the “building blocks” of intact rock, as

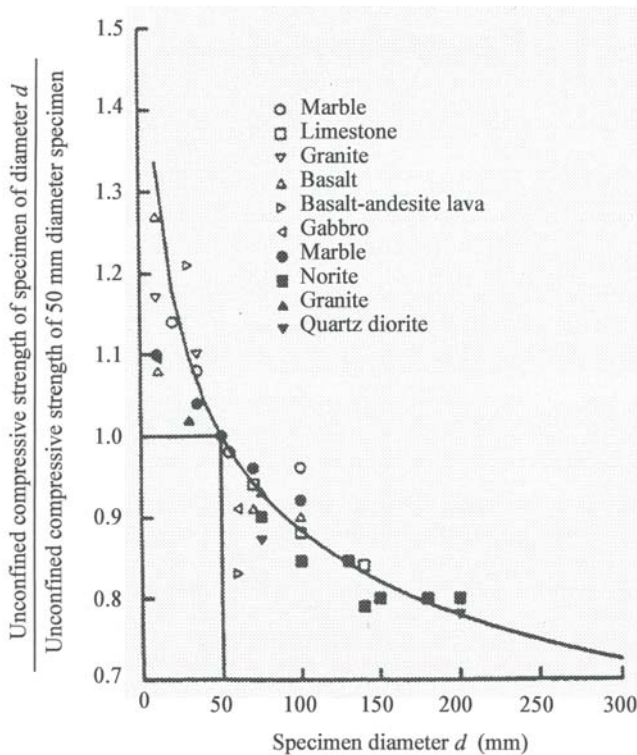


Fig. 7.20 Influence of specimen size on the strength of intact rock (after Hoek & Brown, 1980).

more and more of these grains are included in the test sample. Eventually, when a sufficiently large number of grains are included in the sample, the strength reaches a constant value.

Medhurst and Brown (1996) reported the results of laboratory triaxial tests on 61, 101, 146 and 300 mm diameter samples of a highly cleated mid-brightness coal from the Moura mine in Australia. The results of these tests are as summarized in Table 7.17 and Fig. 7.21. It can be seen that the strength decreases significantly with increasing specimen size. This

Table 7.17 Peak strength of Moura coal in terms of the parameters in equation (7.39), based upon a value of $\sigma_c = 32.7$ MPa.

Diameter (mm)	m_b	s	a
61	19.4	1.0	0.5
101	13.3	0.555	0.5
146	10.0	0.236	0.5
300	5.7	0.184	0.6
Mass	2.6	0.052	0.65

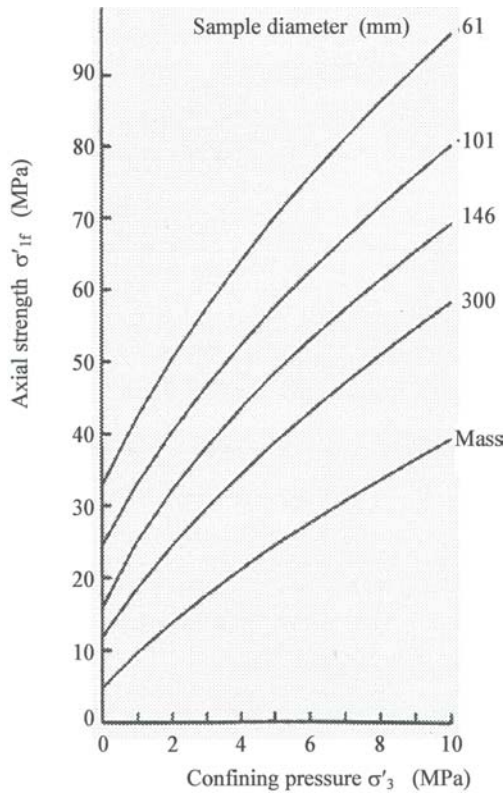


Fig. 7.21 Peak strength for Australian Moura coal (after Medhurst & Brown, 1996).

is attributed to the effects of cleat spacing. For this coal, the persistent cleats are spaced at 0.3-1.0 m while non-persistent cleats within vitrain bands and individual lithotypes define blocks of 1 cm or less. This cleating results in a "critical" sample size of about 1 m above which the strength remains constant. Heuze (1980) conducted an extensive literature search and found results of 77 plate tests as shown in Fig. 7.22. The test volume shown in this figure is calculated in the following way:

1. For a circular plate, the test volume is taken as that of a sphere having a diameter of 4 times the diameter of the plate.
2. For a rectangular or square plate of given area, the diameter of a circle of equal area is first calculated, and the test volume is then determined using the equivalent diameter.

The number shown next to the open triangles in the figure indicates the number of tests performed; the mean value of these test results is plotted as the triangle. The test results

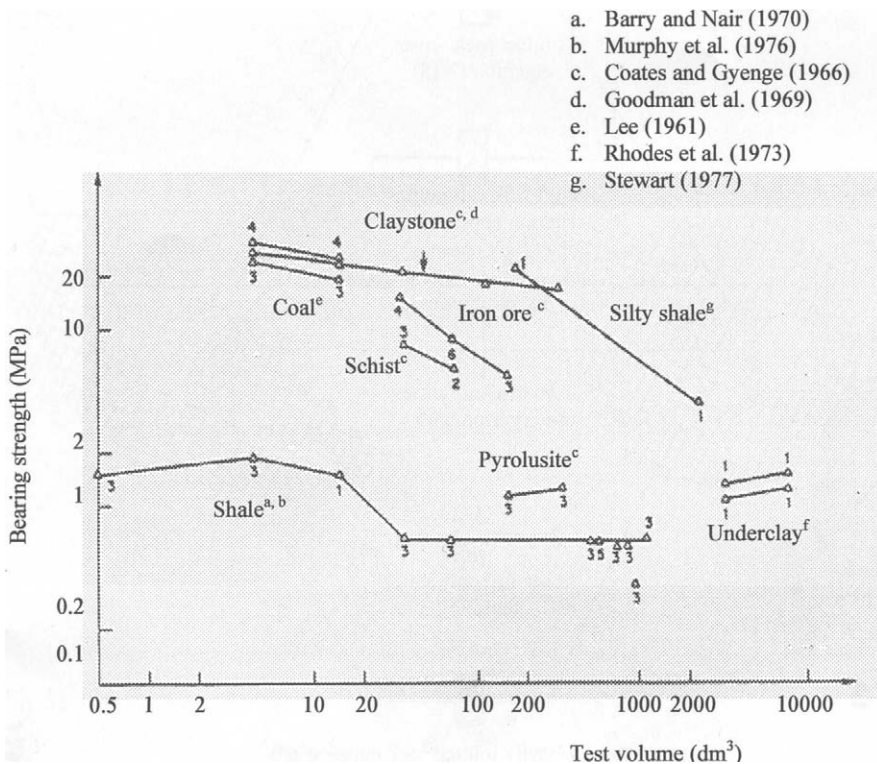


Fig. 7.22 Effect of test volume on measured bearing strength of rock masses. The number next to the triangle indicates the number of tests performed (after Heuze, 1980).

[except those of Coates and Gyenge (1966) and Rhodes et al. (1973)] show that the strength decreases with increasing test volume.

Fig. 7.23 (Hoek et al., 1995) shows a simplified representation of the influence of the relation between the discontinuity spacing and the size of the problem domain on the selection of a rock mass behavior model (Hoek-Brown strength criterion). As the problem domain enlarges, the corresponding rock behavior changes from that of the isotropic intact rock, through that of a highly anisotropic rock mass in which failure is controlled by one or two discontinuities, to that an isotropic heavily jointed rock mass.

7.6 ANISOTROPY OF ROCK STRENGTH

Some intact rocks, such as those composed of parallel arrangements of flat minerals like mica, chlorite and clay, show strong strength anisotropy. Fig. 7.24 shows the anisotropy of compressive strength recorded for a series of tests performed on a slate. The maximum

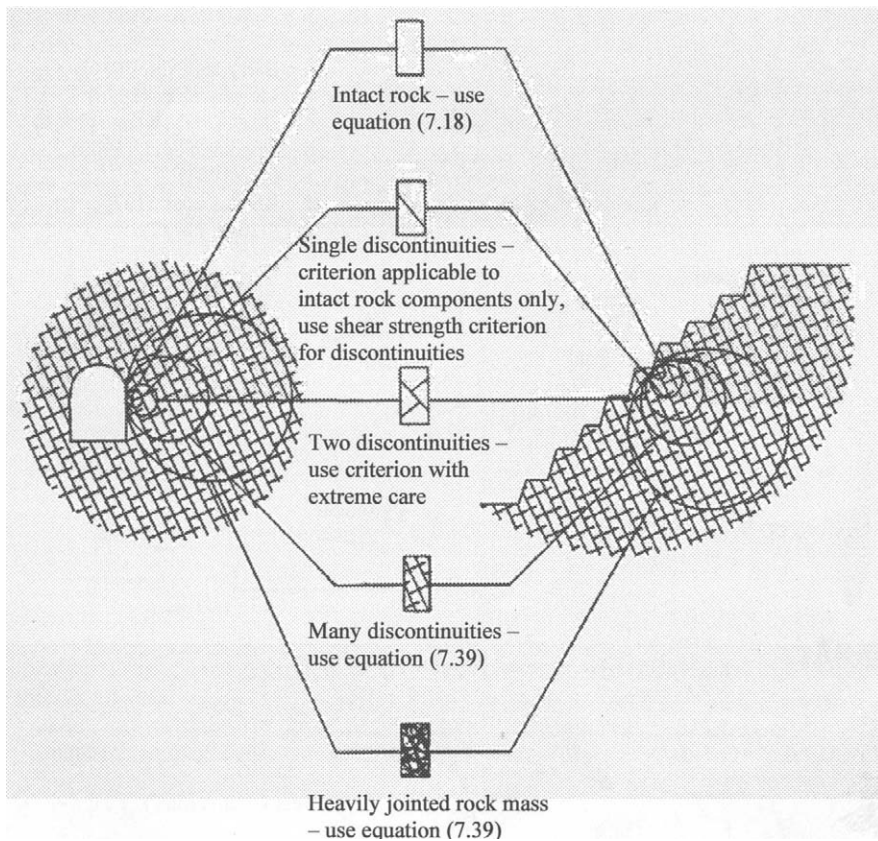


Fig. 7.23 Simplified representation of the influence of scale on the type of rock mass behavior (after Hoek et al., 1995).

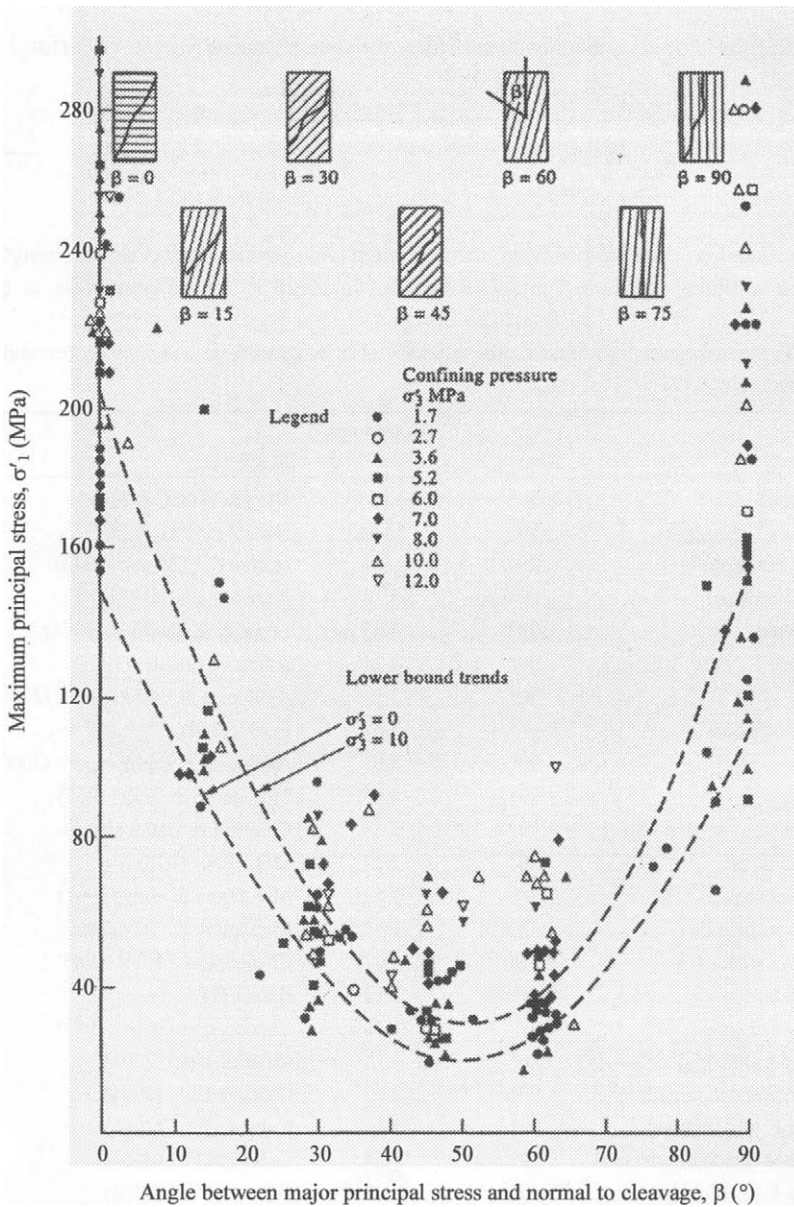


Fig. 7.24 Compressive strength anisotropy in dark gray slate (after Brown, et al., 1977).

strength is generally found when the major principal stress is nearly perpendicular or parallel to the stratification plane. The minimum strength is obtained when the angle β between the major principal stress and the stratification plane is at 30° to 60° . The degree

of strength anisotropy is commonly quantified by the strength anisotropy ratio R_c defined as follows

$$R_c = \frac{\sigma_{cmax}}{\sigma_{cmin}} \quad (7.72)$$

where σ_{cmax} and σ_{cmin} are, respectively, the maximum and minimum compressive strengths at a given confining pressure. Table 7.18 lists the values of R_c for different rocks at the

Table 7.18 Strength anisotropy ratio R_c for different rocks at unconfined compression (expanded from Ramamurthy, 1993).

Rock	β for σ_{cmax}	Anisotropy ratio	
		R_c	Reference
Angers schist	90°	13.48	Duveau et al. (1998)
Martinsburg slate	90°	13.46	Donath (1964)
Fractured sandstone	90°	6.37	Horino & Ellickson (1970)
Barnsley Hard coal	90°	5.18	Pomeroy et al. (1971)
Penrhyn slate	90°	4.85	Attewell & Sandford (1974)
Diatomite	90°	3.74	Allirot & Boehler (1979)
Siltshale	90°	3.70	Ajalloeian & Lashkaripour (2000)
South African slate	0°	3.68	Hoek (1964)
Mudshale	90°	3.01	Ajalloeian & Lashkaripour (2000)
Texas slate	90°	3.00	McLamore & Gray (1967)
Permian shale	90°	2.33	Chnevert & Gatlin (1965)
Crystalline schist	90°	2.24	Moji et al. (1978)
Green River shale I	0°	1.62	McLamore & Gray (1967)
Green River shale II	0°	1.41	McLamore & Gray (1967)
Green River shale	0°, 90°	1.37	Chenenert & Gatlin (1965)
Kota sandstone	0°	1.12	Rao (1984)
Arkansas sandstone	0°	1.10	Chenenert & Gatlin (1965)
Sandstone-A (fine grained)	90°	1.75	Colak & Unlu (2004)
Sandstone-B (fine grained)	90°	1.62	Colak & Unlu (2004)
Sandstone-C (fine grained)	90°	1.15	Colak & Unlu (2004)
Sandstone-D (medium grained)	90°	1.34	Colak & Unlu (2004)
Sandstone-E (medium grained)	90°	1.23	Colak & Unlu (2004)
Siltstone-A	90°	1.94	Colak & Unlu (2004)
Siltstone-B	90°	2.30	Colak & Unlu (2004)
Claystone	90°	3.04	Colak & Unlu (2004)
Chamera phyllites			
Quartzitic	90°	2.19	Singh (1988)
Carbonaceous	90°	2.19	Singh (1988)
Micaceous	90°	6.00	Singh (1988)

conditions of unconfined compression. According to Ramamurthy (1993), the strength anisotropy of intact rocks can be classified as in Table 7.19.

It is noted that the strength anisotropy ratio R_c decreases when the confining pressure is higher (see Fig. 7.25). So the effect of strength anisotropy will be reduced when the confining pressure is increased.

The degree of strength anisotropy can also be quantified by the point load strength anisotropy index $I_{a(50)}$ defined as follows

$$I_{a(50)} = \frac{I_{s(50)v}}{I_{s(50)h}} \quad (7.73)$$

Table 7.19 Classification of strength anisotropy of intact rocks (after Ramamurthy, 1993).

Anisotropy ratio R_c	Class	Rock types
$1.0 < R_c \leq 1.1$	Isotropic	Sandstone Shale Slate, phyllite
$1.1 < R_c \leq 2.0$	Low anisotropy	
$2.0 < R_c \leq 4.0$	Medium anisotropy	
$4.0 < R_c \leq 6.0$	High anisotropy	
$6.0 < R_c$	Very high anisotropy	

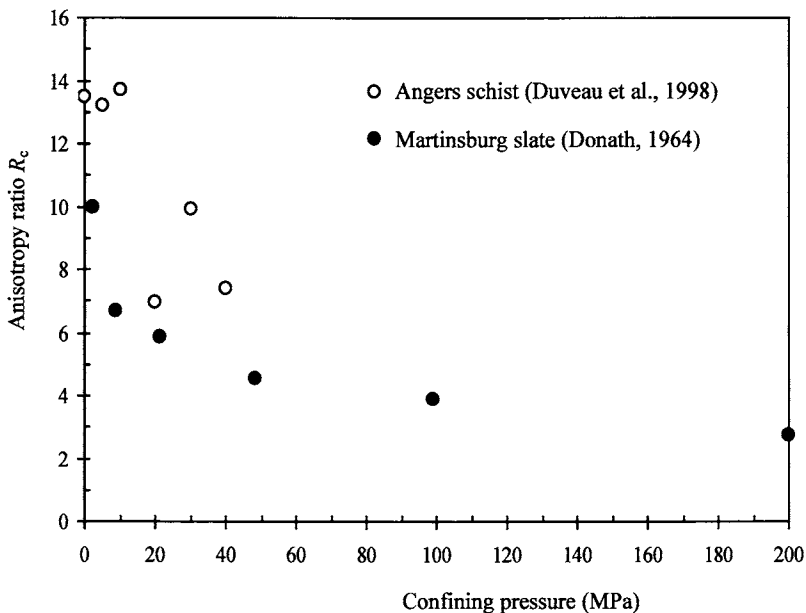


Fig. 7.25 Variation of strength anisotropy ratio with confining pressure (after Donath, 1964; Duveau et al., 1998).

where $I_{s(50)v}$ and $I_{s(50)h}$ are the point load strength index values perpendicular and parallel to the stratification planes, respectively. Table 7.20 shows the anisotropy classification based on $I_{a(50)}$ suggested by Tsidzi (1990).

Rock masses cut by discontinuities also display strength anisotropy. The equivalent continuum models presented in Section 7.4.5 clearly show the variation of compressive strength with the direction of the principal stresses.

Table 7.20 Classification of foliated rocks based on point load strength anisotropy index $I_{a(50)}$ (after Tsidzi, 1990).

Nature of rock	$I_{a(50)}$	Class
Very weakly foliated or non-foliated	$I_{a(50)} \leq 1.1$	Quasi-isotropic
Weakly foliated	$1.1 < I_{a(50)} \leq 1.5$	Fairly anisotropic
Moderately foliated	$1.5 < I_{a(50)} \leq 2.5$	Moderately anisotropic
Strongly foliated	$2.5 < I_{a(50)} \leq 3.5$	Highly anisotropic
Very strongly foliated	$3.5 < I_{a(50)}$	Very highly anisotropic

8

Permeability

8.1 INTRODUCTION

The permeability of a rock is a measure of its capacity for transmitting a fluid. The coefficient of permeability (or hydraulic conductivity) is defined as the discharge velocity through a unit area under a unit hydraulic gradient and is dependent upon the properties of the medium, as well as the viscosity and density of the fluid. According to Darcy's law, the quantity of flow through a cross-sectional area of rock can be calculated by

$$q = KiA \quad (8.1)$$

where q is the quantity of flow; K is the permeability coefficient of the rock, having the units of a velocity; i is the hydraulic gradient (head loss divided by length over which the head loss occurs); and A is the cross-sectional area of flow.

The permeability coefficient of a rock varies for different fluids depending on their density and viscosity as follows:

$$K = k \frac{\rho g}{\mu} = k \frac{g}{\nu} \quad (8.2)$$

where k is the intrinsic (or specific) permeability of the rock, having the units of length squared; ρ , μ , ν are, respectively, the density, viscosity and dynamic viscosity of the fluid; and g is the gravitational acceleration (9.81 m/sec^2). The intrinsic permeability k is independent of the properties of the fluid in the rock.

Very often in rock engineering water is the percolating fluid. In the following discussion, therefore, the fluid in a rock, if not specifically mentioned, will be water.

Because of the presence of discontinuities in a rock mass, the permeability of a rock mass is controlled not only by the intact rock but also by the discontinuities separating the intact rock blocks.

This chapter presents the representative values of the permeability of different rocks and describes various methods for estimating the permeability of rocks. The factors affecting the permeability of rocks are also discussed.

8.2 PERMEABILITY OF INTACT ROCK

The permeability of an intact rock is usually referred to as the primary permeability. The intact rock permeability is governed by the porosity, which varies with factors like the rock type, geological history and in situ stress conditions. Figs. 8.1 and 8.2 are two examples of typical permeability k versus porosity n plots. The increase of permeability with growing porosity follows a quasi-linear $\log k - n$ relationship.

The permeability of intact rocks also varies with the grain size, the higher permeability for larger grain size. Fig. 8.3 shows a logarithmic plot of permeability k versus grain size d . The trend of these data can be represented by

$$\log k = 2.221 \log d - 2.101 \quad (8.3)$$

where k is in md (millidarcy $\approx 10^{-15} \text{ m}^2$) and d is in μm (Schöpfer, 1982).

Since the porosity of intact rocks varies widely (see Table 3.6), the intact rock permeability varies in a great range – at least 8 orders of magnitude. Fig. 8.4(a) shows the range of the intact rock permeability coefficient K for different rock types.

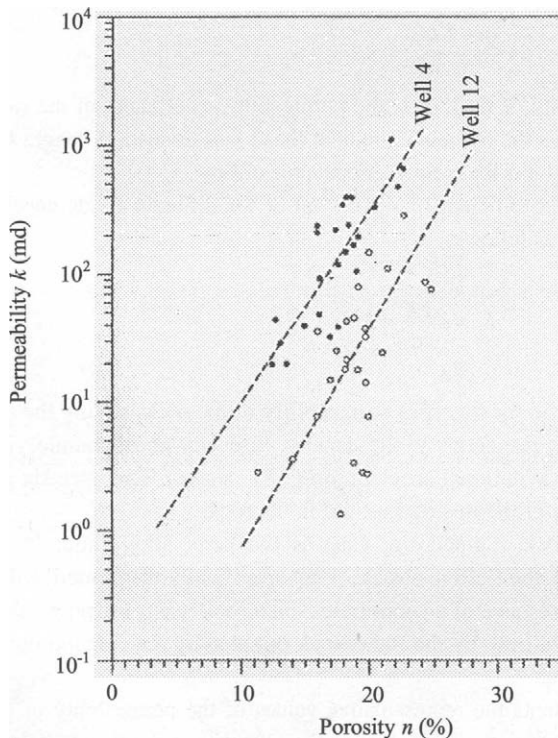


Fig. 8.1 Permeability versus porosity for Totliegend sandstone – data from Diederix (1982) (after Schön, 1996).

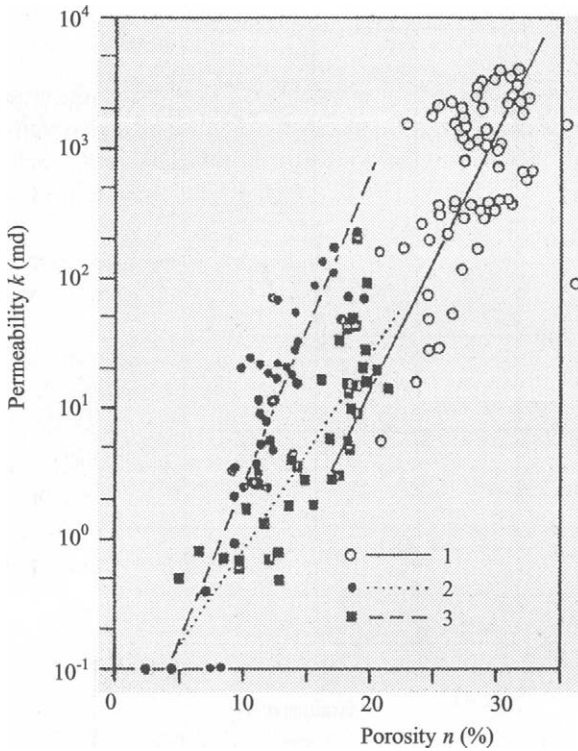


Fig. 8.2 Permeability versus porosity for three sandstones (1 – Gulf Coast Field; 2 – Colorado Field; 3 – California Field) – from Timur (1968) (after Schön, 1996).

8.3 PERMEABILITY OF DISCONTINUITIES

The flow of fluid through discontinuities in rock has been studied in great detail by different researchers, such as Huitt (1956), Snow (1968a, b), Louis (1969), Sharp (1970), and Hoek and Bray (1981). If discontinuities are infilled, the permeability of a discontinuity is simply that of the infilling material. For unfilled discontinuities, by modeling a discontinuity as an equivalent parallel plate conductor, the permeability coefficient along the discontinuity can be determined for the laminar flow by

$$K = \frac{ge^2}{12\nu C} \quad (8.4)$$

where e is the aperture of the discontinuity; ν is the kinematic viscosity of the fluid (which for water can be taken as 1.0×10^{-6} m²/sec); and C is a correction factor representing the discrepancy between the actual physical aperture of the discontinuity and its equivalent hydraulic aperture.

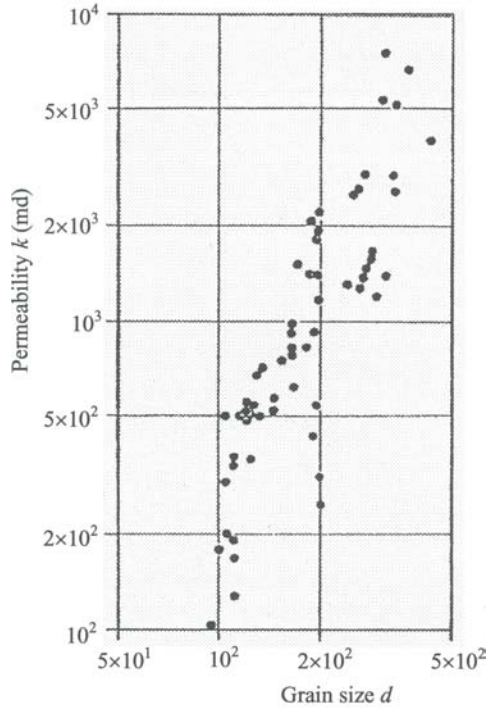


Fig. 8.3 Permeability versus grain size for Bentheim sandstone, Scherhorn oilfield, Germany – from Engelhardt (1960) and Schopper (1982) (after Schön, 1996).

If the equivalent hydraulic aperture is used, equation (8.4) can be rewritten as

$$K = \frac{g e_h^2}{12\nu} \quad (8.5)$$

where e_h is the equivalent hydraulic aperture of the discontinuity, which is related to its physical or mechanical aperture, e , as follows.

$$e_h^2 = \frac{e^2}{C} \quad (8.6)$$

Owing to the wall friction and the tortuosity, the mechanical aperture e is generally larger than the hydraulic aperture e_h . Hakami (1995) showed that the ratio of mechanical mean aperture to hydraulic aperture was 1.1-1.7 for discontinuities with a mean aperture of 100-500 μm . A study by Zimmerman and Bodvarsson (1996)

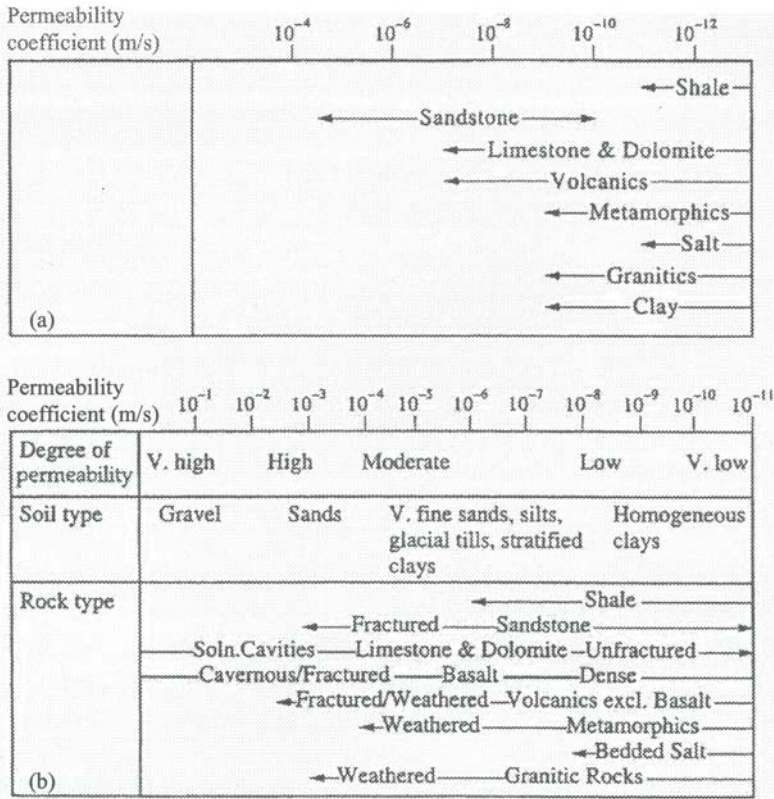


Fig. 8.4 Typical values of permeability coefficient for (a) Intact rocks, and (b) Rock masses (after Isherwood, 1979).

concluded that the mechanic aperture is larger than hydraulic aperture by a factor that depends on the ratio of the mean value of the aperture to its standard deviation. Many researchers have evaluated the factor C , including Lomize (1951), Louis (1969) and Quadros (1982). Their findings can be summarized by the following expression:

$$C = 1 + m \left(\frac{y}{2e} \right)^{1.5} \tag{8.7}$$

where $m = 17$ from Lomize (1951), $m = 8.8$ from Louis (1969), and $m = 20.5$ from Quadros (1982); y is the magnitude of the discontinuity surface roughness. For a smooth parallel discontinuity, y becomes zero and thus C becomes one and $e_h = e$.

Barton et al. (1985) related factor C to the joint roughness coefficient (JRC)

$$C = \frac{\text{JRC}^5}{e^2} \quad (8.8)$$

where C is dimensionless and e is in the unit of μm . The methods for determining JRC have been described in Chapter 6.

Combining equation (8.6) and (8.8) gives

$$e_h = \frac{e^2}{\text{JRC}^{2.5}} \quad (8.9)$$

The background data for equation (8.8) and thus (8.9) mainly comes from normal deformation fluid flow tests. Olsson and Barton (2001) found that equation (8.9) only applies to the case that the shear displacement u_s does not exceed 75% of the peak shear displacement u_{sp} (the shear displacement at peak shear stress). After the peak shear stress ($u_s \geq u_{sp}$), the hydraulic aperture e_h can be calculated from

$$e_h = e^{1/2} \text{JRC}_{\text{mob}} \quad (u_s \geq u_{sp}) \quad (8.10)$$

where JRC_{mob} is the mobilized value of JRC. In the phase of $u_s \geq u_{sp}$, the geometry of the discontinuity wall changes with increasing shear displacement and thus JRC_{mob} should be used. The value of JRC_{mob} is dependent on the strength of the discontinuity wall, on the applied normal stress and on the magnitude of the shear displacement. It is also dependent on the size of the discontinuity plane and on the residual friction angle of the discontinuity. For the calculation of u_{sp} and JRC_{mob} , the reader can refer to Olsson and Barton (2001).

Since the intermediate phase ($0.75u_{sp} < u_s < u_{sp}$) is difficult to define, Olsson and Barton (2001) recommended using a transition curve by connecting the two phases defined by equations (8.9) and (8.10).

For a set of parallel discontinuities, the permeability coefficient parallel to the discontinuities can be determined by

$$K = \frac{g(e_{\text{avg}})^3}{12\nu C_{\text{avg}} s_{\text{avg}}} \quad (8.11)$$

where e_{avg} is the average of individual values of e for discontinuities in the set under consideration; s_{avg} is the average of individual spacing s between discontinuities; and C_{avg} is estimated from equation (8.7) using $(y/e)_{\text{avg}}$ which is the average of the individual values of (y/e) .

Fig. 8.5 shows the variation of permeability coefficient K of a set of smooth parallel discontinuities with the discontinuity aperture and the discontinuity spacing, based on

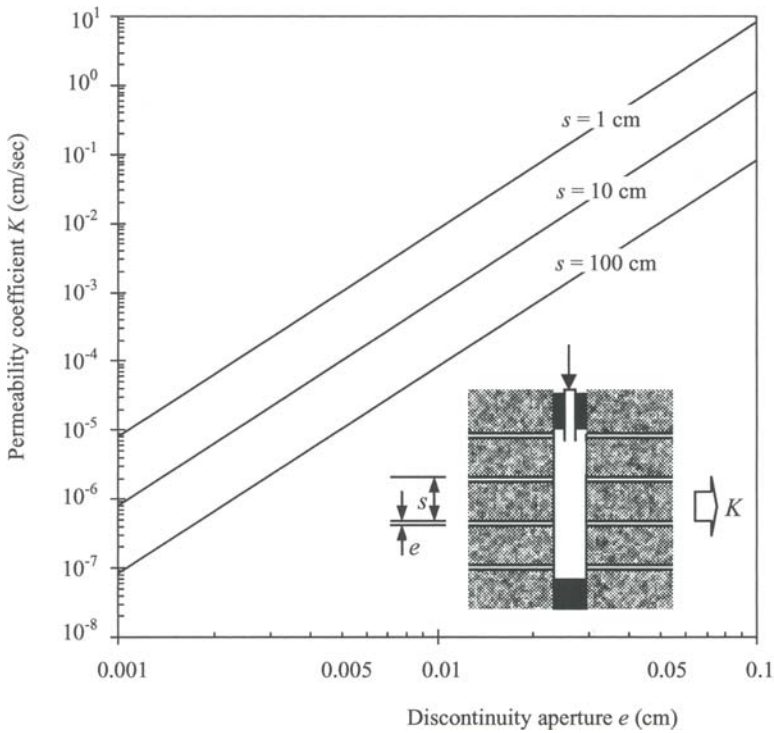


Fig. 8.5 Variation of permeability coefficient K of a set of smooth parallel discontinuities with discontinuity aperture e and spacing s (after Hoek & Bray, 1981).

equation (8.11). The permeability coefficient is very sensitive to small changes in aperture e .

8.4 PERMEABILITY OF ROCK MASS

For a rock mass containing a single set of continuous discontinuities, as illustrated in Fig. 8.6(a), the permeability coefficient of the rock mass in the direction of the discontinuities can be estimated as

$$K = \frac{ge_1^3}{12\nu C_1 s_1} + K_i(1 - e_1/s_1) \quad (8.12)$$

where e_1 , s_1 and C_1 are, respectively, the aperture, spacing and correction factor of discontinuity set 1; and K_i is the permeability coefficient of the intact rock.

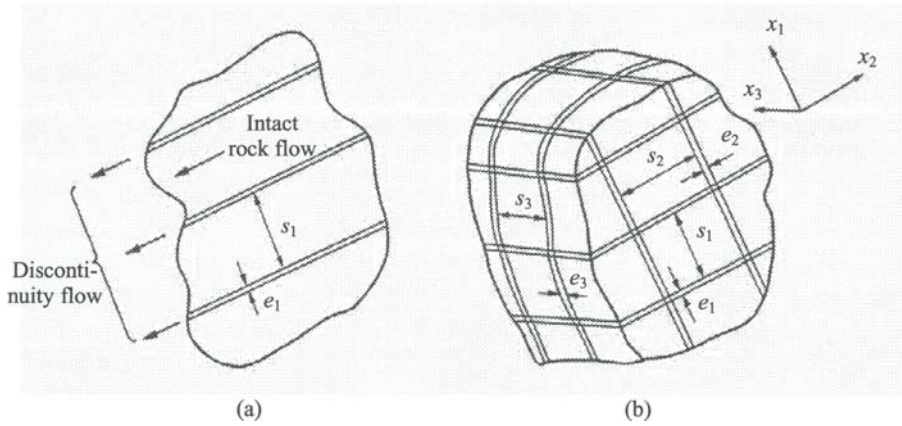


Fig. 8.6 Rock mass containing: (a) a single discontinuity set; and (b) three orthogonal discontinuity sets.

The permeability coefficient of the rock mass in the direction perpendicular to the discontinuities can be simply taken as that of the intact rock.

As further discontinuity sets are added to produce an orthogonal array, the principal magnitudes of permeability coefficient remain coincident with the lines of intersection of the discontinuity sets. The permeability coefficient, K_{11} , in the x_1 direction of Fig. 8.6(b) can be estimated as

$$K_{11} = \frac{g}{12v} \left(\frac{e_2^3}{C_2 s_2} + \frac{e_3^3}{C_3 s_3} \right) + K_i (1 - e_2/s_2)(1 - e_3/s_3) \quad (8.13)$$

The permeability coefficients in the two other orthogonal directions may be determined from equation (8.13) through appropriate permutation. Where discontinuity apertures and spacings between discontinuities differ for each of the sets, permeability of the rock mass will be anisotropic. Commonly, the discontinuity permeability dominates over the intact rock permeability. Consequently, the second term of equations (8.12) and (8.13) may often be neglected.

Fig. 8.4(b) illustrates the range of rock mass permeability coefficient for different rock types. It can be seen that the rock mass permeability coefficient varies in a very great range – 11 orders of magnitude.

8.5 EFFECT OF STRESS ON ROCK PERMEABILITY

Stress has a great effect on the permeability of both intact rocks and rock masses. A number of studies on the variation of intact rock permeability with stress can be found

in the literature (Brace et al., 1968; Gangi, 1978; Kranz et al., 1979; Oda et al., 1989; Read et al., 1989; Jouanna, 1993; Azeemuddin et al., 1995; Indraratna et al., 1999; Ranjith, 2000). Tiller (1953) found an empirical power relationship between the permeability of intact rock and the effective pressure:

$$K = A\sigma^{-m} \quad (\sigma > \sigma_{\text{threshold}}) \quad (8.14)$$

where A and m are constants; and σ is the effective pressure (the difference between the exterior confining pressure and the pore-fluid pressure). This equation is valid only above the threshold effective pressure $\sigma_{\text{threshold}}$.

Louis et al. (1977) presented the following negative exponential relationship between the permeability of intact rock and the effective pressure:

$$K = K_0 e^{-\sigma} \quad (8.15)$$

where σ is the effective pressure (the difference between the exterior confining pressure and the pore-fluid pressure); and K_0 is the permeability at zero effective pressure.

Based on the Hertz theory of deformation of spheres, Gangi (1978) derived the following expression illustrating the effect of confining pressure on the intact rock permeability:

$$K = K_0 \left[1 - C_0 \left(\frac{\sigma + \sigma_i}{p_0} \right)^{2/3} \right]^4 \quad (8.16)$$

where K_0 is the initial permeability of the loose-grain packing; C_0 is a constant depending on the packing and is of the order of 2; σ is the confining pressure; σ_i is the equivalent pressure due to the cementation and permanent deformation of the grains; and p_0 is the effective elastic modulus of the grains and is of the order of the grain material bulk modulus.

Fig. 8.7 shows the variation of the intrinsic permeability of the intact Westerly granite rock with the confining pressure. The intact rock permeability decreases significantly when the confining pressure increases.

Stresses also affect the permeability of discontinuities and thus of rock masses. The effect of stresses on rock mass permeability depends on their direction with respect to the discontinuity orientation. According to Brace (1978), a stress parallel to the discontinuities increases the permeability, while a stress perpendicular to the discontinuities decreases the permeability (Fig. 8.8).

Snow (1968a) presented the following empirical relation between the discontinuity permeability and the normal stress:

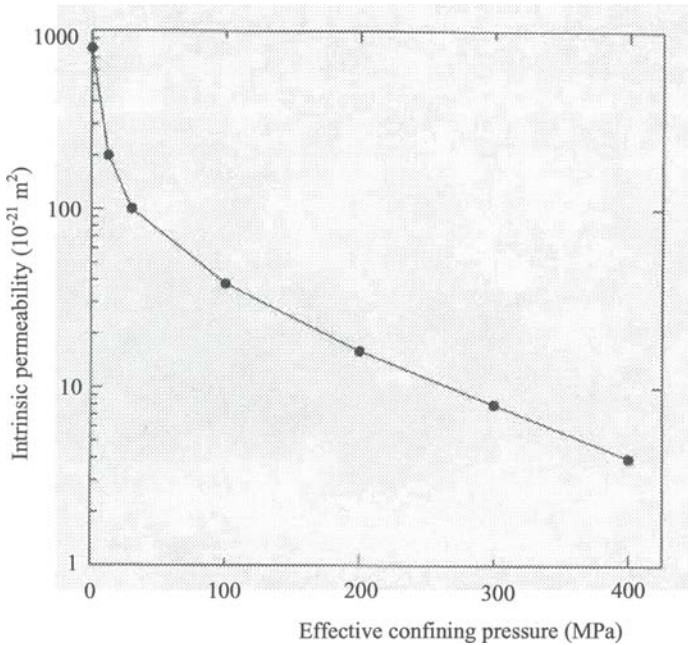


Fig. 8.7 Effect of confining pressure on the permeability of Westerly granite rock (after Indraratna & Ranjith, 2001; data from Brace et al., 1968).

$$K = K_0 + k_n \frac{g e_h^2}{\nu s} (\sigma - \sigma_0) \quad (8.17)$$

where K is the discontinuity permeability at normal stress σ ; K_0 is the initial discontinuity permeability at initial normal stress σ_0 ; k_n is the normal stiffness of the discontinuity; ν is the dynamic viscosity of the fluid; g is the gravitational acceleration (9.81 m/sec^2); s is the discontinuity spacing; and e_h is the hydraulic aperture.

Based on the test results on carbonate rocks, Jones (1975) proposed the following empirical relation between the discontinuity permeability and the confining pressure σ :

$$K = c_0 \left[\log \left(\frac{\sigma_h}{\sigma} \right) \right]^3 \quad (8.18)$$

where σ_h is the confining pressure at which the permeability is zero; and c_0 is a constant that depends on the discontinuity surface and the initial aperture.

By a “bed of nails” model for the asperities of a discontinuity, Gangi (1978) derived the following relation between discontinuity permeability and effective confining stress σ :

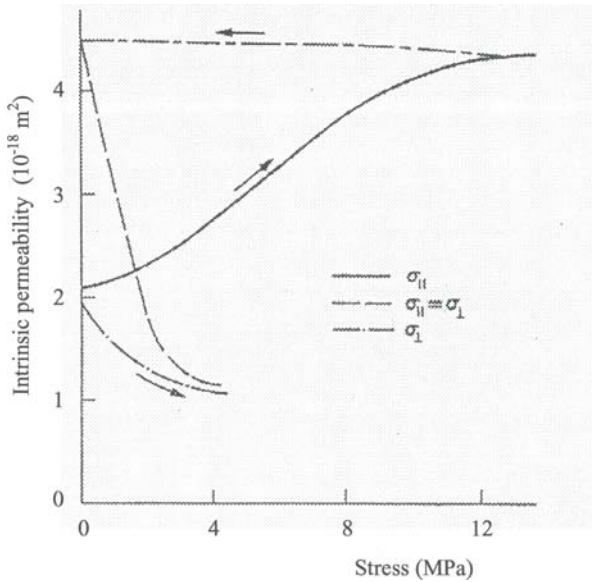


Fig. 8.8 Effect of load acting parallel and perpendicular to a discontinuity on the permeability (after Brace, 1978).

$$K = K_0 \left[1 - \left(\frac{\sigma}{p_1} \right)^m \right]^3 \quad (8.19)$$

where K_0 is the zero pressure permeability; m is a constant ($0 < m < 1$) which characterizes the distribution function of the asperity lengths; and p_1 is the effective modulus of the asperities and is of the order of one-tenth to one-hundredth of the asperity material bulk modulus.

Nelson (1975) proposed the following general expression for the permeability of discontinuities:

$$K = A + B\sigma^{-m} \quad (8.20)$$

where σ is the effective confining stress; and A , B and m are constants determined by regression analysis of test results. These constants vary with the rock type, and even for the same rock type, change with the discontinuity surface.

Based on the simple model of Walsh and Grosenbaugh (1979) for describing the deformation of discontinuities, Walsh (1981) derived the following relation between permeability and confining pressure σ :

$$K = K_0 \left[1 - \left(2 \frac{h}{a_0} \ln \frac{\sigma}{\sigma_0} \right)^{0.5} \right]^3 \left[\frac{1 - b(\sigma - u_w)}{1 + b(\sigma - u_w)} \right] \quad (8.21)$$

where K_0 is the permeability at reference confining pressure σ_0 ; h is the root mean square value of the height distribution of the discontinuity surface; a_0 is the half aperture at the reference confining pressure; u_w is the pore fluid pressure; and

$$b = \left[\frac{3\pi f}{E(1 - \nu^2)h} \right]^{0.5} \quad (8.22)$$

where f is the autocorrelation distance; E and ν are respectively the elastic modulus and Poisson's ratio of the rock.

8.6 VARIATION OF ROCK PERMEABILITY WITH DEPTH

Because in situ rock stress increases with depth (see Chapter 2 for the detailed description of in situ rock stress), the permeability of field rock mass decreases with depth. Figs. 8.9 and 8.10 show the variation of measured rock mass permeability with depth.

Based on field measurements, Louis (1974) found that the rock mass permeability coefficient K decreases with depth z by a negative exponential formula:

$$K = K_0 e^{-Az} \quad (8.23)$$

where K_0 is the surface rock permeability coefficient; and A is an empirical coefficient. On the Grand Maison dam site, he observed that K_0 varied between 10^{-7} and 10^{-6} m/s and A between 7.8 and 3.4×10^{-3} m⁻¹.

Based on the data given by Snow (1968a, b) about the variation of the permeability coefficient of fractured crystalline rocks with depth, Carlsson and Ollsson (1977) proposed the following relation between permeability coefficient K and depth z :

$$K = 10^{-(1.6 \log z + 4)} \quad (8.24)$$

where K and z are, respectively, in the units of m/s and m.

Strack (1989) proposed the following relation between permeability coefficient K and depth z for modeling purposes in crystalline rock masses:

$$K = K_0 \left(1 - \frac{z}{\mu} \right)^\beta \quad (8.25)$$

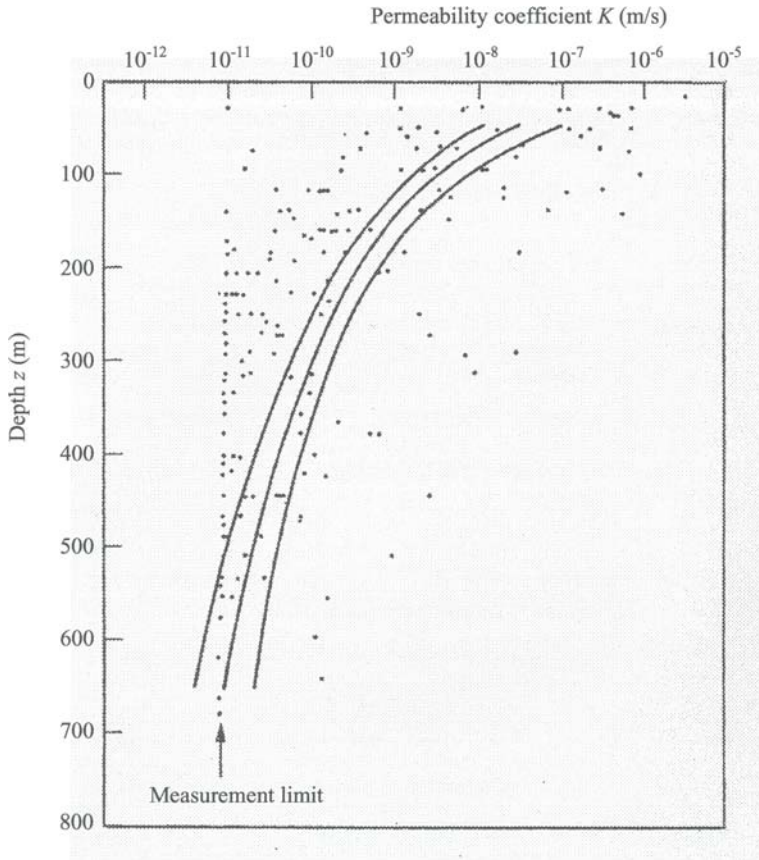


Fig. 8.9 Variation of measured permeability coefficient with depth in granitic rock mass, Sweden (from Carlsson & Olsson, 1993).

where K_0 is the initial rock mass permeability coefficient at the surface; and β and μ are constants.

A numerical study conducted by Wei and others based on rock discontinuity network simulation (Wei and Hudson, 1988; Wei et al., 1995) suggested the following relation between rock mass permeability coefficient K and depth z :

$$K = K_0 \left(1 - \frac{z}{58.0 + 1.02z} \right)^3 \quad (8.26)$$

where K_0 is the rock mass permeability coefficient at initial stage where normal stress approaches to zero.

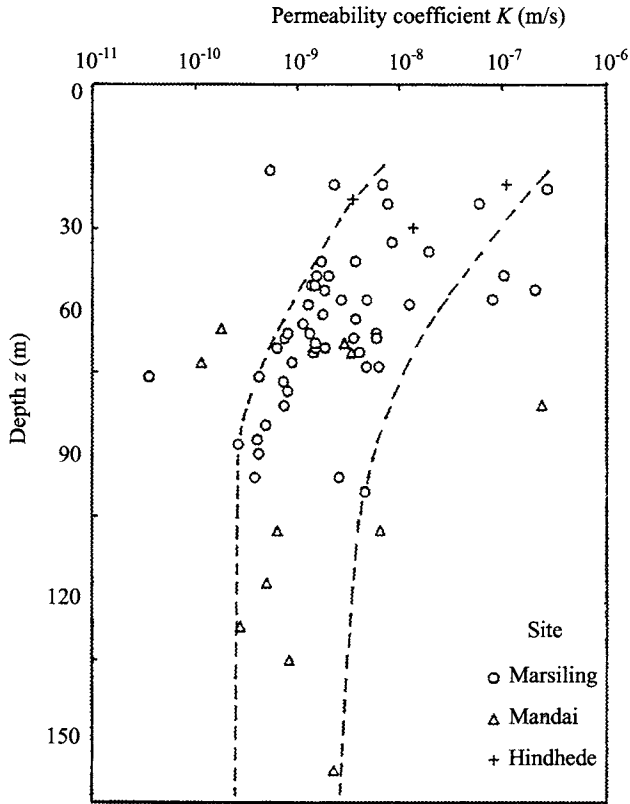


Fig. 8.10 Variation of rock mass permeability coefficient of the Bukit Timah granite with depth at three different sites (from Zhao, 1998).

Based on the measurements in Sweden, Burgess (1977) presented the following empirical relation between the mean horizontal permeability coefficient K and depth z :

$$\log K = 5.57 + 0.352 \log z - 0.978 (\log z)^2 + 0.167 (\log z)^3 \quad (8.27)$$

where K and z are, respectively, in the units of m/s and m.

The effective vertical in situ rock stress due to the weight of the overburden can be simply estimated by:

$$\sigma = \gamma' z \quad (8.28)$$

where γ' is the effective unit weight of the overlying rock mass; and z is the depth below surface. Combining equations (8.20) and (8.28) yields the following general relation between rock mass permeability coefficient K and depth z :

$$K = A + Cz^{-m} \quad (8.29)$$

where A , C ($=B\gamma^m$), and m are constants.

The decrease of rock mass permeability with depth is mainly due to the decrease of discontinuity aperture with depth. Fig. 8.11 shows the variation of discontinuity aperture with depth based on the data of Snow (1968a, b).

8.7 EFFECT OF TEMPERATURE ON ROCK PERMEABILITY

Changes in temperature also affect the rock permeability. An increase in temperature will cause a volumetric expansion of the rock material leading to reduction in discontinuity aperture and thus an overall reduction in the rock mass permeability. Mineral dissolution and precipitation due to increased temperature will also cause redistribution of minerals in the rock, such that asperities are chemically removed while pores and discontinuities are filled leading to reduction of the rock mass permeability (Moore et al., 1994; Polak et al. 2003). Fig. 8.12 shows the reduction of hydraulic

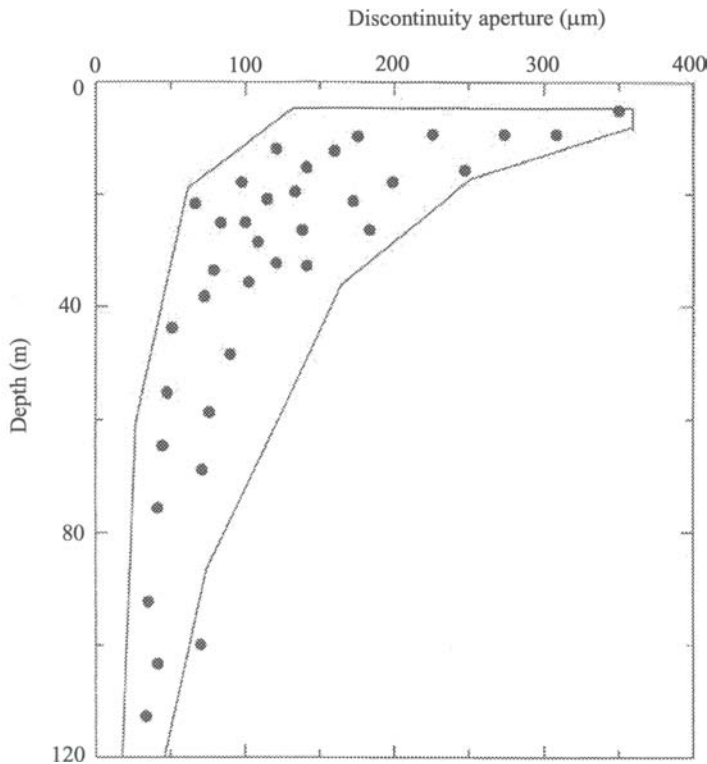


Fig. 8.11 Variation of discontinuity aperture with depth (data from Snow, 1968a, b).

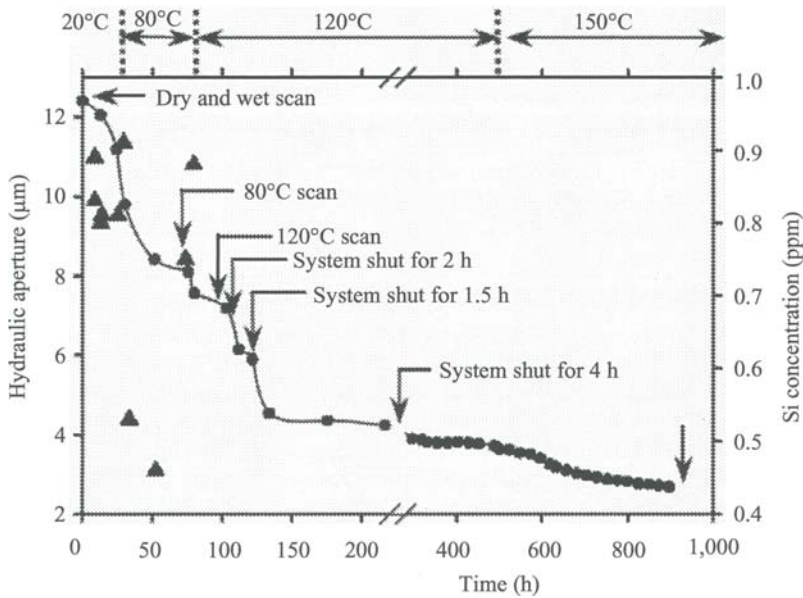


Fig. 8.12 Effect of temperature on hydraulic aperture of a natural discontinuity in novaculite (after Polak et al., 2003).

aperture of a natural discontinuity in novaculite due to temperature increase, under a constant effective stress of 3.5 MPa. The hydraulic aperture decreased from above 12 μm to 2.7 μm as temperature was increased from 20°C to 150°C over a period of 900 hours. Fig. 8.13 shows the variation of the permeability of tuff as temperature was increased from below 30°C to 150°C and then decreased back to below 30°C. The permeability decreased with higher temperature and then increased with lower temperature (Lin et al., 1997).

Studies in the Stripa Iron Ore Mine, Sweden demonstrated a decrease of permeability coefficient for granites from $4 \pm 0.8 \times 10^{-11}$ m/s to $1.8 \pm 0.3 \times 10^{-11}$ m/s when temperature was increased by 25°C by circulating warm water. Considering the change in viscosity of the permeant at the higher temperatures, the intrinsic permeability of the rock mass had been reduced by a factor of approximately four (Lee & Farmer, 1993).

Barton and Lingle (1982) presented the results of tests made in situ on fractured gneiss. The permeability of fractured gneiss was decreased ten fold with a temperature increase of 74°C.

8.8 SCALE EFFECT ON ROCK PERMEABILITY

Research results have shown that the rock mass permeability is strongly scale dependent. As illustrated in Fig. 8.14, the permeability of rock will vary as the problem

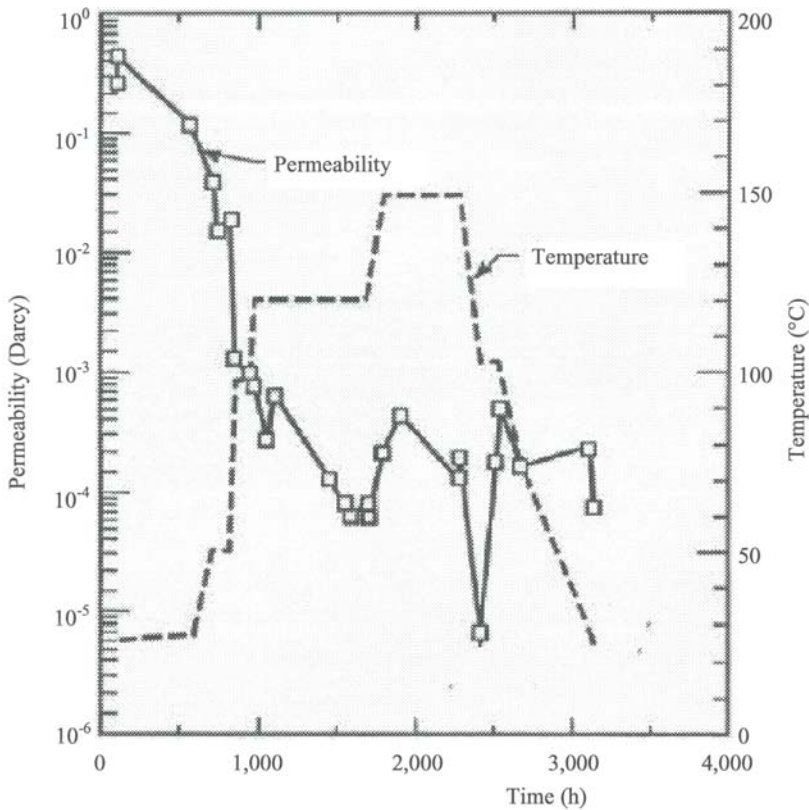


Fig. 8.13 Effect of temperature on the permeability of tuff (after Lin et al., 1997).

domain enlarges. For domain A, water can flow only through the intact rock and the rock mass permeability is simply the intact rock permeability. For domain B, water can flow vertically through the intact rock and along a single discontinuity and thus the rock mass permeability in the vertical direction is the sum of the intact rock permeability and the permeability of that single discontinuity. In the lateral direction, however, the water can flow only through the intact rock and thus the rock mass permeability is simply the intact rock mass permeability. As the domain enlarges to C, water will flow through the intact rock and along discontinuities in both the vertical and lateral directions. Therefore, the rock mass permeability in both the vertical and lateral directions will be the sum of the intact rock permeability and the permeability of the corresponding discontinuities. As the domain further enlarges and thus the number of discontinuities in it increases, water will flow along more discontinuities in both the vertical and lateral directions. When the domain enlarges to a certain volume, called “representative elementary volume” (REV), the rock mass permeability will reach a steady magnitude.

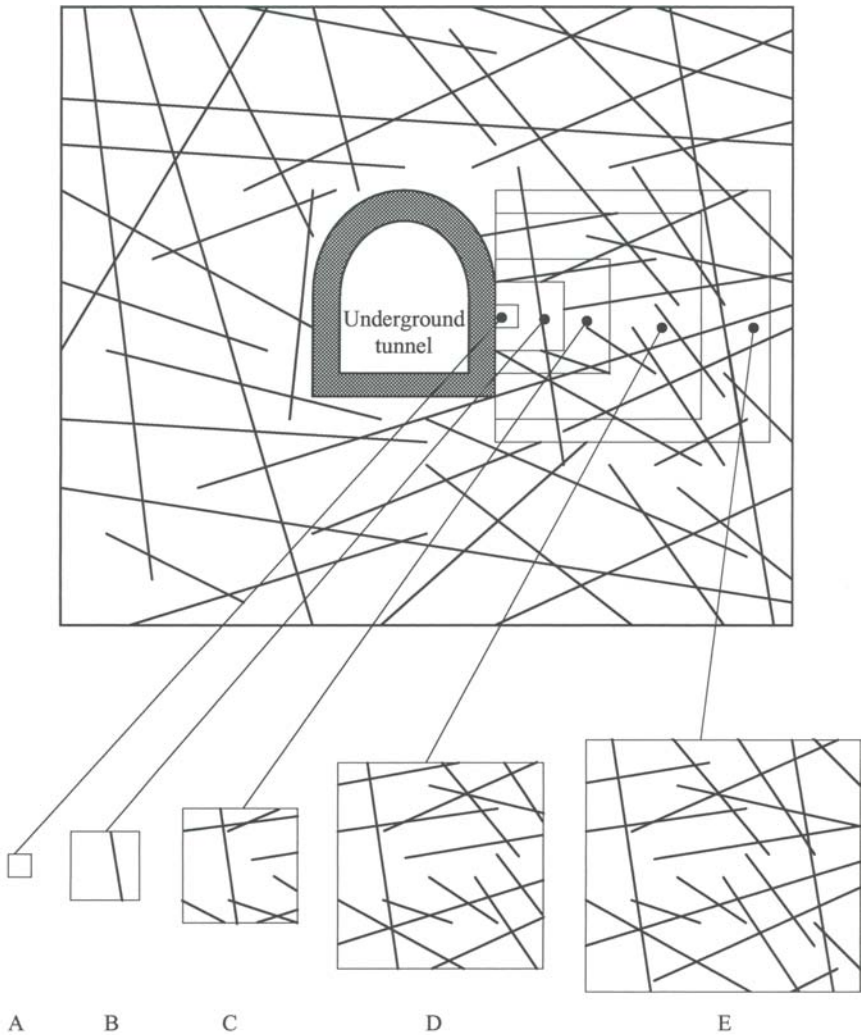


Fig. 8.14 Simplified representation of scale effect on rock mass permeability (modified from Brady & Brown, 1985).

The concept of REV is illustrated in Fig. 8.15. The rock mass permeability will become constant at some REV if the discontinuity occurrence is statistically homogeneous in the region considered. If the discontinuity occurrence is inhomogeneous, the permeability may show further oscillations in the trace or steady increases or decreases.

REV increases in size with larger discontinuity spacing (Kunkel et al., 1988). Fig. 8.16 illustrates how discontinuities affect REV. In rocks without discontinuities, small

REV can be representative of the rock mass [Fig. 8.16(a)]. In rock masses containing discontinuities, REV should be large enough to include sufficient discontinuity intersections to represent the flow domain [Fig. 8.16(b)]. The size of REV will be large compared to the discontinuity lengths in order to provide a good statistical sample of the discontinuity population. In the case of large scale discontinuities, such as faults and dykes, REV may not be feasible as it will be too large an area [Fig. 8.16(c)]. So the REV concept may not be satisfied for every rock mass. The only way to define REV for a rock mass is to investigate in detail the discontinuity geometry. For detailed characterization of discontinuity geometry, the reader can refer to Chapter 4.

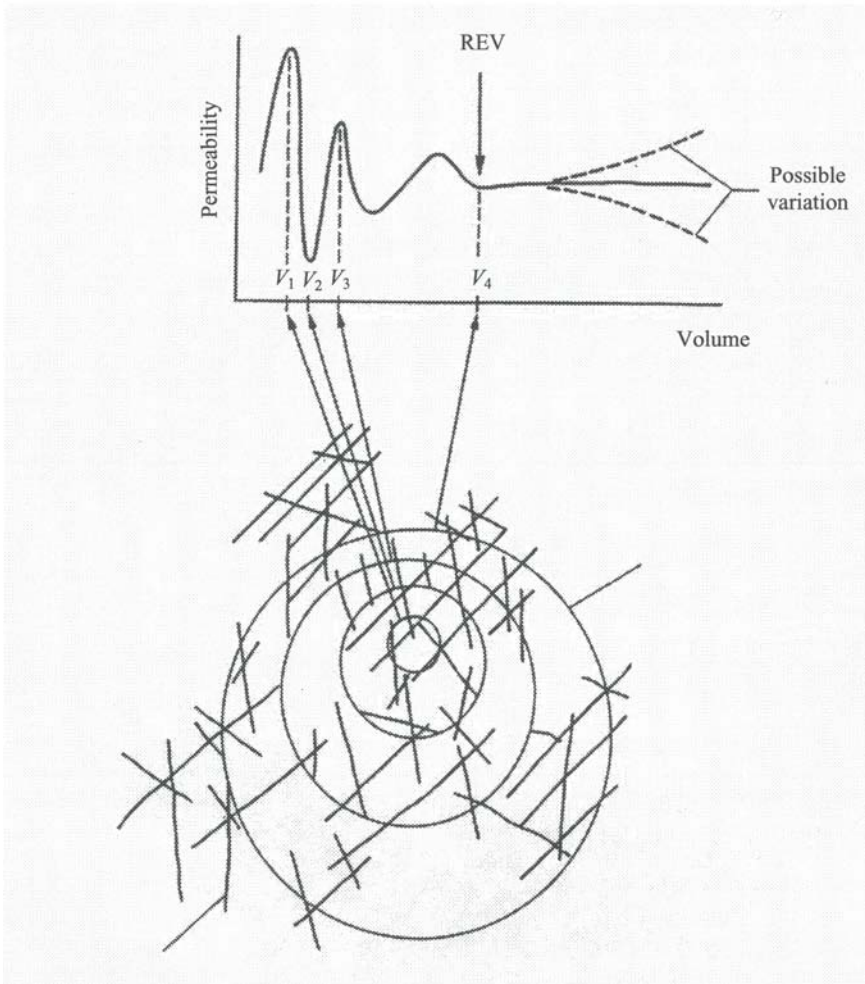


Fig. 8.15 Representative elemental volume (REV) for rock mass permeability (after Elsworth & Mase, 1993).

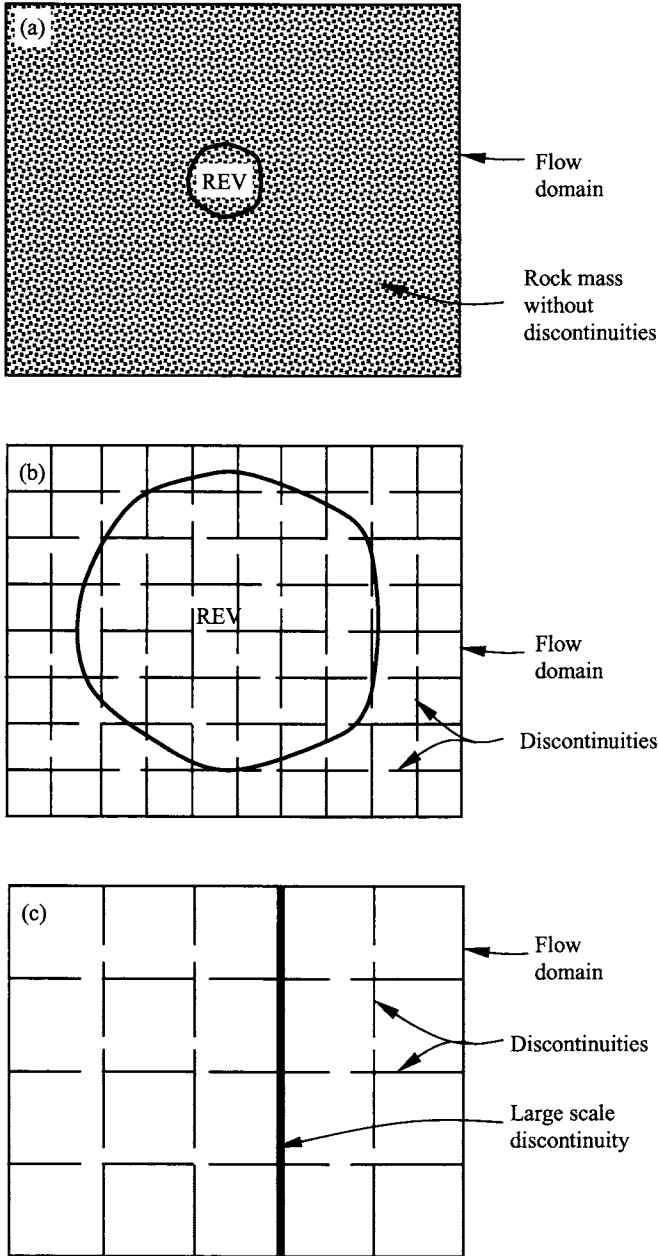


Fig. 8.16 Representative elemental volume (REV) in different rock conditions: (a) Rock mass without discontinuities; (b) Rock mass containing discontinuities where REV includes sufficient discontinuity interactions; and (c) Rock mass containing large-scale discontinuities where REV is either very large or non-existent (after Kunkel et al., 1988).

8.9 INTERCONNECTIVITY OF DISCONTINUITIES

Another important point that can be seen from Fig 8.14 is the interconnection of discontinuities. For example, there are 8 discontinuities included in domain C; but only 5 of them are interconnected and may act as flow path for the lateral and vertical water flow (see Fig. 8.17). Interconnectivity of discontinuities is one of the most important factors affecting the permeability of rock masses. Since all discontinuities are of finite length, a discontinuity can act as a flow path only when it extends completely across the zone interested or is connected to other conductive discontinuities. McCrae (1982) estimated that only about 20% of discontinuities encountered during construction of the Muna highway tunnels, Saudi Arabia, were potential water conduits, of which only about 25% had positive evidence of being so. Andersson et al. (1988) found that only 10-40% of discontinuities in the Brandan aream, Finnsjon, Sweden were conductive. Of the 11,000 discontinuities documented throughout the Äspö Hard Rock Laboratory in Sweden, only 8% were wet when they were excavated (Talbot & Sirat, 2001).

8.10 ANISOTROPY OF ROCK PERMEABILITY

Like mechanical properties, the permeability of rocks also shows appreciable anisotropy. The anisotropy of intact rock permeability is primarily a function of the preferred orientation of mineral particles and micro-discontinuities. The permeability of intact rock parallel to the bedding is usually larger than that perpendicular to it. Table 8.1 lists the ratios of the permeability parallel to bedding to that perpendicular to bedding for different rocks.

Because of the discontinuities, the degree of permeability anisotropy for jointed rock masses may be much higher than that for intact rock. The ratio K_h/K_v may vary from 10^{-2} for rock masses whose discontinuities are mainly vertical to 10^3 for rock masses containing bedding planes. The contribution of discontinuities to the permeability of a rock mass can be estimated using the methods presented in Section 8.4.

Changes in pore pressure can affect the degree of permeability anisotropy. For example, in cases with both significant intact rock and discontinuity permeability



Fig. 8.17 (a) Domain C in Fig. 8.14 containing 8 discontinuities; and (b) 5 discontinuities in domain C are interconnected.

Table 8.1 Ratio of permeability parallel to bedding K_h to permeability perpendicular to bedding K_v for different rocks.

Rock	K_h/K_v	Reference
Rothbach sandstone	7.1	Louis et al. (2005)
Berea sandstone	4.0	Zoback & Byerlee (1976)
Triassic Sherwood sandstone	2.0-3.3	Ayan et al. (1994)
Granite	2.5	Pratt et al. (1977)
Crab Orchard sandstone	2.2	Benson et al. (2005)
Bentheim sandstone	1.2	Louis et al. (2005)

where there is only one dominant discontinuity set, an increase in pore pressure will lower the effective stress. This leads to an increase in anisotropy by opening the discontinuities, thus increasing the permeability parallel to the discontinuity orientation. Where there is more than one discontinuity set, the nature of anisotropy change with stress would depend on which of the sets are more deformable. In a poorly connected discontinuity network, a decrease in pore pressure could theoretically make the rock more isotropic.

References

- AASHTO (1989). *Standard Specifications for Highway Bridges*. 14th edition, American Association of State Highway and Transportation Officials, Washington DC.
- Abad, J., Caleda, B., Chacon, E., Gutierrez, V. and Hidlgo, E. (1984). Application of geomechanical classification to predict the convergence of coal mine galleries and to design their supports. *5th Int. Cong. on Rock Mech.*, E, 15-19.
- Adachi, T. and Yoshida, N. (2002). In situ investigation on mechanical characteristics of soft rocks. *In-Situ Characterization of Rocks*. Ed: V. M. Sharma & K. R. Saxena, Balkema, Lisse, 131-186.
- Adams, J. and Bell, J. S. (1991). Crustal stresses in Canada. *The Geology of North America, Decade Map, Neotectonics of North America*, Geol. Soc. Of America, Boulder, Colorado, 1, 367-386.
- Ajalloeian, R. and Lashkaripour, G. R. (2000). Strength anisotropies in mudrocks. *Bull. Engrg. Geol. Envir.*, 59, 195-199.
- Al-Harhi, A. A., Al-Amri, R. M. and Shehata, W. M. (1999). The porosity and engineering properties of vesicular basalt in Saudi Arabi. *Engrg. Geol.*, 54, 313-320.
- Al-Jassar, S. H. and Hawkins, A. B. (1979). Geotechnical properties of the carboniferous limestone of the Bristol area – the influence of petrography and chemistry. *4th ISRM Conference*, Montreux, 1, 3-14.
- Allirot, D. and Boehler, J.-P. (1979). Evolution of mechanical properties of a stratified rock under confining pressure. *Proc. 4th Int. Cong. Rock Mech.*, Montreux, Balkema, Rotterdam, 1, 15-22 (in French).
- Amadei, B. (1983). *Rock Anisotropy and the Theory of Stress Measurements, Lecture Notes in Engineering*. Eds: C. A. Brebbia & S. A. Orszag, Springer-Verlag Berlin.
- Amadei, B. (1988). Strength of a regularly jointed mass under biaxial and axisymmetric loading conditions. *Int. J. Rock Mech. Min. Sci. & Geomech. Abstr.*, 25, 3-13.
- Amadei, B. and Savage, W. Z. (1989). Anisotropic nature of jointed rock mass strength. *J. Geotech. Engrg.*, ASCE, 115, 525-542.
- Amadei, B. and Savage, W. Z. (1993). Effect of joints on rock mass strength and deformability. *Comprehensive Rock Engineering – Principle, Practice and Projects*. Ed: J. A. Hudson, Pergamon, Oxford, UK, 1, 331-365.
- Amadei, B. and Stephanson, O. (1997). *Rock Stress and its Measurement*. Chapman & Hall, London, UK.
- Anderson, E. M. (1951). *The Dynamics of Faulting and Dyke Formation with Applications to Britain*. Oliver and Boyd, Edinburgh, UK.
- Andersson, J.-E., Ekman, L. and Winberg, A. (1988). Detailed hydraulic characterization of a fracture zone in the Brandan area, Finnsjon, Sweden. *Proc. 4th Canadian/American Conf. on Hydrogeol.*, Ed: B. Hitchon and S. Bachu, Natl. Water Well Assoc., Dublin, Ohio, 32-39.
- Anon (1995). The description and classification of weathered rocks for engineering purposes. Working Party Report. *Q. J. Engrg. Geol.*, 28, 207-242.
- Arel, E. and Onalp, A. (2004). Diagnosis of the transition from rock to soil in a granodiorite. *J. Geotech. Geoenviron. Engrg.*, ASCE, 130, 968-974.
- Arjang, B. (1989). Pre-mining stresses at some hard rock mines in the Canadian shield. *Proc. 30th US Symp. Rock Mech.*, Morgantown, Balkema, Rotterdam, 545-551.

- Arora, V. K. (1987). *Strength and deformational behavior of jointed rocks*. PhD thesis, IIT Delhi, India.
- ASCE (1996). *Rock Foundations: Technical Engineering and Design Guides as Adapted from the US Army Corps of Engineers*. No. 16, ASCE Press, New York, NY.
- Asef, M. R. and Reddish, D. J. (2002). The impact of confining stress on the rock mass deformation modulus. *Geotechnique*, 52, 235-241.
- Asef, M. R., Reddish, D. J. and Lloyd, P. W. (2000). Rock-support interaction analysis based on numerical modeling. *Geotech. Geol. Engrg.*, 18, 23-37.
- ASTM (2004). *Annual Book of ASTM Standards, Vol. 4.08, Soil and Rock*. American Society for Testing and Materials, Philadelphia, PA.
- Atkinson, R. H. (1993). Hardness tests for rock characterization. *Compressive Rock Engineering – Rock Testing and Site Characterization*, Ed: J. A. Hudson, Pergamon, Oxford, UK, 3, 105-117.
- Attewell, P. B. and Sandford, M. R. (1974). Intrinsic shear strength of a brittle anisotropic rock I, experimental and mechanical interpretation. *Int. J. Rock Mech. Min. Sci. & Geomech. Abstr.*, 11, 423-430.
- Aufmuth, R. E. (1973). A systematic determination of engineering criteria for rocks. *Bull. Assoc. Eng. Geol.*, 11, 235-245.
- Ayalew, L., Reik, G. and Busch, W. (2002). Characterizing weathered rock masses – a geostatistical approach. *Int. J. Rock Mech. Min. Sci.*, 39, 105-114.
- Ayan, C., Colley, N. et al. (1994). Measuring permeability anisotropy: The latest approach. *Oilfield Review*, 24-27.
- Aydan, O. and Dalgıç, S. (1998). Prediction of deformation behavior of 3-lanes Bolu tunnels through squeezing rocks of North Anatolian fault zone (NAFZ). *Proc. Regional Symp. Sedimentary Rock Engrg.*, Taipei, 228-233.
- Ayday, C. and Gökten, R. M. (1992). Correlations between L and N-type Schmidt hammer rebound values obtained during field-testing. *Int. ISRM Symp. on Rock Characterization*, Ed: J. A. Hudson, 47-50.
- Aytmatov, I. T. (1986). On virgin stress state of a rock mass in mobile folded areas. *Proc. Int. Symp. on Rock Stress and Rock Stress Measurements*, Stockholm, Centek Publ., Lulea, 55-59.
- Baecher, G. N. and Lanney, N. A. (1978). Trace length biases in joint surveys. *Proc. 19th U.S. Symp. on Rock Mech.*, 1, 56-65.
- Baecher, G. N., Lanney, N. A. and Einstein, H. H. (1977). Statistical description of rock properties and sampling. *Proc. 18th U.S. Symp. on Rock Mech.*, 5C1-8.
- Balmer, G. (1952). A general analytical solution for Mohr's envelope. *American Soci. Test. Mater.*, 52, 1260-1271.
- Bandis, S. C. (1990). Mechanical properties of rock joints. *Proc. Int. Symp. on Rock Joints*, Loen, Norway, Eds: N. Barton & O. Stephanson, Balkema, Rotterdam, 125-140.
- Bandis, S. C., Lumsden, A. C. and Barton, N. R. (1981). Experimental studies of scale effects on the shear behavior of rock joints. *Int. J. Rock Mech. Min. Sci. & Geomech. Abstr.*, 18, 1-21.
- Bandis, S. C., Lumsden, A. C. and Barton, N. R. (1983). Fundamentals of rock joint deformation. *Int. J. Rock Mech. Min. Sci. & Geomech. Abstr.*, 20, 249-268.
- Banks, D. (2005). Rock mass ratings (RMRs) predicted from slope angles of natural rock outcrops. *Int. J. Rock Mech. Min. Sci.*, 42, 440-449.
- Barry, A. J. and Nair, O. B. (1970). *In Situ Tests of Bearing Capacity of Roof and Floor in Selected Bituminous Coal Mines*. A Progress Report – Longwall Mining, US Bureau of Mines, RI 7406.

- Barton, C. M. (1977). Geotechnical analysis of rock structure and fabric in CSA Mine NSW. *Applied Geomechanics Technical Paper 24*, Commonwealth Scientific and Industrial Research Organization, Australia.
- Barton, N. (1976). The shear strength of rock and rock joints. *Int. J. Rock Mech. Min. Sci. & Geomech. Abstr.*, 13, 255-279.
- Barton, N. (1987). *Predicting the Behavior of Underground Openings in Rock*. Manuel Rocha Memorial Lecture, Lisbon, Oslo, Norwegian Geotech. Inst.
- Barton, N. (1995). Permanent support for tunnels using NMT - Special Lecture. *Proc. Symp. of KRMS (Korea Rock Mechanics Society) and KSEG (Korea Society of Engineering Geology)*, 1-26.
- Barton, N. (2002). Some new Q value correlations to assist in site characterization and tunnel design. *Int. J. Rock Mech. Min. Sci. & Geomech. Abstr.*, 39, 185-216.
- Barton, N. and Bandis, S. C. (1982). Effects of block size on the shear behavior of jointed rock. *Proc. 23rd U.S. Symp. on Rock Mech.*, Berkeley, 739-760.
- Barton, N. and Bandis, S. C. (1990). Review of predictive capabilities of JRC-JCS model in engineering practice. *Proc. Int. Symp. on Rock Joints*. Loen, Norway, Eds: N. Barton & O. Stephansson, Balkema, Rotterdam, 603-610.
- Barton, N., Bandis, S. and Bakhtar, K. (1985). Strength, deformation and conductivity coupling of rock joints. *Int. J. Rock Mech. Min. Sci. & Geomech. Abstr.*, 22, 121-140.
- Barton, N. and Choubey, V. (1977). The shear strength of rock joints in theory and practice. *Rock Mech.*, 10, 1-54.
- Barton, N., Lien, R. and Lunde, J. (1974). Engineering classification of rock masses for the design of tunnel support. *Rock Mech.*, 6, 189-236.
- Barton, N. and Lingle, R. (1982). Rock mass characterization methods for nuclear waste repositories in jointed rock. *Rock Mech.: Caverns and Pressure Shafts, ISRM Symp.*, Aachen, 3-18.
- Barton, N., Loset, F., Lien, R. and Lunde, J. (1980). Application of the Q-system in design decisions. *Subsurface Space*, Ed: M. Bergman, 2, 553-561.
- Baumgärtner, J. et al. (1993). Deep hydraulic fracturing stress measurements in the KTB (Germany) and Cajon Pass (USA) scientific drilling projects – a summary. *Proc. 7th Cong. Int. Soc. Rock Mech.*, Aachen, Balkema, Rotterdam, 3, 1685-1690.
- Belikov, B. P., Alexandrov, K. S. and Rysova, T. W. (1970). Uprugie svoistva porodobrasujscich mineralov I gornich porod, Izdat. Nauka, Moskva.
- Bell, F. G. (1987). Properties and behavior of the ground. *Ground Engineer's Reference Book*, Ed: F. G. Bell, Butterworths, London, UK.
- Bell, F. G., Culshaw, M. G. and Cripps, J. C. (1999). A review of selected engineering geological characteristics of English Chalk. *Engng. Geol.*, 54, 237-269.
- Benson, P. M., Meredith, P. G., Platzman, E. S. and White, R. E. (2005). Pore fabric shape anisotropy in porous sandstones and its relation to elastic wave velocity and permeability anisotropy under hydrostatic pressure. *Int. J. Rock Mech. Min. Sci.*, in press.
- Beverly, B. E., Schoenwolf, D. A. and Brierly, G. S. (1979). Correlations of rock index values with engineering properties and the classification of intact rock.
- Bieniawski, Z. T. (1973). Engineering classification of jointed rock masses. *Trans South African Inst. Civil Engrs.*, 15, 335-344.
- Bieniawski, Z. T. (1974). Geomechanics classification of rock masses and its application in tunneling. *Proc. 3rd Int. Cong. on Rock Mech.*, Denver, IIA, 27-32.
- Bieniawski, Z. T. (1975). The point load test in geotechnical practice. *Engineering Geology*, 9, 1-11.
- Bieniawski, Z. T. (1976). Rock mass classification in rock engineering. *Proc. Symp. on Exploration for Rock Engrg.*, Ed: Z. T. Bieniawski, Balkema, Cape Town, 1, 97-106.

- Bieniawski, Z. T. (1978). Determining rock mass deformability: experience from case histories. *Int. J. Rock Mech. Min. Sci. & Geomech. Abstr.*, 15, 237-248.
- Bieniawski, Z. T. (1984). *Rock Mechanics Design in Mining and Tunneling*. Balkema, Rotterdam.
- Bieniawski, Z. T. (1989). *Engineering Rock Mass Classifications*. John Wiley, Rotterdam
- Bieniawski, Z. T. (1993). Design methodology for rock engineering: principles and practice. *Comprehensive Rock Engineering – Principle, Practice and Projects*. Ed: J. A. Hudson, Pergamon, Oxford, UK, 2, 779-793.
- Bieniawski, Z. T. and Van Heerden, W. L. (1975). The significance of in situ tests on large rock specimens. *Int. J. Rock Mech. Min. Sci. & Geomech. Abstr.*, 12, 101-113.
- Birch, F. (1961). The velocity of compressional waves in rocks to 10 kilobars (Part II). *J. Geophys. Res.*, 66, 2199-2224.
- Blyth, G. G. H. and M. H. de Freitas (1974). *A Geology for Engineers*. 6th edition, London, Edward Arnold.
- Bowden, A. J., Spink, T. W. and Mortmore, R. N. (2002). Engineering description of chalk: Its strength, hardness and density. *Q. J. Engrg. Geol. Hydrogeol.*, 35, 355-361.
- Brace, W. F. (1978). A note on permeability changes in geological material due to stress. *Pure Appl. Geophys.*, 116, 627-633.
- Brace, W. F., Walsh, J. B., and Frangos, W. T. (1968). Permeability of granite under high pressure. *J. Geophys. Res.*, 73, 2225-2236.
- Brady, B. H. G. and Brown, E. T. (1985). *Rock Mechanics for Underground Mining*. George Allen & Unwin, London.
- Bridges, M. C. (1976). Presentation of fracture data for rock mechanics. *Proc. 2nd Australia-New Zealand Conf. on Geomech.*, Brisbane, 144-148.
- Broch, E. and Franklin, J. A. (1972). Point load strength test. *Int. J. Rock. Mech. Min. Sci.*, 9, 669-697.
- Brook, N. (1993). The Measurement and estimation of basic rock strength. *Rock Testing and Site Characterization-Compressive Rock Engineering*, Ed: J. A. Hudson, 3, 41-66.
- Brown, E. T. (1970a). Strength of models of rock with intermittent joints. *J. Soil Mech. Found. Div.*, ASCE, 96, 1935-1949.
- Brown, E. T. (1970b). Modes of failure in jointed rock masses. *Proc. 2nd Int. Cong. on Rock Mech.*, Belgrade, 2, 3-42.
- Brown, E. T. (1981). *Rock Characterization, Testing and Monitoring – ISRM Suggested Methods*. Pergamon, Oxford, UK.
- Brown, E. T. (1986). Research and development for design and construction of large rock caverns. *Proc. Int. Symp. on Large Rock Caverns*. Helsinki, Finland, 1937-1948.
- Brown, E. T. (1993). The nature and fundamentals of rock engineering. *Comprehensive Rock Engineering – Principle, Practice and Projects*. Ed: J. A. Hudson, Pergamon, Oxford, UK, 1, 1-23.
- Brown, E. T., Richards, L. R. and Barr, M. V. (1977). Shear strength characteristics of the Delabole Slates. *Proc. Conf. Rock Engrg.* Newcastle University, 33-51.
- Budetta, P., Riso, R. de and Luca, C. de (2001). Correlations between jointing and seismic velocities in highly fractured rock masses. *Bull. Eng. Geol. Env.*, 60, 185-192.
- Bulin, N. K. (1971). The present stress field in the upper parts of the crust. *Geotectonics* (Engl. Transl.), 3, 133-139.
- Burgess, A (1977). *Groundwater Movements around a Repository – Regional Groundwater Flow Analysis*. KBS 54:03, Kaernbraenslesaeckerhet, Stockholm, Sweden.

- Cai, M., Kaiser, P. K., Uno, H., Tasaka, Y. and Minami, M. (2003). Estimation of rock mass deformation modulus and strength of jointed hard rock masses using the GSI System. *Int. J. Rock Mech. Min. Sci.*, 41, 3-19.
- Call, R. D., Savely, J. P. and Nicholas, D. E. (1976). Estimation of joint set characteristics from surface mapping data. *Proc. 17th U. S. Symp. on Rock Mech.*, 2B2, 1-9.
- Call, R. D., Savely, J. P. and Pakalnis, R. (1981). A simple core orientation technique. *3rd Int. Conf. on Stability in Surface Mining*. Vancouver, British Columbia, Canada.
- Cameron-Clarke, I. S. and Budavari, S. (1981). Correlation of rock mass classification parameters obtained from bore core and in-situ observations. *Engineering Geology*, 17, 19-53.
- Carlsson, A., and Olsson, T. (1977). Water leakage in the Foresmark Tunnel, Upland, Sweden, Sever. Geol. Unders., C734, Stockholm.
- Carlsson, A., and Olsson, T. (1993). The analysis of fractures, stress and water flow for rock engineering projects. *Comprehensive Rock Engineering – Principle, Practice & Projects*. Ed: J. A. Hudson, Pergamon, Oxford, UK, 2, 415-437.
- CGS (1985). *Canadian Foundation Engineering Manual*. Part 2, (2nd ed.), Canadian Geotechnical Society, Vancouver, Canada.
- Chan, L. P. (1986). *Application of Block Theory and Simulation Techniques to Optimum Design of Rock Excavations*. Ph.D. thesis, University of California, Berkeley, CA.
- Chang, C. and Haimson, B. (2005). Non-dilatant deformation and failure mechanism in two Long Valley Caldera rocks under true triaxial compression. *Int. J. Rock Mech. Min. Sci.*, 42, 402-414.
- Chappel, B. A. (1974). Load distribution and deformational response in discontinua. *Geotechnique*, London, UK, 24, 641-654.
- Cargill, J. S. and Shakoor, A. (1990). Evaluation of empirical methods for measuring the uniaxial compressive strength. *Int. J. Rock Mech. Min. Sci.*, 27, 495-503.
- Chau, K. T. and Wong, R. H. C. (1996). Uniaxial compressive strength and point load strength of rocks. *Int. J. Rock Mech. Min. Sci. & Geomech. Abstr.*, 33, 183-188.
- Chen, E. P. (1989). A constitutive model for jointed rock mass with orthogonal sets of joints. *J. Applied Mech.*, ASME, 56, 25-32.
- Chenevert, M. E. and Gatlin, C. (1965). Mechanical anisotropies of laminated sedimentary rocks. *Soc. Pet. Engrg. J.*, 5, 67-77.
- Coates, D. F. (1967). *Rock Mechanics Principles*. Energy Mines and Resources, Ottawa, Canada, Monograph 874.
- Coates, D. F. and Gyenge, M. (1966). Plate-load testing on rock for deformation and strength properties. *ASTM Special Technical Publication*, 402, 19-35.
- Colak, K. and Unlu, T. (2004). Effect of transverse anisotropy on the Hoek-Brown strength parameter ' m_i ' for intact rocks. *Int. J. Rock Mech. Min. Sci.*, 41, 1045-1052.
- Colback, P. S. B. and Wild, B. L. (1965). The influence of moisture content on the compressive strength of rock. *Proc. 3rd Canadian Rock Mech. Symp.*, 65-83.
- Coon, R. F. and Merritt, A. H. (1970). Predicting in situ modulus of deformation using rock quality indices. *Determination of the in Situ Modulus of Deformation of Rock*, ASTM STP 477. 154-173.
- Crofton, M. W. (1885). Probability. *Encyclopedia Britannica*. 9th edition, 19, 768.
- Cruden, D. M. (1977). Describing the size of discontinuities. *Int. J. Rock Mech. Min. Sci. & Geomech. Abstr.*, 14, 133-137.
- Christensen, N. J. and Salisbury, U. H. (1975). Structure and constitution of the lower oceanic crust. *Rev. Geophys. Space Phys.*, 13, 57086.

- Curran, J. H. and Ofoegbu, G. I. (1993). Modeling discontinuities in numerical analysis. *Comprehensive Rock Engineering – Principle, Practice & Projects*. Ed: J. A. Hudson, Pergamon, Oxford, UK, 1, 443-468.
- D’Andrea, D. V., Fischer, R. L. and Fogelson, D. E. (1965). *Prediction of compressive strength of rock from other properties*. US Bureau of Mines Rep. Investigation, No. 6702.
- Davis, G. H. and Reynolds, S. J. (1996). *Structural Geology of Rocks and Regions*. John Wiley and Sons, New York.
- Dearman, W. R. (1991). *Engineering Geological Mapping*. Butterworth-Heineman, Oxford.
- Deere, D. U. (1964). Technical description of rock cores for engineering purposes. *Rock Mech. and Rock Engrg.*, 1, 107-116.
- Deere, D. U. (1989). *Rock Quality Designation (RQD) after Twenty Years*. U.S. Army Corps of Engineers Contract Report GL-89-1, Waterways Experiment Station, Vicksburg, MS.
- Deere, D. U., Hendron, A. J., Patton, F. D. and Cording, E. J. (1967). Design of surface and near surface construction in rock. *Failure and Breakage of Rock, Proc. 8th U.S. Symp. Rock Mech.*, Ed: C. Fairhurst, 237-302.
- Deere, D. U. and Miller, R.P. (1966). *Engineering Classification and Index Properties for Intact Rock*. Tech. Rep. No. AFWL-TR-65-116, Air Force Weapons Lab, Kirtland Air Base, New Mexico.
- Dershowitz, W. S., Baecher, G. B. and Einstein, H. H. (1979). Prediction of rock mass deformability. *Proc. 4th Int. Cong. on Rock Mech.*, Montreal, Canada, 1, 605-611.
- Dershowitz, W. S. and Herda, H. H. (1992). Interpretation of fracture spacing and intensity. *Proc. 33rd U.S. Symp. on Rock Mech.*, Santa Fe, NM, 757-766.
- Dershowitz, W. S., Lee., G., Geier, J., Hitchcock, S. and LaPointe, P. (1993). *FracMan Version 2.306, Interactive discrete feature data analysis, geometric modeling, and exploration simulation*. User Documentation. Golder Associates Inc., Seattle, Washington.
- Dey, T. N., and Brown, D. W. (1986). Stress measurements in a deep granitic rock mass using hydraulic fracturing and differential strain curve analysis. *Proc. Int. Symp. on Rock Stress and Rock Stress Measurements*, Stockholm, Centek Publ., Lulea, 351-357.
- Diederix, K. M. (1982). Anomalous relationships between resistivity index and water saturations in the Rotliegend sandstone (the Netherland). *Trans. 23rd Ann. Log. Symp. SPWLA*, paper X.
- Dincer, I., Acar, A., Cobanoglu, I. and Uras, Y. (2004). Correlation between Schmidt hardness, uniaxial compressive strength and Young’s modulus for andesites, basalts and tuffs. *Bull. Engrg. Geol. Env.*, 63, 141-148.
- Donath, F. A. (1964). Strength variation and deformation behavior of anisotropic rocks. *State of Stress in the Earth’s Crust*, Ed: W. R. Judd, Elsevier, New York, 281-318.
- Doruk, P. (1991). *Analysis of the Laboratory Strength Data using the Original and Modified Hoek-Brown Failure Criterion*. MS thesis, Department of Civil Engineering, University of Toronto, Toronto, Ontario, Canada.
- Duncan, J. M. and Chang, C. Y. (1970). Non-linear analysis of stress and strain in soils. *J. Soil Mech. Found. Div.*, ASCE, 96, 1629-1655.
- Duveau, G., Shao, J. F. and Henry, J. P. (1998). Assessment of some failure criteria for strongly anisotropic geomaterials. *Mech. Cohesive-Frictional Materials*, 3, 1-26.
- Dyke, C. J. and Dobereiner, L. (1991). Evaluating the strength and deformability of sandstones. *Q. J. Engrg. Geol.*, 24, 123-134.

- Ebisu, S., Aydan, O., Komura, S. and Kawamoto, T. (1992). Comparative study on various rock mass characterization methods for surface structures. *ISRM Symp.: Eurock '92, Rock Characterization*, Chester, UK, Ed: J. A. Hudson, 203-208.
- Einstein, H. H. and Baecher, G. B. (1983). Probabilistic and statistical methods in engineering geology (part I). *Rock Mech. and Rock Engrg.*, 16, 39-72.
- Einstein, H. H., Baecher, G. B., Veneziano, D., et al. (1979). *Risk Analysis for Rock Slopes in Open Pit Mines*. Parts I-V, USBM Technical Report J0275015.
- Einstein, H. H. and Hirschfeld, R. C. (1973). Model studies on mechanics of jointed rock. *J. Soil Mech. Found. Div.*, ASCE, 99, 229-242.
- Einstein, H. H., Veneziano, D., Baecher, G. B. and O'Reilly, K. J. (1983). The effect of discontinuity persistence on rock slope stability. *Int. J. Rock Mech. Min. Sci. & Geomech. Abstr.*, 20, 227-236.
- Eissa, E. A. and Kazi, A. (1988). Relation between static and dynamic Young's moduli of rocks. *Int. J. Rock Mech. Min. Sci. & Geomech. Abstr.*, 29, 479-482.
- El-Naqa, A. (1994). Rock mass characterization of Wadi Mujib Damsite, Central Jordan. *Engrg. Geol.*, 38, 81-93.
- El-Naqa, A. (1996). Assessment of geotechnical characterization of a rock mass using a seismic geophysical technique. *Geotech. Geol. Engrg.*, 14, 291-305.
- Elsworth, D., and Mase, C. R. (1993). Groundwater in rock engineering. *Comprehensive Rock Engineering – Principle, Practice & Projects*. Ed: J. A. Hudson, Pergamon, Oxford, UK, 2, 201-226.
- Engelhardt, W. V. (1960). *Der Porenraum der Sedimente*. Springer-Verlag Berlin, Göttingen, Heidelberg.
- Fairhurst, C. (1993). Analysis and design in rock mechanics – The general context. *Comprehensive Rock Engineering – Principle, Practice and Projects*. Ed: J. A. Hudson, Pergamon, Oxford, UK, 2, 1-29.
- Fairhurst, C. (2003). Stress estimation in rock: a brief history and review. *Int. J. Rock Mech. Min. Sci.*, 40, 957-973.
- Fossum, A. F. (1985). Effective elastic properties for a randomly jointed rock mass. *Int. J. Rock Mech. Min. Sci. & Geomech. Abstr.*, 22, 467-470.
- Forster, I. R. (1983). The influence of core sample geometry on the axial point-load test. *Int. J. Rock Mech. Min. Sci. & Geomech. Abstr.*, 20, 291-295.
- Freyburg, E. (1972). Der untere und mittlere Buntsandstein SW-Thüringens in seinen gesteintechnischen Eigenschaften. *Ber. Dte. Ges. Geol. Wiss. A*, Berlin, 17, 911-919.
- Gamble, J. C. (1971). *Durability-Plasticity Classification of Shales and other Argillaceous Rocks*, PhD thesis, University of Illinois, IL.
- Gangi, A. F. (1978). Variation of whole and fractured porous rocks permeability with confining pressure. *Int. J. Rock Mech. Min. Sci. & Geomech. Abstr.*, 15, 335-354.
- Gardner, W. S. (1987). Design of drilled piers in the Atlantic Piedmont. *Foundations and Excavations in Decomposed Rock of the Piedmont Province, GSP*, Ed: R. E. Smith RE, ASCE, 9, 62-86.
- Gatlier, N., Pellet, F. and Loret, B. (2002). Mechanical damage of an anisotropic porous rock in cyclic triaxial tests. *Int. J. Rock Mech. Min. Sci.*, 39, 249-257.
- Gaviglio, P. (1989). Longitudinal wave propagation in a limestone: The relationship between velocity and density. *Rock Mech. and Rock Engrg.*, 22, 299-306.
- Gerrard, C. M. (1982a). Elastic models of rock masses having one, two and three sets of joints. *Int. J. Rock Mech. Min. Sci. & Geomech. Abstr.*, 19, 15-23.

- Gerrard, C. M. (1982b). Joint compliances as a basis for rock mass properties and the design of supports. *Int. J. Rock Mech. Min. Sci. & Geomech. Abstr.*, 19, 285-305.
- Gerrard, C. M. (1991). The equivalent elastic properties of stratified and jointed rock masses. *Proc. Int. Conf. on Computer Meth. and Advances in Geomech.*, Cairns, Eds: G. Beer, J. R. Brooker & J. P. Carter, Balkema, Rotterdam, 333-337.
- Ghosh, D. K. and Srivastava, M. (1991). Point-load strength: an index for classification of rock material. *Bull. Int. Assoc. Engrg. Geol.*, 44, 27-33.
- Gnirk, P., Boyle, W. J. and Parrish, D. K. (1992). Quantifying geologic uncertainty in site characterization.' *ISRM Symp.: Eurock '92, Rock Characterization*, Chester, UK, Ed: J. A., Hudson, 468-473.
- Goel, R. K., Jethwa, J. L. and Paithankar, A. G. (1996). Correlation between Barton's Q and Bieniaswki's RMR – A new approach. *Int. J. Rock Mech. Min. Sci. & Geomech. Abstr.*, 33, 179-181.
- Gokceoglu, C., Sonmez, H. and Kayabasi, A. (2003). Predicting the deformation moduli of rock masses. *Int. J. Rock Mech. Min. Sci.*, 40, 701-710.
- Göktan, R. M. (1988). *Theoretical and practical analysis of rock rippability*. Ph.D. thesis, Istanbul Technical University.
- Golubev, A. and Rabinovich, G. J. (1976). Resultaty primeneniya apparatury akusticeskogo karotasa dlja predelenia procnostych svoystv gornych porod na mestorosdeniach tverdykh iskopaemykh. *Prikladnaja Geofizika Moskva*, 73, 109-116.
- Goodman, R. E. (1966). On the distribution of stresses around circular tunnels in non-homogeneous rocks. *Proc. 1st Cong on Rock Mech.*, Lisbon, Portugal, 2, 249-255.
- Goodman, R. E. (1970). The deformability of joints. *Determination of the In-Situ Modulus of Deformation of Rock*, ASTM, Special Technical Publication No. 477, 174-196.
- Goodman, R. E. (1974). The mechanical properties of joints. *Proc. 3rd Int. Cong on Rock Mech.*, Denver, CO, 1-A, 127-140.
- Goodman, R. E. (1976). *Methods in Geological Engineering*. West Publishing Company.
- Goodman, R. E. (1980). *Introduction to Rock Mechanics*. Wiley, New York.
- Goodman, R. E. (1993). *Engineering Geology-Rock in Engineering Construction*. John Wiley & Sons, Inc.
- Goodman, R. E., Taylor and Brekke, T. L. (1968). A model for the mechanics of jointed rock. *J. Soil Mech. Found.*, ASCE, 96, 637-659.
- Goodman, R. E., Van, T. K. and Heuze, F. E. (1969). The measurement of rock deformability in boreholes. *Proc. 10th U.S. Symp. on Rock Mech.*, Austin, TX, 523-555.
- Gorjainov, N. N. and Ljachovickij, F. M. (1979). *Seismiceskie metody v insenernoi geologii*, Izdat. Nedra, Moskva.
- Grasso, P., Xu, S. and Mahtab, A. (1992). Problems and promises of index testing of rocks. *Rock Mechanics*, Balkema, Rotterdam, 879-888.
- Gunsallus, K. L. and Kulhawy, F. H. (1984). A comparative evaluation of rock strength measures. *Int. J. Rock Mech. Min. Sci. Geomech. Abstr.*, 21, 233-248.
- Gupta, A. S. and Rao, K. S. (1998). Index properties of weathered rocks: inter-relationships and applicability. *Bull. Engrg. Geol. Env.*, 57, 161-172.
- Gustkiewicz, J. (1985). Deformation and failure of the Rowa Ruda sandstone in a three-axial state of stress with gas under pressure in the pores. *Archiwum Gornictwa*, 30, 401-424.
- Haimson, B. C. (1977). Recent in-situ stress measurements using the hydrofracturing technique. *Proc. 18th US Symp. Rock Mech.*, Johnson Publ., Golden, 4C2/1-6.
- Haimson, B. C. and Rummel, F. (1982). Hydrofracturing stress measurements in the Iceland drilling project drillhole at Reydasfjordur, Iceland. *J. Geophys. Res.*, 87, 6631-6649.

- Haramy, K. Y. and DeMarco, M. J. (1985). Use of the Schmidt hammer for rock and coal testing. *26th US Symposium on Rock Mechanics*, Rapid City, SD, 549-555.
- Harrison, J. P. (1992). Fuzzy objective functions applied to the analysis of discontinuity orientation data. *ISRM Symp.: Eurock '92, Rock Characterization*, Chester, UK, Ed: J. A., Hudson, 25-30.
- Harrison, J. P. (1999). Selection of the threshold value in RQD assessments. *Int. J. Rock Mech. Min. Sci.*, 36, 673-685.
- Hassani, F. P., Scoble, M. J. and Whittaker, B. N. (1980). Application of the point load index test to strength determination of rock and proposals for a new size-correction chart. *The State of the Art in Rock Mechanics, Proc. 21st US Symp. on Rock Mech.*, 543-553.
- Hawkins, A. B. and McConnell, B. J. (1992). Sensitivity of sandstone strength and deformability to changes in moisture content. *Q. J. Engrg. Geol.*, 62, 115-130.
- Hawkins, A. B. and Olver, J. A. G. (1986). Point load tests: correlation factor and contractual use. An example from the Corallian at Weymouth. *Site Investigation Practice: Assessing BS 5930*. Ed: A. B. Hawkins. Geological Society, London, 269-271.
- Henkel, H., Lee, M K. and Lund, C. E. (1990). An integrated geophysical interpretation of the 200 km FENNOLORA section of the Baltic Shield. *The European Geotraverse: Integrative Studies*, Eds: R. Freeman, P. Giese & St. Mueller, European Science Foundation, Strasbourg, France, 1-47.
- Herget, G. (1974). Ground stress determinations in Canada. *Rock Mech.*, 6, 53-74.
- Herget, G. (1987). Stress assumptions for underground excavations in the Canadian shield. *Int. J. Rock Mech. Min. Sci. & Geomech. Abstr.*, 24, 95-97.
- Herget, G. (1993). Rock stresses and rock stress monitoring in Canada. *Comprehensive Rock Engineering – Principle, Practice and Projects*. Ed: J. A. Hudson, Pergamon, Oxford, UK, 3, 473-496.
- Heuze, F. E. (1980). Scale effects in the determination of rock mass strength and deformability. *Rock Mech.*, 12, 167-192.
- Heuze, F. E. and Barbour, T. G. (1982). New models for rock joints and interfaces. *J. Geotech. Engrg.*, ASCE, 108, 757-776.
- Hills, E. S. (1972). *Elements of Structural Geology*. 2nd edition. Chapman and Hall, London.
- Hobbs, B. E. (1976). *An Outline of Structural Geology*. Wiley, New York.
- Hoek, E. (1964). Fracture of anisotropic rock. *J. S. Afr. Inst. Min. Metall.*, 64, 510-518.
- Hoek, E. (1983). Strength of jointed rock masses - 23rd Rankine Lecture. *Geotechnique*, London, UK, 33(3), 187-223.
- Hoek, E. (1990). Estimating Mohr-Coulomb friction and cohesion values from the Hoek-Brown failure criterion. *Int. J. Rock Mech. Min. Sci. & Geomech. Abstr.*, 27, 227-229.
- Hoek, E. (1994). Strength of rock and rock masses. *News J. of ISRM*, 2, 4-16.
- Hoek, E. (2000). *Rock Engineering*. <http://www.rocsience.com>.
- Hoek, E. (2004). *Personal communication*.
- Hoek, E. and Bray, J. W. (1981). *Rock Slope Engineering*. 3rd edition, Institution of Mining and Metallurgy, London.
- Hoek, E. and Brown, E. T. (1980a). *Underground Excavation in Rock*. Institution of Mining and Metallurgy, London, UK.
- Hoek, E. and Brown, E. T. (1980b). Empirical strength criterion for rock masses. *J. Geotech. Engrg.*, ASCE, 106, 1013-1035.
- Hoek, E. and Brown, E. T. (1988). The Hoek-Brown criterion - a 1988 update. *Proc. 15th Can. Rock Mech. Symp.*, University of Toronto, Canada, 31-38.

- Hoek, E. and Brown, E. T. (1997). Practical estimates of rock mass strength. *Int. J. Rock Mech. Min. Sci.*, 34, 1165-1186.
- Hoek, E., Kaiser, P. K. and Bawden, W. F. (1995). *Support of Underground Excavations in Hard Rock*. Balkema, Rotterdam.
- Hoek, E., Wood, D. and Shah, S. (1992). A modified Hoek-Brown criterion for jointed rock masses. *Proc. Rock Characterization Symp. ISRM: Eurock'92*, Ed: J. A. Hudson, 209-214.
- Horino, F. G. and Ellickson, M. L. (1970). *A method of estimating the strength of rock containing planes of weakness*. U.S. Bureau of Mines, Report Investigation 7449.
- Hudson, J. A. (1992). *Rock characterization - Proc. EUROCK'92 Symp.*, Chester, UK, Telford, London.
- Hudson, J. A. (1993). Rock properties, testing methods and site characterization. *Rock Engineering – Principle, Practice & Projects*. Ed: J. A. Hudson, Pergamon, Oxford, UK, 3, 1-39.
- Hudson, J. A. and Harrison, J. P. (1997). *Rock Engineering Mechanics – An Introduction to the Principles*. Elsevier, Oxford.
- Hudson, J. A., Cornet, F. H. and Christiansson, R. (2003). ISRM suggested methods for rock stress estimation—Part 1: Strategy for rock stress estimation. *Int. J. Rock Mech. Min. Sci.*, 40, 991-998.
- Huitt, J. L. (1956). Fluid flow in simulated fracture. *J. American Inst. Chemical Engrg.*, 2, 259-264.
- Idziak, A. (1981). Seismic study of fractured sedimentary rocks. *Trans. 26th Geophys. Symp.*, Leipzig, 116-123.
- Indraratna, B. and Ranjith, P. (2001). *Hrdromechanical Aspects and Unsaturated Flow in Jointed Rock*. Balkema, Lisse.
- Indraratna, B., Ranjith, P. and Gale, W. (1999). Deformation and permeability characteristics of rocks with interconnected fractures. *9th Int. Cong. on Rock Mech.*, 2, 755-760.
- Inoue, M. and Ohomi, M. (1970). Study on the strength of rocks by the Schmidt hammer test. *Rock Mechanics in Japan*, 1, 177-179.
- Inoue, M. and Ohomi, M. (1981). Relation between uniaxial compressive strength and elastic wave velocity of soft rock. *Int. Symp. on Weak Rock*, Tokyo, 9-13.
- Irfan, T Y. and Dearman, W. R. (1978). Engineering classification and index properties of weathered granite. *Bull. Int. Assoc. Engrg. Geol.*, 17, 79-90.
- Isherwood, D. (1979). *Geoscience Data Base Handbook for Modeling Nuclear Waste Repository*. Vol. 1. NUREG/CR-0912 V1, UCRL-52719, V1.
- ISRM (1978a). Suggested methods for determining sound wave velocity. International Society for Rock Mechanics, Commission on Standardization of Laboratory and Field Tests. *Int. J. Rock Mech. Min. Sci. & Geomech. Abstr.*, 15, 53-58.
- ISRM (1978b). Suggested methods for determining hardness and abrasiveness of rocks. International Society for Rock Mechanics, Commission on Standardization of Laboratory and Field Tests. *Int. J. Rock Mech. Min. Sci. & Geomech. Abstr.*, 15, 89-97.
- ISRM (1978c). Suggested methods for the quantitative description of discontinuities in rock masses. International Society for Rock Mechanics, Commission on Standardization of Laboratory and Field Tests. *Int. J. Rock Mech. Min. Sci. & Geomech. Abstr.*, 15, 319-368.
- ISRM (1979a). Suggested methods for determining the uniaxial compressive strength and deformability of rock materials. International Society for Rock Mechanics, Commission on Standardization of Laboratory and Field Tests. *Int. J. Rock Mech. Min. Sci. & Geomech. Abstr.*, 16, 135-140.

- ISRM (1979b). Suggested methods for determining in situ deformability of rock. International Society for Rock Mechanics, Commission on Standardization of Laboratory and Field Tests. *Int. J. Rock Mech. Min. Sci. & Geomech. Abstr.*, 16, 195-214.
- ISRM (1979c). Suggested methods for determining water content, porosity, density, absorption and related properties and swelling and slake-durability index properties. International Society for Rock Mechanics, Commission on Standardization of Laboratory and Field Tests. *Int. J. Rock Mech. Min. Sci. & Geomech. Abstr.*, 16, 145-156.
- ISRM (1985). Suggested methods for determining the point load strength. International Society for Rock Mechanics, Commission on Standardization of Laboratory and Field Tests. *Int. J. Rock Mech. Min. Sci. & Geomech. Abstr.*, 22, 51-60
- ISRM (1987). Suggested methods for deformability determination using a flexible dilatometer. International Society for Rock Mechanics, Commission on Standardization of Laboratory and Field Tests. *Int. J. Rock Mech. Min. Sci. & Geomech. Abstr.*, 24, 123-134.
- Ivanova, V. (1998). *Geological and Stochastic Modeling of Fracture Systems in Rocks*. PhD thesis, Massachusetts Institute of Technology, Cambridge, MA.
- Jaeger, J. C. (1960). Shear failure of anisotropic rocks. *Geological Magazine*, 97, 65-72.
- Jaeger, J. C. (1971). Friction of rocks and the stability of rock slopes, Rankine Lecture. *Geotechnique*, London, UK, 21, 97-134.
- Jaeger, J. C. and Cook, N. G. W. (1979). *Fundamentals of Rock Mechanics*. 3rd edition, Chapman and Hall, London.
- Jamison, D. B. and Cook, N. G. W. (1979). An analysis of the measured values for the state of stress in the earth's crust. In *Fundamentals of Rock Mechanics* (J. C. Jaeger and N. G. W. Cook). 3rd edition, Chapman and Hall, London.
- Jamscikov, W. S., Schkuratnik, W. L. and Bobrov, A. B. (1985). O kolicestvennoi ozenke mikrotrecinobatocti gornich porod ultrasvukovim velocimmetriceskim metodom. *Akad. Nauk SSSR, Sibirskoe otdelenie*, 4, 110-114.
- Jelic, K. (1984). Odnos gustoce i poroznosti s dubinom litostratigrafskih formacija savske i dravske potoline. *Nafta (Zagreb)*, 35, 637-643.
- Jethwa, J. L., Dube, A. K., Singh, B. and Mithal, R. S. (1982). Evaluation of methods for tunnel support design in squeezing rock conditions. *Proc. 4th Int. Cong. Int. Assoc. Engrg. Geol.*, Balkema, Rotterdam, 5, 125-134.
- John, K. M. (1970). Civil engineering approach to evaluate strength and deformability of closely jointed rock. *Rock Mech. - Theory and Practice, Proc. 14th U. S. Symp. on Rock Mech.*, 69-80.
- John, M. (1972). *The Influence of Length to Diameter Ratio on Rock Properties in Uniaxial Compression: A Contribution to Standardization in Rock Mechanics Testing*. Rep. S. Afr. CSIR, No. ME 1083/5.
- Johnston, I. W. (1985). Strength of intact geomechanical materials. *J. Geotech. Engrg.*, ASCE, 111, 730-749.
- Johnston, I. W., Donald, I. B., Bennett, A. G., and Edwards, J. (1980). "The testing of large diameter pile rock sockets with a retrievable test rig." *Proc. 3rd Australia-New Zealand Conf. on Geomech.*, Wellington, 1, 105-108.
- Jones, F. O. (1975). A laboratory study of the effects of confining pressure on fracture flow and storage capacity in carbonate rocks. *J. Petro. Tech.*, 21, 21-27.
- Kachanov, M. (1980). Continuum model of medium with cracks. *J. Engrg. Mech. Div.*, ASCE, 106, 1039-1051.

- Kahraman, S. (2001a). A correlation between P-wave velocity, number of joints and Schmidt hammer rebound number. *Int. J. Rock Mech. Min. Sci.*, 38, 729-733.
- Kahraman, S. (2001b). Evaluation of simple methods for assessing the uniaxial compressive strength of rock. *Int. J. Rock Mech. Min. Sci.*, 38, 981-994.
- Kahraman, S., Gunaydin, O. and Fener, M. (2005). The effect of porosity on the relation between uniaxial compressive strength and point load index. *Int. J. Rock Mech. Min. Sci.*, 42, 584-589.
- Kaiser, P. K., Mackay, C. and Gale, A. D. (1986). Evaluation of rock classifications at B.C. Rail Tumbler Ridge Tunnels. *Rock Mech. and Rock Engrg.*, 19, 205-234.
- Kalamaras, G. S. and Bieniawski, Z. T. (1993). A rock mass strength concept for coal seams. *Proc. 12th Conf. Ground Control in Mining*, Morgantown, 274-283.
- Karzulovic, A. and Goodman, R. E. (1985). Determination of principal joint frequencies. *Int. J. Rock Mech. Min. Sci. & Geomech. Abstr.*, 22, 471-473.
- Katz, O., Reches, Z. and Roegiers, J-C. (2000). Evaluation of mechanical rock properties using a Schmidt hammer. *Int. J. Rock Mech. Min. Sci.*, 37, 723-728.
- Kawamoto, T., Ichikawa, Y. and Kyoya, T. (1988). Deformation and fracturing behavior of discontinuous rock mass and damage mechanics theory. *Int. J. Numerical & Analytical Methods in Geomech.*, 12, 1-30.
- Kayabasi, A., Gokceoglu, C. and Ercanoglu, M. (2003). Estimating the deformation modulus of rock masses: a comparative study. *Int. J. Rock Mech. Min. Sci.*, 40, 55-63.
- Kidybinski, A. (1980). Bursting liability indices of coal. *Int. J. Rock Mech. Min. Sci. Geomech. Abstr.*, 17, 167-171.
- King, M. S. (1983). Static and dynamic elastic properties of rock from the Canadian Shield. *Int. J. Rock Mech. Min. Sci. Geomech. Abstr.*, 20, 247-241.
- King, M. S., Andrea, M. O. and Shams, K. M. (1994). Velocity anisotropy of Carboniferous mudstones. *Int. J. Rock Mech. Min. Sci. Geomech. Abstr.*, 31, 261-263.
- Klein, R. J. and Brown, E. T. (1983). *The State of Stress in British Rocks*. Report DOE/RW/83.8.
- Koncagül, E. C. and Santi, P. M. (1999). Predicting the unconfined compressive strength of the Breathitt shale using shale durability, shore hardness and rock structural properties. *Int. J. Rock Mech. Min. Sci.*, 36, 139-153.
- Kopf, M. (1977). Fortschritte der Petrophysik. *Physik der Erdkruste*, Ed: R. Lauterbach, Akademite-Verlag Berlin.
- Kopf, M. (1980). Anwendung der Korrelation bei der Ermittlung von Dichte- und Geschwindigkeitswerten für Gravimetrie und Seismik. *Zeitschr. Geol. Wiss.*, Berlin, 8, 449-465.
- Kranz, R. L., Frankel, A. D., Engelder, T., and Scholz, C. H. (1979). The permeability of whole and jointed barre granite. *Int. J. Rock Mech. Min. Sci. & Geomech. Abstr.*, 16, 225-234.
- Kulatilake, P. H. S. W. (1985a). Fitting Fisher distributions to discontinuity orientation data. *J. of Geological Education*, 33, 266-269.
- Kulatilake, P. H. S. W. (1985b). Estimating elastic constants and strength of discontinuous rock. *J. Geotech. Engrg.*, ASCE, 111, 847-864.
- Kulatilake, P. H. S. W. (1986). Bivariate normal distribution fitting on discontinuity orientation clusters. *Mathematical Geology*, 18, 181-195.
- Kulatilake, P. H. S. W. (1988). State-of-the-art in stochastic joint geometry modeling. *Key Questions in Rock Mech.: Proc. 29th U.S. Symp. on Rock Mech.*, 215-299.
- Kulatilake, P. H. S. W. (1993). Application of probability and statistics in joint network modeling in three dimensions. *Proc. Conf. on Probabilistic Methods in Geotech. Engrg.*, Lanberra, Australia, 63-87.

- Kulatilake, P. H. S. W., Ucpirti, H., Wang, S., Radberg, G. and Stephansson, O. (1992). Use of the distinct element method to perform stress analysis in rock with non-persistent joints and to study the effect of joint geometry parameters on the strength and deformability of rock. *Rock Mech. and Rock Engrg.*, 25, 253-274.
- Kulatilake, P. H. S. W., Wang, S. and Stephansson, O. (1993). Effect of finite size joints on the deformability of jointed rock in three dimensions. *Int. J. Rock Mech. Min. Sci. & Geomech. Abstr.*, 30, 479-501.
- Kulatilake, P. H. S. W., Wathugala, D. N. and Stephansson, O. (1993). Stochastic three dimensional joint size, intensity and system modeling and a validation to an area in Stripa Mine, Sweden. *Soils and Found.*, Tokyo, Japan, 33, 55-70.
- Kulatilake, P. H. S. W. and Wu, T. H. (1984a). Sampling bias on orientation of discontinuities. *Rock Mech. and Rock Engrg.*, 17, 243-253.
- Kulatilake, P. H. S. W. and Wu, T. H. (1984b). The density of discontinuity traces in sampling windows. *Int. J. Rock Mech. Min. Sci. & Geomech. Abstr.*, 21, 345-347.
- Kulatilake, P. H. S. W. and Wu, T. H. (1984c). Estimation of mean trace length of discontinuities. *Rock Mech. and Rock Engrg.*, 17, 215-232.
- Kulatilake, P. H. S. W., Wu, T. H. and Wathugala, D. N. (1990). Probabilistic modeling of joint orientation. *Int. J. Numerical & Analytical Methods in Geomech.*, 14, 325-350.
- Kulhawy, F. H. (1978). Geomechanical model for rock foundation settlement. *J. Geotech. Engrg.*, ASCE, 104, 211-227.
- Kunkel, J. R., Way, S. C. and McKee, C. R. (1988). *Comparative evaluation of selected continuum and discrete-fracture models*, U.S. Nuclear Regulatory Commission, NUREG/CR-5240.
- Ladanyi, B. and Archambault, G. (1970). Simulation of shear behavior of a jointed rock mass. *Proc. 11th U.S. Symp. on Rock Mech.*, AIME, New York, 105-125.
- Lade, P. V. (1993). Roc strength criteria: The theories and the evidence. *Comprehensive Rock Engineering – Principle, Practice & Projects*. Ed: J. A. Hudson, Pergamon, Oxford, UK, 1, 255-284.
- Lama, R. D. and Vutukuri, V. S. (1978). Handbook on mechanical properties of rocks. *Trans. Tech. Publ.*, 4, 317-399.
- LaPointe, P. R., Wallmann, P. C. and Dershowitz, W. S. (1993). Stochastic estimation of fracture size through simulated sampling. *Int. J. Rock Mech. Min. Sci. & Geomech. Abstr.*, 30, 1611-1617.
- Lashkaripour, G. R. (2002). Predicting mechanical properties of mudrock from index parameters. *Bull. Engrg. Geol. Envir.*, 61, 73-77.
- Lashkaripour, G. R. and Ghafouri, M. (2002). The engineering geology of the Tabarak Abad Dam. *Engrg. Geol.*, 66, 233-239.
- Laslett, G. M. (1982). Censoring and edge effects in areal and line transect sampling of rock joint traces. *Mathematical Geology*, 14, 125-140.
- Laubscher, D. H. (1984). Design aspects and effectiveness of support system in different mining conditions. *Trans. Inst. Min. Metal.*, 93, A70-81.
- Lauffer, H. (1958). Gebirgsklassifizierung für den Stollenbau. *Geol. Bauwesen*, 24, 46-51.
- Lee, C.-H. and Farmer, I. (1993). *Fluid Flow in Discontinuous Rocks*. Chapman & Hall, London, UK.

- Lee, J-S, Einstein, H. H. and Veneziano, D. (1990). *Stochastic and centrifuge modeling of jointed rock: Part III – Stochastic and topological fracture geometry model*. Grant No. AFOSR-87-0260, MIT.
- Lee, R. D. (1961). Testing mine floors. *Colliery Engrg.*, 38, 255-261.
- Lee, Y. H., Carr, J. R., Barr, D. J. and Haas, C. J. (1990). The fractal dimension as measure of the roughness of rock discontinuity profiles. *Int. J. Rock Mech. Min. Sci. & Geomech. Abstr.*, 27, 453-464.
- Leite, M. H. and Ferland, F. (2001). Determination of unconfined compressive strength and Young's modulus of porous materials by indentation tests. *Engrg. Geol.*, 59, 267-280.
- Lemos, J. V., Hart, R. D. and Cundall, P. A. (1985). A generalized distinct element program for modeling jointed rock mass. *Proc. Symp. on Fundamentals of Rock Joints*, Bjorkliden, Sweden, 335-343.
- Lepper, H. A. Jr. (1949). Compression tests on oriented specimens of Yule marble. *Am. J. Sci.*, 247, 570-575.
- Li, F. (1986). In-situ stress measurements, stress state in the upper crust and their application to rock engineering. *Proc. Int. Symp. on Rock Stress and Rock Stress Measurements*, Stockholm, Centek Publ., Lulea, 69-77.
- Lim, H.-U. and Lee, C.-I. (1995). Fifteen years' experience on rock stress measurements in South Korea. *Proc. Int. Workshop on Rock Stress Measurements at Great Depth*, Tokyo, Japan, 7-12.
- Lin, W., Roberts, J., Glassley, W. and Ruddle, D. (1997). *Fracture and matrix permeability at elevated temperatures. Workshop on significant issues and available data. Near-field/Altered-zone coupled effects expert elicitation project*, San Francisco, November 1997.
- Lindner, E. N. and Halpern, E. N. (1977). In-situ stress: An analysis. *Proc. 18th US Symp. Rock Mech.*, Johnson Publ., Golden, 4C1/1-7.
- Ljunggren, C., Chang, Y., Janson, T. and Christiansson, R. (2003). An overview of rock stress measurement methods. *Int. J. Rock Mech. Min. Sci.*, 40, 975-989.
- Lo, K. Y., Yung, T. C. B. and Lukajic, B. (1987). A field method for the determination of rock-mass modulus. *Can. Geotech. J.*, Ottawa, Canada, 24, 406-413.
- Lomize, G. (1951). *Fluid Flow in Fissured Formation*. Moskva, Leningrad (in Russian).
- Louis, C. A. (1969). *A Study of Groundwater Flow in Jointed Rock and Its Influence on the Stability of Rock Masses*, Rock Mechanics Research Report No. 10, Imperial College, London, England. Available from: Technical Information Center, U. S. Army Engineer Waterways Experiment Station, P. O. Box 631, Vicksburg, MS 39180-0631.
- Louis, C. A. (1974). Rock hydraulics. *Rock Mechanics*, Ed: L. Muller, Springer Verlag, Viena, 299-382.
- Louis, C. A., Dessenne, J.-L. and Feuga, B. (1977). Interaction between water flow phenomena and the mechanical behavior of soil or rock masses. *Finite Elements in Geomechanics*, Ed: G. Gudehus, Wiley, New York, 479-511.
- Louis, L., David, C., Metz, V., Robion, P., Menéndez, B. and Kissel, C. (2005). Microstructural control on the anisotropy of elastic and transport properties in undeformed sandstones. *Int. J. Rock Mech. Min. Sci.*, in press.
- Lundburg, N. (1972). A statistical theory of the polyaxial compressive strength of materials. *Int. J. Rock Mech. Min. Sci.*, 9, 617-624.
- Mahtab, M. A., Bolstad, D. D., Alldredge, J. R. and Shanley, R. J. (1972). *Analysis of Fracture Orientations for Input to Structural Models of Discontinuous Rock*. US Bur. Mines Rep. Invest. 7669.

- Mahtab, M. A. and Yegulalp, T. M., (1984). A similarity test for grouping orientation data in rock mechanics. *Proc. 25th U.S. Symp. on Rock Mech.*, 495-502.
- Marinos, P. and Hoek, E. (2001). Estimating the geotechnical properties of heterogeneous rock masses such as flysch. *Bull. Engrg. Geol. Env.*, 60, 85-92.
- Marle, Chr. (1978). Geophysik und subsequenter Vulkanismus (dargestellt am Beispiel des NW-sächsischen Vulkanitkomplexes). Thesis Universität Leipzig (unpublished).
- Martin, C. D. and Chandler, N. A. (1993). Stress heterogeneity and geological structure. *Int. J. Rock Mech. Min. Sci. & Geomech. Abstr.*, 30, 993-999.
- Mauldon, M. (1994). Intersection probabilities of impersistent joints. *Int. J. Rock Mech. Min. Sci. & Geomech. Abstr.*, 31, 107-115.
- Mauldon, M. (1998). Estimating mean fracture trace length and density from observations in convex windows. *Rock Mech. and Rock Engrg.*, 31, 201-216.
- Mauldon, M. and Mauldon, J. G. (1997). Fracture sampling on a cylinder: From scanline to boreholes and tunnels. *Rock Mech. and Rock Engrg.*, 30, 129-144.
- Mauldon, M., Rohrbaugh, M. B. Jr., Dunne, W. M. and Lawdermilk, W. (1999). Fracture intensity estimates using circular scanlines. *Proc. 37th US Rock Mech. Symp. – Rock Mech. for Industry*, Balkema, Rotterdam, 777-784.
- McCann, D. M. and Entwisle, D. C. (1992). Determination of Young's modulus of the rock mass from geophysical well logs. *Geological Applications of Wireline Logs II*, Eds: Hurst, A., Griffiths, C. M. & Worthington, P. F., Geological Society Special Publication No. 65, 317-325.
- McCrae, R. W. (1982). *Geotechnical Factors Affecting the Design of Highway Tunnels in Hard Rock*, PhD thesis, University of Newcastle, Australia.
- McGarr, A. and Gay, N. C. (1978). State of stress in the Earth's crust. *Ann. Rev. Earth Planet. Sci.*, 6, 405-436.
- McLamore, R. and Gray, K. E. (1967). The mechanical behavior of anisotropic sedimentary rocks. *J. Engrg. Ind.*, 89, 62-76.
- McNally, G. H. (1987). Estimation of coal measures rock strength using sonic and neutron logs. *Geoexploration*, 24, 381-395.
- McWilliams, P. C., Kerkering, J. C. and Miller, S. M. (1990). Fractal characterization of rock fracture roughness for estimating shear strength. *Proc. Int. Conf. on Mech. of Jointed and Faulted Rock*, Vienna, Austria, Ed: H. P. Rossmanith, Balkema, Rotterdam, 331-336.
- Medhurst, T. P. and Brown, E. T. (1996). Large scale laboratory testing of coal. *Proc. 7th Australian-New Zealand Conf. on Geomech.*, Canberra, Australia, 203-208.
- Meigh, A. C. and Wolski, W. (1979). Design parameters for weak rocks. *Proc. 7th European Conf. on Soil Mech. and Found. Engrg.*, Brighton, British Geotechnical Society, 5, 57-77.
- Meyer, T. (1999). *Geologic Stochastic Modeling of Rock Fracture Systems Related to Crustal Faults*. MS thesis, Massachusetts Institute of Technology, Cambridge, MA.
- Militzer, H. and Stoll, R. (1973). Einige Beiträge der Geophysik zur primärdatenerfassung im Bergbau. *Neue Bergbautechnik*, Leipzig, 3, 21-25.
- Miller, S. M. (1983). A statistical method to evaluate homogeneity of structural populations. *Mathematical Geology*. 15, 317-328.
- Mitri, H. S., Edrissi, R. and Henning, J. (1994). Finite element modeling of cable-bolted stopes in hardrock underground mines. *SME Annual Meeting*, Albuquerque, New Mexico, 94-116.
- Moji, K., Kwasniewski, M. and Mochizuki, H. (1978). Fracture of anisotropic rocks under general triaxial compression (abstract). *Seismol. Soc. Japan Bull.*, 1, D 40, 25 (in Japanese).

- Moore, D. E., Lockner, D. A. and Byerlee, J. A. (1994). Reduction of permeability in granite at elevated temperatures, *Science*, New Series, 265, 1558–1561.
- Morales, T., Uribe-Etxebarria, G., Uriarte, J. A. and de Valderrama, I. F. (2004). Probabilistic slope analysis–State-of-play. *Engrg. Geol.*, 71, 343-362.
- Moreno, T. E. (1980). Application de las clasificaciones geomechanicas a los tuneles de parjares. *II Cursode Sostenimientos Activosen Galeriasy Tunnels*, Foundation Gomez-Parto, Madrid.
- Mostyn, G. R. and Li, K. S. (1993). Probabilistic slope analysis–State-of-play. *Proc. Conf. on Probabilistic Methods in Geotech. Engrg.*, Canberra, Australia, 89-109.
- Müller, O. (1930). Untersuchungen an Karbongesteinen zur Klärung von Gebirgsdruckfragen. *Glückauf*, 66, 1601-1612.
- Murphy, D. K., et al. (1976). The LG-2 underground power house. *Proc. RETC Conf.*, Las Vegas, NV, 515-533.
- Murrell, S. A. F. (1963). A criterion for brittle fracture of rocks and concrete under triaxial stress and the effect of pore pressure on the criterion. *Proc. 5th U.S. Symp. on Rock Mech.*, Minneapolis, MN, Ed: C. Fairhurst, Pergamon, Oxford, UK, 563-577.
- Myrvang, A. M. (1993). Rock stress and rock stress problem in Norway. *Comprehensive Rock Engineering – Principle, Practice & Projects*. Ed: J. A. Hudson, Pergamon, Oxford, UK, 3, 461-471.
- Navy (1982). *Foundations and Earth Structures*. NAVFAC DM-7.2, Naval Facilities Engineering Command, US Government Printing Office, Washington DC.
- Nelson, R. (1975). *Fracture Permeability in Porous Reservoirs: Experimental and Field Approach*. PhD dissertation, Dept. of Geology, Texas A&M University.
- Nicholson, G. A. and Bieniawski, Z. T. (1990). A nonlinear deformation modulus based on rock mass classification. *Int. J. Min. Geol. Engrg.*, 8, 181-202.
- Norbury, D. R. (1986). The point load test. *Site Investigation Practice: Assessing BS 5930*. Ed: A. B. Hawkins, Geological Society, London, 325-329.
- Oda, M. (1982). Fabric tensor for discontinuous geological materials. *Soils and Found.*, Tokyo, Japan, 22, 96-108.
- Oda, M., Suzuki, K. and Maeshibu, T. (1984). Elastic compliance for rock-like materials with random cracks. *Soils and Found.*, Tokyo, Japan, 24, 27-40.
- Oda, M. (1988). An experimental study of the elasticity of mylonite rock with random cracks. *Int. J. Rock Mech. Min. Sci. & Geomech. Abstr.*, 25, 59-69.
- Odling, N. E. (1994). Natural fracture profiles, fractal dimension and joint roughness coefficients. *Rock Mech. and Rock Engrg.*, 27, 135-153.
- Olsson, R. and Barton, N. (2001). An improved model for hydromechanical coupling during shear of rock joints. *Int. J. Rock Mech. Min. Sci.*, 38, 317-329.
- Oteo, C. S. (2002). In situ characterization of rocks. *In-Situ Characterization of Rocks*. Ed: V. M. Sharma & K. R. Saxena, Balkema, Lisse, 1-48.
- Ozsan, A. and Akin, M. (2002). Engineering geological assessment of the proposed Urus Dam, Turkey. *Engrg. Geol.*, 66, 271-281.
- Pahl, P. J. (1981). Estimating the mean length of discontinuity traces. *Int. J. Rock Mech. Min. Sci. & Geomech. Abstr.*, 18, 221-228.
- Palchik, V. (1999). Influence of porosity and elastic modulus on uniaxial compressive strength in soft brittle porous sandstones. *Rock Mech. and Rock Engrg.*, 32, 303-309.

- Palchik, V. and Hatzor, Y. H. (2002). Crack damage stress as a composite function of porosity and elastic matrix stiffness in dolomites and limestones. *Engrg. Geol.*, 63, 233-245.
- Palchik, V. and Hatzor, Y. H. (2004). Influence of porosity on tensile and compressive strength of porous chalks. *Rock Mech. and Rock Engrg.*, 37, 331-341.
- Palmström, A. (1982). The volumetric joint count – a useful and simple measure of the degree of rock jointing. *Proc. 41st Int. Congress Int. Ass. Eng. Geol.*, Delphi, 5, 221-228.
- Palmström, A. (1985). Application of the volumetric joint count as a measure of rock mass jointing. *Proc. Int. Symp. on Fundamentals of Rock Joints, Bjorkliden, Sweden*, 103-110.
- Palmström, A. (1986). A general practical method for identification of rock masses to be applied in evaluation of rock mass stability conditions and TBM boring progress. *Proc. Conf. on Fjellsprengningsteknikk, Bergmekanikk, Geoteknikk*, Oslo, Norway, 31, 1-31.
- Palmström, A. (1995). *RMI – A rock mass classification system for rock engineering purposes*. PhD Thesis, University of Oslo.
- Palmström, A. (1996). RMI – A system for characterizing rock mass strength for use in rock engineering. *J. of Rock Mech. and Tunneling Tech.*, India, 1, 69-108.
- Palmström, A. (2002). Measurement and characterization of rock mass jointing. *In-Situ Characterization of Rocks*. Ed: V. M. Sharma & K. R. Saxena, Balkema, Lisse, 49-98.
- Pan, X. D. and Hudson, J. A. (1988). A simplified three-dimensional Hoek-Brown yield criterion. *Rock Mechanics and Power Plants*, Ed: M. Romana, Balkema, Rotterdam, 95-103.
- Patton, F. D. (1966). Multiple modes of shear failure in rock. *Proc. 1st Int. Cong. on Rock Mech.*, Lisbon, 1, 509-515.
- Peck, R. B., Hanson, W. E. and Thornburn, T. H. (1974). *Foundation Engineering*. 2nd edition, John Wiley and Sons, New York.
- Peres Rodrigues, F. (1979). The anisotropy of the moduli of elasticity and of the ultimate stresses in rocks. *Proc. 4th Int. Cong. Rock Mech.*, Montreux, Balkema, Rotterdam, 2, 517-523.
- Petit, J.-P., Massonnat, G., Pueo, F. and Rawnsley, K. (1994). Rapport de forme des fractures de mode 1 dans les roches stratifiées: Une étude de cas dans le Bassin Permian de Lodeve (France). *Bulletin du Centre de Recherches Elf Exploration Production*, 18, 211-229.
- Pine, R. J. and Harrison, J. P. (2003). Rock mass properties for engineering design. *Q. J. Engrg. Geol. Hydrogeol.*, 36, 5-16.
- Pine, R. J. and Kwakwa, K. A. (1989). Experience with hydrofracture stress measurements to depths of 2.6 km and implications for measurements to 6 km in the Carnmenellis granite. *Int. J. Rock Mech. Min. Sci. & Geomech. Abstr.*, 26, 565-571.
- Piteau, D. R. (1970). Geological factors significant to the stability of slopes cut in rock. *Symp. on Planning Open Pit Mines*, South African Inst. of Mining and Metallurgy, Johannesburg, 33-53.
- Piteau, D. R. (1973). Characterizing and extrapolating rock joint properties in engineering practice. *Rock Mech. Supplement*, 2, 5-31.
- Plumb, R. A. (1994). Variation of the least horizontal stress magnitude in sedimentary rocks. *Proc. 1st North Amer. Rock Mech. Symp.*, Austin, Balkema, Rotterdam, 71-78.
- Polak, A., Elsworth, D., Yahuhara, H., Grader, A. S. and Halleck, P. M. (2003). Permeability reduction of a natural fracture under net dissolution by hydrothermal fluids. *Geophy. Res. Lett.*, 30(20), 2020, doi:10.1029/2003GL017575.
- Polak, L. S. and Rapoport, M. B. (1961). Osvjasi skorosti uprugich prodolnych voln s nekotorymi fiziceskimi svoistvami osadocnyh porod. *Prikladnaja geofizika*, Moskva, 29, 12-19.

- Pomeroy, C. D., Hobbs, D. W. and Mahmoud, A. (1971). The effect of weakness plane orientation on the fracture of Barnsley Hards by triaxial compression. *Int. J. Rock Mech. Min. Sci. & Geomech. Abstr.*, 8, 227-238.
- Poon, C. Y., Sayles, R. S. and Jones, T. A. (1992). Surface measurement and fractal characterization of naturally fractured rocks. *J. Phys. D: Applied Phys.*, 25, 1269-1275.
- Pratt, H. R., Black, A. D., Brown, W. S. and Brace, W. F. (1972). The effect of specimen size on the mechanical properties of unjointed diorite. *Int. J. Rock Mech. Min. Sci. & Geomech. Abstr.*, 9, 513-529.
- Price, N. J. (1966). *Fault and Joint Development in Brittle and Semi-Brittle Rock*. Pergamon, Oxford, UK.
- Priest, S. D. (1993). *Discontinuity Analysis for Rock Engineering*. Chapman & Hall.
- Priest, S. D. and Hudson, J. (1976). Discontinuity spacing in rock. *Int. J. Rock Mech. Min. Sci. & Geomech. Abstr.*, 13, 135-148.
- Priest, S. D. and Hudson, J. (1981). Estimation of discontinuity spacing and trace length using scanline surveys. *Int. J. Rock Mech. Min. Sci. & Geomech. Abstr.*, 18, 13-197.
- Quadros, E. F. (1982). *Determinacao das caracteristicas do fluxo de agua em fraturas de rochas*. Dissert. de Mestrado, Dept. of Civil Engrg., Polytech School, University of Sao Paulo.
- Quane, S. L. and Russel, J. K. (2003). Rock strength as a metric of welding intensity in pyroclastic deposits. *Eur. J. Mineral.*, 15, 855-64.
- Radhakrishnan, R., and Leung, C. F. (1989). "Load transfer behavior of rock-socketed piles." *J. Geotech. Engrg.*, ASCE, 115(6), 755-768.
- Ramamurthy, T. (1986). Stability of rock mass, Eighth Indian Geotech. Soc. Annual Lecture. *Indian Geotech. J.*, 16, 1-73.
- Ramamurthy, T. (1993). Strength and modulus responses of anisotropic rocks. *Comprehensive Rock Engineering – Principle, Practice & Projects*. Ed: J. A. Hudson, Pergamon, Oxford, UK, 1, 313-329.
- Ramamurthy, T. and Arora, V. K. (1991). A simple stress-strain model for jointed rocks. *Proc. 7th Int. Cong. on Rock Mech.*, Anchen, Ed: W. Wittke, Balkema, Rotterdam, 1, 323-326.
- Ramamurthy, T., Rao, G. V. and Rao, K. S. (1985). A strength criterion for rocks. *Proc. Indian Geotech. Conf.*, Roorkee, 1, 59-64.
- Ranjith, P. G. (2000). *Analytical and Numerical Investigation of Water and Air Flow through Rock Media*. PhD thesis, Dept. of Civil Engrg., Univ. of Wollongong, Australia.
- Rao, K. S. (1984). *Strength and deformation behavior of sandstones*. PhD thesis, India Institute of Technology, Delhi.
- Raymer, D. S., Hunt, E. R. and Gardner, J. S. (1980). An improved sonic transit time-to-porosity transform. *Proc. SPWLA 21st Ann. Meeting*, paper P.
- Read, J. R. L., Thornton, P. N. and Regan, W. M. (1980). A rational approach to the point load test. *Proc. Aust-N.Z. Geomech. Conf.*, 2, 35-39.
- Read, S. A. L., Perrin, N. D. and Brown, I. R. (1987). Measurement and analysis of laboratory strength and deformability characteristics of schistose rocks. *Proc. 6th Int. Conf. on Rock Mech.*, Montreal, Canada, 1, 233-238.
- Reinecker, J., Heidbach, O., Tingay, M., Connolly, P. and Müller, B. (2004): The 2004 release of the World Stress Map (available online at www.world-stress-map.org)
- Rhodes, G. W., Stephenson, R. W. and Rockaway, J. D. (1973). Plate bearing tests on coal underclay. *Proc. 19th U.S. Symp. on Rock Mech.*, Stateline, NV, 2, 16-27.

- Rives, T., Razack, M., Petit, J.-P. and Rawnsley, K. D. (1992). Joint spacing: analogue and numerical simulations. *J. Struct. Geol.*, 14, 925-937.
- Roberds, W. J. and Einstein, H. H. (1978). Comprehensive model for rock discontinuities. *J. Geotech. Engrg.*, ASCE, 104, 553-569.
- Roberds, W. J., Iwano, M. and Einstein, H. H. (1990). Probabilistic mapping of rock joint surfaces. *Proc. Int. Symp. on Rock Joints*, Loen, Norway, Eds: N. Barton and O. Stephanson, Balkema, Rotterdam, 681-691.
- Robertson, A. (1970). The interpretation of geologic factors for use in slope theory. *Proc. Symp. on the Theoretical Background to the Planning of Open Pit Mines*, Johannesburg, South Africa, 55-71.
- Romana, M. (1999). Correlation between uniaxial compressive and point-load (Franklin test) strengths for different rock classes. *9th ISRM Congress*, Balkema, Paris, 1, 673-676.
- Rowe, R. K., and Armitage, H. H. (1984). *The Design of Piles Socketed into Weak Rock*. Faculty of Engineering Science, The University of Western Ontario, London, Ont., Research Report GEOT-11-84.
- Rummel, F. (1986). Stresses and tectonics of the upper continental crust – a review. *Proc. Int. Symp. on Rock Stress and Rock Stress Measurements*, Stockholm, Centek Publ., Lulea, 177-186.
- Rummel, F. (2002). Crustal stress derived from fluid injection tests in boreholes. *In-Situ Characterization of Rocks*. Ed: V. M. Sharma & K. R. Saxena, Balkema, Lisse, 205-244.
- Rutledge, J. C. and Preston, R. L. (1978). Experience with engineering classifications of rock. *Proc. Int. Tunneling Symp.*, Tokyo, A3.1-A3.7.
- Rzhewski, W. W. and Novik, G. J. (1978). *Osnovy fiziki gornich porod*, Izdat. Nauka, Moskva 1964.
- Sabatini, P. J., Bachus, R. C., Mayne, P. W., Schneider, J. A. and Zettler, T. E. (2002). *Evaluation of Soil and Rock Properties*. Geotechnical Engineering Circular No. 5, Report No.: FHWA-IF-034, FHWA, US.
- Sachpazis, C. I. (1990). Correlating Schmidt hardness with compressive strength and Young's modulus of carbonate rocks. *Bull. Int. Assoc. Engrg. Geol.*, 42, 75-84.
- Savic, A. J., Koptev, W. J., Nikitin, W. N. and Jascenko, Z. D. (1969). *Seismoakusticeskie metody izucenia massivov skalnych porod*. Izdat. Nedra, Moskva.
- Schön, J. H. (1996). *Physical Properties of Rocks – Fundamentals and Principles of Petrophysics*. Pergamon, Oxford, UK.
- Schopper, J. R. (1982). Porosity and permeability. *Numerical Data and Functional Relationships in Science and Technology, New Series; Group V Geophysics and Space Research, Vol. 1 Physical properties of Rocks, Subvol. A*, Springer-Verlag Berlin.
- Schultz, R. A. (1996). Relative scale and the strength and deformability of rock masses. *J. Struct. Geol.*, 18, 1139-1149.
- Sen, Z. (1993). RQD-fracture frequency chart based on a Weibull distribution. *Int. J. Rock Mech. Min. Sci. & Geomech. Abstr.*, 30, 555-557.
- Sen, Z. and Kazi, A. (1984). Discontinuity spacing and RQD estimates from finite length scanlines. *Int. J. Rock Mech. Min. Sci. & Geomech. Abstr.*, 21, 203-212.
- Serafim, J. L., Pereira, J. P. (1983). Considerations of the geomechanics classification of Bieniawski. *Proc. Int. Symp. Eng. Geol. Underground Constr.*, Lisbon, 1, II33-II42.
- Shanley, R. J. and Mahtab, M. A. (1976). Delineation and analysis of centers in orientation data. *Mathematical Geology*, 8, 9-23.

- Sharp, J. C. (1970). *Fluid Flow through Fissured Media*. Ph.D. Thesis, University of London (Imperial College).
- Sheorey, P. R. (1994). A theory for in situ stresses in isotropic and transversely isotropic rock. *Int. J. Rock Mech. Min. Sci. Geomech. Abstr.*, 31, 23–34.
- Sheorey, P. R. (1997). *Empirical Rock Failure Criteria*. Balkema, Rotterdam.
- Sheorey, P. R., Barat, D., Das, M. N., Mukherjee, K. P. and Singh, B. (1984). Schmidt hammer rebound data for estimation of large scale in situ coal strength. *Int. J. Rock Mech. Min. Sci.*, 21, 39-42.
- Sheorey, P. R., Murali Mohan, G. and Sinha, A. (2001). Influence of elastic constants on the horizontal in situ stress. *Int. J. Rock Mech. Min. Sci.*, 38, 1211-1216.
- Singh, B. (1973). Continuum characterization of jointed rock masses. Part I – The constitutive equations. *Int. J. Rock Mech. Min. Sci. & Geomech. Abstr.*, 10, 311-335.
- Singh, B., and Goel, R. K. (1999). *Rock Mass Classifications – A practical Approach in Civil Engineering*. Elsevier, Amsterdam.
- Singh, D. P. (1981). Determination of some engineering properties of weak rocks. *Proc. Int. Sym. on Weak Rock*, Ed: IAKai K., Balkema, Rotterdam, 21-24.
- Singh, J. (1988). *Strength prediction of anisotropic rocks*. PhD thesis, India Institute of Technology, Delhi.
- Singh, M., Rao, K. S. and Ramamurthy, T. (2002). Strength and deformational behavior of jointed rock mass. *Rock Mech. and Rock Engrg.*, 35, 45-64.
- Singh, V. K. and Singh, D. P. (1993). Correlation between point load index and compressive strength for quartzite rocks. *Geotech. Geol. Engrg.*, 11, 269-272.
- Sjögren, B, Øvsthus, A. and Sandberg, J. (1979). Seismic classification of rock mass qualities. *Geophys. Prospect.*, 27, 409-442.
- Smith, H. J. (1997). The point load test for weak rock in dredging applications. *Int. J. Rock Mech. Min. Sci.*, 34, 702.
- Snow, D. T. (1968a). Anisotropic permeability of fractured media. *Water Resour. Res.*, 5, 1273-1289.
- Snow, D. T. (1968b). Rock fracture spacings, openings and porosities. *J. Soil. Mech. Found. Div.*, ASCE, 94, 73-91.
- Sonmez, H. and Ulusay, R. (1999). Modifications to the geological strength index (GSI) and their applicability to stability of slopes. *Int. J. Rock Mech. Min. Sci.*, 36, 743-760.
- Sonmez, H. and Ulusay, R. (2002). A discussion on the Hoek-Brown failure criterion and suggested modification to the criterion verified by slope stability case studies. *Yerbilimleri (Earthsciences)*, 26, 77–99.
- Sousa, L. M. O., del Rio, L. M. S, Calleja, L., de Argandona, V. G. R. and Rey, A. R. (2005). Influence of microfractures and porosity on the physico-mechanical properties and weathering of ornamental granites. *Engrg. Geol.*, 77, 153-168.
- Spencer, E. W. (1969). *Introduction to the Structure of the Earth*. McGraw-Hill, New York.
- Stacey, T. R., van Veerden, W. L. And Vogler, U. W. (1987). Properties of intact rock. *Ground Engineer's Reference Book*, Ed: F. G. Bell, Butterworths, London, UK.
- Starzec, P. (1999). Dynamic elastic properties of crystalline rocks from south-west Sweden. *Int. J. Rock Mech. Min. Sci.*, 36, 265-272.
- Steffen, O., et al. (1975). Recent developments in the interpretation of data from joint surveys in rock masses. *6th Reg. Conf. Africa on Soil Mech. and Found.*, II, 17-26.
- Stegena, L. (1964). The structure of the earth crust in Hungary. *Acta Geologica*, Budapest, 8, 413-431.
- Stephans, R. E. and Banks, D. C. (1989). Moduli of deformation studies of the foundation and abutments of the Portugues Dam – Puerto Rico. *Rock Mechanics as a Guide for Efficient*

- Utilization of Natural Resources: Proc. 30th U.S. Symp. on Rock Mech.*, Morgantown, WV, 31-38.
- Stephansson, O. (1993). Rock stress in the Fennoscandian shield. *Comprehensive Rock Engineering – Principle, Practice & Projects*. Ed: J. A. Hudson, Pergamon, Oxford, UK, 3, 445-459.
- Stewart, C. L. (1977). Subsurface rock mechanics instrumentation program for demonstration of shield-type long wall supports at York Canyon, Raton, New Mexico. *Proc. 18th U.S. Symp. on Rock Mech.*, Keystone, CO, 1C-2, 1-13.
- Stimpson, B. (1981). A suggested technique for determining the basic friction angle of rock surfaces using core. *Int. J. Rock Mech. Min. Sci. Geomech. Abstr.*, 18, 63-65.
- Strack, O. D. L. (1989). *Groundwater Mechanics*. Prentice Hall, Englewood Cliffs, NJ.
- Sugawara, K. and Obara, Y. (1993). Measuring rock stress. *Comprehensive Rock Engineering – Principle, Practice & Projects*. Ed: J. A. Hudson, Pergamon, Oxford, UK, 3, 533-552.
- Szlavin, J. (1974). Relationships between some physical properties of rock determined by laboratory tests. *Int. J. Rock Mech. Min. Sci. Geomech. Abstr.*, 11, 57-66.
- Talbot, C. J. and Sirat, M. (2001). Stress control of hydraulic conductivity in fractured-saturated Swedish bedrock. *Engrg. Geol.*, 61, 145-153.
- Talesnick, M. L., Hatzor, Y. H. and Tsearsky, M. (2001). The elastic deformability and strength of high porosity anisotropic chalk. *Int. J. Rock Mech. Min. Sci.*, 38, 543-555.
- Te Kamp, L., Rummel, F. and Zoback, M. D. (1995). Hydrofrac stress profile to 9 km at the German KTP site. *Proc. Workshop on Rock Stresses in the North Sea*, Trondheim, Norway, NTH and SINTEF Publ., Trondheim, 147-153.
- Terzaghi, K. (1946). Rock defects and loads on tunnel supports. *Rock Tunneling with Steel Supports*, Youngstown, OH, Eds: R. V. Proctor and T. L. White, 1, 17-99.
- Terzaghi, K. and Richard, F. E. (1952). Measurement of stresses in rock. *Geotechnique*, 12, 105-124.
- Terzaghi, R. (1965). Sources of error in joint surveys. *Geotechnique*, London, UK, 5, 287-304.
- Tiller, F. M. (1953). *Chem. Engrg. Prog.* 49, 467.
- Timur, A. (1968). An investigation of permeability, porosity, and residual water saturation relationships for sandstone reservoirs. *Log Analyst*, Jul-Aug., 8-17.
- Titley, S. R., Thompson, R. C., Haynes, F. M., Manske, S. L., Robison, L. C. and White, J. L. (1986). Evaluation of fractures and alteration in the Sierrita-Esperanza Hydrothermal System, Pima County, Arizona. *Economic Geol.*, 81, 343-370.
- Trueman, R. (1988). *An evaluation of strata support techniques in dual life gateroads*. Ph.D. Thesis, University of Wales, Cardiff.
- Tse, R. and Cruden, D. M. (1979). Estimating joint roughness coefficients. *Int. J. Rock Mech. Min. Sci. & Geomech. Abstr.*, 16, 303-307.
- Tsiambaos, G. and Sabatakakis, N. (2004). Considerations on strength of intact sedimentary rocks. *Engrg. Geology*, 72, 261-273.
- Tsidzi, K. E. N. (1990). The influence of foliation on point load strength anisotropy of foliated rocks. *Engrg. Geol.*, 29, 49-58.
- Tsidzi, K. E. N. (1991). Point load-uniaxial compressive strength correlation. *Proc. 7th ISRM Cong.*, Ed: Wittke W., Balkema, Rotterdam, 1, 637-639.
- Turgul, A. (2004). The effect of weathering on pore geometry and compressive strength of selected rock types from Turkey. *Engrg. Geol.*, 75, 215-227.
- Turgul, A. and Zarif, I. H. (1999). Correlation of mineralogical and textural characteristics with engineering properties of selected granitic rocks from Turkey. *Engrg. Geol.*, 51, 303-317.

- Ulusay, R., Tureli, K. and Ider, M. H. (1994). Prediction of engineering properties of a selected litharenite sandstone from its petrographic characteristics using correlation and multivariate statistical techniques. *Engrg. Geol.*, 38, 135-157.
- Vallejo, L. E., Welsh, R. A. and Robinson, M. K. (1989). Correlation between unconfined compressive and point load strength for Appalachian rocks. *Proc. 30th US Symp. Rock Mech.*, Ed: Khair A. W., Balkema, Rotterdam, 461-468.
- Van Heerden, W. L. (1976). Practical application of the CSIR triaxial strain cell for rock stress measurements. *Proc. ISRM Symp. on Investi. of Stress in Rock, Advances in Stress Measurement*, Sydney, The Institution of Engineers, Australia, 1-6.
- Vasarhelyi, B. (2003). Some observations regarding the strength and deformability of sandstones in case of dry and saturated conditions. *Bull. Engrg. Geol. Envir.*, 62, 245-249.
- Vasarhelyi, B. (2005). Statistical analysis of the influence of water content on the strength of the Miocene limestone. *Rock Mech. and Rock Engrg.*, 38, 69-76.
- Verman, M., Singh, B., Viladkar, M. N. and Jethwa, J. L. (1997). Effect of tunnel depth on modulus of deformation of rock mass. *Rock Mech. Rock Engrg.*, 30, 121-127.
- Villaescusa, E. (1993). Statistical modeling of rock jointing. *Proc. Conf. on Probabilistic Methods in Geotech. Engrg.*, Lanberra, Australia, 221-231.
- Villaescusa, E. and Brown, E. T. (1992). Maximum likelihood estimation of joint size from trace length measurements. *Rock Mech. and Rock Engrg.*, 25, 67-87.
- Voight, B. (1966). Interpretation of in-situ stress measurements - Panel Report on Theme IV. *Proc. 1st Cong. Int. Soc. Rock Mech.*, Lisbon, 3, 332-348.
- Voight, B. (1968). On the functional classification of rocks for engineering purposes. *Int. Symp. on Rock Mech.*, Madrid, 131-135.
- Volarovich, M. P. and Bajuk, E. I. (1977). Elastic properties of rocks. *Issledovanie Fiziceskich svoit sv Mineralnogo Vescstva Zemli pri Vysokich Termodinamiceskich Parametrach*, Eds: M. P. Volarovic, H. Stiller and T. S. Lebedev, Izd. Nakova dumka, Kiev 43-49.
- Voss, R. (1988). Fractals in nature. *The Science of Fractal Images*, Eds: H. Peitgen and D. Saupe, Springer, New York, 21-69.
- Wallis, P. F. and King, M. S. (1980). Discontinuity spacing in a crystalline rock. *Int. J. Rock Mech. Min. Sci. & Geomech. Abstr.*, 17, 63-66.
- Walsh, J. B. (1981). Effects of pore pressure and confining pressure on fracture permeability. *Int. J. Rock Mech. Min. Sci. & Geomech. Abstr.*, 18, 429-434.
- Walsh, J. B. and Grosenbaugh, M. A. (1979). A new model for analyzing the effect of fractures on compressibility. *J. Geophys. Res.*, 84, 3532-3536.
- Wang, S. (1992). *Fundamental Studies of the Deformability and Strength of Jointed Rock Masses at Three Dimensional Level*. PhD Dissertation, University of Arizona, Tucson.
- Wang, S. and Kulatilake, P. H. S. W. (1993). Linking between joint geometry models and a distinct element method in three dimensions to perform stress analyses in rock masses containing finite size joints. *Soils and Found.*, Tokyo, Japan, 33, 88-98.
- Warburton, P. M. (1980a). A stereological interpretation of joint trace data. *Int. J. Rock Mech. Min. Sci. & Geomech. Abstr.*, 17, 181-190.
- Warburton, P. M. (1980b). Stereological interpretation of joint trace data: Influence of joint shape and implications for geological surveys. *Int. J. Rock Mech. Min. Sci. & Geomech. Abstr.*, 17, 305-316.

- Wathugala, D. N. (1991). *Stochastic Three Dimensional Joint Geometry Modeling and Verification*. Ph.D. Dissertation, University of Arizona, Tucson.
- Wathugala, D. N., Kulatilake, P. H. S. W., Wathugala, G. W. and Stephansson, O. (1990). A general procedure to correct sampling bias on joint orientation using a vector approach. *Computers and Geomech.*, 10, 1-31.
- Wei, Z. Q. and Hudson, J. A. (1988). Permeability of jointed rock masses. *Proc. Int. Symp. Rock Mech. and Power Plants*, Balkema, Rotterdam, 613-625.
- Wei, Z. Q., Egger, P. and Descoedres, F. (1995). Permeability predictions for jointed rock masses. *Int. J. Rock Mech. Min. Sci. & Geomech. Abstr.*, 32, 251-261.
- Wickham, G. E., Tiedemann, H. R. and Skinner, E. H. (1972). Support determination based on geologic predictions. *Proc. North American Rapid Excav. Tunneling Conf.*, Chicago, Eds: K. S. Lane and L.A. Garfield, 43-46.
- Wines, D. T. and Lilly, P. A. (2003). Estimates of rock joint shear strength in part of the Fimiston open pit operation in Western Australia. *Int. J. Rock Mech. Min. Sci.*, 40, 929-937.
- Worotnicki, G. and Denham, D. (1976). The state of stress in the upper part of the earth's crust in Australia according to measurements in mines and tunnels and from seismic observations. *Proc. ISRM Symp. on Investi. of Stress in Rock, Advances in Stress Measurement*, Sydney, The Institution of Engineers, Australia, 71-82.
- Worotnicki, G. and Walton, R. J. (1976). Triaxial hollow inclusion gauges for determination of rock stresses in-situ. *Supplement to Proc. ISRM Symp. on Investi. of Stress in Rock, Advances in Stress Measurement*, Sydney, The Institution of Engineers, Australia, 141-150.
- Wuerker, R. G. (1953). The status of testing strength of rocks. *Trans. Min. Eng., AIME*, 1108-1113.
- Wyllie, D. C. (1999). *Foundations on Rock*. 2nd edition, E & FN SPON.
- Wyllie, M. R. J., Gregory, A. R. and Gardner, L. W. (1956). Elastic wave velocities in heterogeneous and porous media. *Geophysics*, 21, 41-70.
- Xu, S., Grasso, P. and Mahtab, A. (1990). Use of Schmidt hammer for estimating mechanical properties of weak rock. *6th Int. LAEG Cong.*, Balkema, Rotterdam, 511-519.
- Yasar, E. and Erdogan, Y. (2004a). Estimation of rock physicomaterial properties using hardness methods. *Engrg. Geology*, 71, 281-288.
- Yasar, E. and Erdoğan, Y. (2004b). Correlating sound velocity with the density, compressive strength and Young's modulus of carbonate rocks. *Int. J. Rock Mech. Min. Sci.*, 41, 871-875.
- Yilmaz, I. and Sendir, H. (2002). Correlation of Schmidt hardness with unconfined compressive strength and Young's modulus in gypsum from Sivas (Turkey). *Engrg. Geology*, 66, 211-219.
- Yokoyama, T., Ogawa, K., Kanagawa, T., Tanak, M., and Ishida, T. (2003). Regional in-situ stress in Japan based on measurements. *Rock Stress: Proc. 3rd Int. Symp. on Rock Stress*, Kumamoto, Japan, Eds: K. Sugawara, Y. Obara and A. Sato, Balkema, Rotterdam, 335-341.
- Yoshinaka, R. and Yambe, T (1986). Joint stiffness and the deformation behavior of discontinuous rock. *Int. J. Rock Mech. Min. Sci. & Geomech. Abstr.*, 23, 19-28.
- Yu, X. and Vayssade, B. (1990). Joint profiles and their roughness parameters. *Proc. Int. Symp. on Rock Joints*, Loen, Norway, Eds: N. Barton and O. Stephanson, Balkema, Rotterdam, 781-785.
- Yudhbir, Lemanza, W. and Prinzl, F. (1983). An empirical failure criterion for rock masses. *Proc. 5th Int. Cong. on Rock Mech.*, Melbourne, 1, B1-B8.
- Zanbak, C. (1977). Statistical interpretation of discontinuity contour diagrams. *Int. J. Rock Mech. Min. Sci. & Geomech. Abstr.*, 14, 111-120.

- Zhang, L. (1999). *Analysis and Design of Drilled Shafts in Rock*. PhD thesis, Massachusetts Institute of Technology, Cambridge, MA.
- Zhang, L. (2004). *Drilled Shafts in Rock – Analysis and Design*. Balkema, Leiden.
- Zhang, L. and Einstein, H. H. (1998a). End bearing capacity of drilled shafts in rock. *J. Geotech. Geoenviron. Engrg.*, ASCE, 124, 574-584.
- Zhang, L. and Einstein, H. H. (1998b). Estimating the mean trace length of rock discontinuities. *Rock Mech. and Rock Engrg.*, 31, 217-235.
- Zhang, L. and Einstein, H. H. (2000). Estimating the intensity of rock discontinuities. *Int. J. Rock Mech. Min. Sci.*, 37, 819-837.
- Zhang, L. and Einstein, H. H. (2004). Estimating the deformation modulus of rock masses. *Int. J. Rock Mech. Min. Sci.*, 41, 337-341.
- Zhang, L., Einstein, H. H. and Dershowitz, W. S. (2002). Stereological relationship between trace length distribution and size distribution of elliptical discontinuities. *Geotechnique*, London, UK, 52, 419-433.
- Zhao, J. (1998). Rock mass hydraulic conductivity of the Bukit Timah granite, Singapore. *Engrg. Geol.*, 50, 211-216.
- Zimmerman, R. R. (1991). Deformability of sandstones. *Developments in Petroleum Science*, Elsevier, Amsterdam.
- Zobak, M. D. and Byerlee, J. D. (1976). Effect of high-pressure deformation on the permeability of Ottawa Sand. *Bull. Am. Assoc. Petro. Geol.*, 60, 1531.
- Zobak, M. L. et al. (1989). Global patterns of tectonic stress. *Nature*, 341, 291-298.

Index

(Page numbers in italics show entries found in figures and tables)

- AASHTO (American Association of State Highway and Transportation Officials), 121, 138
- Amadei model, 215–17
- American Association of State Highway and Transportation Officials *see* AASHTO
- American Society for Testing Materials *see* ASTM
- anisotropy,
 - deformability, 171–3
 - anisotropy of elastic modulus of intact rocks, 172
 - deformability anisotropy ratio, 173, 173
 - permeability, 251–2
 - permeability of rock shows appreciable anisotropy, 251
 - ratio of permeability parallel to bedding to permeability perpendicular to bedding, 252
 - strength, 226–30
 - classification of strength anisotropy ratio, 229
 - compressive strength anisotropy in slate, 227
 - point load strength anisotropy index, 229, 230
 - strength anisotropy ratio, 228, 228
 - variation of strength anisotropy ratio with pressure, 229
- aperture,
 - classification, 96, 97
 - decrease of aperture with depth, 245
 - defined, 95, 96
 - hydraulic aperture, 128, 234–6
 - variation of hydraulic aperture with temperature, 246
- ASTM (American Society for Testing Materials), vii, 5, 7, 12, 175

- Barton model, 199–201
- basic friction angle, 8, 9, 131, 132, 198
- Bentheim Sandstone, 37, 39, 234
- bias, 78–9, 80–1
- Bieniawski-Yudhbir criterion, 193, 194, 208, 209
- bilinear strength model, 198, 198, 199
- block size, discontinuity, 72–3, 73

- Canadian Foundation Engineering Manual*, 34
- correlation between,
 - cone indenter number and unconfined compressive strength, 181–2
 - deformation modulus and P-wave velocity, 146
 - deformation modulus and Q, 145
 - deformation modulus and RMR or GSI, 143–5
 - deformation modulus and RQD, 138–43
 - deformation modulus and unconfined compressive strength, 146
 - density and depth, 40–1
 - density and porosity, 44–5

density and unconfined compressive strength, 186, 187
discontinuity areal and volumetric frequency, 68–71, 70
dynamic elastic properties, 122
elastic modulus and porosity, 124
elastic modulus and Schmidt hammer rebound number, 122
elastic modulus at saturated condition and that at dry condition, 124, 125
L and N-type Schmidt hammer rebound numbers, 43
linear discontinuity frequency and P-wave velocity, 63–4, 65
P-wave velocity and density, 46, 47, 49
P-wave velocity and point load index, 46, 49
P-wave velocity and porosity, 46, 46, 47
P-wave velocity and Schmidt hammer rebound number, 51
P-wave velocity and unconfined compressive strength, 182, 183–4
permeability and depth, 242–5, 243–4
permeability and grain size, 232, 234
permeability and porosity, 232, 232, 233
permeability and stress, 238–42, 240–1
permeability and temperature, 245–6, 247
point load index and porosity, 48, 49
point load index and Schmidt hammer rebound number, 50, 51
point load index and unconfined compressive strength, 176–8, 177–8
porosity and depth, 37–8
porosity and grain size, 37, 39
porosity and unconfined compressive strength, 182–5, 183–5
Q and P-wave velocity, 106
RMR and P-wave velocity, 104
RMR and Q, 114–115, 114
RQD and linear discontinuity frequency, 64–8, 67
RQD and P-wave velocity, 68, 69
RQD and volumetric frequency, 71
RQD, volumetric frequency and block volume, 73, 73
Schmidt hammer rebound number and density, 50
Schmidt hammer rebound number and porosity, 48, 50
Schmidt hammer rebound number and unconfined compressive strength, 178, 179–80
Shore Sclerscope hardness and unconfined compressive strength, 178–81, 181
static modulus and dynamic modulus, 123
static modulus and P-wave velocity, 124
unconfined compressive strength at saturated condition and that at dry condition, 187, 188
water content and unconfined compressive strength, 186–7, 188

Darcy's law, 231

deformability, 119–73

deformability of intact rock,

anisotropy of rock deformability, 171–3

anisotropy of elastic modulus of intact rocks, 172

deformability anisotropy ratio, 173, 173

comparison of static and dynamic elastic modulus, 123

correlation between,

dynamic elastic properties, 122

elastic modulus and porosity, 124, 125

elastic modulus and Schmidt hammer rebound number, 122

elastic modulus at saturated condition and that at dry condition, 124

- static modulus and dynamic modulus, 123
- static modulus and P-wave velocity, 124
- effect of confining stress, 169–71
- elastic modulus values, 120, 121
- Poisson's ratio values, 120, 121
- variation of elastic modulus with porosity, 124, 125
- variation of elastic modulus with water content, 124, 126
- deformability of rock discontinuities,
 - dilation of discontinuities, 136–7
 - defined, 136
 - expression for discontinuity deformation including dilation, 136, 137
 - normal stiffness, 125–34
 - basic friction angle, 131, 132, 132
 - discontinuity roughness coefficient JRC, 128–131, 133
 - discontinuity wall compressive strength JCS, 128–130, 134
 - hydraulic aperture, 128
 - residual friction angle, 130–1
 - roughness profiles, 130–1
 - stress-relative displacement relationship, 125–127
 - tangential normal stiffness, 125–128
 - tilt test, 132, 132
 - shear stiffness, 135–6
 - shear strength of a discontinuity, 136
 - stress-relative displacement relationship, 127, 135
 - tangential shear stiffness, 135
- deformability of rock mass,
 - anisotropy of rock deformability, 171–3
 - effect of confining stress, 169–71
 - empirical methods for estimation of rock mass deformation modulus, 137–46
 - limitations of empirical methods, 146
 - method relating deformation modulus with,
 - P-wave velocity, 146
 - unconfined compressive strength, 146
 - methods relating deformation modulus with Q, 145
 - methods relating deformation modulus with RMR or GSI, 143–5
 - correlations between E_m/E_r and RMR, 145
 - correlations between rock mass deformation modulus and RMR or GSI, 143, 144, 144
 - methods relating deformation modulus with RQD, 138–43
 - insensitivity of RQD to discontinuity frequency, 141, 142
 - reasons for data scatter, 140–1
 - relations between rock mass deformation and RQD, 139, 142, 142, 143
 - variation of E_m/E_r with RQD and average discontinuity spacing, 138, 139, 141
 - equivalent continuum approach for estimating rock mass deformation modulus, 146–68
 - rock mass with non-persistent discontinuities, 153–68
 - constitutive model for discontinuities, 157, 160
 - constitutive model for intact rock, 157, 159
 - deformation moduli related to fracture tensor components, 163, 164, 166
 - DEM analysis of the rock block, 157–8, 161, 162
 - discrete element method (DEM), 153, 157–8
 - fracture tensor equations, 162, 163
 - generated discontinuity networks, 157
 - limitations of the method, 167–8

- procedure for evaluating the effect of discontinuities, 154–6, 156
- shear moduli related to fracture tensor components, 163, 165–6
- values for parameters of intact rock, fictitious and actual discontinuities, 157, 158
- rock mass with persistent discontinuities, 146–53
 - Dershowitz analytical model, 152
 - Fossum model, 151
 - jointed rock mass under uniaxial loading, 150
 - Kulhawy three-dimensional equivalent continuum, 147, 147
 - limitations of models, 153
 - modulus reduction factor, 148
 - modulus reduction factor versus discontinuity spacing, 149
 - modulus reduction factor versus RQD, 150
 - relationships between deformation modulus and RQD, 154, 155
 - RQD versus number of discontinuities, 149
- scale effect on rock deformability, 168–9
 - variation of measured dynamic modulus with test volume of rock, 170
- deformation modulus, 119–20
 - importance of discontinuities, 119
 - stress-strain curve of rock mass, 119, 120
 - deformation modulus, 120
 - elastic modulus, 119
 - initial tangent modulus, 119
 - recovery modulus, 120
- density, 39–41
 - defined, 39
 - definition of terms, 39
 - density versus depth for sedimentary rocks, 41
 - relation between depth and density, 40, 41
- Dershowitz analytical model, 152
- discontinuities in rocks, 53–97
 - aperture, 95–7
 - classification, 96, 97
 - defined, 95, 96
 - areal and volumetric frequency, 68–71
 - areal frequency defined, 68
 - circular scanline sampling, 69, 70
 - ISRM relationship between volumetric frequency and RQD, 71
 - measures for discontinuity intensity, 68, 70
 - relationship between areal frequency and volumetric frequency, 71
 - volumetric frequency defined, 71
- block size, 72–3
 - adjectives for describing block shape, 73
 - block volume calculation, 72
 - examples of block shapes, 72
 - ranges of block volume, volumetric frequency and RQD, 73
 - terms for describing block size, 73
- discontinuity defined, 53
- filling, 96–7
 - defined, 96
 - effect on shear strength, 97
- fracture tensor, 92–3
 - tensor equations, 92–3

- major types of discontinuity, 53–5
 - bedding planes, 54
 - cleavage, 54–5
 - faults, 53–4
 - joints, 54
- orientation, 56–60
 - assignment of poles into discontinuity sets, 58
 - equation for trend and plunge of the pole, 58
 - pole of a discontinuity as a vector, 58, 59
 - contours of pole concentrations, 56, 57
 - data in the form of dip direction, 56
 - orientation defined, 56
 - polar stereonet plot, 56, 57
 - probability distributions, 60
 - procedure for obtaining mean orientation, 58–60
- persistence, 74–8
 - defined, 74
 - ISRM classification of persistence, 74
 - persistence ratio (PR), 75
 - definition as area ratio, 75
 - definition as length ratio, 76
 - estimation of PR for a finite sample length, 75
 - failure of low-angle transitions, 76, 77
 - in-plane failure of intact rock, 76, 78
 - mathematical definitions, 75, 77, 78, 79
- rock quality designation (RQD), 64–8
 - defined, 64
 - ISRM recommendations, 64
 - procedure for measurement, 64, 66
 - relationship between linear discontinuity frequency and RQD, 64, 65, 67
 - relationship between P-wave velocity and RQD, 68, 69
 - variation of RQD with length of sampling line, 66, 67
- roughness, 93–5
 - classification, 94, 95
 - defined, 93
 - scales of roughness, 93, 94
- shape, 84–5
 - assumed equidimensional, 85, 86
 - definition of elliptical discontinuity, 87, 88
 - limited information on shape, 84
 - unrestricted and restricted discontinuities, 84
 - variation of mean trace length, 88, 89
- size, 85–91
 - expressions relating mean and standard deviation respectively of discontinuity size and trace length, 87, 88, 89
 - size distribution, 86, 87, 90, 91
- spacing and linear frequency, 61–4
 - classification of spacing, 61
 - frequency defined, 61–2
 - function for discontinuity spacing values, 62
 - linear discontinuity frequency related to the P-wave velocity, 63, 64, 65
 - spacing defined, 61

- spacing histogram, 62
- ten characteristic ISRM parameters, 55–6
- trace length, 78–84
 - corrected mean trace length, 80–3
 - discontinuities intersecting a circular sampling window, 82, 83
 - discontinuities intersecting a vertical rock face, 81
 - effect of bias, 80–1
 - equations for mean trace length, 81, 82
 - special cases, 83
 - errors caused by bias, 78–9
 - probability distribution of measured trace length, 80
 - trace length distribution on an infinite surface, 83–4
- discontinuity roughness coefficient *see* JRC
- discontinuity wall compressive strength *see* JCS
- discrete element method (DEM), 153, 157–8

- engineering properties of rocks, determination of, 5–12
 - accuracy required for rock mass properties, 5
 - examples, 7–12
 - estimation of rock discontinuity shear strength, 7–9
 - determination of basic friction angle, 8, 9
 - determination of JRC and JCS, 8
 - shear strength criterion parameters, 8
 - estimation of strength and deformability of rock masses, 9–12
 - borings to obtain RQD and TCR values, 11
 - characterization of discontinuities, 11
 - GSI values, 12
 - Hoek-Brown criterion, 12
 - laboratory test results, 11
 - laboratory and in situ tests, 6, 6, 7
 - methods for determining rock mass properties, direct and indirect, 5, 6
- engineering problems in rocks, 1–4
 - components of a general rock mechanics program, 4
 - discontinuities in rock, 1
 - influence of scale on rock mass behaviour, 1, 3
 - intact rock defined, 1
 - rock mass defined, 1
 - three-tier approach to problems, 2, 3
 - types of structure built on, in or of rock, 1, 2

- filling, discontinuity, 96–7
 - defined, 96
 - effect on shear strength, 97
- Fossum model, 151
- FracMan discrete fracture code, 84
- fracture tensor, 92–3, 162–8,
 - tensor equations, 92–3, 162–3,

- geological strength index *see* GSI
- Geomechanics Classification System *see* RMR (rock mass rating)
- grain size,
 - correlation between permeability and grain size, 232, 234

- correlation between porosity and grain size, 37, 39
- GSI (geological strength index), vii, 12, 99, 106–14
- hardness, 31, 32
- Hoek-Brown criterion, 12, 189, 192, 193, 206–8
- HTPE (hydraulic testing of pre-existing fractures), 15–16
- initial tangent modulus, 119
- intact rock, 31–51 *see also* strength of intact rock
 - correlations between, 44–51
 - density and depth, 40–1
 - density and porosity, 44–5
 - L and N-type Schmidt hammer rebound numbers, 43
 - P-wave velocity and density, 46, 47, 48
 - P-wave velocity and point load index, 46, 49
 - P-wave velocity and porosity, 46, 46, 47
 - P-wave velocity and Schmidt hammer rebound number, 51
 - point load index and porosity, 48, 49
 - point load index and Schmidt hammer rebound number, 50, 51
 - porosity and depth, 37–8
 - porosity and grain size, 37, 39
 - Schmidt hammer rebound number and density, 50
 - Schmidt hammer rebound number and porosity, 48, 50
 - definition, 31
 - density, 39–41
 - defined, 39
 - definition of terms, 39
 - density versus depth for sedimentary rocks, 41
 - relation between depth and density, 40, 41
 - engineering classification, 34–7
 - Deere and Miller classification, 35, 36, 37
 - ISRM classification, 34, 35
 - geological classification, 31–4
 - elementary rocks, 32–4
 - igneous, 32, 33
 - metamorphic, 32, 33
 - sedimentary, 33, 34
 - rock-forming minerals, 31–2
 - point load index, 42–3
 - for different rocks, 35
 - test method, 43
 - porosity, 37–9
 - decreases with increasing depth, 37
 - exponential function, 37
 - relationship for sandstones, 38
 - defined, 37
 - typical values, 38
 - variation of porosity with grain size, 37, 39
 - Schmidt hammer rebound number, 43–4
 - correlation between L and N-type hammer rebound numbers, 43
 - typical number for different rocks, 44
 - slake durability index, 44

- classification, 45
- wave velocity, 42
 - methods for laboratory determination, 42
 - P-wave and S-wave velocity ranges, 42
- International Journal of Rock Mechanics and Mining Sciences (Rock Stress Estimation Special Issue)*, 16, 18
- interconnectivity of discontinuities, 248, 251, 251
- International Lithosphere Program, 26
- International Society for Rock Mechanics *see* ISRM
- ISRM (International Society for Rock Mechanics),
 - categories of,
 - roughness, 93, 94
 - test methods, 6
 - characterization of discontinuities, 11
 - classification of,
 - aperture, 96, 97
 - discontinuity spacing, 61
 - persistence, 74
 - correlation between volumetric frequency and RQD, 71
 - density of rock, 39
 - discontinuities, 53, 55
 - engineering classification of rock by strength, 35
 - measurement of unconfined compressive strength, vii, 175
 - point load test, 42
 - porosity of rock, 37
 - rock quality designation (RQD), 64
 - rock stress tensor measurement, 17
 - Schmidt hammer rebound number, 43
 - Shore Sclerscope hardness measurement, 179
 - slake durability index, 44
 - standards for procedures, 12
 - wave velocity measurements, 42
 - weathering grades of rock mass, 116
- Jaeger model, 212–15
- JCS (discontinuity wall compressive stress), 8
- Johnston criterion, 193, 194, 209
- JRC (discontinuity roughness coefficient), 8
- Kulhawy three-dimensional equivalent continuum, 147, 147
- laboratory tests, 5–7, 11, 6
- Lauffer's Classification, 99
- methods for determining rock mass properties, direct and indirect, 5–7, 6
- Mohr-Coulomb,
 - cohesion and friction angle for different rocks, 197
 - criterion, 194, 212
 - model, 196–8
 - parameters, 196, 210–12
- Moh's scale of hardness, 31, 32

National Coal Board *see* British Coal Corporation

orientation, 56–60

- assignment of poles into discontinuity sets, 58
- contours of pole concentrations, 56, 57
- data in the form of dip direction, 56
- equation for trend and plunge of the pole, 58
- orientation defined, 56
- polar stereonet plot, 56, 57
- pole of a discontinuity as a vector, 58, 59
- probability distributions, 60
- procedure for obtaining mean orientation, 58–60

P-wave velocity, 42, 46, 51, 63, 64, 65, 68, 69, 104, 106, 182, 184 *see also* wave velocity

permeability, 231–52

- anisotropy, 251–2
 - permeability of rocks shows appreciable anisotropy, 251
 - ratio of permeability parallel to bedding to permeability perpendicular to bedding, 252

Darcy's law, 231

defined, 231

discontinuities, 233–7

- correction factors, 235, 236
- permeability coefficient, 233, 234
- variability of permeability coefficients, 237

effect of stress, 238–42

- effect of load acting parallel/perpendicular to discontinuities, 241
- empirical relationships between discontinuity permeability and normal stress, 240, 241
- relationships involving pressure, 239
- variation of permeability with pressure on granite, 240

effect of temperature, 245–6

- increase in temperature reduces permeability, 245
- temperature effect on the permeability of tuff, 247
- variation of hydraulic aperture with temperature, 246

intact rock, 232–3

- permeability coefficient, 235
- permeability versus grain size, 232, 234
- relation between permeability and porosity, 232, 232, 233

interconnectivity of discontinuities, 248, 251, 251

permeability coefficient, 231

rock mass, 237–8

- single discontinuity, 237, 238
- three orthogonal discontinuity sets, 238, 238

scale effect, 246–50

- effect of scale on rock permeability, 246, 248
- representative elementary volume (REV), 247, 248, 249, 250

variation with depth, 242–5

- decrease of discontinuity aperture with depth, 245
- relationship between permeability and depth, 242, 243, 243, 244, 244

persistence, 74–8

defined, 74

ISRM classification of persistence, 74

persistence ratio (PR), 75

- definition as area ratio, 75
- definition as length ratio, 76
- estimation of PR for a finite sample length, 75
- failure of low-angle transitions through intact rock, 76, 77
- in-plane failure of intact rock, 76, 78
- point load index, 42–3
 - for different rocks, 35
 - test method, 43
- Poisson's ratio, 120–2, 121
- porosity, 37–9
 - decreases with increasing depth, 37
 - exponential function, 37
 - relationship for sandstones, 38
 - defined, 37
 - typical values, 38
 - variation of porosity with grain size, 37, 39
- Q (Q-System), vii, 99, 104–6, 145, 204–5 *see also* rock masses
- Ramamurthy criterion, 195, 196, 209, 210
- Recovery modulus, 120
- representative elementary volume (REV), 247, 248, 249, 250
- residual friction angle, 8, 130–1, 199–201
- RMR (rock mass rating), vii, 99–104, 114–5, 143–5, 202–5 *see also* rock masses
- rock masses, 99–117
 - classification, 99–114
 - geological strength index (GSI), 106–14
 - characterization of rock masses, 112
 - quantification of GSI chart, 113
 - rock mass quality (Q), 104–111
 - classification of rock mass based on Q-values, 111
 - correlations with P-wave velocity, 106
 - rock mass rating (RMR), 100–4
 - correlation with P-wave velocity, 104
 - relation between RMR and slope angle, 104
 - rock quality designation (RQD), 99–100
 - correlation with rock quality, 100
 - classification of weathering of rock, 115–18
 - porosity and density of weathering rocks, 116, 118
 - qualitative weathering grade, 116, 117
 - quantitative weathering grades for granite, 116, 118
 - relationship between weathering and RQD, 116, 118
 - weathering defined, 115
 - correlations between classification indices, 114–15
 - relationships between GSI, RMR and Q, 115
 - relationships between Q and RMR, 114, 114, 115
- rock quality designation *see* RQD
- roughness, 93–5
 - classification, 94, 95
 - defined, 93
 - scales of roughness, 93, 94
- RQD (rock quality designation), vii, 11, 64–8, 99–100

- RSR concept, 99
- S-wave velocity, 42, 122
- scale effect,
 deformability, 168–9
 variation of measured dynamic modulus with test volume of rock, 170
 permeability, 246–50
 representative elementary volume (REV), 247, 248, 249, 250
 strength, 223–6
 effect of test volume on measured bearing strength, 225
 influence of scale on type of rock mass behaviour, 226
 peak strength for Moura coal, 224
 scale effect on components of shear strength of a rough discontinuity, 200
 specimen size and strength of intact rock, 223
- Schmidt hammer, vii, 43–4, 48–50, 51, 122, 178
- seismic wave velocity *see* wave velocity
- Shore Sclerscope hardness measurement, 178–81
- Standard Specification for Highway Bridges* (AASHTO), 138
- strength of intact rock, 175–96
 empirical strength criteria of intact rock, 192–6
 Bieniawski-Yudhbir criterion, 193
 values of parameter, 194
 Hoek-Brown criterion, 192, 193
 Johnston criterion, 193, 194
 Ramamurthy criterion, 195, 196
 Mohr-Coulomb parameters of intact rock, 196
 cohesion and friction angle for different rocks, 197
- tensile strength, 187–92
 estimating methods, 189
 relationships between tensile strength and unconfined compressive strength for three rock types, 191, 192
 simple correlation between tensile strength and unconfined compressive strength, 187
 variation of tensile strength with water content, 192, 193
- unconfined compressive strength, 175–87
 cone indenter number versus unconfined compressive strength, 181–2
 test equipment and procedure, 181
 density versus unconfined compressive strength, 186
 data and trend line for chalk, 187
 empirical relationship, 186
 P-wave velocity versus unconfined compressive strength, 182
 correlations, 183
 variation of unconfined compressive strength with P-wave velocity, 184
- point load index versus unconfined compressive strength, 176–8
 effect of porosity, 178
 empirical correlations, 177, 178
- porosity versus unconfined compressive strength, 182–5
 empirical relationships, 183
 equation constants for different rocks, 184
 variation of strength with porosity, 185
- range of strength, 176
- Schmidt hammer rebound number versus unconfined compressive strength, 178, 179
 empirical correlations, 180

- Shore Sclerscope hardness versus unconfined compressive strength, 178–81
 - empirical correlations, 181
 - standardised measurement procedures, 175–6
 - water content,
 - ratio of unconfined compressive strength at saturated condition to that at dry condition, 187, 188
 - variation of unconfined compressive strength with water content, 186–7, 188
- strength of rock discontinuities, 196–202
 - Barton model, 199–201
 - peak shear strength for different rock types, 201
 - scale effect on components of shear strength of a rough discontinuity, 200
 - bilinear shear strength model, 198, 198, 199
 - Mohr-Coulomb model, 196–8
 - shear strength of filled discontinuities, 202
 - shear strength parameters of filled discontinuities and filling materials, 203
- strength of rock mass, 202–22
 - empirical strength criteria, 206–10
 - Bieniawski-Yudhbir criterion, 208, 209
 - Hoek-Brown criterion, 206–8
 - effect of water, 208
 - limitations on use, 208
 - Johnston criterion, 209
 - Ramamurthy criterion, 209, 210
 - equivalent continuum method for estimating strength, 212–22
 - Amadei model, 215–17
 - discontinuity plane in a triaxial stress field, 216
 - equations for the criteria, 215, 216, 217
 - forms of equation for different parameters, 217
 - geometrical representation of the failure surface, 217, 219
 - shape of the failure surface, 218, 220
 - comments, 217–22
 - rock mass with two discontinuity sets, 217, 221
 - strength variation with angle of discontinuity plane, 222
 - defined, 212
 - Jaeger model, 212–15
 - Mohr-Coulomb parameters of rock mass, 210–12
 - cohesive strength and friction angles for different GSI and m , values, 213
 - equations for estimation of cohesion and friction angle, 211
 - tensile strength, 205
 - unconfined compressive strength, 202–5
 - empirical correlations, 204
 - variation with GSI or RMR, 205
- stresses, in-situ, 15–30
 - activities requiring knowledge of stresses, 15, 16
 - components of the stress tensor, 15, 17
 - effect of complex topography, 27, 29
 - measurement methods, 15
 - motivations for determination of stress, 15
 - strategy for estimating stresses, 17–18
 - steps in developing knowledge of tensor components, 18
 - variation with depth, 19–26
 - horizontal stress, 20–6

- average horizontal to vertical stress ratio (k), 25 26, 27
- coefficient of linear thermal expansion of rock, 25
- related to vertical stress, 20, 21, 23
- types of fault and state of stresses, 21
- variation of average horizontal stress to vertical stress ratio versus depth, 21, 23, 24
- variation of horizontal stress with depth, 22–3
- worldwide average horizontal stress to vertical stress ratio versus depth, 23, 24
- vertical stress, 19–20
 - variation of vertical stress with depth, 20
 - worldwide data, 19
- world stress map (WSM), 26, 28
 - four categories of stress indicators for tectonic stress orientation, 26
 - map showing orientations of maximum horizontal stress, 28
- Suggested methods for the quantitative description of discontinuities in rock masses (ISRM)*, 55
- TCR (total core recovery), 11
- temperature, effect of, 245–6
 - increase in temperature reduces permeability, 245
 - temperature effect on the permeability of tuff, 247
 - variation of hydraulic aperture with temperature, 246
- tensile strength,
 - intact rock, 187–92
 - estimating methods, 189
 - relationships between tensile strength and unconfined compressive strength for three rock types, 191, 192
 - simple correlation between tensile strength and unconfined compressive strength, 187
 - variation of tensile strength with water content, 192, 193
 - rock mass, 205
- Terzaghi's Rock Load Height Classification, 99
- Tilt test, 132, 132
- Trace length,
 - corrected mean trace length, 80–3
 - discontinuities intersecting a circular sampling window, 82, 83
 - discontinuities intersecting a vertical rock face, 81
 - effect of bias, 80–1
 - equations for mean trace length, 81, 82
 - special cases, 83
 - errors caused by bias, 78–9
 - probability distribution of measured trace length, 80
 - trace length distribution on an infinite surface, 83–4
 - variation of mean trace length, 88, 89
- UCS (unconfined compressive strength), vii *see also* unconfined compressive strength
- unconfined compressive strength,
 - intact rock, 175–87
 - cone indenter number versus unconfined compressive strength, 181–2
 - test equipment and procedure, 181
 - density versus unconfined compressive strength, 186
 - data and trend line for chalk, 187
 - empirical relationship, 186
 - P-wave velocity versus unconfined compressive strength, 182
 - correlations, 183

- variation of unconfined compressive strength with P-wave velocity, 184
- point load index versus unconfined compressive strength, 176–8
 - effect of porosity, 178
 - empirical correlations, 177, 178
- porosity versus unconfined compressive strength, 182–5
 - empirical relationships, 183
 - equation constants for different rocks, 184
 - variation of strength with porosity, 185
- range of strength, 176
- Schmidt hammer rebound number versus unconfined compressive strength, 178, 179
 - empirical correlations, 180
- Shore Sclerscope hardness versus unconfined compressive strength, 178–81
 - empirical correlations, 181
- standardised measurement procedures, 175–6
- water content,
 - ratio of unconfined compressive strength at saturated condition to that at dry condition, 188
 - variation of unconfined compressive strength with water content, 186, 188
- rock mass, 202–5
 - empirical correlations, 204
 - variation with GSI or RMR, 205
- vertical stress, 19–20, 20
- water content,
 - ratio of unconfined compressive strength at saturated condition to that at dry condition, 188
 - variation of elastic modulus with water content, 124, 126
 - variation of tensile strength with water content, 192, 193
 - variation of unconfined compressive strength with water content, 186, 188
- wave velocity,
 - correlation between,
 - deformation modulus and P-wave velocity, 146
 - elastic modulus and P-wave velocity, 124
 - linear discontinuity frequency and P-wave velocity, 63, 64, 65
 - P-wave velocity and density, 46, 47, 49
 - P-wave velocity and point load index, 46, 49
 - P-wave velocity and porosity, 46, 46, 47
 - P-wave velocity and RQD, 68, 69
 - P-wave velocity and Schmidt hammer rebound number, 51
 - P-wave velocity and unconfined compressive strength, 182, 183, 184
 - rock mass quality (Q) and P-wave velocity, 106
 - rock mass rating (RMR) and P-wave velocity, 104
 - methods for laboratory determination, 42
 - P-wave and S-wave velocity ranges, 42
- weathering of rock, 115–18
 - defined, 115
 - porosity and density of weathering rocks, 116, 118
 - qualitative weathering grade, 116, 117
 - quantitative weathering grades for granite, 116, 118
 - relationship between weathering and RQD, 116, 118
- WSM (world stress map), 26, 28